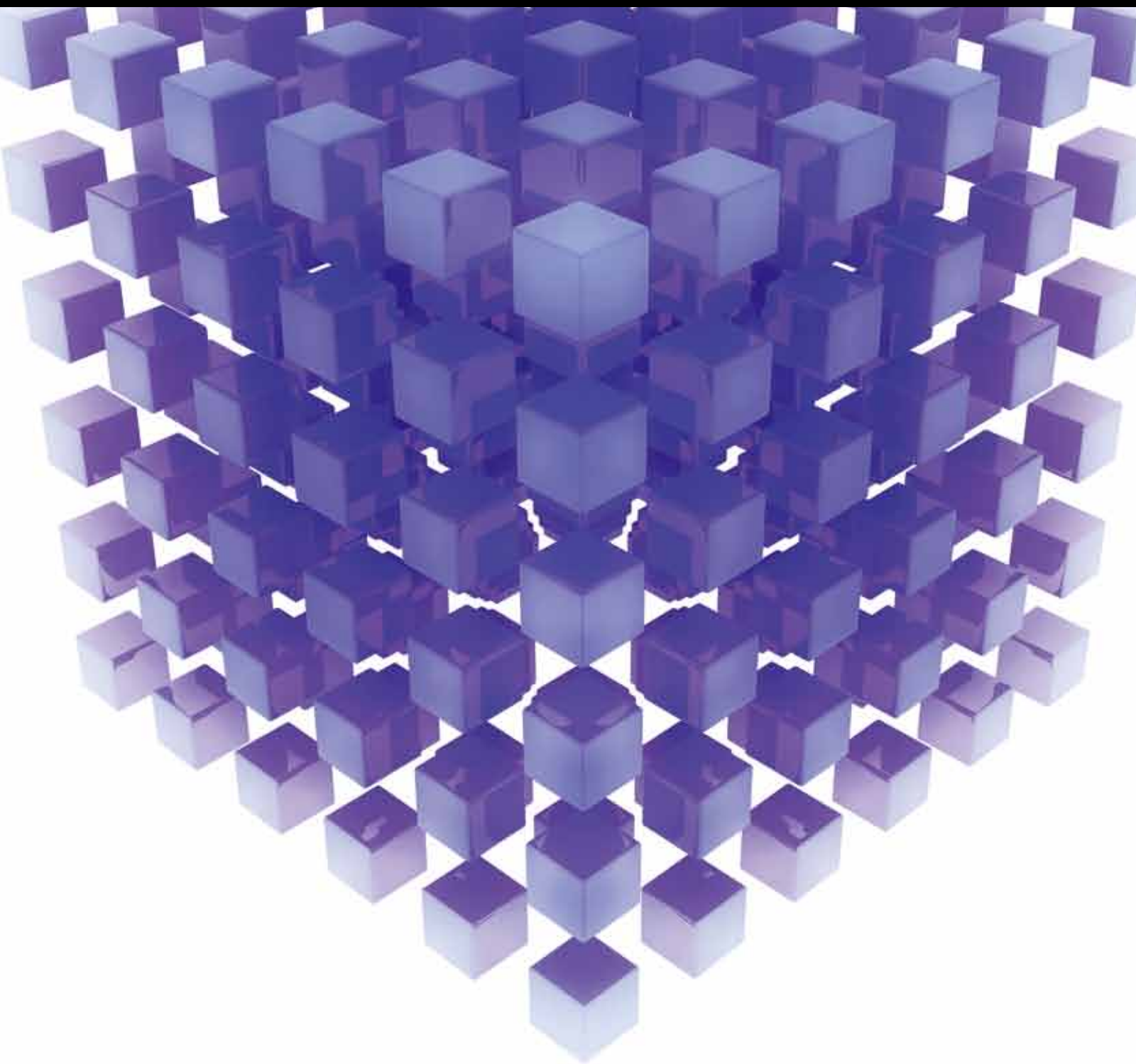


MATHEMATICAL PROBLEMS IN ENGINEERING

# Nonlinear Time Series 2013

GUEST EDITORS: MING LI, CARLO CATTANI, S. C. LIM, AND MASSIMO SCALIA





---

## **Nonlinear Time Series 2013**

Mathematical Problems in Engineering

---

## **Nonlinear Time Series 2013**

Guest Editors: Ming Li, Carlo Cattani, S. C. Lim,  
and Massimo Scalia



---

Copyright © 2014 Hindawi Publishing Corporation. All rights reserved.

This is a special issue published in “Mathematical Problems in Engineering.” All articles are open access articles distributed under the Creative Commons Attribution License, which permits unrestricted use, distribution, and reproduction in any medium, provided the original work is properly cited.



## Editorial Board

M. Abd El Aziz, Egypt  
E. M. Abdel-Rahman, Canada  
R. K. Abu Al-Rub, USA  
Sarp Adali, South Africa  
Salvatore Alfonzetti, Italy  
Igor Andrianov, Germany  
Sebastian Anita, Romania  
W. Assawinchaichote, Thailand  
Erwei Bai, USA  
Ezzat G. Bakhoun, USA  
José M. Balthazar, Brazil  
R. K. Bera, India  
C. Bérenguer, France  
Jonathan N. Blakely, USA  
Stefano Boccaletti, Spain  
Stephane P.A. Bordas, USA  
Daniela Boso, Italy  
M. Boutayeb, France  
Michael J. Brennan, UK  
Salvatore Caddemi, Italy  
Piermarco Cannarsa, Italy  
Jose E. Capilla, Spain  
Carlo Cattani, Italy  
M. M. Cavalcanti, Brazil  
Diego J. Celentano, Chile  
Mohammed Chadli, France  
Arindam Chakraborty, USA  
Yong-Kui Chang, China  
Michael J. Chappell, UK  
Kui Fu Chen, China  
Xinkai Chen, Japan  
Kue-Hong Chen, Taiwan  
Jyh-Horng Chou, Taiwan  
Slim Choura, Tunisia  
C. Cruz-Hernandez, Mexico  
Swagatam Das, India  
Filippo de Monte, Italy  
Antonio Desimone, Italy  
Yannis Dimakopoulos, Greece  
Baocang Ding, China  
Joao B. R. Do Val, Brazil  
Daoyi Dong, Australia  
B. Dubey, India  
Horst Ecker, Austria  
M. Onder Efe, Turkey

Elmetwally Elabbasy, Egypt  
A. Elías-Zúñiga, Mexico  
Anders Eriksson, Sweden  
Vedat S. Erturk, Turkey  
Moez Feki, Tunisia  
Ricardo Femat, Mexico  
Robertt A. Valente, Portugal  
C. Fuerte-Esquivel, Mexico  
Zoran Gajic, USA  
Ugo Galvanetto, Italy  
Furong Gao, Hong Kong  
Xin-Lin Gao, USA  
Behrouz Gatmiri, Iran  
Oleg V. Gendelman, Israel  
Didier Georges, France  
P. Gonçalves, Brazil  
Oded Gottlieb, Israel  
Fabrizio Greco, Italy  
Quang Phuc Ha, Australia  
M. R. Hajj, USA  
Tony S. W. Hann, Taiwan  
Thomas Hanne, Switzerland  
K. R. (Stevanovic) Hedrih, Serbia  
M.I. Herreros, Spain  
Wei-Chiang Hong, Taiwan  
Jaromir Horacek, Czech Republic  
Huabing Huang, China  
Chuangxia Huang, China  
Gordon Huang, Canada  
Yi Feng Hung, Taiwan  
Hai-Feng Huo, China  
Asier Ibeas, Spain  
Anuar Ishak, Malaysia  
Reza Jazar, Australia  
Zhijian Ji, China  
Jun Jiang, China  
J. J. Judice, Portugal  
Tadeusz Kaczorek, Poland  
Tamas Kalmar-Nagy, USA  
Tomasz Kapitaniak, Poland  
Hamid Reza Karimi, Norway  
Metin O. Kaya, Turkey  
Nikolaos Kazantzis, USA  
Farzad Khani, Iran  
K. Krabbenhoft, Australia

Ren-Jieh Kuo, Taiwan  
Jurgen Kurths, Germany  
Claude Lamarque, France  
Usik Lee, Korea  
Marek Lefik, Poland  
Stefano Lenci, Italy  
Roman Lewandowski, Poland  
Shanling Li, Canada  
Ming Li, China  
Jian Li, China  
Shihua Li, China  
Teh-Lu Liao, Taiwan  
Panos Liatsis, UK  
Shueei M. Lin, Taiwan  
Yi-Kuei Lin, Taiwan  
Jui-Sheng Lin, Taiwan  
Yuji Liu, China  
Wanquan Liu, Australia  
Bin Liu, Australia  
Paolo Lonetti, Italy  
V. C. Loukopoulos, Greece  
Junguo Lu, China  
Chien-Yu Lu, Taiwan  
Alexei Mailybaev, Brazil  
M. K. Maiti, India  
O. D. Makinde, South Africa  
R. Martinez-Guerra, Mexico  
Driss Mehdi, France  
Roderick Melnik, Canada  
Xinzhu Meng, China  
Yuri V. Mikhlin, Ukraine  
G. Milovanovic, Serbia  
Ebrahim Momoniat, South Africa  
Trung Nguyen Thoi, Vietnam  
Hung Nguyen-Xuan, Vietnam  
Ben T. Nohara, Japan  
Sotiris K. Ntouyas, Greece  
Gerard Olivar, Colombia  
Claudio Padra, Argentina  
Bijaya Ketan Panigrahi, India  
Francesco Pellicano, Italy  
Matjaz Perc, Slovenia  
Vu Ngoc Phat, Vietnam  
M. do Rosário Pinho, Portugal  
A. Pogromsky, The Netherlands

Seppo Pohjolainen, Finland  
Stanislav Potapenko, Canada  
Sergio Preidikman, USA  
Carsten Proppe, Germany  
Hector Puebla, Mexico  
Justo Puerto, Spain  
Dane Quinn, USA  
K. R. Rajagopal, USA  
Gianluca Ranzi, Australia  
Sivaguru Ravindran, USA  
G. Rega, Italy  
Pedro Ribeiro, Portugal  
J. Rodellar, Spain  
R. Rodriguez-Lopez, Spain  
A. J. Rodriguez-Luis, Spain  
Ignacio Romero, Spain  
Hamid Ronagh, Australia  
Carla Roque, Portugal  
R. R. García, Spain  
Manouchehr Salehi, Iran  
Miguel A. Sanjuán, Spain  
Ilmar F. Santos, Denmark  
Nickolas S. Sapidis, Greece  
E. J. Sapountzakis, Greece  
Bozidar Sarler, Slovenia  
Andrey V. Savkin, Australia  
Massimo Scalia, Italy  
Mohamed A. Seddeek, Egypt  
A. P. Seyranian, Russia  
Leonid Shaikhet, Ukraine

Cheng Shao, China  
Bo Shen, Germany  
Jian-Jun Shu, Singapore  
Zhan Shu, UK  
Dan Simon, USA  
Luciano Simoni, Italy  
Grigori M. Sisoiev, UK  
Christos H. Skiadas, Greece  
Davide Spinello, Canada  
Sri Sridharan, USA  
Rolf Stenberg, Finland  
Changyin Sun, China  
Jitao Sun, China  
Xi-Ming Sun, China  
Andrzej Swierniak, Poland  
Yang Tang, Germany  
Allen Tannenbaum, USA  
Cristian Toma, Romania  
Irina N. Trendafilova, UK  
Alberto Trevisani, Italy  
Jung-Fa Tsai, Taiwan  
K. Vajravelu, USA  
Victoria Vampa, Argentina  
Josep Vehi, Spain  
Stefano Vidoli, Italy  
Xiaojun Wang, China  
Dan Wang, China  
Youqing Wang, China  
Yongqi Wang, Germany  
Cheng C. Wang, Taiwan

Moran Wang, China  
Yijing Wang, China  
Gerhard-Wilhelm Weber, Turkey  
J. S. Witteveen, The Netherlands  
Kwok-Wo Wong, Hong Kong  
Ligang Wu, China  
Zhengguang Wu, China  
Gongnan Xie, China  
Wang Xing-yuan, China  
Xi Frank Xu, USA  
Xuping Xu, USA  
Jun-Juh Yan, Taiwan  
Xing-Gang Yan, UK  
Suh-Yuh Yang, Taiwan  
Mahmoud T. Yassen, Egypt  
Mohammad I. Younis, USA  
Bo Yu, China  
Huang Yuan, Germany  
S.P. Yung, Hong Kong  
Ion Zaballa, Spain  
A. M. Zenkour, KSA  
Jianming Zhan, China  
Xu Zhang, China  
Yingwei Zhang, China  
Lu Zhen, China  
Liancun Zheng, China  
Jian Guo Zhou, UK  
Zexuan Zhu, China  
Mustapha Zidi, France

# Contents

**Nonlinear Time Series 2013**, Ming Li, Carlo Cattani, S. C. Lim, and Massimo Scalia  
Volume 2014, Article ID 492874, 2 pages

**Tool Wear Detection Using Lipschitz Exponent and Harmonic Wavelet**, Song Wanqing, Li Qing, and Wang Yuming  
Volume 2013, Article ID 489261, 8 pages

**A Hybrid Fuzzy Time Series Approach Based on Fuzzy Clustering and Artificial Neural Network with Single Multiplicative Neuron Model**, Ozge Cagcag Yolcu  
Volume 2013, Article ID 560472, 9 pages

**Italian Residential Buildings: Economic Assessments for Biomass Boilers Plants**, Maurizio Carlini, Sonia Castellucci, Silvia Cocchi, Elena Allegrini, and Ming Li  
Volume 2013, Article ID 823851, 10 pages

**Identification of Nonstandard Multifractional Brownian Motions under White Noise by Multiscale Local Variations of Its Sample Paths**, Kwang-Il Ahn and Kichun Lee  
Volume 2013, Article ID 794130, 10 pages

**A Reconfigurable Logic Cell Based on a Simple Dynamical System**, Lixiang Li, Chunyu Yang, Sili Hui, Wenwen Yu, Jürgen Kurths, Haipeng Peng, and Yixian Yang  
Volume 2013, Article ID 735189, 7 pages

**Topology Identification of Complex Network via Chaotic Ant Swarm Algorithm**, Haipeng Peng, Lixiang Li, Jürgen Kurths, Shudong Li, and Yixian Yang  
Volume 2013, Article ID 401983, 5 pages


**Sensor Scheduling with Intelligent Optimization Algorithm Based on Quantum Theory**, Zhiguo Chen, Yi Fu, and Wenbo Xu  
Volume 2013, Article ID 853430, 8 pages

**First-Order ARMA Type Fuzzy Time Series Method Based on Fuzzy Logic Relation Tables**, Cem Kocak  
Volume 2013, Article ID 769125, 12 pages

**Residual ISI Obtained by Nonblind Adaptive Equalizers and Fractional Noise**, Monika Pinchas  
Volume 2013, Article ID 830517, 7 pages

**Wild Fluctuations of Random Functions with the Pareto Distribution**, Ming Li and Wei Zhao  
Volume 2013, Article ID 767502, 3 pages

**Set Pair Analysis Based on Phase Space Reconstruction Model and Its Application in Forecasting Extreme Temperature**, Yin Zhang, Xiao-hua Yang, Ling Zhang, Wan-ying Ma, and Ling-xia Qiao  
Volume 2013, Article ID 516150, 7 pages



---

**Symbol Error Rate as a Function of the Residual ISI Obtained by Blind Adaptive Equalizers for the SIMO and Fractional Gaussian Noise Case**, Monika Pinchas

Volume 2013, Article ID 860389, 9 pages

**An ARMA Type Fuzzy Time Series Forecasting Method Based on Particle Swarm Optimization**, Erol Egrioglu, Ufuk Yolcu, Cagdas Hakan Aladag, and Cem Kocak

Volume 2013, Article ID 935815, 12 pages

**Convergence of Sample Autocorrelation of Long-Range Dependent Traffic**, Ming Li and Wei Zhao

Volume 2013, Article ID 725730, 7 pages

**Adaptive Synchronization of Complex Dynamical Multilinks Networks with Similar Nodes**,

Weiping Wang, Lixiang Li, Haipeng Peng, Jialiang Yuan, Jinghua Xiao, and Yixian Yang

Volume 2013, Article ID 736585, 12 pages

**On the Long-Range Dependence of Fractional Brownian Motion**, Ming Li

Volume 2013, Article ID 842197, 5 pages

## Editorial

# Nonlinear Time Series 2013

**Ming Li,<sup>1</sup> Carlo Cattani,<sup>2</sup> S. C. Lim,<sup>3</sup> and Massimo Scalia<sup>4</sup>**

<sup>1</sup> School of Information Science & Technology, East China Normal University, Shanghai 200241, China

<sup>2</sup> Department of Mathematics, University of Salerno, Via Ponte Don Melillo, 84084 Fisciano, Italy

<sup>3</sup> Faculty of Engineering, Multimedia University, 63100 Cyberjaya, Selangor, Malaysia

<sup>4</sup> CIRPS, University of Rome, "La Sapienza", Piazza San Pietro in Vincoli 10, 00184 Rome, Italy

Correspondence should be addressed to Ming Li; ming\_lihk@yahoo.com

Received 12 December 2013; Accepted 12 December 2013; Published 12 January 2014

Copyright © 2014 Ming Li et al. This is an open access article distributed under the Creative Commons Attribution License, which permits unrestricted use, distribution, and reproduction in any medium, provided the original work is properly cited.

Nonlinear time series plays a fundamental role in various fields of sciences and engineering, ranging from physical and life sciences to telecommunication engineering.

One of the most challenging tasks of research is to face nonlinear problems which nonlinearly depend on a large number of parameters and/or are based on unpredictable, random, or fractal-like behavior. Some of the more intriguing and modern topics such as telecommunication, traffic dynamics, complex networks, optimization, and fractional dynamics, can be described by nonlinear time series. However, the extraction of useful information from the nonlinear time series by the commonly used analytical techniques is often difficult due the presence of noise in the signals. In this issue, we have selected papers on the main theme of identifying correct methods for the optimal understanding of the relevant information hidden in a signal representing a nonlinear phenomenon. We believe that there is a strong interest on this topic, although a widely accepted methodology for a proper investigation of nonlinear time series is still an open question. Through the collected papers of this issue we want to illustrate some of the interesting approaches and smart techniques which we hope can be regarded as a small step towards a systematic method for analyzing nonlinear time series.

This special issue collects 16 papers with respect to nonlinear time series, its computations, and applications.

M. Li and W. Zhao's paper entitled "*Convergence of sample autocorrelation of long-range dependent traffic*" exhibits

a radical property of teletraffic time series. The paper "*Identification of nonstandard multifractional Brownian motions under white noise by multiscale local variations of its sample paths*" by K. Ahn and I. Lee provides stable and simultaneous estimators of two parameters for nonstandard multifractional Brownian motions under white noise. M. Li's paper "*On the long-range dependence of fractional Brownian motion*" clarifies that fractional Brownian motion is long-range dependent on the Hurst parameter  $0 < H < 1$ . The paper by Li and Zhao, entitled "*Wild fluctuations of random functions with the Pareto distribution*," introduces the terms wild and wildest fluctuations of time series that follow heavy-tailed distributions, such as the Pareto distribution.

Peng et al.'s paper "Topology identification of complex network via chaotic ant swarm algorithm" studies the issue of topology identification from the point of view of parameter optimization for complex networks. It is a pioneering work revealing an important phenomenon of Lorenz chaotic equation that was used in their simulation of the  $i$ th node from a view of the golden ratio with respect to chaotic ant swarm algorithm. M. Pinchas' two papers, entitled "*Symbol error rate as a function of the residual ISI obtained by blind adaptive equalizers for the SIMO and fractional Gaussian noise case*" and "*Residual ISI obtained by nonblind adaptive equalizers and fractional noise*," provide examples of applying fractional Gaussian noise to communication engineering. These two papers provide of a set of theories of adaptive equalizers essential to communication systems. The paper "*Adaptive synchronization of complex dynamical multilinks*

*networks with similar nodes*” by W. Wang et al. proposes a novel method of adaptive synchronization to describe the similarity of similar nodes in complex multilinks networks. The paper entitled “*A reconfigurable logic cell based on a simple dynamical system*” by L. Li et al. introduces a new scheme to achieve a dynamic logic gate that can be flexibly varied to obtain different logic functions by adjusting specific parameters of a dynamical system, discovering that it is resistant to system noise. In addition, the paper contributes a significant result in electronics engineering that the system can be considered as a leaky integrator.

O. C. Yolcu’s paper entitled “*A hybrid fuzzy time series approach based on fuzzy clustering and artificial neural network with single multiplicative neuron model*” studies fuzzy time series forecasting by using artificial neural networks with single multiplicative neuron model in the identification of fuzzy relation such that the architecture selection problem can be eliminated without the need for defuzzification step by constituting target values from real observations of time series. The paper “*An ARMA type fuzzy time series forecasting method based on particle swarm optimization*” by E. Egrioglu et al. discusses fuzzy time series forecasting. Its novelty in time series prediction is in presenting a novel first-order fuzzy time series by taking into account both autoregressive and moving average structures. Its practical significance is that the proposed model is time invariant. The paper by C. Kocak “*First-order ARMA type fuzzy time series method based on fuzzy logic relation tables*” attempts to carry out fuzzy time series prediction a step further by considering autoregressive moving average ARMA (1, 1) in order to eliminate the deficiency of conventional fuzzy time series predictors. The paper “*Set pair analysis based on phase space reconstruction model and its application in forecasting extreme temperature*” by Y. Zhang et al. establishes a forecasting approach called set pair analysis based on phase space reconstruction model to improve forecasting precision of a time series.

Z. Chen et al. in their paper “*Sensor scheduling with intelligent optimization algorithm based on quantum theory*” proposes an improved particle swarm optimization (PSO) algorithm using a best dimension mutation technique. M. Carlini et al.’s paper “*Italian residential buildings: economic assessments for biomass boilers plants*” deals with the economic feasibility of biomass boiler plants with specific regard to an existing residential building. It further investigates an Italian case that focuses on the attention on European and national regulations on energy efficiency and considers the recent public incentives and supporting measures. The paper by S. Wanqing et al., “*Tool wear detection using Lipschitz exponent and harmonic wavelet*,” explains singularity analysis with harmonic wavelet for data processing.

work in part by Macau Science and Technology Development Fund under Grant nos. 061/2011/A3, 009/2010/A1, and 021/2009/A1 and by the National Natural Science Foundation of China under the Project Grant nos. 61272402, 61070214, and 60873264.

Ming Li  
Carlo Cattani  
S. C. Lim  
Massimo Scalia

## Acknowledgments

We are grateful to all the authors of this special issue for their contributions and to the reviewers for their valuable comments. Ming Li acknowledges the supports for his

## Research Article

# Tool Wear Detection Using Lipschitz Exponent and Harmonic Wavelet

**Song Wanqing, Li Qing, and Wang Yuming**

*College of Electronic and Electrical Engineering, Shanghai University of Engineering and Science, Shanghai 201620, China*

Correspondence should be addressed to Song Wanqing; [swqls@126.com](mailto:swqls@126.com)

Received 20 July 2013; Accepted 31 August 2013

Academic Editor: Carlo Cattani

Copyright © 2013 Song Wanqing et al. This is an open access article distributed under the Creative Commons Attribution License, which permits unrestricted use, distribution, and reproduction in any medium, provided the original work is properly cited.

The paper researches a novel engineering application of Lipschitz exponent function and harmonic wavelet for detecting tool condition. Tool wear affects often the quality grade of products and is gradually formed during cutting process. Meanwhile, since cutting noise is very strong, we think tool wear belongs to detecting weak singularity signals in strong noise. It is difficult to obtain a reliable worn result by raw sampled data. We propose singularity analysis with harmonic wavelet for data processing and a new concept of Lipschitz exponent function. The method can be quantitative tool condition and make maintaining decision. Test result was validated with 27 kinds of cutting conditions with the sharp tool and the worn tool; 54 group data are sampled by acoustic emission (AE).

## 1. Introduction

In recent years, great achievements in tool wear monitoring have been made based on the advanced mathematical models [1–8], even though none of these methods was successful online monitoring due to the complex performance of the machining processes. How to be quantitative tool condition monitoring is very important for practical engineering applications. This is a signal process problem that detects weak singularity signals in strong noise. However, the classical signal process is Fourier theory which has four defects [9–11]: (1) suits stationary stochastic signal, this kind of signal does not almost exists in engineering; (2) for discrete Fourier, Fourier analysis is precise with time series long from zero to infinite, otherwise truncation error is made; (3) weak singularity signal, relatively strange signal, is omitted in FFT however, weak singularity signal often contains important fault information; (4) when signal frequency happen a sudden change with adjacent time intervals, Fourier method only obtains two frequencies, it cannot display the moment two frequency changes or occurs (i.e., the singularities) in frequency domain. In order to overcome the above four defects to improve the measuring precision of weak singular signal in strong noise, we propose the combination between Lipschitz exponent index and complex wavelet for the detection of quantitative tool wear.

Lipschitz functions appear almost everywhere in mathematics [12]. Lipschitz functions are an important class of strong variations originating from smooth deformations of corresponding nonsmooth function [13]; the local regularity is often measured by Lipschitz exponents (LE); the singular variations can be viewed as combinations of weak increasing and decreasing variations; it means the case of discontinuity occurrence on smooth function. Since the paper [14] is published in 1992 to detect signal's singularities, which proposed that the instantaneous frequencies can be approximately identified from the modulus maxima of a real wavelet based on general maxima, which are the locations of the largest modulus along maxima lines through an extension of [14], the complex-wavelet modulus maxima can detect and characterize singularities [15, 16] and has taken excellent result for measuring weak singularities of signal. Harmonic wavelet is one kind of complex wavelet; it is very sensitive to singularity feature of the signal that contains weak faults [17–20] and satisfies multiwavelets frames with arbitrary integer dilation factor [21]. The paper combines the modulus maxima of using a harmonic wavelet, and Lipschitz functions can be quantitative tool condition during cutting process. By 27 kinds of cutting conditions and turning experiments on HL-32 NC turning center, 54 group data are sampled by acoustic emission (AE). We have demonstrated



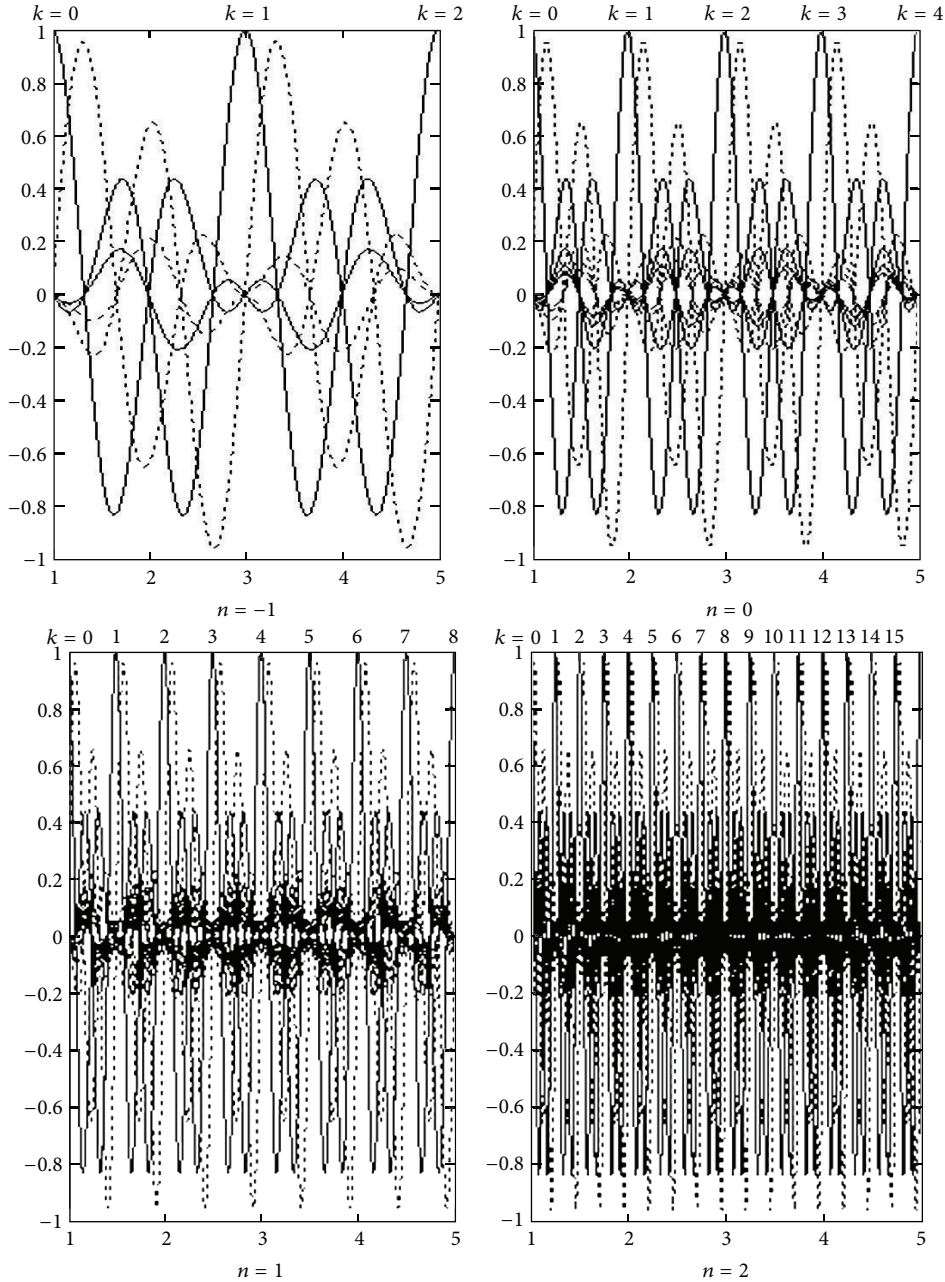


FIGURE 1: Real (thick line) and imaginary (thin line).

that combining the modulus maxima of harmonic wavelet and Lipschitz functions is better for detecting and estimating tool wear when a worn tool generates a singular signal in a strong noise.

## 2. Harmonic Wavelet Transform Algorithm

Discrete harmonic wavelets are given by

$$\psi_k^n(2^n x - k) \stackrel{\text{def}}{=} \frac{\exp(4\pi i(2^n x - k)) - \exp(2\pi i(2^n x - k))}{2\pi i(2^n x - k)}, \quad (1)$$

where  $n = -1, 0, 1, 2, \dots, N$ .  $n$  is different levels (scale), and  $k$  is different steps (time). The functions of its scale and time are given by Figure 1.

The Fourier transform of (1) is as below:

$$|\hat{\psi}_k^n(\omega)| = \begin{cases} \frac{1}{2\pi 2^n}, & 2\pi 2^n \leq \omega \leq 2\pi 2^{n+1}, \\ 0, & \text{other.} \end{cases} \quad (2)$$

The amplitude-frequency characteristics of (2) is exactly like a box with band limited, as shown Figure 2. This characteristic is the best than any real wavelets for decomposed signal to difference frequency band.



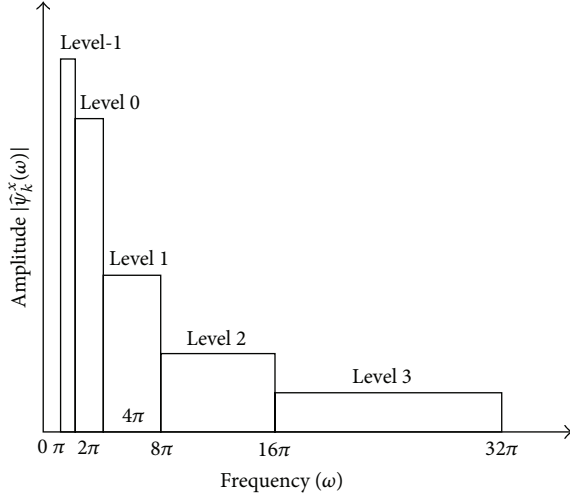
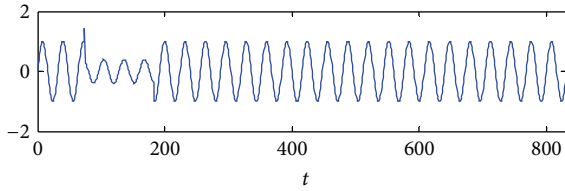
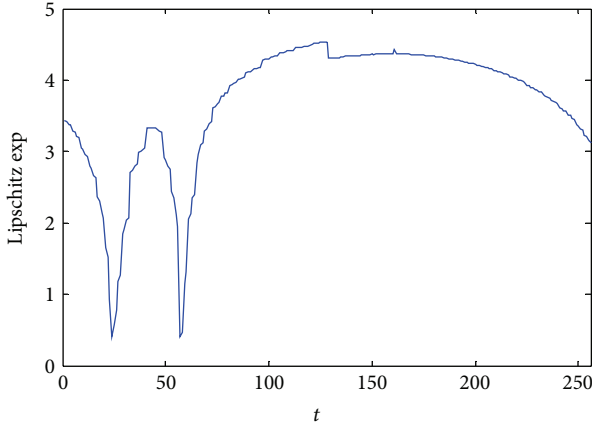


FIGURE 2: Amplitude-frequency characteristics of the discrete harmonic wavelets.



(a) Sine function with two singular points



(b)  $\alpha(t)$  along the temporal axis  $t$

FIGURE 3: Extracting Lipschitz exponent function  $\alpha(t)$ .

### 3. The Definition of Lipschitz Exponent

Lipschitz is from Taylor formula [16, 22, 23] Suppose that function  $f(x)$  is  $m$  times differentiable in  $[x_0 - h, x_0 + h]$ ; then, Taylor expands in the neighborhood of  $x_0$ :

$$f_{x_0}(x) = \sum_{k=0}^{m-1} \frac{f^{(k)}(x_0)}{k!} (x - x_0)^k \quad (3)$$

exists one approximate error:

$$e(x) = f(x) - f_{x_0}(x) \quad (4)$$

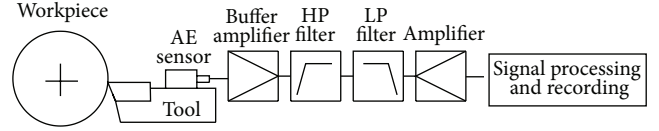


FIGURE 4: AE measurement in metal cutting.

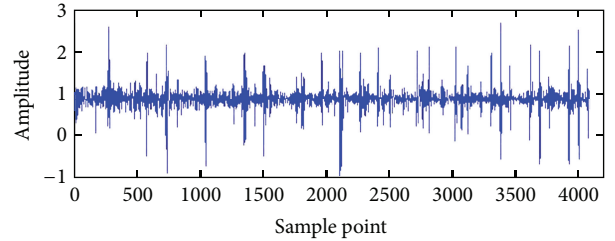


FIGURE 5: Waveform of sharp tool in first condition.

which satisfies:

$$\begin{aligned} \forall x \in [x_0 - h, x_0 + h], \\ |e(x)| \leq \frac{|x - x_0|^m}{m!} \sup_{\zeta \in [x_0 - h, x_0 + h]} |f^{(m)}(\zeta)|. \end{aligned} \quad (5)$$

The  $m$ th order differentiability of  $f(x)$  in the neighborhood of  $x_0$  yields an upper bound on the error  $e(x)$  when  $x$  tends to  $x_0$ . The Lipschitz regularity refines this upper bound with noninteger exponents. The definition of Lipschitz exponent is as follows: a function  $f(x)$  is of Lipschitz  $\alpha$  at  $x_0$ , if and only if there exists a constant  $A$  such that for all  $x$  in a neighborhood of  $x_0$

$$|f(x) - f(x_0)| \leq A|x - x_0|^\alpha. \quad (6)$$

We say that  $f(x)$  is uniformly Lipschitz  $\alpha$  for all  $x$ . Equation (6) is a kind of fractional order [20]. In a neighborhood of  $x_0$ ,  $f(x)$  is singular when  $\alpha \neq 1$ , and  $f(x)$  is continuous when  $\alpha > 0$ . In other words, If  $f(x)$  is discontinuous and bounded in a neighborhood of  $x_0$ , then  $\alpha = 0$ . If  $f(x)$  is continuously differentiable then  $\alpha = 1$  and  $f(x)$  is not singular.

### 4. Modulus Maxima of Wavelet

Reference [14] depicts the modulus maxima of real wavelet to detect singular signal, and [15] extends to the modulus maxima of complex wavelet, and algorithm is deduced in detail. We say a function  $f(x)$  is a modulus maximum of wavelet at the point  $(2^n, x_0)$ ; then,

$$|\psi f(2^n, x)| < |\psi f(2^n, x_0)| \quad (7)$$

or

$$\frac{\partial \psi f(2^j, x_0)}{\partial x} = 0, \quad (8)$$

where  $x$  belongs to either the right or the left neighborhood of  $x_0$ . A maxima line is consisted of a connected curve of the

TABLE 1: Experimental cutting conditions.

No.	Speed r/min	Depth of cut mm	Feed mm/r	No.	Speed r/min	Depth of cut mm	Feed mm/r
1	1500	1	0.1	15	1000	0.2	0.05
2	1500	0.5	0.1	16	800	1	0.05
3	1500	0.2	0.1	17	800	0.5	0.05
4	1000	1	0.1	18	800	0.2	0.05
5	1000	0.5	0.1	19	1500	1	0.02
6	1000	0.2	0.1	20	1500	0.5	0.02
7	800	1	0.1	21	1500	0.2	0.02
8	800	0.5	0.1	22	1000	1	0.02
9	800	0.2	0.1	23	1000	0.5	0.02
10	1500	1	0.05	24	1000	0.2	0.02
11	1500	0.5	0.05	25	800	1	0.02
12	1500	0.2	0.05	26	800	0.5	0.02
13	1000	1	0.05	27	800	0.2	0.02
14	1000	0.5	0.05				

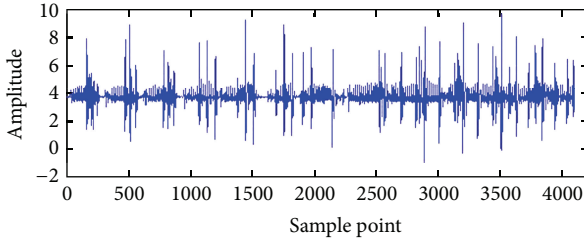


FIGURE 6: Waveform of wear tool in first condition.

modulus maxima in the scale space  $n = -1, 0, 1, 2, \dots, N$ . These multiscale modulus maxima are used to locate discontinuities [16], and if  $\psi f(2^n, x)$  has no modulus maxima at fine scales, then  $f(x)$  is locally regular. Singular point can be recognized by modulus maxima.

## 5. Lipschitz Exponent Based on Modulus Maxima of Harmonic Wavelet

It has been shown that the Lipschitz exponent of a local singularity can be characterized by being placed on their local modulus maxima at each scale [14, 16]. References [15, 24] extend to using the modulus maxima of a complex wavelet. Here, we research that the modulus maxima of harmonic wavelet can be used to detect singularities, by means of a Lipschitz exponent of a function, and quantitative analysis on signal's singularities is measured. By examining the asymptotic decay of wavelet modulus maxima from coarser scale to finer scale, the strength of the singularity can be characterized by Lipschitz exponent.

Let  $s = 2^n$ ,  $n = -1, 0, \dots, N$ , in terms of [15, 25], function  $f(x)$ ,  $x \in (a, b)$ , and let  $n$ th ( $n > 0$ ) derivative of  $\text{Re}(\psi f(s, x))$  and  $\text{Im}(\psi f(s, x))$  be finite deviations for each scale  $s$ . If a scale  $s_0 > 0$  and constants  $C$  and  $A$  exist such that for  $x \in (a, b)$  and

$s > s_0$ , all the modulus maxima of  $\psi f(s, x)$  belong to a cone defined by

$$|x - x_0| \leq Cs \quad (9)$$

such that at each modulus maxima  $(s, x)$  in the cone

$$|\psi f(s, x)| \leq As^\alpha \quad (10)$$

then  $f(x)$  is uniformly Lipschitz  $\alpha$  at  $x$  when  $x \neq x_0$ , and  $f(x)$  is Lipschitz  $\alpha$  at  $x_0$  when  $\alpha < n$ , and  $\alpha$  is a noninteger. Equation (10) takes the logarithm on both sides:

$$\log_2 |\psi f(s, x)| \leq \log_2 A + \alpha \log_2 s. \quad (11)$$

In [15, 24],  $A$  and  $\alpha$  are computed by

$$\min_{A, \alpha} \sum_s [\log_2 |Wf(s, x)| - \log_2 A - \alpha \log_2 s]^2. \quad (12)$$

The problem of estimating  $\alpha$  transforms into optimization based on a nonlinear least squared, and when (12) is minimized at all scale,  $A$  and  $\alpha$  are obtained.

According to [24] description of the results, we use  $s = 2^n$  instead of  $s$ , we get the following:

$$\begin{aligned} \alpha(x) &= \left( \sum_{n=-1}^N (\log_2 |Wf(2^n, x)| * \log_2 2^n) \right. \\ &\quad \left. - \frac{(\sum_{n=-1}^N \log_2 |Wf(2^n, x)|)(\sum_{n=-1}^N \log_2 2^n)}{N} \right) \\ &\quad \times \left( \sum_{n=-1}^N (\log_2 2^n)^2 - \frac{\sum_{n=-1}^N (\log_2 2^n)}{N} \right)^{-1}. \end{aligned} \quad (13)$$

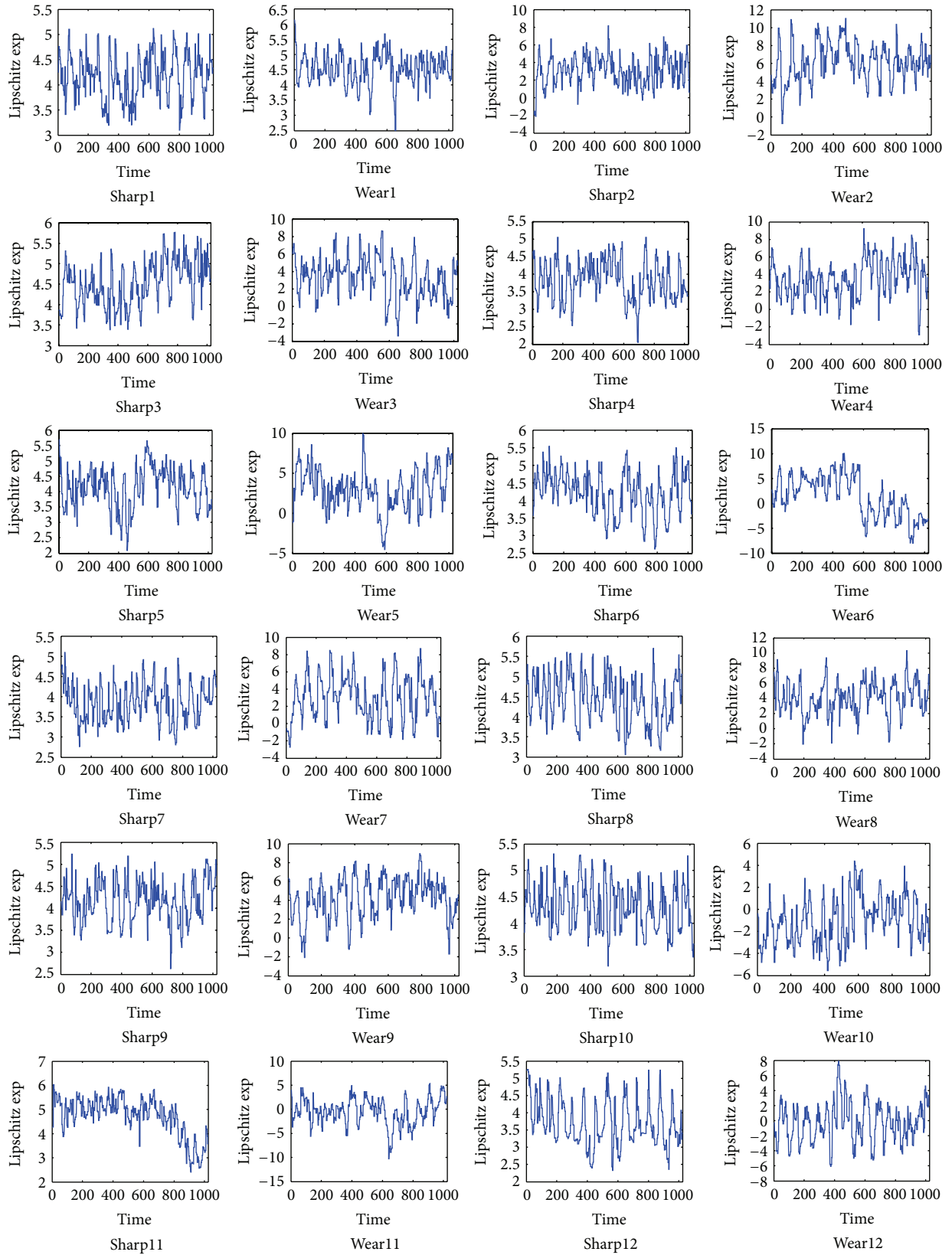


FIGURE 7: Continued.

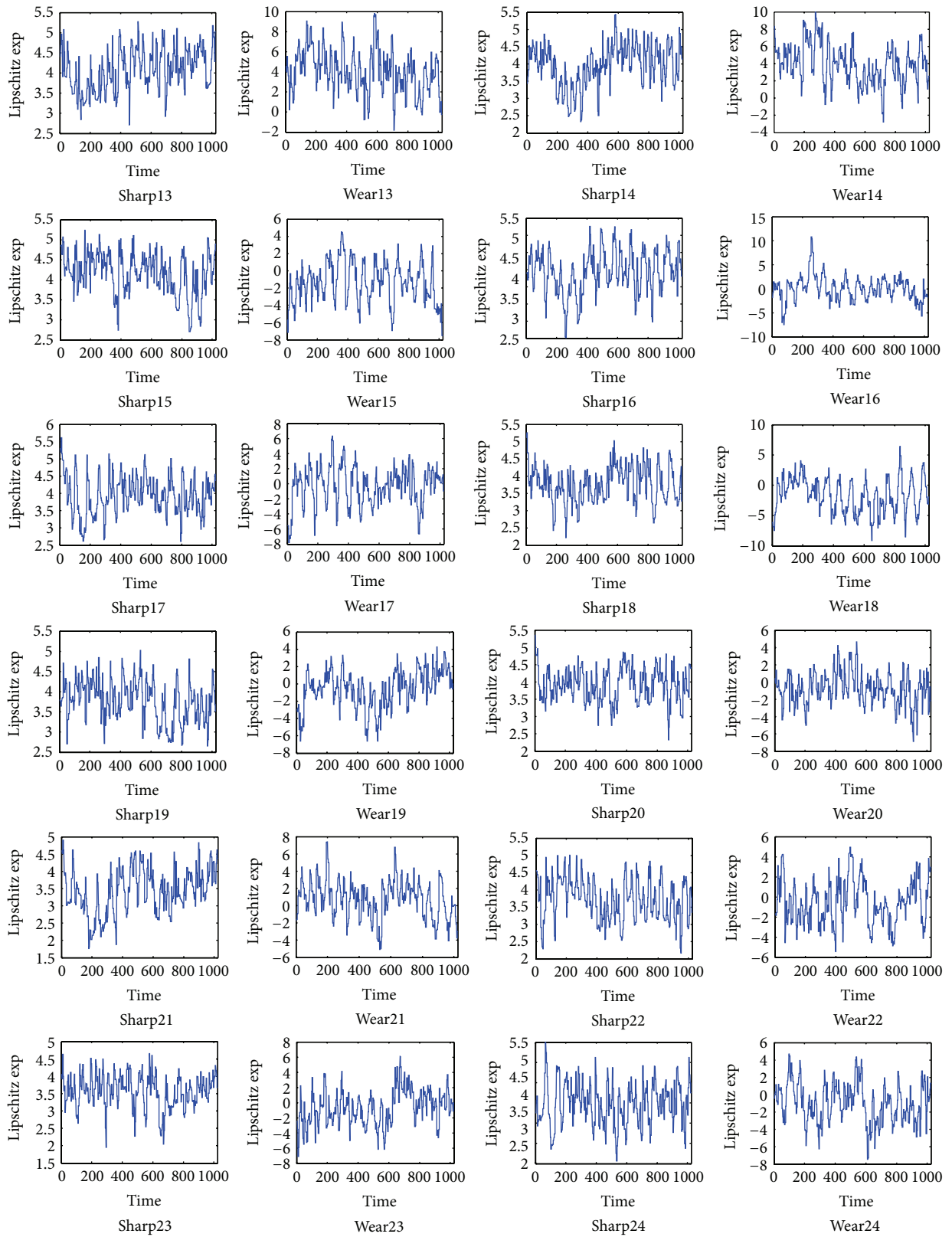


FIGURE 7: Continued.

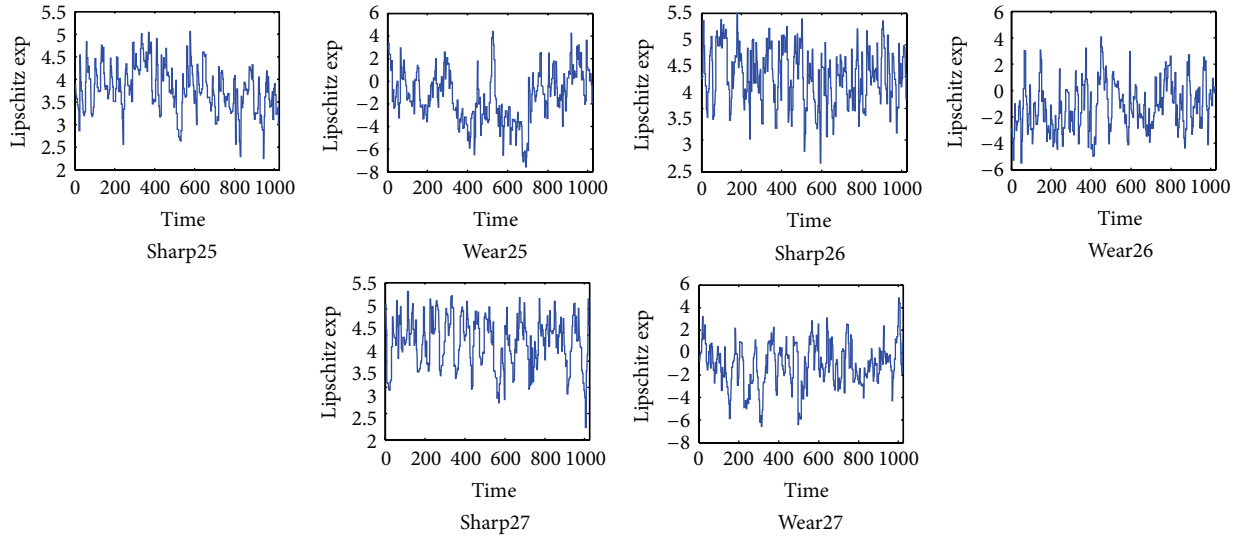


FIGURE 7: Lipschitz exponent function of 54 group data.

$\alpha(x)$  is called Lipschitz exponent function that describes the change of Lipschitz exponent value  $\alpha$  along the temporal axis  $x$ . The variable  $x$  is sampling point by acoustic emission (AE) during cutting process. Figure 5 is a simulation example of extracting Lipschitz exponent function  $\alpha(x)$  on a sine function with singular points. Here, we set  $N = 10$  in (13).

Figure 3 demonstrates the potential ability of singularity detection (or fault detection) with Lipschitz exponent function  $\alpha(x)$ .

## 6. Application Platform

In turning experiments, the feasibility for tool condition monitoring is demonstrated by 27 kinds of cutting conditions (see Table 1); 54 group data are sampled by AE; they are shaper1~shaper27 and wear1~wear27, respectively. Machining tests were carried out on HL-32 NC turning center [26]. The work material was chosen for ease of machining, allowing for generation of surfaces of varying quality without the use of cutting fluids. The experiment equipment is shown in Figure 4. Currently, AE-based sensing technology is the area of most intense research activity for developing intelligent tool condition systems. The reason is that the sensitivity of AE to tool wear and fracture is coupled with a high response rate of the signal. Sharp1 signal and wear1 signal show Figures 5 and 6, respectively in time domain.

According to (13), we set harmonic wavelet decomposed level  $N = 10$ , and Lipschitz exponent function  $\alpha(x)$  of 54 group data is shown in Figure 7.

In Figure 7, all sharp tools are of positive Lipschitz exponent function  $\alpha(t) > 0$ , and all wear tools are of a negative Lipschitz exponent function  $\alpha(t) < 0$ . Wear tool and sharp tool can be distinguished by Lipschitz exponent function  $\alpha(t)$ . A threshold value  $\alpha(t) = 0$  is obtained as a criterion of the tool condition monitoring during cutting process.

## 7. Conclusion

The proposed research provides a new theoretical basis and a new engineering application on the online tool monitoring which can distinguish between worn tool and sharp tool during cutting process. The results of experiment demonstrate that this method is more precise and robust.

The method which was described in this paper can be used as a valuable method for tool condition monitoring. In comparison to conventional data processing, the advantages of Lipschitz exponent and harmonic wavelet were shown. The zero threshold is determined conveniently which can distinguish between worn tool and sharp tool. For the future development of the presented techniques in laboratory, several approaches will be tested, including new broadband sensors application.

## Acknowledgment

This project is supported by Shanghai Municipal Education Commission of China (Grant no. 13XKCZ07/YLJX12-7).

## References

- [1] V. B. Magdum and V. R. Naik, "Tool wear monitoring when turning EN 8 Steel with HSS-M2 tool," *International Journal of Innovative Research in Science, Engineering and Technology*, vol. 2, no. 5, pp. 1706–1711, 2013.
- [2] Y. Huang and S. Y. Liang, "Modeling of cutting forces under hard turning conditions considering tool wear effect," *Journal of Manufacturing Science and Engineering, Transactions of the ASME*, vol. 127, no. 2, pp. 262–270, 2005.
- [3] C.-W. Hung and M.-C. Lu, "Model development for tool wear effect on AE signal generation in micromilling," *The International Journal of Advanced Manufacturing Technology*, vol. 66, no. 9–12, pp. 845–1858, 2013.

- [4] M. A. Xavier and M. Adithan, "Determining the influence of cutting fluids on tool wear and surface roughness during turning of AISI 304 austenitic stainless steel," *Journal of Materials Processing Technology*, vol. 209, no. 2, pp. 900–909, 2009.
- [5] R. Quiza, L. Figueira, and J. P. Davim, "Comparing statistical models and artificial neural networks on predicting the tool wear in hard machining D2 AISI steel," *International Journal of Advanced Manufacturing Technology*, vol. 37, no. 7-8, pp. 641–648, 2008.
- [6] S. Cho, S. Binsaeid, and S. Asfour, "Design of multisensor fusion-based tool condition monitoring system in end milling," *International Journal of Advanced Manufacturing Technology*, vol. 46, no. 5–8, pp. 681–694, 2010.
- [7] D. Iliescu, D. Gehin, M. E. Gutierrez, and F. Girot, "Modeling and tool wear in drilling of CFRP," *International Journal of Machine Tools and Manufacture*, vol. 50, no. 2, pp. 204–213, 2010.
- [8] F. Girardin, D. Rémond, and J.-F. Rigal, "Tool wear detection in milling—An original approach with a non-dedicated sensor," *Mechanical Systems and Signal Processing*, vol. 24, no. 6, pp. 1907–1920, 2010.
- [9] A. E. Zonst, *Understanding FFT Applications: A Tutorial for Laymen, Students, Technicians & Working Engineers*, Citrus Press, Titusville, Fla, USA, 2nd edition, 2003.
- [10] J. F. James, *A Student's Guide to Fourier Transforms: With Applications in Physics and Engineering*, Cambridge University Press, London, UK, 3rd edition, 2011.
- [11] A. H. Kaiser, *Digital Signal Processing Using the Fast Fourier Transform (FFT)*, GRIN Verlag, Munich, Germany, 2013.
- [12] J. Heinonen, "Lectures on Lipschitz Analysis, Lectures at the 14th Jyväskylä Summer School in August 2004," Supported by NSF grant DMS 0353549 and DMS 0244421.
- [13] Y. Grabovsky, V. A. Kucher, and L. Truskinovsky, "Weak variations of Lipschitz graphs and stability of phase boundaries," *Continuum Mechanics and Thermodynamics*, vol. 23, no. 2, pp. 87–123, 2011.
- [14] S. Mallat and W. L. Hwang, "Singularity detection and processing with wavelets," *IEEE Transactions on Information Theory*, vol. 38, no. 2, pp. 617–643, 1992.
- [15] C.-L. Tu, W.-L. Hwang, and J. Ho, "Analysis of singularities from modulus maxima of complex wavelets," *IEEE Transactions on Information Theory*, vol. 51, no. 3, pp. 1049–1062, 2005.
- [16] S. Mallat, *A Wavelet Tour of Signal Processing*, Academic Press, San Diego, Calif, USA, 3rd edition, 2008.
- [17] C. Cattani, "Harmonic wavelet approximation of random, fractal and high frequency signals," *Telecommunication Systems*, vol. 43, no. 3-4, pp. 207–217, 2010.
- [18] D. E. Newland, *An Introduction to Random Vibrations, Spectral and Wavelet Analysis*, Dover, London, UK, 3rd edition, 2005.
- [19] D. E. Newland, "Harmonic wavelet analysis," *Proceedings of the Royal Society of London. Series A*, vol. 443, pp. 203–222, 1993.
- [20] D. E. Newland, "Wavelet analysis of vibration, part 2: wavelet maps," *Journal of Vibration and Acoustics*, vol. 116, no. 4, pp. 417–425, 1994.
- [21] Y. Huang, Q. Li, and M. Li, "Minimum-energy multiwavelet frames with arbitrary integer dilation factor," *Mathematical Problems in Engineering*, vol. 2012, Article ID 640789, 37 pages, 2012.
- [22] K. A. Innanen, "Local signal regularity and lipschitz exponents as a means to estimate  $Q_s$ ," *Journal of Seismic Exploration*, vol. 12, no. 1, pp. 53–74, 2003.
- [23] J. Lindenstrauss, D. Preiss, and J. Tiser, *Fréchet Differentiability of Lipschitz Functions and Porous Sets in Banach Spaces (AM-179)*, Princeton University Press, Princeton, NJ, USA.
- [24] Q. Miao, H.-Z. Huang, and X. Fan, "Singularity detection in machinery health monitoring using Lipschitz exponent function," *Journal of Mechanical Science and Technology*, vol. 21, no. 5, pp. 737–744, 2007.
- [25] P. Venkatakrishnan, S. Sangeetha, and M. Sundar, "Measurement of Lipschitz exponent (LE) using wavelet transform modulus maxima (WTMM)," *International Journal of Scientific & Engineering Research*, vol. 3, no. 6, 2012.
- [26] W. Song and J. Zhang, "Tool state detection by harmonic wavelet and sample entropy," *Chinese Journal of Mechanical Engineering*, vol. 24, no. 6, pp. 1068–1073, 2011.



## Research Article

# A Hybrid Fuzzy Time Series Approach Based on Fuzzy Clustering and Artificial Neural Network with Single Multiplicative Neuron Model

**Ozge Cagcag Yolcu**

*Department of Statistics, Faculty of Arts and Sciences, Ondokuz Mayıs University, 55139 Samsun, Turkey*

Correspondence should be addressed to Ozge Cagcag Yolcu; [ozgecagcag@yahoo.com](mailto:ozgecagcag@yahoo.com)

Received 19 July 2013; Revised 11 September 2013; Accepted 25 September 2013

Academic Editor: Ming Li

Copyright © 2013 Ozge Cagcag Yolcu. This is an open access article distributed under the Creative Commons Attribution License, which permits unrestricted use, distribution, and reproduction in any medium, provided the original work is properly cited.

Particularly in recent years, artificial intelligence optimization techniques have been used to make fuzzy time series approaches more systematic and improve forecasting performance. Besides, some fuzzy clustering methods and artificial neural networks with different structures are used in the fuzzification of observations and determination of fuzzy relationships, respectively. In approaches considering the membership values, the membership values are determined subjectively or fuzzy outputs of the system are obtained by considering that there is a relation between membership values in identification of relation. This necessitates defuzzification step and increases the model error. In this study, membership values were obtained more systematically by using Gustafson-Kessel fuzzy clustering technique. The use of artificial neural network with single multiplicative neuron model in identification of fuzzy relation eliminated the architecture selection problem as well as the necessity for defuzzification step by constituting target values from real observations of time series. The training of artificial neural network with single multiplicative neuron model which is used for identification of fuzzy relation step is carried out with particle swarm optimization. The proposed method is implemented using various time series and the results are compared with those of previous studies to demonstrate the performance of the proposed method.

## 1. Introduction

Nowadays, it is of vital importance to make predictions about the future in terms of planning and strategy formulation. This can be realized by accurate and realistic analysis of information and data that have emerged from past to present. Different approaches, namely, stochastic and nonstochastic approaches, have been proposed in the literature for the analysis of time series. Nowadays, the use of nonstochastic models such as fuzzy time series approach for the analysis of time series has become widespread. In some cases, expressing the observations of time series by linguistic values or fuzzy sets is more realistic. These types of time series are called fuzzy time series and their analysis should be made via fuzzy time series analysis methods rather than traditional ones. In recent years, to analyse the nonlinear time series such as time series of 1/f noise time series, Li et al. [1], Li et al. [2], and Li and Zhao [3] presented different approaches which are expressed

as stochastic models. In addition, Li et al. [4] stated that a sufficient condition for 1/f noise type time series to be predictable is that variance of its predication errors exists and described that there are some challenges in prediction of 1/f noise type time series. The main advantage of fuzzy time series approaches is that they do not need assumptions that stochastic models do. Particularly, since fuzzy time series methods do not need linear model assumption and probability distribution assumption, they can be effectively used to analyse the nonlinear time series which is frequently encountered in the real-world problems.

The concept of fuzzy time series was first introduced by Song and Chissom [5] based on fuzzy set theory proposed by Zadeh [6]. Fuzzy time series can be evaluated under two main headings as time-variant and time-invariant. Song and Chissom [5] have reported that internal relations belonging to fuzzy time series are supposed to change over time in time-variant fuzzy time series but not in time-invariant ones.

Song and Chissom [7] proposed an algorithm for the solution of time-invariant fuzzy time series which are the subject of almost all the studies in the literature. As the subject of this study is time-invariant fuzzy time series, in the remainder of the paper the term of “fuzzy time series” will be used instead of “time-invariant fuzzy time series.” As in fuzzy inference systems, fuzzy time series forecasting models consist of three steps as fuzzification, identification of fuzzy relation, and defuzzification which have an influence on forecasting performance of the method. Many researchers have carried out studies using different approaches on these three steps.

Universe of discourse has been used in fuzzification step until recently. Song and Chissom [5, 7, 8] and Chen [9, 10] determined fixedly interval lengths arbitrarily whereas Huarng [11] used average and distribution-based and Egrioglu et al. [12] used optimization-based methods. In addition, for the analysis of time series containing trend, a ratio-based length of intervals is proposed by Huarng and Yu [13]. Furthermore, Yolcu et al. [14] proposed a new approach and used a single-variable constrained optimization to determine the ratio for the length of intervals which change in time in partition of universe of discourse. More recently, Kuo et al. [15, 16], Davari et al. [17], Park et al. [18], Hsu et al. [19], and Egrioglu et al. [20] used particle swarm optimization whereas Chen and Chung [21] and Lee et al. [22, 23] proposed methods using genetic algorithms for determination of the changing length of intervals.

Although subjective judgments are avoided in these studies using optimization techniques, membership values are still determined subjectively and all membership values are not considered. The problem that membership values are determined subjectively may eliminate by using some fuzzy clustering techniques. In this regard, Cheng et al. [24], Li et al. [25], Aladag et al. [26], Alpaslan et al. [27], Egrioglu et al. [12, 28], and Alpaslan and Cagcag [29] eliminated by using fuzzy C-means (FCM) and Gustafson-Kessel fuzzy clustering techniques, respectively.

Identification of fuzzy relation is the step in which the appropriate model is determined. Therefore, this step plays the most important role in forecasting performance. In this stage, Song and Chissom [5, 7, 8] used fuzzy relation matrix and represented the fuzzy logic relations with only one matrix. Sullivan and Woodall [30] used transition matrices based on Markov chain instead of using fuzzy logic relation matrix. Chen [9] proposed a simpler approach using fuzzy logic group relationships tables by claiming that matrix calculations are based on complex processes. The approach proposed by Chen [9] is the most commonly used approach in the literature. Huarng and Yu [31] proposed a first-order fuzzy time series approach which uses feedforward neural networks (FFANN) in this step. Aladag et al. [32] developed the approach proposed by Huarng and Yu [31] and proposed a high-order fuzzy time series forecasting model which uses FFANN in the determination of fuzzy relations. In all of these approaches, when determining the fuzzy relations representing the internal relation of fuzzy time series, only the fuzzy set having the highest membership value was considered and membership values were ignored. Although Yu and Huarng [33] proposed an approach which considers the membership

values, their approach has determined membership values subjectively. Alpaslan et al. [27] and Yolcu et al. [34] used FCM technique instead of determining the membership values subjectively. The use of ANN in identification of fuzzy relations has many advantages and disadvantages as well. Determination of unit number in hidden layer (architecture structure) and excessive number of parameters to be used during the analysis are the most prominent ones. Although Aladag [35] eliminated this problem by using artificial neural network with single multiplicative neuron model (SMNM-ANN) in the determination of fuzzy relations, membership values were not considered. Nevertheless, as the system output of these approaches consists of fuzzy set number or membership values, fuzzification step is necessary. This may be a factor that increases the model error. An approach not requiring defuzzification step would eliminate forecasting error that may occur in this step and improve the performance of the method.

Almost all approaches proposed in the literature focus on autoregressive (AR) model; in other words, in these approaches it is supposed that time series is affected by only its own lagged variables. Otherwise, there are various approaches which included autoregressive moving average (ARMA) model such as the method proposed by Egrioglu et al. [20] and seasonal autoregressive moving average (SARIMA) model such as methods proposed by Egrioglu et al. [36], Uslu et al. [37], Aladag et al. [38], and Alpaslan et al. [27].

The proposed method uses Gustafson-Kessel fuzzy clustering technique in fuzzification step and membership values are obtained more systematically. The use of SMNM-ANN in identification of fuzzy relations eliminates architecture selection problem and the need for defuzzification step by constituting the target values from observations of the real-time series. The training of SMNM-ANN which was used in the determination of fuzzy relations is carried out with particle swarm optimization. The proposed method comprises first-order fuzzy time series model and it can be referred to as an AR model. Main differences of proposed method from previous studies are that it does not need the defuzzification stage and also identification of architecture of ANN.

The rest of this paper is designed as follows. In Section 2, the basic concepts of fuzzy time series are briefly reviewed. In Section 3, PSO, Gustafson-Kessel fuzzy clustering technique, and SMNM-ANN are briefly presented under the related methods main heading. In Section 4, we introduce new hybrid fuzzy time series method. In Section 5, we apply the proposed method to different time series and make a comparison of the forecasted results of the proposed method with that of the existing methods. In the last section, the conclusions are discussed.

## 2. Fuzzy Time Series

The fuzzy time series was firstly introduced by Song and Chissom [5]. The fuzzy time series and time-variant and time-invariant fuzzy time series definitions are given below by Song and Chissom [5].



**Definition 1.** Let  $Y(t) (t = \dots, 0, 1, 2, \dots)$ , a subset of real numbers, be the universe of discourse on which fuzzy sets  $f_j(t)$  are defined. If  $F(t)$  is a collection of  $f_1(t), f_2(t), \dots$ , then  $F(t)$  is called a fuzzy time series defined on  $Y(t)$ .

**Definition 2.** Suppose that  $F(t)$  is caused by  $F(t-1)$  only; that is,  $F(t-1) \rightarrow F(t)$ . Then, this relation can be expressed as  $F(t) = F(t-1) \circ R(t, t-1)$ , where  $R(t, t-1)$  is the fuzzy relationship between  $F(t-1)$  and  $F(t)$ , and  $F(t) = F(t-1) \circ R(t, t-1)$  is called the first-order model of  $F(t)$ . “ $\circ$ ” represents max-min composition of fuzzy sets.

**Definition 3.** Suppose that  $R(t, t-1)$  is a first-order model of  $F(t)$ . If for any  $t$ ,  $R(t, t-1)$  is independent of  $t$ , that is, for any  $t$ ,  $R(t, t-1) = R(t-1, t-2)$ , then  $F(t)$  is called a time-invariant fuzzy time series; otherwise, it is called a time-variant fuzzy time series.

Song and Chissom [7] firstly introduced an algorithm based on the first-order model for forecasting time-invariant  $F(t)$ . In Song and Chissom's work [7], the fuzzy relationship matrix  $R(t, t-1) = R$  is obtained by many matrix operations. The fuzzy forecasts are obtained based on max-min composition as follows:

$$F(t) = F(t-1) \circ R. \quad (1)$$

The dimension of  $R$  matrix is dependent number of fuzzy sets which are partition number of universe and discourse. If we want to use more fuzzy sets, we need different matrix operations to obtain  $R$  matrix.

### 3. Related Methods

**3.1. Particle Swarm Optimization (PSO).** Particle swarm optimization, which is a population-based heuristic algorithm, was firstly proposed by Eberhart and Kennedy [39]. Distinguishing feature of this heuristic algorithm is that it simultaneously examines different points in different regions of the solution space to find the global optimum solution. Local optimum traps can be avoided because of this feature.

In the literature, it was shown that using some time-varying parameters can increase the convergence speed of the algorithm. Ma et al. [40] employed time-varying acceleration coefficient in standard particle swarm optimization method. In another study, Shi and Eberhart [41] used time-varying inertia weight. In the modified particle swarm optimization, this time-varying constituents are used together. This is the only difference between standard and modified particle swarm optimization methods.

**Algorithm 4.** The modified particle swarm optimization.

**Step 1.** Positions of each  $k$ th, ( $k = 1, 2, \dots, pn$ ) particles' positions are randomly determined and kept in a vector  $X_k$  given as follows:

$$X_k = \{x_1^k, x_2^k, \dots, x_d^k\}, \quad k = 1, 2, \dots, pn, \quad (2)$$

where  $x_i^k$  ( $i = 1, 2, \dots, d$ ) represents  $i$ th position of  $k$ th particle.  $pn$  and  $d$  represent the numbers of particles in swarm and positions, respectively.

**Step 2.** Velocities are randomly determined and stored in a vector  $V_k$  as follow:

$$V_k = \{v_1^k, v_2^k, \dots, v_d^k\}, \quad k = 1, 2, \dots, pn. \quad (3)$$

**Step 3.** According to the evaluation function,  $pbest$  and  $gbest$  particles given in (4), respectively, are determined:

$$\begin{aligned} pbest_i &= (p_{i1}, p_{i2}, \dots, p_{id}) \quad i = 1, 2, \dots, d, \\ pbest_g &= gbest = (p_{g1}, p_{g2}, \dots, p_{gd}), \end{aligned} \quad (4)$$

where  $pbest$  is a vector which stores the positions corresponding to the  $k$ th particle's best individual performance and  $gbest$  represents the best particle, which has the best evaluation function value, found so far.

**Step 4.** Let  $c_1$  and  $c_2$  represent cognitive and social coefficients, respectively, and  $w$  is the inertia parameter. Let  $(c_{1i}, c_{1f})$ ,  $(c_{2i}, c_{2f})$ , and  $(w_1, w_2)$  be the intervals which include possible values for  $c_1$ ,  $c_2$ , and  $w$ , respectively. At each iteration, these parameters are calculated by using the following formulas:

$$\begin{aligned} c_1 &= (c_{1f} - c_{1i}) \frac{t}{\max t} + c_{1i}, \\ c_2 &= (c_{2f} - c_{2i}) \frac{t}{\max t} + c_{2i}, \\ w &= (w_2 - w_1) \frac{\max t - t}{\max t} + w_1, \end{aligned} \quad (5)$$

where  $\max t$  and  $t$  represent maximum iteration number and current iteration number, respectively.

**Step 5.** Values of velocities and positions are updated by using the following formulas.

$$\begin{aligned} v_{ij}^{k+1} &= [w \times v_{ij}^k + c_1 \times \text{rand}_1 \times (pbest_{ij} - x_{ij}) \\ &\quad + c_2 \times \text{rand}_2 \times (gbest_j - x_{ij})], \end{aligned} \quad (6)$$

$$x_{ij}^{k+1} = x_{ij} + v_{ij}^{k+1}, \quad (7)$$

where  $\text{rand}_1$  and  $\text{rand}_2$  are random values from the interval  $[0 \ 1]$ .

**Step 6.** Steps 3 to 5 are repeated until a predetermined maximum iteration number ( $\max t$ ) is reached.

**3.2. The Gustafson-Kessel Fuzzy Clustering Technique.** The algorithm of Gustafson-Kessel fuzzy clustering is firstly proposed by Gustafson and Kessel [42]. Let  $\Sigma_i$  be the covariance matrix of the cluster,  $c_i$  the center of the  $i$ th cluster,  $u_{ij}$  the membership degree, and  $\beta$  fuzziness index. For the  $i$ th cluster, its associated Mahalanobis distance is defined as

$$d^2(x_j, c_i, \Sigma_i) = (x_j - c_i)^T \sum_{i=1}^{-1} (x_j - c_i). \quad (8)$$

The covariance matrices are computed as follows:

$$\begin{aligned} \Sigma_i &= \frac{\Sigma_i^*}{\sqrt[p]{\det(\Sigma_i^*)}}, \\ \Sigma_i^* &= \frac{\sum_{j=1}^n u_{ij} (x_j - c_i)(x_j - c_i)^T}{\sum_{j=1}^n u_{ij}}. \end{aligned} \quad (9)$$

The objective function is defined as

$$J(X, C, \Sigma, U) = \sum_{i=1}^c \sum_{j=1}^n u_{ij}^\beta d^2(x_j, c_i, \Sigma_i). \quad (10)$$

The objective function  $J(X, C, \Sigma, U)$  is, then, minimized under the following constraints:

$$\begin{aligned} 0 &\leq u_{ij} \leq 1, \quad \forall i, j, \\ 0 &< \sum_{j=1}^n u_{ij} \leq n, \quad \forall i, \\ \sum_{i=1}^c u_{ij} &= 1. \end{aligned} \quad (11)$$

In this minimization problem, the center  $c_i$  and the membership degrees  $u_{ij}$  are updated according to the expressions given below:

$$\begin{aligned} c_i &= \frac{\sum_{j=1}^n u_{ij}^\beta x_j}{\sum_{j=1}^n u_{ij}^\beta}, \\ u_{ij} &= \frac{1}{\sum_{k=1}^c (d(x_j, c_i) / d(x_j, c_k))^{2/(\beta-1)}}. \end{aligned} \quad (12)$$

**3.3. Single Multiplicative Neuron Model.** In neurons of feed-forward neural networks, the input signal is calculated based on addition function. Yadav et al. [43] proposed a single multiplicative neuron model. In the model, the input signal of the neuron is estimated by the multiplication function. Yadav et al. [43] showed that single multiplicative neuron model gives better forecasting performance for time series forecasting. Zhao and Yang [44] recommended the use of PSO instead of backpropagation learning algorithm proposed by Yadav et al. [43] in the training of single multiplicative neuron model. The structure of single multiplicative neuron model for 5 inputs is given in Figure 1.

This model has a single neuron, and unlike feed forward neural network, multiplication is performed to the signal coming into the neuron. Function  $\Omega(x, \theta)$  is the product of the weighted inputs. The multiplicative neural model with five inputs given in Figure 1 ( $x_i, i = 1, 2, \dots, 5$ ) has 10 weights. Of these, five are the weights corresponding to the inputs ( $w_i, i = 1, 2, \dots, 5$ ) and five to the sides of the weights ( $b_i, i = 1, 2, \dots, 5$ ). Suppose that activation function is taken as logistic given below:

$$f(x) = \frac{1}{1 + e^{-x}}. \quad (13)$$

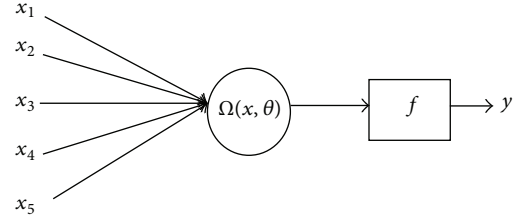


FIGURE 1: The structure of single multiplicative neuron model.

In this case, the net value of the neuron is obtained as follows:

$$\text{net} = \Omega(x, \theta) = \prod_{i=1}^5 (w_i x_i + b_i). \quad (14)$$

Thus, as the net value passes through activation function, output of the weight is obtained as  $y = f(\text{net})$ . The fitness function to be calculated during the training of multiplicative neuron model with PSO can be used as a criterion as the sum of squares which was calculated from the difference between output values for all learning samples and target values:

$$\text{SSE} = \sum_{i=1}^n (d_i - y_i)^2, \quad (15)$$

where  $d_i$  and  $y_i$  represent the target value and the output of the network corresponding to  $i$ th learning sample.

## 4. Proposed Method

In fuzzy time series approaches, each stage plays a decisive role in the forecasting performance of the method. Many studies on these steps have been conducted in the literature. As well as more systematical approaches in fuzzification step, flexible and superior calculation abilities of ANN in identification of fuzzy relation have been widely used recently. These studies have many advantages and disadvantages as well such as determination of unit number in hidden layer (architecture structure), identification of membership values subjectively, and excessive number of parameters to be used during the analysis. In this study, it was aimed to propose a model which is free from all these problems. In the proposed method, membership values were obtained more systematically by using Gustafson-Kessel fuzzy clustering technique in fuzzification step. The use of SMNM-ANN in identification of fuzzy relation eliminated architecture selection problem and the necessity for defuzzification step by constituting target values from real observations of time series; thus, the forecasting performance of the method was improved. The training of artificial neural network with single multiplicative neuron model which was used in identification of fuzzy relations is carried out with particle swarm optimization. The main advantages of the proposed method can be summarized as follows.

- (i) With the use of fuzzy clustering method in fuzzification step, subjective judgments are not needed anymore.

TABLE 1: An example of fuzzification.

		Center of Set 1 ( $v_1$ )	Center of Set 2 ( $v_2$ )	Center of Set 3 ( $v_3$ )
		25.4718	51.3607	79.4108
$t$	$X(t)$	Memberships of Observations to Fuzzy Sets		
		Set 1 ( $L_1$ )	Set 2 ( $L_2$ )	Set 3 ( $L_3$ )
1	20	0.9625	0.0293	0.0082
2	30	0.9494	0.0427	0.0080
3	40	0.3608	0.5901	0.0490
4	30	0.9494	0.0427	0.0080
5	20	0.9625	0.0293	0.0082
6	50	0.0031	0.9948	0.0021
7	60	0.0497	0.7932	0.1571
8	80	0.0001	0.0004	0.9995

- (ii) With the use of ANN in identification of fuzzy relation, complex matrix operations and complex fuzzy relation tables are not needed. In addition, one may benefit from the flexible modeling advantage of ANN.
- (iii) The use of SMNM-ANN eliminates the problem of determining the number of units in hidden layer.
- (iv) Again, having inputs of SMNM-ANN which is used for identification of fuzzy relation from membership values leads to increases in the amount of information used in the solution process and thus providing a more appropriate approach for fuzzy set theory.
- (v) Defuzzification step is no longer needed by constituting SMNM-ANN target values with real values of time series and thus forecasting error that may occur in this step is prevented and forecasting performance of the method is improved.

The algorithm of the proposed method is given below in steps.

*Step 1.* For  $2 \leq c \leq n$ , where  $c$  is the number of fuzzy sets, Gustafson-Kessel algorithm is applied to the crisp time series. The centers of fuzzy sets and membership degrees, which are calculated for every observation according to this center, are obtained. Finally, ordered fuzzy sets,  $L_r$ ,  $r = 1, 2, \dots, c$ , are obtained according to the ascending order centers, which are denoted by  $v_r$ ,  $r = 1, 2, \dots, c$ .

For better understanding, we consider a time series data with 8 observations such as 20, 30, 40, 30, 20, 50, 60, and 80. Let  $c$ , the number of fuzzy sets, be 3. When we applied the method of Gustafson-Kessel to this data, the centroid of the fuzzy sets and the membership degrees of each observation, which denote the belonging degree of that observation to the related fuzzy set, are given in Table 1. According to Table 1, the membership degree of belonging to the second fuzzy set ( $L_2$ ) of the first observation ( $t = 1$ ) is  $\mu_{L_2}(X(1)) = 0.0293$ .

*Step 2.* Define the fuzzy relationship with SMNM-ANN.

The number of inputs of SMNM-ANN, used for determining fuzzy relationships, is equal to the number of fuzzy

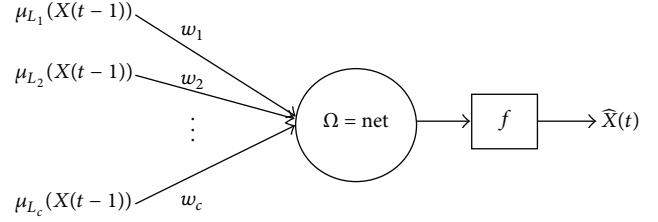


FIGURE 2: The structure of SMNM-ANN.

TABLE 2: An example of determine fuzzy relation.

Training Sample	$t$	Input 1 $\mu_{L_1}(X(t-1))$	Input 2 $\mu_{L_2}(X(t-1))$	Input3 $\mu_{L_3}(X(t-1))$	Target
1	2	0.9625	0.0293	0.0082	30
2	3	0.9494	0.0427	0.0080	40
3	4	0.3608	0.5901	0.0490	30
4	5	0.9494	0.0427	0.0080	20
5	6	0.9625	0.0293	0.0082	50
6	7	0.0031	0.9948	0.0021	60
7	8	0.0497	0.7932	0.1571	80

sets ( $c$ ). The architecture of the network is shown in Figure 2. In Figure 2,  $\mu_{L_i}(X(t-1))$  denotes the membership degree of belonging to  $i$ th fuzzy set of related observation of time series  $X(t-1)$ . Then, the target values of SMNM-ANN are real observation of time series at  $t$  while the inputs of the networks are every membership degree of belonging to  $c$  fuzzy sets of the observation of time series at  $t-1$ .

For example, suppose that we consider the time series given in Table 1. When we defined the architectural structure as given in Figure 2, the input and the targets of ANN would be as in Table 2.

Function  $\Omega$  is comprised of multiplication of the weighted inputs and is obtained by (16), where  $f$  is the activation function and  $\hat{X}(t)$  is the output of the model. The output of the model is calculated as in (17):

$$\Omega(\mu, w, b) = \text{net} = \prod_{i=1}^c [w_i \times \mu_{L_i}(X(t-1)) + b_i], \quad (16)$$

$$\hat{X}(t) = f(\text{net}) = \frac{1}{1 + \exp(-\text{net})}. \quad (17)$$

In the case where the number of fuzzy sets defined for the fuzzification process is  $c$ , there are  $2 \times c$  variables to be optimized by PSO. The position of these variables for a particle can be shown as in Figure 3, where  $w_i$ ,  $i = 1, 2, \dots, c$ , and  $b_i$ ,  $i = 1, 2, \dots, c$ , are weights and biases of SMNM-ANN, respectively.

The training SMNM-ANN given in Figure 2 is carried out via PSO with the following substeps.

*Step 2.1.* The parameters of PSO algorithm ( $c_{1i}, c_{1f}, c_{2i}, c_{2f}, w_1, w_2, pn, \max t, vm$ ) are determined. ( $c_{1i}, c_{1f}$ ), ( $c_{2i}, c_{2f}$ ), and ( $w_1, w_2$ ) are the possible starting and end values for cognitive component coefficient ( $c_1$ ), social component coefficient ( $c_2$ ), and inertia parameter ( $w$ ), respectively.  $\max t$  represents the maximum number of iterations,  $t$  is the number of the valid

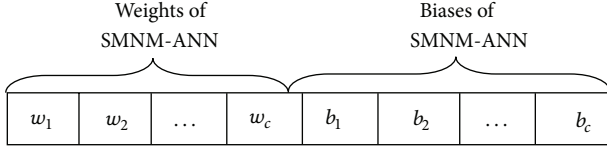


FIGURE 3: The structure of a particle.

iterations, and  $vm$  is the velocities of each particle for weights and biases of SMNM-ANN, respectively.

**Step 2.2.** Starting positions of the variables to be optimized by PSO are randomly generated. Positions of each  $k$ th ( $k = 1, 2, \dots, pn$ ) particle's positions and velocities are randomly determined and kept in vectors  $X_k$  and  $V_k$  given as follows:

$$\begin{aligned} X_k &= \{x_{k,1}, x_{k,2}, \dots, x_{k,2 \times c}\}, \\ V_k &= \{v_{k,1}, v_{k,2}, \dots, v_{k,2 \times c}\}, \end{aligned} \quad (18)$$

where  $x_{k,i}$  ( $i = 1, 2, \dots, 2 \times c$ ) represent  $i$ th position of  $k$ th particle for weights and biases of SMNM-ANN.  $pn$  and  $d = 2 \times c$  represent the number of particles in swarm and positions, respectively. The initial positions and velocities of each particle in a swarm are randomly generated from uniform distribution  $(0, 1)$  and  $(-vm, vm)$ , respectively.

**Step 2.3.** Evaluation function values for each particle are computed. Root mean square error (RMSE) given below is used as evaluation function:

$$RMSE = \sqrt{\frac{1}{T} \sum_{t=1}^T (X(t) - \widehat{X}(t))^2}, \quad (19)$$

where  $T$  represents the number of learning sample for SMNM-ANN and  $X(t)$  and  $\widehat{X}(t)$  are real observation and forecasting of time series at  $t$ , respectively.

**Step 2.4.**  $Pbest_k$ , ( $k = 1, 2, \dots, pn$ ) and  $Gbest$  are determined according to evaluation function values calculated in the previous step.  $Pbest_k$  is a vector stores the positions corresponding to the  $k$ th particle's best individual performance, and  $Gbest$  is the best particle, which has the best evaluation function value, found so far:

$$\begin{aligned} Pbest_k &= \{p_{k,1}, p_{k,2}, \dots, p_{k,d}\}, \quad (k = 1, 2, \dots, pn), \\ Gbest &= \{p_{g,1}, p_{g,2}, \dots, p_{g,d}\}, \end{aligned} \quad (20)$$

function values for each particle are computed.

**Step 2.5.** New values of positions and velocities are calculated. New values of positions and velocities for each particle are computed by using the following formulas:

$$\begin{aligned} v_{i,d}^{t+1} &= [w \times v_{i,d}^t + c_1 \times rand_1 \times (p_{i,d} - x_{i,d}) \\ &\quad + c_2 \times rand_2 \times (p_{g,d} - x_{i,d})], \\ x_{i,d}^{t+1} &= x_{i,d} + v_{i,d}^{t+1}, \end{aligned} \quad (21)$$

where  $rand_1$  and  $rand_2$  are randomly generated from uniform distribution  $(0, 1)$ .

Steps 2.1–2.5 are repeating the number of maximum iteration times. Finally, the elements of  $Gbest$  are taken as the optimal solution.

## 5. Applications

The proposed method was applied to five different time series, namely, Taiwan stock index (TAIEX) in years 2000, 2001, 2002, 2003, and 2004. In the analysis of TAIEX, we used observations of the last three months as the out-of-sample observations (test data). Therefore, we carried out five different analyses to evaluate of performance of the proposed method.

In the implementation of the proposed method, a new time series which was constituted from first-order differences of time series rather than time series was used as in Yu and Huarng's study [33]. The creation of new time series can be summarized as follows.

Firstly, the differences between every two consecutive observations at  $t$  and  $t - 1$  are obtained:

$$d(t - 1, t) = \text{observation}(t) - \text{observation}(t - 1). \quad (22)$$

The differences may turn out to be negative. To ensure that all the universes of discourse are positive, we add different positive constants to the differences for different years:

$$d'(t - 1, t) = d(t - 1, t) + \text{constant}. \quad (23)$$

On behalf of a better understanding of the implementation of the proposed method, let us examine the time series of the TAIEX in 2004. The stock index for 2000/1/5 is 6125.42 and that for 2004/1/6 is 6144.01. Hence,

$$\begin{aligned} d(2004/1/5, 2004/1/6) &= \text{observation}(2004/1/6) \\ &\quad - \text{observation}(2004/1/5) \\ &= 6144.01 - 6125.42 = 18.59. \end{aligned} \quad (24)$$

For the year 2004, the minimum of all the differences is  $-455.17$ . Hence, 500 is considered to be appropriate as the constant for the year 2004:

$$\begin{aligned} d'(2004/1/5, 2004/1/6) &= d(2004/1/5, 2004/1/6) + \text{constant} \\ &= 18.59 - 500 \\ &= 518.59. \end{aligned} \quad (25)$$

Moreover, the outputs from the SMNM-ANN are the forecasted for the next difference. For example, when the forecasted difference between 10/4 and 10/5 is obtained as



$fd(2004/10/4, 2004/10/5) = 498.66$ , the forecast is calculated as follows:

$$\begin{aligned} fd'(2004/10/4, 2004/10/5) \\ &= fd(2004/10/4, 2004/10/5) - \text{constant} \\ &= 498.66 - 500 \\ &= -1.34. \end{aligned} \quad (26)$$

Hence,

$$\begin{aligned} \text{forecast}(2004/10/5) \\ &= fd'(2004/10/4, 2004/10/5) + \text{observation}(2004/10/4) \\ &= -1.34 + 6077.96 \\ &= 6076.62. \end{aligned} \quad (27)$$

700, 300, 300, 200, and 500 are considered to be appropriate as the constant for the years 2000, 2001, 2002, 2003, and 2004, respectively. Moreover, in the analysis of all TAIEX data, the number of fuzzy sets is varied between 5 and 15 and parameters of PSO are determined as  $(c_{1i}, c_{1f}) = (2, 3)$ ,  $(c_{2i}, c_{2f}) = (2, 3)$ ,  $(w_1, w_2) = (0.4, 0.9)$ , and  $vm = 10$ .

RMSE criteria were used in the evaluation of the results obtained by the analyses and the other methods in the literature.

The optimal results are obtained from nine, thirteen, six, seven, and five fuzzy sets for TAIEX data of years 2000, 2001, 2002, 2003, and 2004, respectively. Prediction error for the optimal results obtained from the proposed method as well as prediction error of other fuzzy time series methods is presented in Table 3.

Considering Table 3, it can be concluded that forecasting performances of the proposed method for all TAIEX data are better than those found in the literature with respect to RMSE criterion.

## 6. Conclusions and Discussion

It is of vital importance to make predictions about the future in terms of planning and strategy formulation. This can be realized by accurate and realistic analysis of information and data that have emerged from past to present. Expressing observations of time series with linguistic and fuzzy clusters and analyzing these types of time series via fuzzy time series methods rather than conventional ones would provide more realistic approaches and more accurate outcomes.

Many studies aiming at making fuzzy time series more systematic approaches have been introduced in the literature. Therefore, some fuzzy clustering methods and artificial neural networks with different structures are used in the fuzzification of observations and determination of fuzzy relationships, respectively. Considering membership values especially in identification of fuzzy relations seems to be a factor that improves the forecasting performance of the method. In approaches considering the membership values, the membership values are determined subjectively or fuzzy outputs of

TABLE 3: Performance evaluation of methods for RMSE criteria.

Methods	Years				
	2000	2001	2002	2003	2004
Chen (1996) [9]	176	148	101	74	84
Huarng and Yu (2006) [31]	152	130	84	56	116
Huarng et al. (2007) [45]	154.42	124.02	93.48	65.51	72.35
Yu and Huarng (2010) [33]	131	130	80	58	67
Chen and Chang (2010) [46]	129.42	113.33	66.82	53.51	60.48
Chen and Chen (2011) [47]	123.62	115.33	71.01	58.06	57.73
Chen et al. (2012) [48]	119.98	114.47	67.17	52.49	52.27
The Proposed Method	99.19	98.53	59.34	41.25	44.15

the system are obtained by considering that there is a relation between membership values in identification of relation. This necessitates defuzzification step and increases model error. The study aimed to overcome all these problems. For this purpose, membership values were obtained more systematically by using Gustafson-Kessel fuzzy clustering technique in fuzzification step. In identification of fuzzy relations, problems such as architecture selection were eliminated by using artificial neural network with single multiplicative neuron SMNM-ANN and defuzzification step is no longer needed by constituting target values with real values of time series. The training of artificial neural network with single multiplicative neuron model is carried out with particle swarm optimization. Main differences of proposed method from previous studies are that it does not need the defuzzification and also identification of architecture of artificial neural network. In conclusion, considering the advantages and the superior forecasting performance of the method proved via different solutions, it can be argued that the proposed method would be applicable and make contributions to the fuzzy time series literature. In the future studies, proposed method can be extended to the high order structure. Moreover feedback mechanism can be added to model like moving average terms in ARMA.

## References

- [1] M. Li, C. Cattani, and S.-Y. Chen, "Viewing sea level by a one-dimensional random function with long memory," *Mathematical Problems in Engineering*, vol. 2011, Article ID 654284, 13 pages, 2011.
- [2] M. Li, Y. Q. Chen, J. Y. Li, and W. Zhao, "Hölder scales of sea level," *Mathematical Problems in Engineering*, vol. 2012, Article ID 863707, 22 pages, 2012.
- [3] M. Li and W. Zhao, "On  $1/f$  noise," *Mathematical Problems in Engineering*, vol. 2012, Article ID 673648, 23 pages, 2012.
- [4] M. Li, W. Zhao, and B. Chen, "Heavy-tailed prediction error: a difficulty in predicting biomedical signals of  $1/f$  noise type," *Computational and Mathematical Methods in Medicine*, vol. 2012, Article ID 291510, 5 pages, 2012.
- [5] Q. Song and B. S. Chissom, "Forecasting enrollments with fuzzy time series—part I," *Fuzzy Sets and Systems*, vol. 54, no. 1, pp. 1–9, 1993.
- [6] L. A. Zadeh, "Fuzzy sets," *Information and Computation*, vol. 8, pp. 338–353, 1965.

- [7] Q. Song and B. S. Chissom, "Fuzzy time series and its models," *Fuzzy Sets and Systems*, vol. 54, no. 3, pp. 269–277, 1993.
- [8] Q. Song and B. S. Chissom, "Forecasting enrollments with fuzzy time series—part II," *Fuzzy Sets and Systems*, vol. 62, no. 1, pp. 1–8, 1994.
- [9] S.-M. Chen, "Forecasting enrollments based on fuzzy time series," *Fuzzy Sets and Systems*, vol. 81, no. 3, pp. 311–319, 1996.
- [10] S.-M. Chen, "Forecasting enrollments based on high-order fuzzy time series," *Cybernetics and Systems*, vol. 33, no. 1, pp. 1–16, 2002.
- [11] K. Huarng, "Effective lengths of intervals to improve forecasting in fuzzy time series," *Fuzzy Sets and Systems*, vol. 123, no. 3, pp. 387–394, 2001.
- [12] E. Egrioglu, C. H. Aladag, M. A. Basaran, U. Yolcu, and V. R. Uslu, "A new approach based on the optimization of the length of intervals in fuzzy time series," *Journal of Intelligent and Fuzzy Systems*, vol. 22, no. 1, pp. 15–19, 2011.
- [13] K. Huarng and T. H.-K. Yu, "Ratio-based lengths of intervals to improve fuzzy time series forecasting," *IEEE Transactions on Systems, Man, and Cybernetics B*, vol. 36, no. 2, pp. 328–340, 2006.
- [14] U. Yolcu, E. Egrioglu, V. R. Uslu, M. A. Basaran, and C. H. Aladag, "A new approach for determining the length of intervals for fuzzy time series," *Applied Soft Computing Journal*, vol. 9, no. 2, pp. 647–651, 2009.
- [15] I.-H. Kuo, S.-J. Horng, T.-W. Kao, T.-L. Lin, C.-L. Lee, and Y. Pan, "An improved method for forecasting enrollments based on fuzzy time series and particle swarm optimization," *Expert Systems with Applications*, vol. 36, no. 3, pp. 6108–6117, 2009.
- [16] I.-H. Kuo, S.-J. Horng, Y.-H. Chen et al., "Forecasting TAIEX based on fuzzy time series and particle swarm optimization," *Expert Systems with Applications*, vol. 37, no. 2, pp. 1494–1502, 2010.
- [17] S. Davari, M. H. F. Zarandi, and I. B. Turksen, "An improved fuzzy time series forecasting model based on particle swarm intervalization," in *Proceedings of the 28th North American Fuzzy Information Processing Society (NAFIPS '09)*, pp. 1–5, Cincinnati, Ohio, USA, June 2009.
- [18] J.-I. Park, D.-J. Lee, C.-K. Song, and M.-G. Chun, "TAIEX and KOSPI 200 forecasting based on two-factors high-order fuzzy time series and particle swarm optimization," *Expert Systems with Applications*, vol. 37, no. 2, pp. 959–967, 2010.
- [19] L.-Y. Hsu, S.-J. Horng, T.-W. Kao et al., "Temperature prediction and TAIEX forecasting based on fuzzy relationships and MTPSO techniques," *Expert Systems with Applications*, vol. 37, no. 4, pp. 2756–2770, 2010.
- [20] E. Egrioglu, U. Yolcu, C. H. Aladag, and C. Kocak, "An ARMA type fuzzy time series forecasting method based on particle swarm optimization," *Mathematical Problems in Engineering*, vol. 2013, Article ID 935815, 12 pages, 2013.
- [21] S.-M. Chen and N.-Y. Chung, "Forecasting enrollments using high-order fuzzy time series and genetic algorithms," *International Journal of Intelligent Systems*, vol. 21, no. 5, pp. 485–501, 2006.
- [22] L.-W. Lee, L.-H. Wang, and S.-M. Chen, "Temperature prediction and TAIEX forecasting based on fuzzy logical relationships and genetic algorithms," *Expert Systems with Applications*, vol. 33, no. 3, pp. 539–550, 2007.
- [23] L.-W. Lee, L.-H. Wang, and S.-M. Chen, "Temperature prediction and TAIEX forecasting based on high-order fuzzy logical relationships and genetic simulated annealing techniques," *Expert Systems with Applications*, vol. 34, no. 1, pp. 328–336, 2008.
- [24] C.-H. Cheng, G.-W. Cheng, and J.-W. Wang, "Multi-attribute fuzzy time series method based on fuzzy clustering," *Expert Systems with Applications*, vol. 34, no. 2, pp. 1235–1242, 2008.
- [25] S.-T. Li, Y.-C. Cheng, and S.-Y. Lin, "A FCM-based deterministic forecasting model for fuzzy time series," *Computers & Mathematics with Applications*, vol. 56, no. 12, pp. 3052–3063, 2008.
- [26] C. H. Aladag, U. Yolcu, E. Egrioglu, and A. Z. Dalar, "A new time invariant fuzzy time series forecasting method based on particle swarm optimization," *Applied Soft Computing*, vol. 12, pp. 3291–3299, 2012.
- [27] F. Alpaslan, O. Cagcag, C. H. Aladag, U. Yolcu, and E. Egrioglu, "A novel seasonal fuzzy time series method," *Hacettepe Journal of Mathematics and Statistics*, vol. 41, no. 3, pp. 375–385, 2012.
- [28] E. Egrioglu, C. H. Aladag, and U. Yolcu, "A hybrid fuzzy time series forecasting model based on fuzzy c-means and artificial neural networks," *Expert Systems With Applications*, vol. 40, pp. 854–857, 2013.
- [29] F. Alpaslan and O. Cagcag, "A seasonal fuzzy time series forecasting method based on gustafson-kessel fuzzy clustering," *Journal of Social and Economic Statistics*, vol. 2, no. 1, pp. 1–13, 2012.
- [30] J. Sullivan and W. H. Woodall, "A comparison of fuzzy forecasting and Markov modeling," *Fuzzy Sets and Systems*, vol. 64, no. 3, pp. 279–293, 1994.
- [31] K. Huarng and T. H.-K. Yu, "The application of neural networks to forecast fuzzy time series," *Physica A*, vol. 363, no. 2, pp. 481–491, 2006.
- [32] C. H. Aladag, M. A. Basaran, E. Egrioglu, U. Yolcu, and V. R. Uslu, "Forecasting in high order fuzzy times series by using neural networks to define fuzzy relations," *Expert Systems with Applications*, vol. 36, no. 3, pp. 4228–4231, 2009.
- [33] T. H.-K. Yu and K.-H. Huarng, "A neural network-based fuzzy time series model to improve forecasting," *Expert Systems with Applications*, vol. 37, no. 4, pp. 3366–3372, 2010.
- [34] U. Yolcu, C. H. Aladag, E. Egrioglu, and V. R. Uslu, "Time series forecasting with a novel fuzzy time series approach: an example for Istanbul stock market," *Journal of Computational and Statistics Simulation*, vol. 83, no. 4, pp. 597–610, 2013.
- [35] C. H. Aladag, "Using multiplicative neuron model to establish fuzzy logic relationships," *Expert Systems with Applications*, vol. 40, pp. 850–853, 2013.
- [36] E. Egrioglu, C. H. Aladag, U. Yolcu, M. A. Basaran, and V. R. Uslu, "A new hybrid approach based on SARIMA and partial high order bivariate fuzzy time series forecasting model," *Expert Systems with Applications*, vol. 36, no. 4, pp. 7424–7434, 2009.
- [37] V. R. Uslu, C. H. Aladag, U. Yolcu, and E. Egrioglu, "A new hybrid approach for forecasting a seasonal fuzzy time series," in *Proceedings of the International Symposium Computing Science and Engineering Proceeding Book*, pp. 1152–1158, 2010.
- [38] S. Aladag, C. H. Aladag, T. Menten, and E. Egrioglu, "A new seasonal fuzzy time series method based on the multiplicative neuron model and SARIMA," *Hacettepe Journal of Mathematics and Statistics*, vol. 41, no. 3, pp. 337–345, 2012.
- [39] J. Kennedy and R. Eberhart, "Particle swarm optimization," in *Proceedings of the IEEE International Conference on Neural Networks*, pp. 1942–1948, December 1995.
- [40] Y. Ma, C. Jiang, Z. Hou, and C. Wang, "The formulation of the optimal strategies for the electricity producers based on the particle swarm optimization algorithm," *IEEE Transactions on Power Systems*, vol. 21, no. 4, pp. 1663–1671, 2006.

- [41] Y. Shi and R. C. Eberhart, "Empirical study of particle swarm optimization," in *Proceedings of the Congress on Evolutionary Computation (CEC '99)*, vol. 3, pp. 1945–1950, 1999.
- [42] D. E. Gustafson and W. C. Kessel, "Fuzzy clustering with a fuzzy covariance matrix," in *Proceedings of the IEEE Conference on Decision and Control Including the 17th Symposium on Adaptive Processes*, pp. 761–766, San Diego, Calif, USA, January 1979.
- [43] R. N. Yadav, P. K. Kalra, and J. John, "Time series prediction with single multiplicative neuron model," *Applied Soft Computing Journal*, vol. 7, no. 4, pp. 1157–1163, 2007.
- [44] L. Zhao and Y. Yang, "PSO-based single multiplicative neuron model for time series prediction," *Expert Systems with Applications*, vol. 36, no. 2, pp. 2805–2812, 2009.
- [45] K.-H. Huarng, T. H.-K. Yu, and Y. W. Hsu, "A multivariate heuristic model for fuzzy time-series forecasting," *IEEE Transactions on Systems, Man, and Cybernetics B*, vol. 37, no. 4, pp. 836–846, 2007.
- [46] S.-M. Chen and Y.-C. Chang, "Multi-variable fuzzy forecasting based on fuzzy clustering and fuzzy rule interpolation techniques," *Information Sciences*, vol. 180, no. 24, pp. 4772–4783, 2010.
- [47] S.-M. Chen and C.-D. Chen, "TAIEX forecasting based on fuzzy time series and fuzzy variation groups," *IEEE Transactions on Fuzzy Systems*, vol. 19, no. 1, pp. 1–12, 2011.
- [48] S.-M. Chen, H.-P. Chu, and T.-W. Sheu, "TAIEX forecasting using fuzzy time series and automatically generated weights of multiple factors," *IEEE Transactions on Systems, Man, and Cybernetics Part A*, vol. 42, no. 6, pp. 1485–1495, 2012.

## Research Article

# Italian Residential Buildings: Economic Assessments for Biomass Boilers Plants

**Maurizio Carlini,<sup>1</sup> Sonia Castellucci,<sup>2</sup> Silvia Cocchi,<sup>1</sup> Elena Allegrini,<sup>1</sup> and Ming Li<sup>3</sup>**

<sup>1</sup> DAFNE, University of Tuscia, Via San Camillo de Lellis snc, 01100 Viterbo, Italy

<sup>2</sup> CIRDER, University of Tuscia, Via Santa Maria in Gradi 4, 01100 Viterbo, Italy

<sup>3</sup> School of Information Science & Technology, East China Normal University, No. 500, Dong-Chuan Road, Shanghai 200241, China

Correspondence should be addressed to Silvia Cocchi; [silvia.cocchi@unitus.it](mailto:silvia.cocchi@unitus.it)

Received 29 July 2013; Accepted 19 September 2013

Academic Editor: Carlo Cattani

Copyright © 2013 Maurizio Carlini et al. This is an open access article distributed under the Creative Commons Attribution License, which permits unrestricted use, distribution, and reproduction in any medium, provided the original work is properly cited.

Biomass is increasingly used for energy generation since it represents a useful alternative to fossil fuel in order to face the pollutions and the global warming problem. It can be exploited for heating purposes and for supplying domestic hot water. The most common applications encompass wood and pellet boilers. The economic aspect is becoming an important issue in order to achieve the ambitious targets set by the European Directives on Renewable Sources. Thus, the present paper deals with the economic feasibility of biomass boiler plants with specific regard to an existing residential building. An Italian case study is further investigated, focusing the attention on European and national regulations on energy efficiency and considering the recent public incentives and supporting measures. The main thermoclimatic parameters—that is, heating degree days (HDDs), building thermal insulation and thermal needs—are taken into account. Moreover, the following economic indicators are calculated: cumulative cash flow, discounted cumulative cash flow, payback period (PP), net present value (NPV), Internal rate of return (IRR), discounted payback period (DPP), and profit index (PI).

## 1. Introduction

The problem of global warming, the growing pollutant emissions, and the increasing energy demand together with the reduction of fossil fuel sources have led many countries to consider and develop the Renewable Energy Sources sector and Europe to adopt some specific regulations on this matter [1, 2].

The European Directive 2009/28/EC—also well known as “Directive 20-20-20”—set many climate and energy targets in order to achieve and ensure a clean and sustainable living for the future generations: reduction of greenhouse gases emissions by 20%, energy production from renewable sources in percentage of 20%, and improvement of the energy efficiency by 20% in order to reduce the energy consumption [3, 4].

In this context, the biomass represents a good solution for RES developing since it is widespread in many different areas; indeed, it encompasses all organic matter of vegetable or animal origin. Biomass from plant is a product of photosynthesis process and can be considered carbon neutral

since the amount of the released carbon, during its energetic conversion process, is similar to the quantity absorbed during its life time [5–7]. The cycle from biomass and fossil fuel to energy can be shortly represented as follows: biomass consumes CO<sub>2</sub> through photosynthesis, which is the process used by plants and other organisms to capture sun's energy, and the solar energy is stored in the chemical bonds of their structural components; when this energy is extracted, CO<sub>2</sub> becomes available to produce new biomass; the process is cyclical. Burning fossil fuels, old biomass (whose conversion took millions of years), is exploited, so that new CO<sub>2</sub> is generated through the combustion, increasing the greenhouse effect. In contrast, burning new biomass does not add new CO<sub>2</sub> since replanting new biomass permits carbon dioxide to be absorbed and returned cyclically [8]. For this reason, biomass can be seen as a neutral fuel: combustion produces the same amount of CO<sub>2</sub> which is absorbed during the whole life cycle of plants [9, 10]. Furthermore, during the biomass conversion into energy, low pollutants are emitted. Polycyclic Aromatic Hydrocarbons (PAHs) and CO<sub>2</sub> emissions can be



reduced by simply varying some parameters of conversion technologies [11]; moreover, since biomass has low nitrogen and sulphur contents, low emissions of  $\text{NO}_x$  and  $\text{SO}_x$  occur [12, 13]. In addition, biomass has a small content of pollutants and ashes, despite the possible variations of some chemical components and moisture [14].

In order to convert biomass into energy, several categories of processes can be exploited depending on biomass characteristics, namely, thermochemical conversion, biochemical conversion, and mechanical extraction. Direct combustion, gasification, and pyrolysis belong to the first category [15, 16]. Combustion is the most widespread process, and it mainly exploits wood biomass; the most common and commercial application is represented by biomass boiler, using wood or pellet.

In the present work, an economic assessment of a biomass boiler installation in Italian residential buildings has been investigated using the main financial indicators: cumulative cash flow, discounted cumulative cash flow, payback period (PP), net present value (NPV), internal rate of return (IRR), discounted payback period (DPP), and profit index (PI).

A two-storey single building located in Viterbo has been considered. In the current condition, the building has a methane traditional boiler for heating and domestic hot water (DHW) supply. A study on the energy improvement has been carried out considering the replacement of the methane boiler with a biomass one. The DHW demand has been covered with a solar collector. The study has been carried out on two different cases concerning the thermal insulation of the building.

*Case 1.* A not well thermally insulated building, for which a replacement of the fixtures and an insulation cover for the external walls have been considered in order to lead it to Case 2 conditions; in the economical assessment, the thermal insulation costs have been taken into account.

*Case 2.* A thermally insulated building for which the thermal insulation costs are not to be considered.

The use of the biomass boiler and the solar collector permits us to gain access to the Italian Renewable Heat Incentive. In the following paragraph, a brief description of the European and Italian Regulations and the supporting measures are reported.

*1.1. European Regulations and Italian Incentive Measures.* Energy efficiency improvement in Italian buildings is an extremely important aspect to ensure energy saving and green-house gases (GHGs) emissions reduction. According to ENEA, most of the dwellings in our country were built before the first law on reducing building energy consumption (Legislative Decree 373/76) came into force. More than 2.7 million residential buildings, heterogeneously distributed in the whole territory and mostly belonging to the coldest climatic areas and having a low-thermal performance building envelope, are present in Italy. This is the reason why the residential sector is characterised by the highest energy consumptions corresponding to 36% (48 262 ktoe) of the

TABLE 1: Eligible projects included in category 1 (Legislative Decree 28th December 2012).

Project identification code	Eligible projects
1.A	Thermal insulation of opaque enclosures
1.B	Replacement of transparent enclosures
1.C	Replacement of existing winter heating systems with condensing heat generator
1.D	Shadowing and shielding systems for transparent enclosures

national demands and whose mean value is equal to 150–200 kWh/(m<sup>2</sup> × year). The thermal need represents 85% of the building energy demand, including space heating (70%) and domestic hot water (15%) (year 2007) [17, 18].

Hence, in order to speed up the transition from existing heating systems towards more efficient alternatives, in recent years, many incentive schemes have been adopted in Italy [19]. In more detail on 28th December 2012 the so-called “Renewable Energy for Heating and Cooling Support Scheme” has been established; it represents the Italian Supporting Measures and implements the previous Legislative Decree number 28 of 3rd March 2011. This policy strongly encourages the use of wood and pellet boilers [20]. Indeed, according to the European Directive 2009/28, public support is needed to reach the community’s purposes on renewable energy sources (RES) use [21].

The Italian incentive mechanism carefully defines the supporting scheme for small-scale projects concerning energy efficiency improvements in existing buildings (called “category 1”) and thermal energy production by the use of RES and high efficiency systems (“category 2”), as shown in Tables 1 and 2. The term “replacement” means the substitution of an existing power system with a new solution, whose capacity must not exceed more than 10% of the old system. If this constraint is not respected, the corresponding incentive will not be awarded [20].

According to the national regulation, two different parties are eligible, namely, public administrations and private parties. The first parties may apply for both categories, while private parties may require incentives only for category 2. Moreover, focusing the attention on new buildings or on those subject to major renovation, the supporting measure will cover only the part of the project exceeding the mandatory targets set by Legislative Decree number 28. The supporting measures will be granted only for those projects which do not benefit other incentives from the government [20].

In order to further improve the energy efficiency in new or existing buildings—both for thermal behaviour and heating/cooling systems—it is fundamental to analyse the thermal and electrical needs. This goal is successfully reached by carrying out the so-called Energy Performance Certificate (EPC) which was laid down by the European Directive 2002/91. With regards to the regulation, “energy performance of a building” is meant as the amount of energy actually consumed or estimated to meet the different needs associated with a standardised use of the building itself, which may

TABLE 2: Eligible projects included in category 2 (Legislative Decree 28th December 2012).

Project identification code	Eligible projects
2.A	Replacement of existing winter heating systems with heat pumps, whose thermal capacity must be less than 1000 kW
2.B	Replacement of existing heating or cooling systems for greenhouses or agricultural buildings with heat generators supplied by biomass, whose thermal capacity must be less than 1000 kW
2.C	Solar thermal collector, whose total area must not exceed 1000 m <sup>2</sup>
2.D	Replacement of electrical boilers with heat pump boilers

include heating, hot water heating, cooling, ventilation, and lighting. When buildings are constructed, sold, or rented out, the EPC is made available to the owner or by the owner to the prospective buyer or tenant, as the case might be. The validity of the certificate should not exceed 10 years [22].

The above-mentioned regulation was repealed by the European Directive 2010/31 with effect from 1 February 2012. Since buildings account for 40% of total energy consumption in the Union and the sector is still expanding, member states should ensure that all new buildings occupied and owned by public authorities are nearly zero-energy buildings, by 31 December 2020 and 31 December 2018, respectively. In more detail, a “nearly zero-energy building” is referred to, a very high energy performance structure as determined in accordance with Annex I. A very limited amount of energy required should be covered—to a very significant extent—by energy from renewable sources, especially on-site or nearby [23].

The European Directive 2012/27 establishes a common framework of measures for promoting energy efficiency within the Union in order to ensure the achievement of the Union’s 2020 20% headline target on energy efficiency and to pave the way for further energy efficiency improvements beyond that date [24].

With specific regard to Italy, the concepts of energy savings in buildings, rational utilisation of energy, and sustainable use of RES were introduced by the National Law 10/91 [25]. In recent years, the legislative framework has been further developed and is still changing in order to comply with the above-described European Directives. The following national regulations must be taken into account to carry out the Energy Performance Certificate.

- (i) Legislative Decree 192/05 on energy efficiency of buildings [26].
- (ii) Legislative Decree 311/06 which encompasses corrections and integrations to the Legislative Decree 192/05 [27].
- (iii) Presidential Decree 59/09 which enforced Legislative Decree 192/05 [28].
- (iv) National guidelines for energy performance set by the Ministerial Decree 26/06/2009 [29].
- (v) Ministerial Decree 22/11/2012, including corrections and integrations to the Ministerial Decree 26/06/2009 [30].

In order to benefit the incentives laid down by the Renewable Energy for Heating and Cooling Support Scheme, the EPC must be carried out in case of replacement of existing winter heating systems with biomass boiler if the renovation is applied to the whole building, having a nominal power more than 100 kW.

## 2. Materials and Methods

The system considered in the present study consists of a single building located in Viterbo (Northern Latium, Central Italy). The structure is a 2-storey, rectangular-shaped building, with external gross dimensions of 6 m × 10 m. The total footprint area is 102 m<sup>2</sup>, leading to a total heated volume of 275.4 m<sup>3</sup> since each floor is 2.7 m high. External walls are made of 28 cm of brick elements, without any insulation cover. Moreover, an internal and external layer of plaster—whose thickness is equal to 20 mm in both cases—is added. Table 3 shows the main thermal parameters of the current wall layers in the building. The roof and the ground floor consist of ordinary concrete structure. Windows are 1 or 2 double glass panes-solutions with wooden frame and are located in the eastern, southern, and western sides of the considered dwelling. The overall thermal transmittance of the transparent enclosures is equal to 2.8 W/(m<sup>2</sup> × K). Windows account for 19.48 m<sup>2</sup>, corresponding to 10% of the external wall surface. Space heating and domestic hot water (DHW) are supplied by means of a 24 kW methane-traditional heat generator, whose parameters are summarized in Table 4. The heat distribution system is ensured by traditional radiators. The building in this condition represents the studied Case 1 in the present paper.

Since the dwelling is represented by a residential building (belonging to category E1 according to the Presidential Decree 412/93), the set point for indoor temperature is assumed to be equal to 20°C to ensure thermal comfort [31].

Broadly speaking, the working period of the heating systems depends on climatic conditions and on the so-called heat degree days (HDDs). The heating requirements for a given structure at a specific location are considered to be directly proportional to the number of HDDs at that location. HDDs are defined relative to a base temperature which is the outside temperature above which a building does not need heating. In order to evaluate HDD, an approximation method is used by taking the average temperature on any given day and subtracting it from the base temperature. If the value is

TABLE 3: Main thermal parameters for the current wall stratigraphy of the building (Case 1—*ante operam*).

Materials	Thickness (mm)	Thermal conductivity (W/m × K)	Density (kg/m <sup>3</sup> )	Resistance factor (dimensionless)	Specific heat (J/kg × °C)	Thermal resistance (m <sup>2</sup> × K/W)	Overall thermal transmittance (W/m <sup>2</sup> × K)
Internal plaster	20	0.35	1200	10	835	0.057	1.642
Brick	280	0.777	1800	15	835	0.36	
External plaster	20	0.9	1800	20	835	0.022	

TABLE 4: Main parameters of the traditional heat generator (Case 1—*ante operam*).

Parameters	Values
Nominal power for heating (min/max)	11.0/24.6 kW
Nominal power for DHW (min/max)	11.0/24.6 kW
Useful power output (min/max)	9.6/22.9 kW
Temperature range for heating	82/40°C
Temperature range for DHW	60/36°C
Efficiency considering the nominal power	93.0%
Efficiency considering 30% of the nominal power	92.8%

TABLE 5: HDD, heating hours per day, and heating period (Decree 412/93).

Climatic area	HDD	Maximum heating hours per day	Heating period
A	<600	6	December 1–March 15
B	601–900	8	December 1–March 31
C	901–1400	10	November 15–March 31
D	1401–2100	12	November 1–April 15
E	2101–3000	14	October 15–April 15
F	>3000	No limitations	No limitations

less than or equal to zero, that day has zero HDD; if the value is positive, that number represents the number of HDDs on that day. Thus, only the positive differences of temperature must be considered. HDDs are calculated with (1) [32] as follows:

$$\text{HDD} = \sum_{i=1}^{\text{nhd}} (T_0 - T_i), \quad (1)$$

where  $i$  is value varying from 1 to the number of heating days (nhd),  $T_0$  is the base temperature (°C), and  $T_i$  is the mean daily external temperature (°C). According to the value given by (1), Italy is divided into six different areas—from zone A (the hottest one) to zone F (the coldest one)—as shown in Table 5. More precisely, HDDs increase when the climate becomes colder. Viterbo belongs to zone D, having 1989 HDDs.

Considering all the input data mentioned in Tables 3, 4, and 5, the software DoCeT has been used in order to calculate the total primary energy consumption for space heating, DHW, and electrical purposes and, as a consequence, the energy class of the building. The obtained results are summarized in Table 6 [33].

TABLE 6: Output data generated by DoCeT for the residential building (Case 1—*ante operam*).

Output data	Case 1
Primary energy for space heating	299.5 kWh/m <sup>2</sup>
Primary energy for DHW	21.8 kWh/m <sup>2</sup>
Primary energy for electrical uses	4.1 kWh/m <sup>2</sup>
Total primary energy consumption	325.4 kWh/m <sup>2</sup>
Thermal need for space heating	204.9 kWh/m <sup>2</sup>
Thermal need for DHW	17.1 kWh/m <sup>2</sup>
Cooling need	18.6 kWh/m <sup>2</sup>
Global energy class (space heating and DHW)	G
Partial energy class with regard to heating and cooling	G
Building envelope performance	II
Partial energy class with regard to DHW	E
CO <sub>2</sub> emissions	88.2 kg/m <sup>2</sup>

In order to improve the energy and thermal performance of the building, the following actions can be carried out:

- (i) insulation layer within the external wall;
- (ii) supplying DHW demand by installing solar collectors on the roof;
- (iii) providing space heating and DHW by means of a pellet boiler.

With specific regard to the first stage, Tables 7 and 8 show the main thermal parameters of the building in case of insulating the external wall and the improvements of the building envelope in terms of thermal behaviour. In order to access the 65% tax deduction regulation, the overall transmittance of the wall must not exceed the limit values reported in the Ministerial Decree 59/09, if the project is carried out in climatic areas belonging to classes C, D, E, and F [34].

The transparent enclosures may be replaced by double glass panes-solutions with PVC frame, whose overall thermal transmittance is given by 1.1 W/m<sup>2</sup> × K.

An energy analysis has been carried out with DoCet software for the thermally insulated building too, considering a methane boiler for heating and DHW supply. The building in these conditions represents Case 2 studied in the present paper. The results are reported in Table 9.

For both Cases 1 and 2, the installation of solar collectors and pellet boiler has been evaluated in order to enhance the energy properties of the building.

TABLE 7: Main thermal parameters for the current wall stratigraphy of the building (Case 1—*post operam* and Case 2).

Materials	Thickness (mm)	Thermal conductivity (W/m × K)	Density (kg/m <sup>3</sup> )	Resistance factor (dimensionless)	Specific heat (J/kg × °C)	Thermal resistance (m <sup>2</sup> × K/W)	Overall thermal transmittance (W/m <sup>2</sup> × K)
Internal plaster	20	0.35	1200	10	835	0.057	0.359
Brick	280	0.777	1800	15	835	0.36	
Insulating layer	50	0.023	38	89900	1392	2.174	
External plaster	20	0.9	1800	20	835	0.022	

TABLE 8: Overall transmittance of the building envelope (Case 1—*post operam* and Case 2).

Overall transmittance Case 1— <i>post operam</i> and Case 2 (W/m <sup>2</sup> × K)	Limit value according to Presidential Decree 59/2009	Overall transmittance Case 1— <i>ante operam</i> (W/m <sup>2</sup> × K)	Overall transmittance reduction (W/m <sup>2</sup> × K)
0.359	0.36	1.642	−1.283

TABLE 9: Output data generated by DoCeT software for the residential building (Case 2—*ante operam*).

Output data	Case 2
Primary energy for space heating	160 kWh/m <sup>2</sup>
Primary energy for DHW	21.8 kWh/m <sup>2</sup>
Primary energy for electrical uses	4.1 kWh/m <sup>2</sup>
Total primary energy consumption	186 kWh/m <sup>2</sup>
Thermal need for space heating	102 kWh/m <sup>2</sup>
Thermal need for DHW	17.1 kWh/m <sup>2</sup>
Cooling need	19.7 kWh/m <sup>2</sup>
Global energy class (space heating and DHW)	F
Partial energy class with regard to heating and cooling	F
Building envelope performance	II
Partial energy class with regard to DHW	E
CO <sub>2</sub> emissions	37 kg/m <sup>2</sup>

TABLE 10: Main characteristics of the biomass boiler.

Characteristics	Values
Fuel	Pellet
Rated power ( $P_n$ )	12 kW
Efficiency	93%
Consumption	0.9–2.75 kg/h
Heatable volume	315 m <sup>3</sup>
Water buffer tank	600 L

The solar collectors to be located on the roof have been preliminarily designed assuming 4 occupants and 50 L/person as water demand. This leads us to calculate the collector surface (3 m<sup>2</sup>) and the diameter of the pipe within the collector (16 mm). The tank volume is equal to 220 L.

As for the heating system, the chosen biomass boiler has the characteristics reported in Table 10 (according to UNI EN 303-5-2012 standard).

Considering all the above-mentioned input data and the results coming from the design procedures, the software DoCeT has led us to calculate an approximate estimation

TABLE 11: Output data generated by DoCeT for the residential building (*post operam* both Cases 1 and 2).

Output data	Values
Primary energy for space heating	137.3 kWh/m <sup>2</sup>
Primary energy for DHW	0 kWh/m <sup>2</sup>
Primary energy for electrical uses	4.2 kWh/m <sup>2</sup>
Total primary energy consumption	141.5 kWh/m <sup>2</sup>
Thermal need for space heating	102 kWh/m <sup>2</sup>
Thermal need for DHW	17.1 kWh/m <sup>2</sup>
Cooling need	19.7 kWh/m <sup>2</sup>
Global energy class (space heating and DHW)	E
Partial energy class with regard to heating and cooling	F
Building envelope performance	II
Partial energy class with regard to DHW	A
CO <sub>2</sub> emissions	0.3 kg/m <sup>2</sup>

of the total primary energy consumption for space heating, DHW, and electrical purposes and, as a consequence, the energy class of the buildings in *post operam* conditions, as summarized in Table 11 [33].

The chosen solar collectors and biomass boiler fulfil the technical requirements set by the Renewable Energy for Heating and Cooling Support Scheme.

With specific regard to the cases described, the EPC is not needed. However, it has been carried out since it is fundamental to understand the current energy class of the dwelling and the future and possible improvements by modifying the building envelope and the energy supply plants [19]. As it is commonly known, the energy efficiency is given on a scale from A<sup>+</sup>—the most efficient homes—to G—the most energy consuming one. According to the national regulations, the EPC can be successfully carried out using the software DoCeT in case of existing residential buildings whose total area does not exceed 3000 m<sup>2</sup> [26–31].

The biomass boiler fulfils the technical requirements set by the support scheme, such as the observance of class 5 of the EN 303-5 technical standard, the efficiency higher than



TABLE 12: Utilization coefficient  $h_r$  (Decree 28th December 2012).

Climatic zone	$h_r$ (hours)
A	600
B	850
C	1100
D	1400
E	1700
F	1800

TABLE 13: Coefficient  $C_i$  (Decree 28th December 2012).

	<35 KW	35–500 kW	>500 kW
Biomass boilers	0.045 [€/kWh <sub>t</sub> ]	0.020 [€/kWh <sub>t</sub> ]	0.018 [€/kWh <sub>t</sub> ]

TABLE 14:  $C_e$  coefficient values depending on the primary particulate emissions (Decree 28th December 2012).

PPBT (mg/Nm <sup>3</sup> )	$C_e$
20 < emissions ≤ 30	1
10 < emissions ≤ 20	1.2
emissions ≤ 10	1.5

TABLE 15: Yearly incentive calculation for biomass boiler.

Parameters	Values
$I_{a,tot}$	907.2 €/year
$P_n$	12 kW
$h_r$	1400 hours
$C_i$	0.045 €/kWh
$C_e$	1.2
PPBT	10 ÷ 20

$87 + \log(P_n)$ , and the observance of the pellet characteristics according to classes A1 and A2 of EN 14961-2.

According to the Italian supporting measures, the incentive for biomass boilers has been calculated as follows [20]:

$$I_{a,tot} = P_n \times h_r \times C_i \times C_e, \quad (2)$$

where

- $I_{a,tot}$  is the yearly awarded incentive (€/year),
- $P_n$  is thermal power of the plant (kW),
- $h_r$  is the utilization coefficient in hours (Table 12),
- $C_i$  is a coefficient depending on the thermal power of the plant (Table 13),
- $C_e$  is a coefficient depending on the particulate emissions (Table 14).

The primary particulate emissions can be determined by following the CEN/TS 15883 or EN 13284-1 standards and with a formula described in Decree 28th December 2012.

The parameters and the yearly incentive for the biomass boiler are reported in Table 15.

TABLE 16: Incentive calculation for solar collectors.

Parameters	Values
$I_{a,tot}$	510 €/year
$C_i$	170 €/m <sup>2</sup>
$S_l$	3 m <sup>2</sup>

The yearly incentive ( $I_{a,tot}$ ) awarded for the installation of the solar collectors is reported in Table 16 and is defined by the following formula [20]:

$$I_{a,tot} = S_l \cdot C_i, \quad (3)$$

where  $S_l$  is the gross surface of the solar collectors (m<sup>2</sup>) and  $C_i$  is a coefficient depending on the total surface of the system.

Thus, the total yearly incentive is 1 417.2 €/year, and it is dispensed in two years.

Furthermore, private parties might benefit of the supporting measures for the energy efficiency improvement in the existing residential buildings by accessing the so-called “65% tax deduction,” laid down by the recent Legislative Decree number 63 of 6th June 2013. The latter awards incentives for those projects which will be carried out until 31st December 2012 or 30th June 2014 in case of block apartments and involving the building envelope (both opaque and transparent enclosures), the installation of solar collectors, or the replacement of existing heating generators by means of a condensing boiler [34]. Thus, the tax deduction on the thermal insulation of the building has been taken into account for the studied Case 1.

### 3. Results

All costs for the above-described installations are reported for both Cases 1 and 2 in Table 17.

The energy consumption costs before and after installing biomass boiler and solar collector are reported in Table 18 for both Cases 1 and 2.

The benefits of the investment are shown for both cases in Table 19.

All the above-listed costs and benefits are useful in order to calculate the main financial parameters.

The cash flows ( $CF_t^*$ ) are obtained by adding all the costs ( $C_{i,t}$ ) and all the profits ( $P_{i,t}$ ) related to the generic  $t$ th year, as shown in (4) [3] as follows:

$$CF_t^* = \sum_i P_{i,t} - \sum_i C_{i,t}. \quad (4)$$

The discounted cash flows have been calculated by [3]

$$CF_t = \frac{CF_t^*}{(1+r)^t}, \quad (5)$$

where  $r$  represents the weighted average cost of capital (WACC). It refers to the index which defines the average expected return considering the assets of the plant's owner. The cumulative cash flow and the discounted cumulative cash flow are reported in Figures 1, 2, 3, and 4.

TABLE 17: Table of costs for studied Case 1 and Case 2.

References	Components	Costs	Total (€)	Operating maintenance (€)
Market research	Pellet boiler	2750 €	2750	100
Market research	Water buffer tank	1300 €	1300	6.5
Latium region price list 2012 CODES A.11.02.1.c1 A.11.02.1.c2	Thermal insulation for external walls (Polyiso)	40.16 €/m <sup>2</sup> (up to 2 cm) 2.83 €/m <sup>2</sup> (for additional cm)	8393	—
Latium region price list 2012 CODE E.1.17.4	Solar collector	516.46 €/m <sup>2</sup>	1549.38	—
Market research	Water tank	1250 €	1250	7.74
Latium region price list 2012 CODE A.16.01.a-b-c-d	Transparent enclosures	380 €/m <sup>2</sup>	702	—
Total costs Case 1			22645	127
Total costs Case 2			6850	127

TABLE 18: Costs for energy consumption (Case 1 and Case 2).

Energy consumption before installing biomass boiler and solar collector			
	Consumption (kWh/year)	Cost of methane (€/kWh)	Total (€/year)
Case 1			
Heating + DHW	20899.8	0.093	2105.9
Case 2			
Heating + DHW	12148.2	0.093	1129.78
Energy consumption after installing biomass boiler and solar collector			
	Consumption (kWh/year)	Pellet cost (€/kWh)	Total (€/year)
Heating + DHW	12148.2	0.058	704

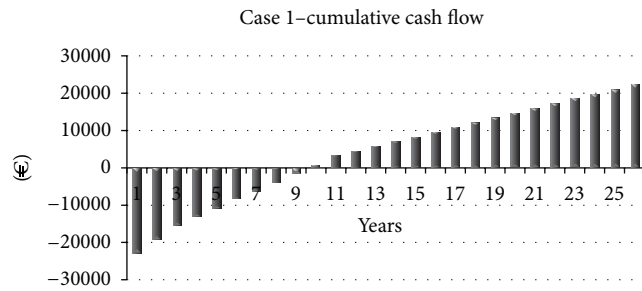


FIGURE 1: Trend of the cumulative cash flow for Case 1.

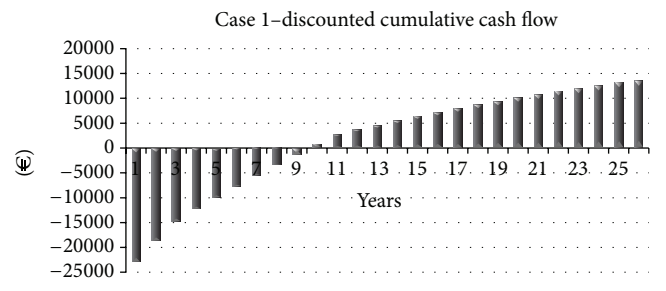


FIGURE 2: Trend of discounted cumulative cash flow for Case 1.

It can be easily seen that the payback period (PP) of the investment is 9 years for Case 1 and 13 for Case 2.

The net present value (NPV) has been evaluated using [3]

$$\begin{aligned}
 \text{NPV} &= \sum_{t=1}^N \frac{\text{CF}_t^*}{(1+r)^t} - C_0 \\
 &= \frac{P_1 - C_1}{(1+r)^1} + \dots + \frac{P_N - C_N}{(1+r)^N} - C_0,
 \end{aligned} \quad (6)$$

where  $N$  is the lifetime of the investment, considered equal to 20 years.

The discounted payback period (DPP) can be observed in Figures 5 and 6.

The internal rate of return (IRR) can be calculated through the following conditions:

$$\begin{aligned}
 \text{NPV} &= \sum_{t=0}^N \frac{\text{CF}_t^*}{(1+\text{IRR})^t} = 0, \\
 \text{PI} &= \frac{\sum_{t=0}^N (P_t / (1+\text{IRR})^t)}{\sum_{t=0}^N (C_t / (1+\text{IRR})^t)} = 1.
 \end{aligned} \quad (7)$$

The values of the IRR can be observed in Figures 7 and 8.

TABLE 19: Table of the benefits for studied Case 1 and Case 2.

Benefits	€/year	Period
Italian renewable heat incentive for biomass boiler	907.2	2 years
Italian renewable heat incentive for solar collector	510	2 years
65%-tax deduction—thermal insulation for external walls—Case 1	545.55	10 years
65%-tax deduction—transparent enclosures—Case 1	481.13	10 years
Annual cost saving for energy production—Case 2	425.2	
Annual cost saving for energy production—Case 1	1401.3	

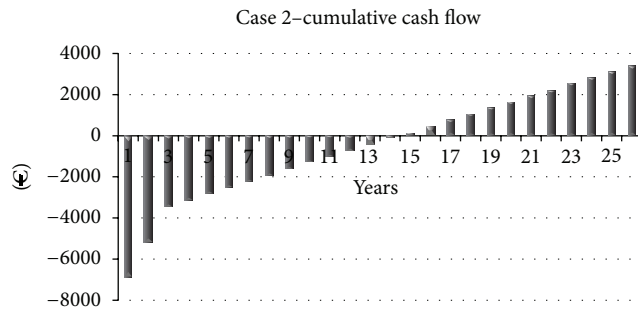


FIGURE 3: Trend of cumulative cash flow for Case 2.

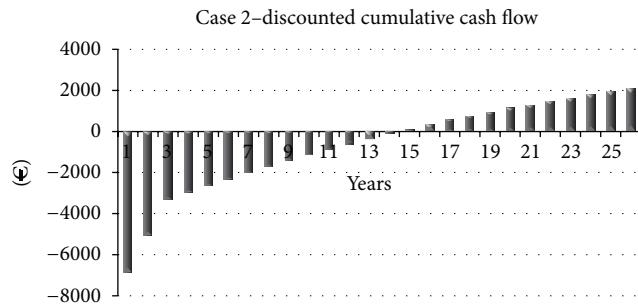


FIGURE 4: Trend of discounted cumulative cash flow for Case 2.

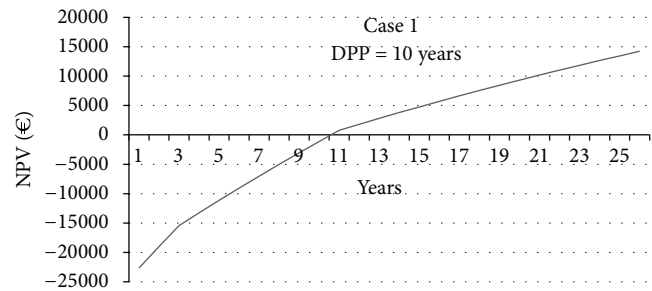


FIGURE 5: Trend of NPV depending on time for Case 1.

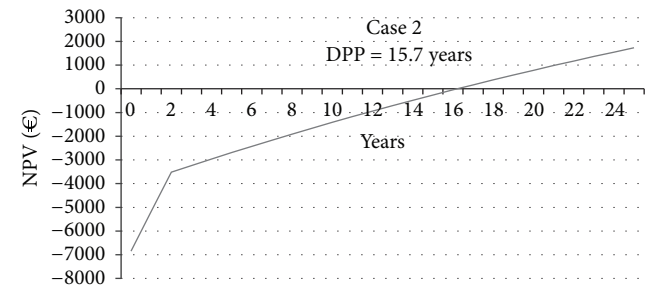


FIGURE 6: Trend of NPV depending on time for Case 2.

The profitability index has been calculated using the following:

$$\begin{aligned}
 PI &= \frac{\sum_{t=0}^N (P_t / (1+r)^t)}{\sum_{t=0}^N (C_t / (1+r)^t)} \\
 &= \frac{P_0 / (1+r)^0 + \dots + P_N / (1+r)^N}{C_0 / (1+r)^0 + \dots + C_N / (1+r)^N}.
 \end{aligned} \quad (8)$$

The main financial parameters are summarized in Table 20.

#### 4. Conclusion

Two analyses have been carried out in order to assess the economical feasibility of biomass boiler plants in standard Italian residential buildings located in Viterbo. The first case studied concerns a not well thermally insulated building for which the following actions have been considered: energy efficiency improvement through insulation of the external walls and replacement of the transparent enclosures; installation of a

TABLE 20: Main financial indicators for both Case 1 and, Case 2.

Case 1	
Lifetime of the investment	20 years
PP	9 years
NPV	10170.11 €
DPP	10 years
IRR	7.5%
PI	1.41
Case 2	
Lifetime of the investment	20 years
PP	14 years
NPV	782.12 €
DPP	15.7 years
IRR	3.7%
PI	1.08

solar collector to supply DHW; and installation of a pellet boiler to provide space heating and DHW if needed. The second case studied involves the same thermally insulated

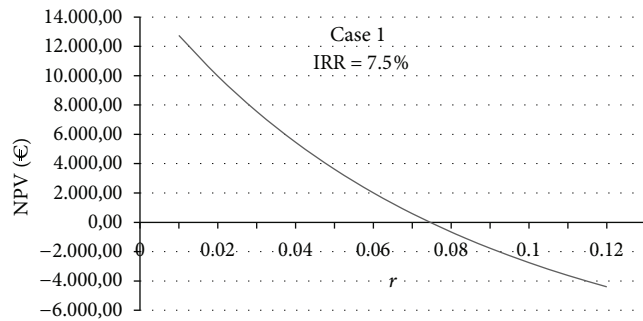


FIGURE 7: IRR for Case 1.

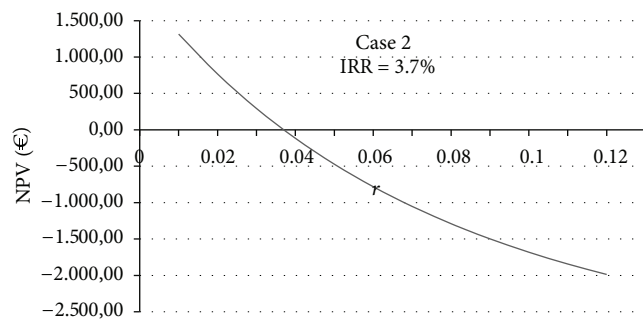


FIGURE 8: IRR for Case 2.

building for which the actions concern the solar collector and pellet boiler installations only.

All the installations fulfil the technical requirements set by the Italian Renewable Energy for Heating and Cooling Support scheme (Decree 28th December 2012) and 65% tax deduction (Legislative Decree no. 63 of 6th June 2013).

The supporting measures permit us to obtain good economic indicators for Case 1 which represents the condition with the highest investment costs. This is possible especially thanks to the 65% tax deduction and to the consumption reduction due to the energy efficiency improvement of the building.

In both studied cases, the major advantages are due to the energy and economic saving achieved with solar collector and pellet boiler installation compared to the use of the methane boiler.

However, the economic subsidy represents a fundamental tool for the payback period reduction and the dissemination of renewable energy sources for heating purposes and domestic hot water supply.

## Acknowledgment

Ming Li acknowledges the support in part by the National Natural Science Foundation of China under the project Grant numbers 61272402, 61070214, and 60873264.

## References

- [1] S. Cocchi, S. Castellucci, and A. Tucci, "Modeling of an air conditioning system with geothermal heat pump for a residential building," *Mathematical Problems in Engineering*, vol. 2013, Article ID 781231, 6 pages, 2013.
- [2] M. Carlini and S. Castellucci, "Efficient energy supply from ground coupled heat transfer source," in *Proceedings of the ICCSA*, vol. 6017 of *Lecture Notes in Computer Science*, pp. 177–190, 2010.
- [3] E. M. Mosconi, M. Carlini, S. Castellucci, E. Allegrini, L. Mizzelli, and M. Arezzo di Trifiletti, "Economical assessment of large scale photovoltaic plants: an Italian case study," in *Proceedings of the ICCSA*, vol. 7972 of *Lecture Notes in Computer Science*, pp. 160–175, 2013.
- [4] European Directive 2009/28/EC.
- [5] M. Carlini, S. Castellucci, S. Cocchi, and A. Manzo, "Waste wood biomass from pruning of Urban Green in viterbo town: energy characterization and potential uses," in *Proceedings of the ICCSA*, vol. 7972 of *Lecture Notes in Computer Science*, pp. 245–255, 2013.
- [6] A. Di Carlo, D. Borello, and E. Bocci, "Process simulation of a hybrid SOFC/mGT and enriched air/steam fluidized bed gasifier power plant," *International Journal of Hydrogen Energy*, vol. 38, pp. 5857–5874, 2013.
- [7] A. Di Carlo, E. Bocci, and V. Naso, "Process simulation of a SOFC and double bubbling fluidized gasifier power plant," *International Journal of Hydrogen Energy*, vol. 38, pp. 532–542, 2013.
- [8] P. McKendry, "Energy production from biomass (part 1): overview of biomass," *Bioresource Technology*, vol. 83, no. 1, pp. 37–46, 2002.
- [9] E. Biagini, F. Barontini, and L. Tognotti, "Devolatilization of biomass fuels and biomass components studied by TG/FTIR technique," *Industrial and Engineering Chemistry Research*, vol. 45, no. 13, pp. 4486–4493, 2006.
- [10] A. Di Carlo, E. Bocci, and A. Dell'Era, "Comparison by the use of numerical simulation of a MCFC-IR and a MCFC-ER when used with syngas obtained by atmospheric pressure biomass gasification," *International Journal of Hydrogen Energy*, vol. 36, no. 13, pp. 7976–7984, 2011.
- [11] A. T. Wijayanta, M. Saiful Alam, K. Nakaso, J. Fukai, and M. Shimizu, "Optimized combustion of biomass volatiles by varying  $O_2$  and  $CO_2$  levels: a numerical simulation using a highly detailed soot formation reaction mechanism," *Bioresource Technology*, vol. 110, pp. 645–651, 2012.
- [12] Z. Li, W. Zhao, R. Li, Z. Wang, Y. Li, and G. Zhao, "Combustion characteristics and NO formation for biomass blends in a 35-ton-per-hour travelling grate utility boiler," *Bioresource Technology*, vol. 100, no. 7, pp. 2278–2283, 2009.
- [13] S. Sethuraman, C. V. Huynh, and S.-C. Kong, "Producer gas composition and  $NO_x$  emissions from a pilot-scale biomass gasification and combustion system using feedstock with controlled nitrogen content," *Energy and Fuels*, vol. 25, no. 2, pp. 813–822, 2011.
- [14] W. Heschel, L. Rweyemamu, T. Scheibner, and B. Meyer, "Abatement of emissions in small-scale combustors through utilisation of blended pellet fuels," *Fuel Processing Technology*, vol. 61, no. 3, pp. 223–242, 1999.
- [15] D. Monarca, A. Colantoni, M. Cecchini, L. Longo, M. Carlini, and A. Manzo, "Energy characterization and gasification of biomass derived by hazelnut cultivation: analysis of produced syngas by gas chromatography," *Mathematical Problems in Engineering*, vol. 2012, Article ID 102914, 9 pages, 2012.
- [16] A. Monarca, M. Cecchini, A. Colantoni, and A. Marucci, "Feasibility of the electric energy production through gasification processes of biomass: technical and economic aspects," in *Proceedings of the ICCSA*, vol. 6785 of *Lecture Notes in Computer Science*, pp. 307–315.



- [17] M. Citterio, B. Dipietra, and F. Margiotta, “Recupero Energetico dell’Edilizia Sociale, Potenzialità e opportunità, il caso di edifici ATC di Biella,” VIII Congresso Nazionale CIRIAF—Sviluppo Sostenibile e Tutela dell’Ambiente e della Salute Umana, 2008.
- [18] Italian Regulation, Legge 373/76.
- [19] M. Villarini, M. Limiti, and R. Impero Abernavoli, “Overview and comparison of global concentrating solar power incentives schemes by means of computational models,” in *Proceedings of the ICCSA*, vol. 6785 of *Lecture Notes in Computer Science*, pp. 258–269, 2011.
- [20] Italian Regulation, D.M. 28 dicembre 2012.
- [21] European Directive 2009/28/EC.
- [22] European Directive 2002/91/EC.
- [23] European Directive 2010/31/EC.
- [24] European Directive 2012/27/EU.
- [25] Italian Regulation, Legge 10/91.
- [26] Italian Regulation, Decreto Legislativo 192/05.
- [27] Italian Regulation, Decreto Legislativo 311/06.
- [28] Italian Regulation, Decreto Legislativo 59/09.
- [29] Italian Regulation, D.M. 26 giugno 2009.
- [30] Italian Regulation, D.M. 22 novembre 2012.
- [31] Italian Regulation, D.P.R. 412/1993.
- [32] M. Carlini, S. Castellucci, E. Allegrini, and A. Tucci, “Down-hole heat exchangers: modelling of a low-enthalpy geothermal system for district heating,” *Mathematical Problems in Engineering*, vol. 2012, Article ID 845192, 11 pages, 2012.
- [33] Software DOCET Manual.
- [34] Italian Regulation, Decreto legge 4 giugno 2013, n. 63.

## Research Article

# Identification of Nonstandard Multifractional Brownian Motions under White Noise by Multiscale Local Variations of Its Sample Paths

Kwang-Il Ahn and Kichun Lee

Industrial Engineering Department, Hanyang University, 222 Wangsimni-ro, Seongdong-gu, Seoul 133-791, Republic of Korea

Correspondence should be addressed to Kichun Lee; [skylee@hanyang.ac.kr](mailto:skylee@hanyang.ac.kr)

Received 18 July 2013; Accepted 9 August 2013

Academic Editor: Ming Li

Copyright © 2013 K.-I. Ahn and K. Lee. This is an open access article distributed under the Creative Commons Attribution License, which permits unrestricted use, distribution, and reproduction in any medium, provided the original work is properly cited.

The Hurst exponent and variance are two quantities that often characterize real-life, high-frequency observations. Such real-life signals are generally measured under noise environments. We develop a multiscale statistical method for simultaneous estimation of a time-changing Hurst exponent  $H(t)$  and a variance parameter  $C$  in a multifractional Brownian motion model in the presence of white noise. The method is based on the asymptotic behavior of the local variation of its sample paths which applies to coarse scales of the sample paths. This work provides stable and simultaneous estimators of both parameters when independent white noise is present. We also discuss the accuracy of the simultaneous estimators compared with a few selected methods and the stability of computations with regard to adapted wavelet filters.

## 1. Introduction

Fractional Brownian motion (fBm) has been commonly used to characterize a wide range of complex signals in natural phenomena that exhibit self-similarity and long-range dependence since the pioneering work of Mandelbrot and Van Ness [1]. Examples of such complex signals in time are abundant in medicine, economics, and geoscience, to list a few. The fBm model is characterized by two parameters of the regularity level and the variance level of a signal. The regularity attribute, also called the Hurst exponent, expresses the strength of statistical similarity at many different frequencies, and the variance attribute describes an order of energy magnitude.

To model path regularity varying with time, multifractional Brownian motion (mBm) has been proposed as a generalization of fractional Brownian motion (fBm). The theory and applications of both fBm and mBm models have attracted the interests of researchers in numerous problems of, for example, sea level fluctuations [2], currency exchange rates [3], and network traffic [4–6]. To model mBm, Lévy-Véhel and Peltier [7] proposed a mean average approach, and Benassi et al. [8] introduced a spectral approach. Lim

and Muniandy [9, 10] also proposed a mBm model based on the fBm defined by the Riemann-Liouville type of fractional integral. The proposed models represent mBm as a Gaussian process  $W(t)$  with a covariance function involving Hurst exponent  $H$  by a function of time,  $H(t)$ , and variance parameter  $C$ . Specifically, a Gaussian process  $(W(t))_{t \geq 0}$  is called mBm with Hurst function  $H(t)$  and its variance level (scaling factor)  $C$  if its covariance function is represented as

$$\begin{aligned} \mathbb{E}[W(t)W(s)] &= \frac{C^2}{2} g(H(t), H(s)) \\ &\times \left\{ |t|^{H(t)+H(s)} + |s|^{H(t)+H(s)} - |t-s|^{H(t)+H(s)} \right\} \end{aligned} \quad (1)$$

for  $H \in \mathcal{C}^\eta([0, 1])$ ;  $t, s \in [0, 1]$ ;  $g(x, y) = \sqrt{K(2x)K(2y)}/K(x+y)$ ; and  $K(\alpha) = \Gamma(\alpha+1) \sin(\alpha\pi/2)/\pi$ ,  $0 < \alpha < 2$ . The process is well defined, or square-integrable, if function  $H(t)$  is the Hölderian of order  $0 < \eta \leq 1$  on  $[0, 1]$ . Clearly, the process  $W(t)$  is not weakly stationary since the covariance function  $\mathbb{E}[W(t)W(s)]$  does not depend on  $t-s$  only. From (1), we have  $\mathbb{E}[W(t)^2] = C^2 t^{H(t)}$ , and consequently,  $\text{Var}[W(1)] = C^2$ . In this sense,  $C$  is called the variance level of the process.

The time-changing Hurst exponent  $H(t)$  characterizes the path regularity of process  $W$  at time  $t$  since sample paths near  $t$  with small  $H(t)$ , close to 0, are space filling and highly irregular, while paths with large  $H(t)$ , close to 1, are very smooth. The variance constant  $C$  determines the energy level of the process. Alternatively, a spectral representation of mBm is given by

$$W(t) = C \sqrt{\frac{K(2H(t))}{2}} \int_{\mathbb{R}} \frac{e^{it\lambda} - 1}{|\lambda|^{H(t)+1/2}} dB(\lambda), \quad (2)$$

where  $C$  is a constant scale (variance) parameter and  $B$  the standard Brownian [7].

Several approaches were proposed to estimate time-changing Hurst exponent  $H(t)$  and variance  $C$  from sample paths of mBm signals. Benassi et al. [8] investigated estimation of a continuously differentiable  $H(t)$  without the direct estimation of  $C$ . A local version of quadratic variations was used in several researches to estimate the constant Hurst exponent [11–13]. Recently Fhima et al. [14] adopted the increment ratio statistic method for  $H(t)$  estimation only. For an overview of estimating constant  $H(t)$ , the reader is also referred to Beran [15] including various statistical methods or Bardet and Bertrand [16] concentrating on wavelet approaches. Estimation of both  $H(t)$  and variance parameter  $C$  has received little attention from the statistics community while  $C$  is mostly treated as a nuisance parameter. When a signal is modeled with mBm, the estimation of  $H(t)$  can be improved by the accurate estimation of  $C$  from covariance structures involving both  $H(t)$  and  $C$ . For that purpose, the application of a local version of quadratic variations for estimating  $H(t)$  and  $C$  in mBm was discussed in Coeurjolly [17], in which  $C$  was, however, locally estimated in each sample path. Moreover, the existence of noise in mBm signals has not been dealt with in the literature though real-life signals are commonly measured under noise environments.

The main objective of this paper is to develop a stable and accurate estimation procedure for unknown parameters  $(H(t), C)$  given a path of  $W(t)$  in the presence of independent white noise. Previous approaches by Coeurjolly [17] relied on local sample paths in the absence of white noise that resulted in estimators of  $C$  sensitive to the sampled paths. It is widely accepted that noise occurs from a variety of sources such as measurement devices.

In this paper, we assume that mBm signals are contaminated by a moderate amount of noise. We extend the quadratic variations method to estimate  $H(t)$  and  $C$  simultaneously for mBm by applying dilated high-pass filters to all sampled paths (all subsample paths from a given sample path) and aggregating all local conditions from the previous filtering step. This method includes filtering all sampled paths with a dilated filter possessing a sufficient number of vanishing moments to capture regularity conditions at associated coarse scales and generating stationary filtered signals. The method further calculates empirical moments of the filtered signals and then estimates  $H(t)$  and  $C$  simultaneously together with

a noise level in a regression setup specified by the empirical moments.

This paper is organized as follows. Section 2 introduces local variations in a mBm setting, discussing the procedures and justification for the simultaneous estimators of unknown parameters. Section 3 discusses numerical simulations and computational issues with adapted wavelet filters. The appendix presents proofs for the propositions in the preceding sections.

## 2. Multiscale Local Variations of Multifractional Brownian Motion

Let us consider a case in which a discretized sample path  $(W')$  is given by

$$W' \left( \frac{i}{N} \right) = W \left( \frac{i}{N} \right) + \sigma \varepsilon \left( \frac{i}{N} \right), \quad i = 1, \dots, N, \quad (3)$$

in which  $\varepsilon(i/N)$  is independent white noise and  $\sigma$  is the noise level. Hurst function  $H(t)$ , generated by  $W(i/N)$ , is assumed to be Hölderian function of order  $0 < \eta \leq 1$  on  $[0, 1]$ . In addition, noise magnitude  $\sigma$  is assumed to be sufficiently small compared to the variance of mBm. The covariance function of  $(W')$  is

$$\begin{aligned} \mathbb{E} [W'(t) W'(s)] &= \frac{C^2}{2} g(H(t), H(s)) \\ &\times \left\{ |t|^{H(t)+H(s)} + |s|^{H(t)+H(s)} \right. \\ &\quad \left. - |t-s|^{H(t)+H(s)} \right\} + \sigma^2 \mathbf{1} \quad (t = s), \end{aligned} \quad (4)$$

where  $\mathbf{1}(A)$  is an indicator of relation  $A$  and  $g(x, y) = \sqrt{K(2x)K(2y)}/K(x+y)$  as defined above. From the above covariance function, we have  $\mathbb{E}[W(t)^2] = C^2 t^{2H(t)} + \sigma^2$ , and consequently,  $\text{Var}[W(1)] = C^2 + \sigma^2$ . Noticeably the estimation of  $C$  is nontrivial because of the dependence structure from the covariance function; that is to say, the sample variance of a sample path does not lead to the direct expression of  $C$  alone but to an expression mixed with all unknown parameters. The entries in (4) generate covariance matrix  $\Sigma$ , which depends on unknown parameters  $\theta := (H(t), C, \sigma) \in \mathbb{R}^{N+2}$ . The covariance matrix consists of  $N(N+1)/2$  parameters (due to symmetry) that can be organized into an  $N(N+1)/2 \times 1$  vector  $\Gamma(\theta)$ . Model (4) is locally identifiable almost everywhere if Jacobian matrix  $\partial \Gamma(\theta)/\partial \theta'$ , which is  $N(N+1)/2 \times (N+2)$ , has full column rank [18].

In order to weaken the dependence in  $W'(t)$  in (3), a differencing filter  $\mathbf{a}$  of length  $l+1$  and order  $p > 1$  (the number of vanishing moments) is applied. Filter  $\mathbf{a}$  is defined by its taps  $(a_0, \dots, a_l)$  such that

$$\begin{aligned} \sum_{q=0}^l a_q q^i &= 0, \quad i = 0, \dots, p-1, \\ \sum_{q=0}^l a_q q^i &\neq 0, \quad i = p. \end{aligned} \quad (5)$$

Let us also introduce  $\mathbf{a}^{(m)}$  based on filter  $\mathbf{a}$ , defined by

$$a_i^{(m)} = \begin{cases} a_{i/m}, & \frac{i}{m} \text{ is an integer,} \\ 0, & \text{otherwise.} \end{cases} \quad (6)$$

We observe that  $\mathbf{a}^{(m)}$ , the filter  $\mathbf{a}$  dilated  $m$  times, focuses on a resolution at a low frequency, corresponding to a coarse space, as  $m$  increases. For  $m = 1$ , it captures the finest level of detail. For example,  $\mathbf{a}^{(1)} = \mathbf{a}$  by definition, and for a second-order filter  $\mathbf{a} := (1, -2, 1)$ ,  $\mathbf{a}^{(2)}$  becomes  $(1, 0, -2, 0, 1)$ . Furthermore, we can choose  $\mathbf{a}$  as high-pass wavelet filters corresponding to orthogonal wavelets such as Daubechies and Symlet wavelets. A detailed discussion of wavelet filters can be found in Daubechies [19] and Vidakovic [20].

Let  $(V_{\mathbf{a}^{(m)}}')$  be a process consisting of  $(W')$  filtered by  $\mathbf{a}^{(m)}$ , that is,

$$V_{\mathbf{a}^{(m)}}' \left( \frac{j}{N} \right) = \sum_{q=0}^{ml} a_q^{(m)} W' \left( \frac{j-q}{N} \right), \quad \text{for } j = ml + 1, \dots, N. \quad (7)$$

For example, when  $\mathbf{a}$  is  $(1, -2, 1)$ , the filter is of order 2, and  $(V_{\mathbf{a}}')$  represents the second-order differences of  $(W')$ . The process  $(V_{\mathbf{a}^{(m)}}')$  is defined similarly with  $(W)$  instead of  $(W')$ :  $(V_{\mathbf{a}^{(m)}}')$  is a process consisting of  $(W)$  filtered by  $\mathbf{a}^{(m)}$ . The filtering by  $\mathbf{a}^{(m)}$  breaks the dependence structure between observations. Specifically the process  $(V_{\mathbf{a}^{(m)}}')$  is stationary due to the vanishing moment property of filter  $\mathbf{a}^{(m)}$ . To verify it, we need to introduce a sufficiently small neighborhood covering  $j$ . Let  $\nu(t)$  be an index set of a neighborhood of  $t$ , defined as

$$\nu(t) = \left\{ j \in \mathbb{Z} \mid l < j \leq N, \left| \frac{j}{N} - t \right| \leq \epsilon \right\} \quad (8)$$

for a parameter  $\epsilon > 0$ . We set  $\epsilon$  to be a function of  $N$  in such a way that  $\epsilon \rightarrow 0$ ,  $\epsilon N \rightarrow \infty$ , and  $\epsilon^\eta \log(N) \rightarrow 0$  as  $N \rightarrow \infty$ . In other words, for a sufficiently large  $N$ , the size of one neighbor becomes sufficiently small while maintaining the summation of the sizes of all the neighbors that are sufficiently large. In addition, it is possible to make  $\epsilon^\eta$  converge to zero faster than  $\log(N)$  grows. Then we derive the covariance of  $(V_{\mathbf{a}^{(m)}}')$  as follows.

**Proposition 1.** *Let  $j_1 \in \nu(t_1)$ ,  $j_2 \in \nu(t_2)$ . Then, the covariance of  $V_{\mathbf{a}^{(m)}}'(j/N)$  in (7),  $\mathbb{E}[V_{\mathbf{a}^{(m)}}'(j_1/N)V_{\mathbf{a}^{(m)}}'(j_2/N)]$ , depends on  $j_1 - j_2$  as follows:*

$$\begin{aligned} & \mathbb{E} \left[ V_{\mathbf{a}^{(m)}}' \left( \frac{j_1}{N} \right) V_{\mathbf{a}^{(m)}}' \left( \frac{j_2}{N} \right) \right] \\ &= \frac{C^2 g(H(t_1), H(t_2))}{N^{H(t_1)+H(t_2)}} \\ & \times \pi_{\mathbf{a}^{(m)}, H(t_1)/2+H(t_2)/2}(j_1 - j_2) \\ & + \sigma^2 \sum_{p=q=j_1-j_2} a_p^{(m)} a_q^{(m)} + \mathcal{O}(\epsilon^\eta \log N), \end{aligned} \quad (9)$$

where

$$\pi_{\mathbf{a}^{(m)}, h}(k) = -\frac{1}{2} \sum_{p,q=0}^{ml} a_p^{(m)} a_q^{(m)} |k - p + q|^{2h}. \quad (10)$$

The above proposition states that  $V_{\mathbf{a}^{(m)}}'(j/N)$  is weakly stationary as Gaussian. Particularly for  $j_1 = j_2 = j$ , as  $N \rightarrow \infty$ , it simplifies to

$$E \left[ V_{\mathbf{a}^{(m)}}' \left( \frac{j}{N} \right)^2 \right] = C^2 \left( \frac{m}{N} \right)^{2H(t)} \pi_{\mathbf{a}, H(t)}(0) + \sigma^2 \sum_q a_q^2. \quad (11)$$

Observably the above proposition deals with two pointwise positions,  $j_1$  and  $j_2$ , for two neighborhoods near  $t_1$  and  $t_2$ , respectively. Thus an aggregate behavior of each neighborhood is analyzed via the following setup.

Let us define the second empirical moment of the filtered signal  $V_{\mathbf{a}^{(m)}}'$  as follows:

$$S'(t, \mathbf{a}^{(m)}) = \frac{1}{|\nu(t)|} \sum_{j \in \nu(t)} V_{\mathbf{a}^{(m)}}' \left( \frac{j}{N} \right)^2, \quad \text{for } t \in [0, 1], \quad (12)$$

which represents the average squared energy of the  $\mathbf{a}^{(m)}$ -filtered signal in the neighborhood of  $t$ . We notice that  $S'(t, \mathbf{a}^{(m)})$  is random because  $V_{\mathbf{a}^{(m)}}'(j/N)$  is random and its expectation  $E[S'(t, \mathbf{a}^{(m)})]$  equals that of  $V_{\mathbf{a}^{(m)}}'(j/N)^2$  because  $V_{\mathbf{a}^{(m)}}'(j/N)$  is weakly stationary. That is to say,

$$\begin{aligned} E[S'(t, \mathbf{a}^{(m)})] &= E \left[ V_{\mathbf{a}^{(m)}}' \left( \frac{j}{N} \right)^2 \right] \\ &= C^2 \left( \frac{m}{N} \right)^{2H(t)} \pi_{\mathbf{a}, H(t)}(0) + \sigma^2 \sum_q a_q^2. \end{aligned} \quad (13)$$

Now, to relate  $S'(t, \mathbf{a}^{(m)})$  to  $E[S'(t, \mathbf{a}^{(m)})]$  more specifically, we define a statistic  $V(t, \mathbf{a}^{(m)})$ , called the  $m$ -scale local variation of  $(W)$ , as

$$V(t, \mathbf{a}^{(m)}) = \frac{1}{|\nu(t)|} \sum_{j \in \nu(t)} \left\{ \frac{V_{\mathbf{a}^{(m)}}(j/N)^2}{\mathbb{E}[V_{\mathbf{a}^{(m)}}(j/N)^2]} - 1 \right\}, \quad (14)$$

where  $|\nu(t)|$  is the cardinal number of  $\nu(t)$ . The statistic  $V(t, \mathbf{a}^{(m)})$  captures the amount of deviations of the  $\mathbf{a}^{(m)}$ -filtered signal from the standard normal distribution near  $t$  because  $V_{\mathbf{a}^{(m)}}$  is normalized by its standard deviation, the square root of  $\mathbb{E}[V_{\mathbf{a}^{(m)}}(j/N)^2]$ . The definition based on the second order can be extended to the  $k$ th order Hermite polynomial in the summation of (14): the second Hermite polynomial is defined by  $t^2 - 1$ . In this paper, we use local variations based on the second Hermite polynomial as the minimum asymptotic variance estimators, as shown in Coeurjolly [13] for fBm settings. Next, we connect the  $m$ -scale local variation  $V(t, \mathbf{a}^{(m)})$  with the empirical moment  $S'(t, \mathbf{a}^{(m)})$  through the following relationship.

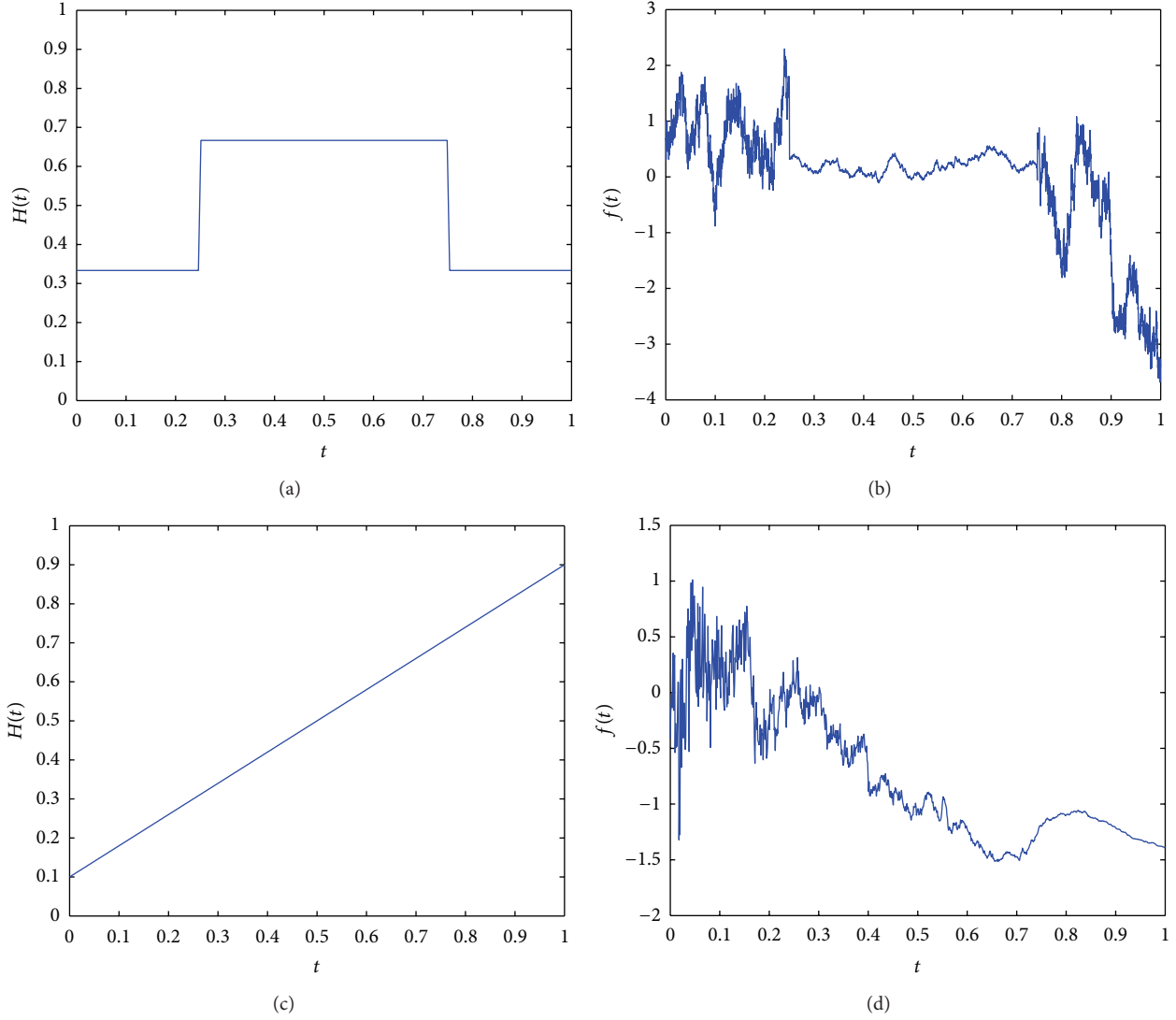


FIGURE 1: Tested Hurst functions are shown in (a) step-function  $H(t)$  and (c) straight-line  $H(t)$ ; their illustrations of signals are shown in (b) and (d), correspondingly.

**Proposition 2.** Let  $m$ -scale local variation  $V(t, \mathbf{a}^{(m)})$  and the empirical moment  $S'(t, \mathbf{a}^{(m)})$  be defined by (14) and (12), respectively, given  $W'(t)$  as above and  $\mathbf{a}$  of order  $> 1$ . Then

$$\log S'(t, \mathbf{a}^{(m)}) = \log \mathbb{E} [S'(t, \mathbf{a}^{(m)})] + V(t, \mathbf{a}^{(m)}) (1 + o(1)),$$

as  $N \rightarrow \infty$ .  
(15)

The proposition connects the empirical moment  $S'(t, \mathbf{a}^{(m)})$  and the log of its expectation through  $m$ -scale local variation  $V(t, \mathbf{a}^{(m)})$ . Since the  $m$ -scale local variation converges almost surely to 0 and its distribution follows normal distribution asymptotically [17], the above relationship establishes a regression setup. We also note that a filter of an order of at least 2 ensures asymptotic normality for all the values of the function  $H(t)$ . For a filter of order 1, this convergence is available if and only if  $0 < \sup_t H(t) < 3/4$ .

Next the relationship between the log of the expectation of the empirical moment  $S'(t, \mathbf{a}^{(m)})$  and the parameters of interest ( $H(t)$ ,  $C$ , and  $\sigma$ ) is derived naturally in the light of Proposition 2 and (13). Thus for  $t_1, \dots, t_d \in [0, 1]$  we obtain a regression model for  $\log S'(t_i, \mathbf{a}^{(m)})$  as  $N \rightarrow \infty$ :

$$\log S'(t_i, \mathbf{a}^{(m)}) \sim \log \left( C^2 \left( \frac{m}{N} \right)^{2H(t_i)} \pi_{\mathbf{a}, H(t_i)}(0) + \sigma^2 \sum_q a_q^2 \right),$$

$\forall i, m,$   
(16)

which is nonlinear with respect to  $H(t_i)$ ,  $C$ , and  $\sigma$ . In particular, when the noise level  $\sigma$  is considered to be zero, the regression model simplifies to, for all  $i$  and  $m$ ,

$$\log S'(t_i, \mathbf{a}^{(m)}) \sim 2 \log C + 2H(t_i) \log \left( \frac{m}{N} \right) + \log (\pi_{\mathbf{a}, H(t_i)}(0))$$

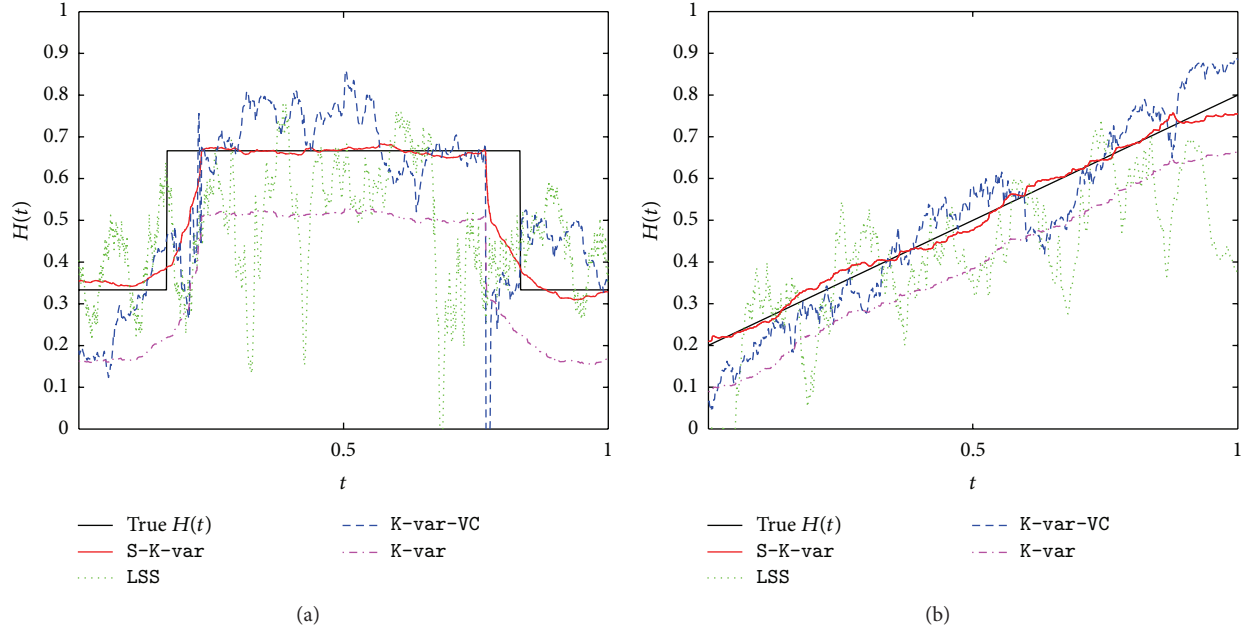


FIGURE 2: Illustrations of the estimators: in panel (a), variance  $C$  was 2; in panel (b), variance  $C$  was 4; the best match to the true  $H(t)$  was the method of S-K-var among the four.

$$= \left[ 1 \quad 2 \log \left( \frac{m}{N} \right) \right] \times \left[ \begin{array}{c} 2 \log C + \log \left( \pi_{\mathbf{a}, H(t_i)}(0) \right) \\ H(t_i) \end{array} \right], \quad (17)$$

which turns out to be linear with respect to  $H(t_i)$  with intercept  $2 \log C$ , if  $\log(\pi_{\mathbf{a}, H(t_i)}(0))$  is negligible. The above regression model possesses a computational advantage though ignoring the presence of noise.

When  $\sigma$  is nonzero, the following least square estimator of  $(\mathbf{H}, C, \sigma)$  is introduced:

$$(\hat{\mathbf{H}}, \hat{C}, \hat{\sigma}) = \arg \min_{(\mathbf{H}, C, \sigma)} \times \sum_{i=1}^d \sum_{m=1}^M \left( \log S(t_i, \mathbf{a}^{(m)}) - \log \mathbb{E} [S(t_i, \mathbf{a}^{(m)})] \right)^2. \quad (18)$$

The computation of the least-square estimator is feasible because, based on (16), for fixed  $C$  as  $C_o$  and  $\sigma$  as  $\sigma_o$ , the computation of  $\mathbf{H}$  is separable into each  $H(t_i)$ . In other words, a solution of  $H(t_i)$  is given by

$$\hat{H}(t_i) = \arg \min_h \times \sum_{m=1}^M \left( \log S'(t_i, \mathbf{a}^{(m)}) - \log \left( C_o^2 \left( \frac{m}{N} \right)^{2h} \pi_{\mathbf{a}, h}(0) + \sigma_o^2 \sum_q a_q^2 \right) \right)^2. \quad (19)$$

Numerical approaches such as the bisection method can be used for the above procedure, which is nonlinear in  $h$ . The bisection method achieves a desired precision level,  $\tau$ , for  $\hat{H}(t_i)$  with the number of iterations greater than  $\log_2 \tau^{-1}$ . In other words, 10 iterations, for example, results in precision  $\tau < 0.001$ .

### 3. Simulations and Comparisons

We present here a simulation study of the performance of the approach suggested in this paper, denoted by S-K-var. Simulation is done with the “known truth” of Hurst function  $H(t)$  the controlled signal variance and the signal-to-noise (SNR) ratio. Test functions are shown in Figure 1 with the *step function* for  $H(t)$  in Figure 1(a) and the *straight-line* function in Figure 1(c). Their illustrations of  $W'(t)$  are shown in Figures 1(b) and 1(d), correspondingly. For the sake of comparison, we chose several popular methods such as the local spectra slope, which is summarized in Gao [21] and denoted by LSS, and  $k$ -variation of variance-uncorrected, denoted by K-var, and the  $k$ -variation of variance-corrected version in Coeurjolly [13], denoted by K-var-VC. The average mean squared error (AMSE) was used as a performance measure to capture the difference between true  $H(t)$  and estimated  $\hat{H}(t)$ . To simulate a sample path from a fBm on  $[0, 1]$ , we used the method of Wood and Chan [22]. One can simulate a standard mBm  $W$  with covariance matrix  $C_{H(\cdot)}$  by generating  $Z \sim N(0, I_N)$  and estimating  $W := C_{H(\cdot)}^{1/2} Z$ . This method is exact in theory and sufficiently fast for a reasonable sample size  $N$ .

In this section we will use the following notations regarding filters: Diff . i denoting the filter of differences of order  $i$ ,



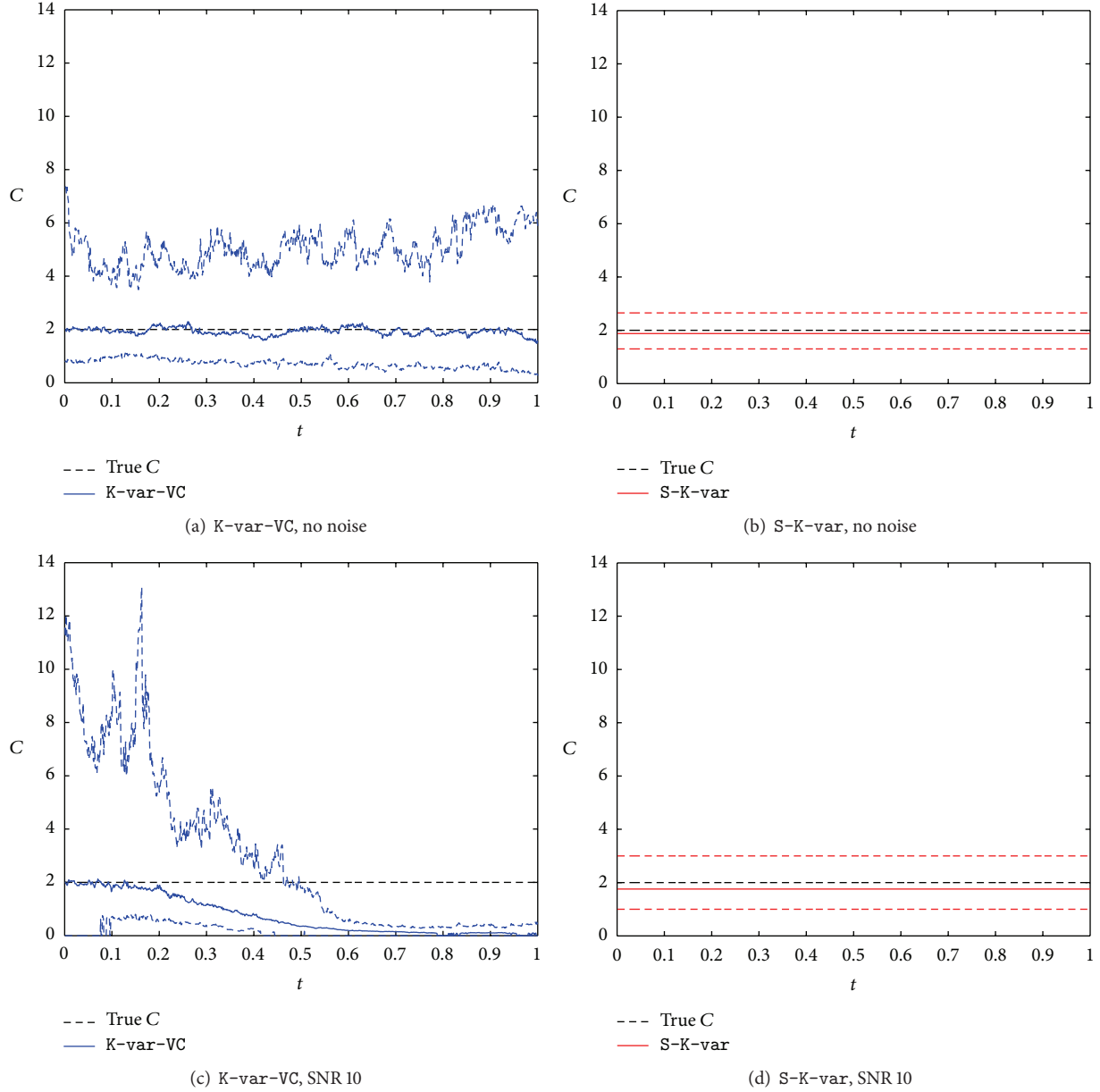


FIGURE 3: Estimation of  $C$  by K-var-VC with empirical 95% confidence intervals in blue is shown in (a) for no noise and (c) for SNR 10 when true  $C = 2$ . Similarly, estimation of  $C$  by S-K-var in red is shown in (b) for no noise and (d) for SNR 10. S-K-var yields more stable and shorter confidence intervals.

Db.  $i$  denoting a Daubechies wavelet filter of order  $i$ , and Sym.  $i$  denoting a Symlet wavelet filter of order  $i$ . We generate 1,000 series of length  $N = 4096$  for step-function  $H(t)$  and  $N = 1024$  for straight-line function  $H(t)$ . A simple difference filter  $[1 \ -2 \ 1]$  (Diff. 2) was used for straight-line  $H(t)$ , and Db. 6 was used for step-function  $H(t)$ . For the local spectra slope of LSS, the length of the subsignal was set to be 512, which is sufficient for its numerical stability, and the two levels, by which spectral slopes are calculated, were 3 and 7. The size of a neighborhood of  $t$ ,  $\nu(t)$  in (8), is set to be 50 for S-K-var, K-var, and K-var-VC.

Illustrations of the estimators under no noise are shown in Figure 2. Estimation by K-var-VC most accurately follows true  $H(t)$  among the tested methods. Estimation results by

K-var, considering no scale parameter  $C$ , notably deviate from true  $H(t)$ . We note that the distance between K-var estimation and true  $H(t)$  relates to  $C$ . Estimators by LSS are bumpy because it assumes that subsignals during its computation follow fBm without considering the variability of  $H(t)$ . We also observe that K-var-VC is more unstable than S-K-var.

Regarding the estimation of  $C$ , the comparison between K-var-VC and S-K-var is shown in Figure 3, in which empirical confidence intervals for true  $C = 2$  are shown with the upper panels for no noise and the lower panels for SNR 10. We sampled 1000 series of  $W'(t)$  with  $C = 2$  and straight-line  $H(t)$  under white noise of SNR 10. Consistently, the estimation results by S-K-var at the right

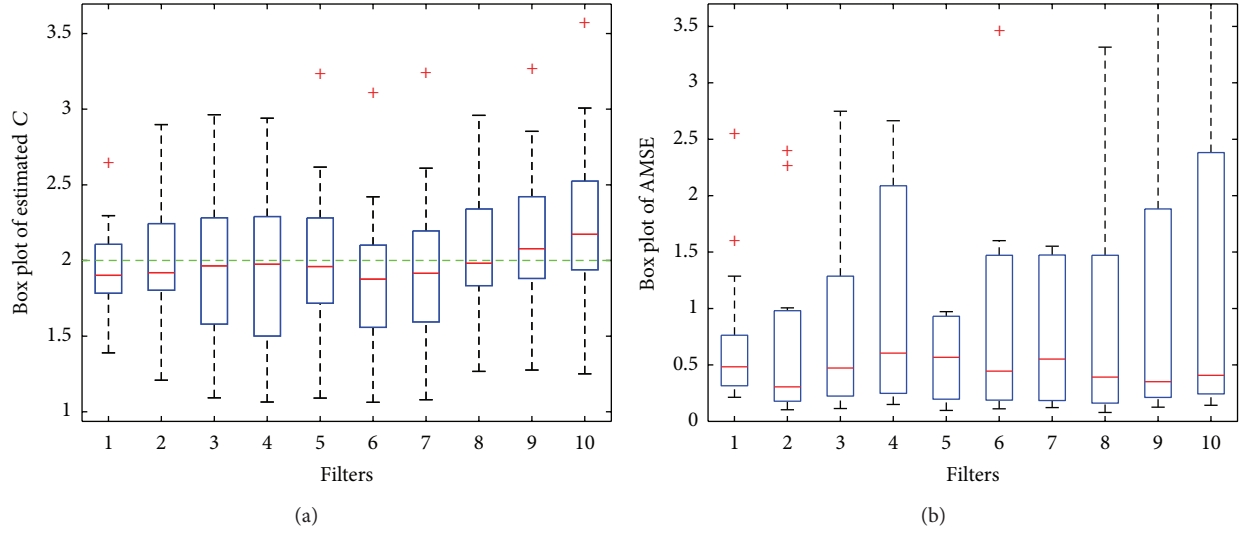


FIGURE 4: Performance according to different filters with straight-line  $H(t)$ ; in panel (a), box plots for estimations of  $C = 2$ ; in (b), box plots for AMSE of  $H(t)$ . Filter numbers represent the following: 1, Diff . 1; 2, Diff . 2; 3, Diff . 3; 4, Diff . 4; 5, Sym . 4; 6, Sym . 6; 7, Sym . 8; 8, Db . 2; 9, Db . 3; and as well as 10, Db . 4.

TABLE 1: Average mean squared error for the S-K-var, K-var-VC, and K-var methods in various settings of variance constant  $C$  and SNR levels based on 1000 sample paths of  $W'(t)$  for each of step-function and straight-line  $H(t)$ . The asterisk marks show that S-K-var outperformed the other methods.

Parameters	Average mean squared error					
	Step-function $H(t)$			Straight-line $H(t)$		
	S-K-var	K-var-VC	K-var	S-K-var	K-var-VC	K-var
$C = 1$ , SNR 10	31.54*	178.6	1071	84.62	215.5	81.31
30	22.85*	89.64	64.59	25.48	147.8	23.53
$\infty$	9.940*	26.31	48.16	.8242*	9.508	.9376
$C = 4$ , SNR 10	15.56*	212.5	82.29	46.16*	176.9	175.2
30	4.406*	152.2	39.91	36.11*	92.07	120.2
$\infty$	.9706*	10.00	8.173	10.04*	24.73	93.21
$C = 10$ , SNR 10	61.80*	178.2	281.5	89.94*	216.5	223.9
30	55.97*	87.35	237.0	42.21*	150.9	144.6
$\infty$	33.86*	26.08	193.1	1.425*	9.288	77.32

panels are more accurate, and their confidence intervals are sharper than those by K-var-VC. We also note that the confidence intervals by S-K-var in Figures 3(b) and 3(d) are constant in time since S-K-var employs a global constant in regression model (16). A noise level of SNR 10 heavily worsened the estimation results by K-var-VC while those by S-K-var yielded a slight increase in the confidence intervals. Accurate estimation of variance level  $C$  by K-var-VC leads to accurate estimation of  $H(t)$ , which will be demonstrated in the following tests.

We compared S-K-var with K-var-VC and K-var in terms of AMSE in various settings. The method LSS was dropped due to obvious poor performance as is shown in Figure 2. We varied the levels of variance  $C$  from 1 to 4 and 10 under SNR levels of 10, 30, and the infinity. The number of sample path  $W'(t)$  was 1000 in each setting, and AMSE was computed for each of the methods. The results are shown in Table 1 for each step-function and straight-line  $H(t)$ . We observe that our proposed method S-K-var

consistently outperforms the other methods except for only a few settings. Overall, there was little difference between K-var-VC and K-var in performance. This experimental result is not surprising since S-K-var reflects the existence of white noise and globally includes variance constant  $C$ .

The effects of adapted filters are summarized in Figure 4. The experiments were done with straight-line  $H(t)$ , variance  $C = 2$ , and SNR = 7. We observe that the performance of S-K-var on the estimation of  $C$  does not change much depending on the filter it uses. However, we mention that the variance of AMSEs tends to increase according to the filter size.

## 4. Conclusion

To conclude, we proposed the joint estimators of the time-changing Hurst exponent  $H(t)$  and its variance coefficient  $C$  for mBm under white noise. The proposed method is based on filtering sampled paths with dilated high-pass

filters to derive regularity conditions at associated scales. The second empirical moment, average squared energy, of the filtered signals near a time position is connected to the theoretical expectation and used to establish a regression setup through the asymptotic distribution of multiscale local variation statistics. The effectiveness of the approach was verified through numerical experiments that compared it with that of several other approaches. Simulation results show that the proposed approach yields more precise and stable estimation of Hurst exponents and variance constants under noiseless or noised conditions.

## Appendices

### A. Proof of Proposition 1

Let  $G(t)$  denote  $C\sqrt{K(2H(t))/2}$  for the sake of simplicity. Then, the covariance  $\mathbb{E}[V'_a(j_1/N)V'_a(j_2/N)]$  becomes, by  $u = \lambda/N$ ,

$$\begin{aligned} & \sum_{p,q} a_p a_q \left( G\left(\frac{j_1-p}{N}\right) G\left(\frac{j_2-q}{N}\right) \right. \\ & \quad \times \int \frac{\exp(\mathbf{i}((j_1-p)/N)\lambda) - 1}{|\lambda|^{H((j_1-p)/N)+1/2}} \\ & \quad \times \frac{\exp(-\mathbf{i}((j_2-q)/N)\lambda) - 1}{|\lambda|^{H((j_2-q)/N)+1/2}} d\lambda \\ & \quad \left. + \sigma^2 \mathbb{E} \left[ \varepsilon \left( \frac{j_1-p}{N} \right) \varepsilon \left( \frac{j_2-q}{N} \right) \right] \right) \\ &= \sum_{p,q} a_p a_q \frac{G((j_1-p)/N) G((j_2-q)/N)}{N^{H((j_1-p)/N)+H((j_2-q)/N)}} \\ & \quad \times \int \frac{\exp(\mathbf{i}(j_1-p)u) - 1}{|u|^{H((j_1-p)/N)+1/2}} \times \frac{\exp(-\mathbf{i}(j_2-q)u) - 1}{|u|^{H((j_2-q)/N)+1/2}} du \\ & \quad + \sigma^2 \sum_{p-q=j_1-j_2} a_p a_q. \end{aligned} \quad (\text{A.1})$$

By Taylor's expansion and Hölderian order  $\eta$  of  $H(t)$ , for  $j_1-p$  in the neighborhood of  $t_1$  we approximate  $G((j_1-p)/N)$  with

$$\begin{aligned} G\left(\frac{j_1-p}{N}\right) &= G(t_1) + \mathcal{O}\left(\left|H\left(\frac{j_1-p}{N}\right) - H(t_1)\right|\right) \\ &= G(t_1) + \mathcal{O}(\epsilon^\eta). \end{aligned} \quad (\text{A.2})$$

Similarly,  $G((j_2-q)/N)$  is approximated with  $G((j_2-q)/N) = G(t_2) + \mathcal{O}(\epsilon^\eta)$ . In addition, by Taylor's expansion

of  $N^x/\log(N)N^k$  around the point  $k$ ,  $N^x/\log(N)N^k = 1/\log(N) + \mathcal{O}(|x-k|)$ , we have

$$\begin{aligned} \frac{1}{N^{H((j_1-p)/N)+H((j_2-q)/N)}} &= \frac{1}{N^{H(t_1)+H(t_2)}} (1 + \mathcal{O}(\epsilon^\eta \log N)), \\ \frac{1}{|u|^{H((j_1-p)/N)+H((j_2-q)/N)}} &= \frac{1}{|u|^{H(t_1)+H(t_2)}} (1 + \mathcal{O}(\epsilon^\eta \log u)). \end{aligned} \quad (\text{A.3})$$

Using also  $\epsilon^\eta \rightarrow 0$  as  $N$  goes to infinity, the covariance can be written as follows:

$$\begin{aligned} & \sum_{p,q} a_p a_q \frac{G(t_1) G(t_2)}{N^{H(t_1)+H(t_2)}} \\ & \quad \times \int \frac{\exp(\mathbf{i}(j_1-p)u) - 1}{|u|^{H(t_1)+1/2}} \times \frac{\exp(-\mathbf{i}(j_2-q)u) - 1}{|u|^{H(t_2)+1/2}} du \\ & \quad + \sigma^2 \sum_{p-q=j_1-j_2} a_p a_q + \mathcal{O}(\epsilon^\eta \log N). \end{aligned} \quad (\text{A.4})$$

Since the order of filter  $\mathbf{a}$  is at least 1,  $\sum_q a_q = 0$ , (A.4) becomes

$$\begin{aligned} & \sum_{p,q} a_p a_q \frac{G(t_1) G(t_2)}{N^{H(t_1)+H(t_2)}} \int \frac{\cos((j_1-p-j_2+q)u) - 1}{|u|^{H(t_1)+H(t_2)+1}} du \\ & \quad + \sigma^2 \sum_{p-q=j_1-j_2} a_p a_q + \mathcal{O}(\epsilon^\eta \log N). \end{aligned} \quad (\text{A.5})$$

Since  $K(\alpha) \int ((1 - \cos(\kappa u))/|u|^{\alpha+1}) du = |\kappa|^\alpha$ , for all  $\kappa$ ,  $0 < \alpha < 2$ ,

$$\begin{aligned} \mathbb{E} \left[ V'_a \left( \frac{j_1}{N} \right) V'_a \left( \frac{j_2}{N} \right) \right] &= - \sum_{p,q} a_p a_q \frac{G(t_1) G(t_2)}{N^{H(t_1)+H(t_2)}} \\ & \quad \times \frac{|j_1-p-j_2+q|^{H(t_1)+H(t_2)}}{K(H(t_1)+H(t_2))} \\ & \quad + \sigma^2 \sum_{p-q=j_1-j_2} a_p a_q + \mathcal{O}(\epsilon^\eta \log N) \\ &= - \frac{C^2 g(H(t_1), H(t_2))}{N^{H(t_1)+H(t_2)}} \\ & \quad \times \sum_{p,q} \frac{a_p a_q}{2} |j_1-p-j_2+q|^{H(t_1)+H(t_2)} \\ & \quad + \sigma^2 \sum_{p-q=j_1-j_2} a_p a_q + \mathcal{O}(\epsilon^\eta \log N) \\ &= \frac{C^2 g(H(t_1), H(t_2))}{N^{H(t_1)+H(t_2)}} \\ & \quad \times \pi_{\mathbf{a}, H(t_1)/2+H(t_2)/2}(j_1-j_2) \\ & \quad + \sigma^2 \sum_{p-q=j_1-j_2} a_p a_q + \mathcal{O}(\epsilon^\eta \log N), \end{aligned} \quad (\text{A.6})$$

where  $\pi_{a,h}(k) = -(1/2) \sum_{p,q=0}^l a_p a_q |k - p + q|^{2h}$ . When we replace  $\mathbf{a}$  with  $\mathbf{a}^{(m)}$ , the proof is completed.

## B. Proof of Proposition 2

Let  $A$  and  $B$  denote, respectively,

$$A = \frac{1}{|\nu(t)|} \sum_{j \in \nu(t)} \sum_{p,q}^l a_p a_q W\left(\frac{j-p}{N}\right) \varepsilon\left(\frac{j-q}{N}\right), \quad (\text{B.1})$$

$$B = \frac{1}{|\nu(t)|} \sum_{j \in \nu(t)} \left( \sum_q^l a_q \varepsilon\left(\frac{j-q}{N}\right) \right)^2.$$

Then  $\log S'(t, \mathbf{a})$  can be written as

$$\begin{aligned} \log S'(t, \mathbf{a}) &= \log \frac{1}{|\nu(t)|} \sum_{j \in \nu(t)} V'_a\left(\frac{j}{N}\right)^2 \\ &= \log \frac{1}{|\nu(t)|} \\ &\quad \times \sum_{j \in \nu(t)} \left( \left( \sum_q^l a_q W\left(\frac{j-q}{N}\right) \right)^2 \right. \\ &\quad \left. + 2\sigma \sum_{p,q}^l a_p a_q W\left(\frac{j-p}{N}\right) \varepsilon\left(\frac{j-q}{N}\right) \right. \\ &\quad \left. + \sigma^2 \left( \sum_q^l a_q \varepsilon\left(\frac{j-q}{N}\right) \right)^2 \right) \\ &= \log S(t, \mathbf{a}) + \left( 2\sigma \frac{A}{S(t, \mathbf{a})} + \sigma^2 \frac{B}{S(t, \mathbf{a})} \right) \\ &\quad \times (1 + o(1)) \end{aligned} \quad (\text{B.2})$$

by Taylor's expansion of  $\log(1+x) = x(1+o(1))$  near  $x=0$ . Similarly,  $\log \mathbb{E}[S'(t, \mathbf{a})]$  is expressed as

$$\begin{aligned} \log \mathbb{E}[S'(t, \mathbf{a})] &= \log \left( \mathbb{E}[S(t, \mathbf{a})] + \sigma^2 \sum_q^l a_q^2 \right) \\ &= \log(\mathbb{E}[S(t, \mathbf{a})]) + \left( \frac{\sigma^2 \sum_q^l a_q^2}{\mathbb{E}[S(t, \mathbf{a})]} \right) \quad (\text{B.3}) \\ &\quad \times (1 + o(1)). \end{aligned}$$

Using independence of  $W(t)$  and  $\varepsilon(t)$ , the property of white noise  $\varepsilon(t)$ , and the convergence of  $S(t, \mathbf{a})$  to  $\mathbb{E}[S(t, \mathbf{a})]$  almost surely as  $N \rightarrow \infty$ , we approximate  $A \rightarrow 0$ ,  $B \rightarrow \sum_q^l a_q^2$ , and  $\sigma^2(B/S(t, \mathbf{a})) \rightarrow \sigma^2(\sum_q^l a_q^2/\mathbb{E}[S(t, \mathbf{a})])$ . Then the

difference between  $\log S'(t, \mathbf{a})$  in (B.2) and  $\log \mathbb{E}[S'(t, \mathbf{a})]$  in (B.3) becomes

$$\begin{aligned} &\log S'(t, \mathbf{a}) - \log \mathbb{E}[S'(t, \mathbf{a})] \\ &= \log S(t, \mathbf{a}) - \log \mathbb{E}[S(t, \mathbf{a})] + o(1) \\ &= \log \left( \frac{1}{|\nu(t)|} \sum_{j \in \nu(t)} \frac{V_a(j/N)^2}{\mathbb{E}[S(t, \mathbf{a})]} \right) + o(1) \\ &\quad (\text{by the definition of } S(t, \mathbf{a})) \\ &= \log \left( \frac{1}{|\nu(t)|} \sum_{j \in \nu(t)} \frac{V_a(j/N)^2}{\mathbb{E}[V_a(j/N)^2]} \right) + o(1) \quad (\text{B.4}) \\ &\quad (\text{by the stationarity of } V_a) \\ &= \left( \left( \frac{1}{|\nu(t)|} \sum_{j \in \nu(t)} \frac{V_a(j/N)^2}{\mathbb{E}[V_a(j/N)^2]} \right) - 1 \right) (1 + o(1)) \\ &\quad (\text{by Taylor's expansion}) \\ &= V(t, \mathbf{a}) (1 + o(1)). \end{aligned}$$

## Conflict of Interests

The authors declare that there is no conflict of interests regarding the publication of this paper.

## Acknowledgments

This research was provided by Hanyang University (201300000001465). The authors give special thanks to Brani Vidakovic and Jean-Francois Coeurjolly for their careful comments.

## References

- [1] B. B. Mandelbrot and J. W. Van Ness, "Fractional Brownian motions, fractional noises and applications," *SIAM Review*, vol. 10, pp. 422–437, 1968.
- [2] M. Li, Y. Chen, J. Y. Li, and W. Zhao, "Hölder scales of sea level," *Mathematical Problems in Engineering*, vol. 2012, Article ID 863707, 22 pages, 2012.
- [3] S. V. Muniandy, S. C. Lim, and R. Murugan, "Inhomogeneous scaling behaviors in Malaysian foreign currency exchange rates," *Physica A*, vol. 301, no. 1–4, pp. 407–428, 2001.
- [4] R. H. Riedi, M. S. Crouse, V. J. Ribeiro, and R. G. Baraniuk, "A multifractal wavelet model with application to network traffic," *IEEE Transactions on Information Theory*, vol. 45, no. 3, pp. 992–1018, 1999.
- [5] M. Li, W. Zhao, and S. Chen, "mBm-based scalings of traffic propagated in internet," *Mathematical Problems in Engineering*, vol. 2011, Article ID 389803, 21 pages, 2011.
- [6] M. Li and W. Zhao, "Quantitatively investigating locally weak stationarity of modified multifractional gaussian noise," *Physica A*, vol. 391, no. 24, pp. 6268–6278, 2012.

- [7] J. Lévy-Véhel and R. Peltier, "Multifractional brownian motion: definition and preliminary results," *Rapport de Recherche de l'INRIA* n2645, 1995.
- [8] A. Benassi, S. Cohen, and J. Istas, "Identifying the multifractional function of a gaussian process," *Statistics & Probability Letters*, vol. 39, no. 4, pp. 337–345, 1998.
- [9] S. C. Lim and S. V. Muniandy, "On some possible generalizations of fractional Brownian motion," *Physics Letters. A*, vol. 266, no. 2-3, pp. 140–145, 2000.
- [10] S. V. Muniandy and S. C. Lim, "Modeling of locally self-similar processes using multifractional brownian motion of Riemann-Liouville type," *Physical Review E*, vol. 63, no. 4, pp. 461041–461047, 2001.
- [11] J. Istas and G. Lang, "Quadratic variations and estimation of the local Hölder index of a Gaussian process," *Annales de l'Institut Henri Poincaré B*, vol. 33, no. 4, pp. 407–436, 1997.
- [12] J. T. Kent and A. T. A. Wood, "Estimating the fractal dimension of a locally self-similar gaussian process by using increments," *Journal of the Royal Statistical Society B*, vol. 59, no. 3, pp. 679–699, 1997.
- [13] J. F. Coeurjolly, "Estimating the parameters of a fractional brownian motion by discrete variations of its sample paths," *Statistical Inference for Stochastic Processes*, vol. 4, no. 2, pp. 199–227, 2001.
- [14] M. Fhima, A. Guillin, and P. R. Bertrand, "Fast change point analysis on the Hurst index of piecewise fractional Brownian motion," <http://arxiv.org/abs/1103.4029>.
- [15] J. Beran, *Statistics for Long-Memory Processes*, vol. 61 of *Monographs on Statistics and Applied Probability*, Chapman & Hall, London, UK, 1994.
- [16] J.M. Bardet and P. Bertrand, "Definition, properties and wavelet analysis of multiscale fractional Brownian motion," *Fractals*, vol. 15, no. 1, pp. 73–87, 2007.
- [17] J.F. Coeurjolly, "Identification of multifractional brownian motion," *Bernoulli*, vol. 11, no. 6, pp. 987–1008, 2005.
- [18] A. Shapiro, "Statistical inference of moment structures," in *Handbook of Latent Variable and Related Models*, pp. 229–260, 2007.
- [19] I. Daubechies, *Ten Lectures on Wavelets*, vol. 61 of *CBMS-NSF Regional Conference Series in Applied Mathematics*, SIAM, Philadelphia, Pa, USA, 1992.
- [20] B. Vidakovic, *Statistical Modeling by Wavelets*, Wiley Series in Probability and Statistics: Applied Probability and Statistics, John Wiley & Sons, Hoboken, NJ, USA, 1999.
- [21] J. Gao, *Multiscale Analysis of Complex Time Series: Integration of Chaos and Random Fractal Theory, and Beyond*, John Wiley & Sons, Hoboken, NJ, USA, 2007.
- [22] A. Wood and G. Chan, "Simulation of stationary gaussian processes in  $[0, 1]$  d," *Journal of Computational and Graphical Statistics*, vol. 3, no. 4, pp. 409–432, 1994.



## Research Article

# A Reconfigurable Logic Cell Based on a Simple Dynamical System

**Lixiang Li,<sup>1,2,3</sup> Chunyu Yang,<sup>2</sup> Sili Hui,<sup>2</sup> Wenwen Yu,<sup>2</sup> Jürgen Kurths,<sup>4</sup> Haipeng Peng,<sup>2</sup> and Yixian Yang<sup>5</sup>**

<sup>1</sup> Institute of Network Coding, The Chinese University of Hong Kong, Shatin N.T., Hong Kong

<sup>2</sup> Information Security Center, State Key Laboratory of Networking and Switching Technology, Beijing University of Posts and Telecommunications, P.O. Box 145, Beijing 100876, China

<sup>3</sup> Shenzhen Research Institute, The Chinese University of Hong Kong, Shenzhen 518063, China

<sup>4</sup> Potsdam Institute for Climate Impact Research, 14473 Potsdam, Germany

<sup>5</sup> School of Information Engineering, Beijing Institute of Graphic Communication, Beijing 102600, China

Correspondence should be addressed to Lixiang Li; [li.lixiang2006@163.com](mailto:li.lixiang2006@163.com)

Received 21 June 2013; Accepted 7 July 2013

Academic Editor: Ming Li

Copyright © 2013 Lixiang Li et al. This is an open access article distributed under the Creative Commons Attribution License, which permits unrestricted use, distribution, and reproduction in any medium, provided the original work is properly cited.

This paper introduces a new scheme to achieve a dynamic logic gate which can be adjusted flexibly to obtain different logic functions by adjusting specific parameters of a dynamical system. Based on graphical tools and the threshold mechanism, the distribution of different logic gates is studied, and a transformation method between different logics is given. Analyzing the performance of the dynamical system in the presence of noise, we discover that it is resistant to system noise. Moreover, we find some part of the system can be considered as a leaky integrator which has been already widely applied in engineering. Finally, we provide a proof-of-principle hardware implementation of the proposed scheme to illustrate its effectiveness. With the proposed scheme in hand, it is convenient to build the flexible, robust, and general purpose computing devices such as various network coding routers, communication encoders or decoders, and reconfigurable computer chips.

## 1. Introduction

For years, the construction of integrated circuits has required a vast amount of time and money for combining different logic gates. In 1985, when the first field-programmable gate array (FPGA) was introduced to the world, the era of reusable “field-programming” began which led to a more flexible implementation of integrated circuits. However, the speed of an FPGA reconfigurable scheme is typically slow, since it needs some time for “rewiring” [1].

In 1998, a novel way of configuring dynamic logic gates was introduced by Sinha and Ditto [2]. Based on a threshold mechanism and chaotic maps, they proposed a scheme to construct dynamic computing systems with flexible logic functions. Their method permitted faster switching (typically within only 0.5 clock cycle) between any two kinds of logics. Nowadays, more schemes have been conducted to construct

new types of dynamic logic gates, including synchronization of a nonlinear system [3] as well as the interplay of square waves and noise [4]. Recently, piecewise linear systems were also suggested to construct the dynamic logic architecture [5]. The development of dynamic computing has brought about the appearance of commercial chaotic computer [6].

In this work, we propose a scheme to obtain dynamic logic functions by controlling simple dynamical systems. Based on the threshold mechanism, we give a transformation method between different logics and analyze its antinoise and time-delay characteristics. We find that the scheme is robust to system noise. Furthermore, the main part of the system can be designed based on the leaky integrator which has been applied into different research fields, such as in neuronal or cell analysis and filters related to signal processing. Finally, the scheme is proved to be effective by simulation results of a logic gate circuit.

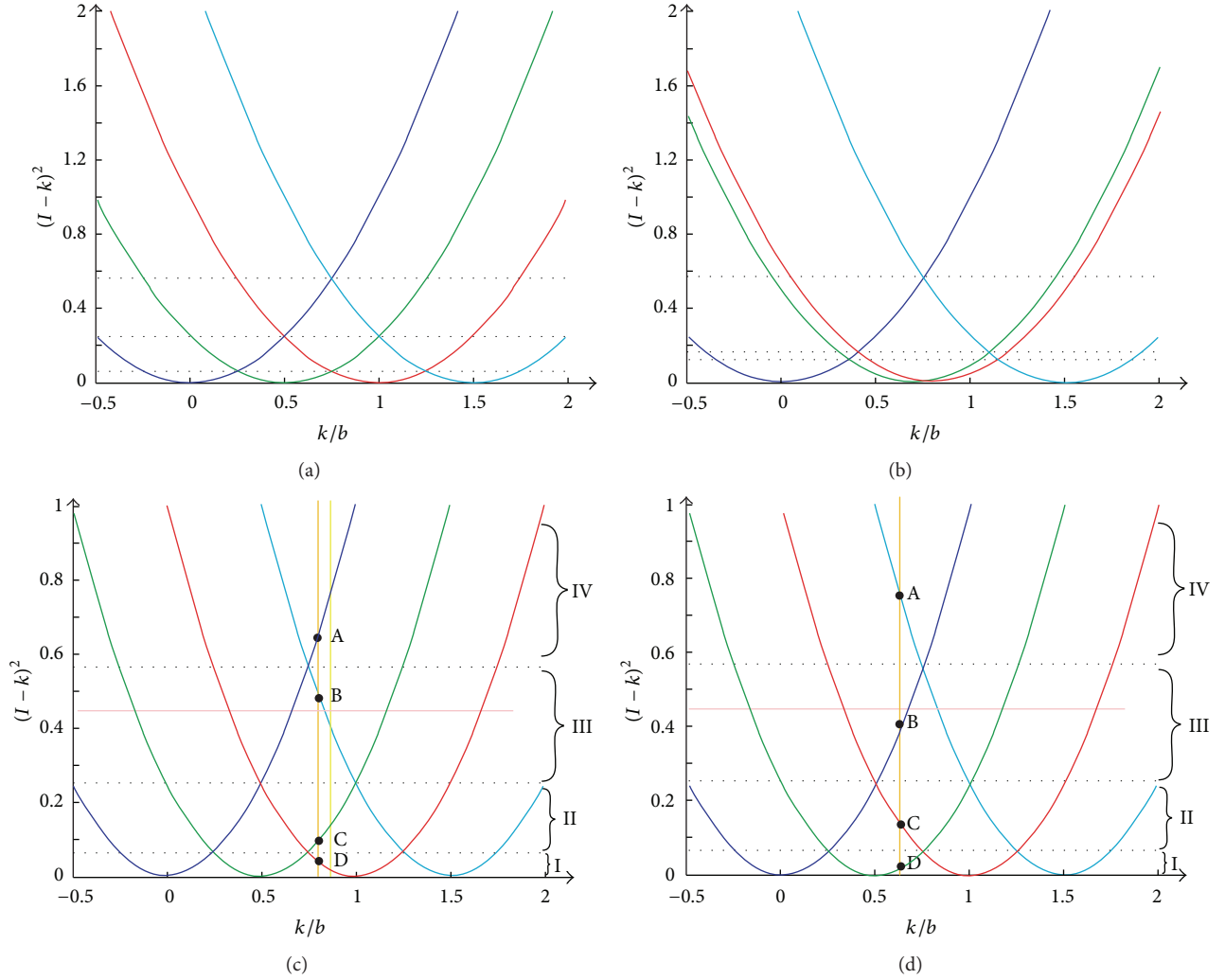


FIGURE 1: (Color online) the judging method of the system output, where the navy blue, green, red, and baby blue lines represent the situations of inputs (0, 0), (0, 1), (1, 0), and (1, 1), respectively.

## 2. A Scheme of Dynamic Logic Gate

We now propose a new method to change the function of a logic gate flexibly by altering only one parameter or two specific parameters. The formula of its implementation is

$$\dot{x} = -px + p(I - k)^2, \quad (1)$$

where  $x$  is the state of system (1),  $I$  is the input of the logic gate,  $p > 1$  determines the convergence rate of the system, and  $k$  is the control parameter to achieve a transformation between different logics.

When system (1) is stable, its state  $x$  will converge to the constant as follows:

$$x = (I - k)^2. \quad (2)$$

Based on the threshold mechanism introduced by Murali et al. [4], the output of the logic gate can be determined by

$$I_{\text{out}} = 0 \quad \text{if } x < \beta; \quad I_{\text{out}} = 1 \quad \text{else.} \quad (3)$$

To implement the dynamic logics, the most significant step is to set  $p$ ,  $k$ , and  $\beta$  based on some specific applications. A general situation will be discussed in this paper.

## 3. Explanation and Discussion of the Proposed Scheme

Typically, we consider that a logic gate has two inputs and one output, for example, we suppose that

$$I = a \cdot I_0 + b \cdot I_1, \quad (4)$$

where  $I_0$  and  $I_1$  are two logic inputs being either 0 or 1, and  $a$  and  $b$  are the parameters.  $(I_0, I_1)$  has four possible values. The relationship between the inputs and the output is shown in Table 1.

Figure 1(a) shows the situation of  $b = 2a$ , while in Figure 1(b),  $a$  and  $b$  do not have to have any relationships. We can see that both Figures 1(a) and 1(b) can be divided into four logical areas based on the intersections among these four

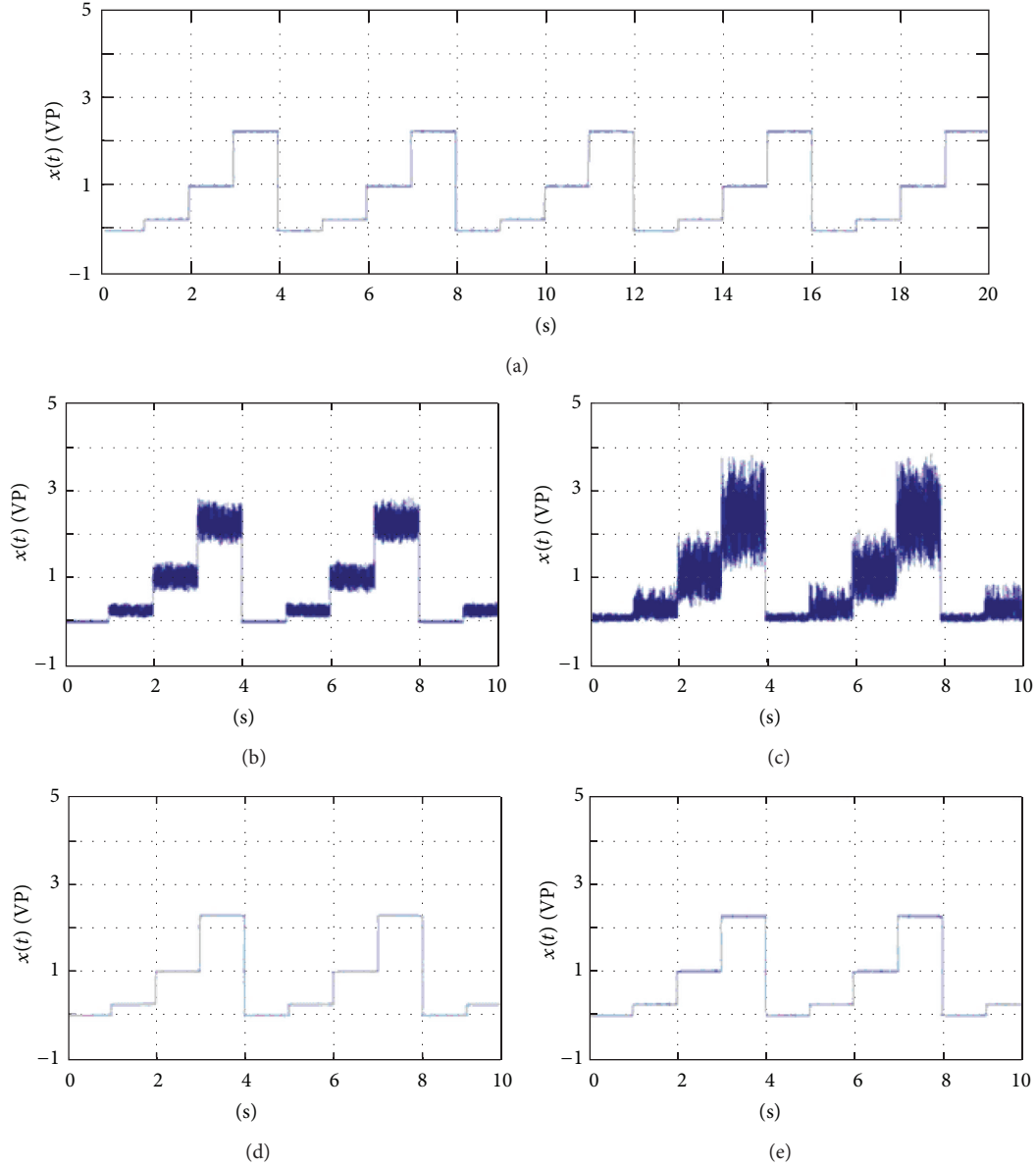


FIGURE 2: (Color online) the influences of input and system noises on the performance of the system, where (a) in a noiseless case; (b) in the presence of input noise whose range is  $[-0.2, +0.2]$  V; (c) in the presence of input noise whose range is  $[-0.5, +0.5]$  V; (d) in the presence of system noise whose range is  $[-0.5, +0.5]$  V; and (e) in the presence of system noise whose range is  $[-10, +10]$  V.

TABLE 1: The relationship between the inputs and the output.

(a) For arbitrary $a$ and $b$				
Input 0	0	0	1	1
Input 1	0	1	0	1
Output	0	$b$	$a$	$a + b$
(b) For $b = 2a$				
Input 0	0	0	1	1
Input 1	0	1	0	1
Output	0	$2a$	$a$	$3a$

curves, which states that there are four possible ranges for the threshold  $\beta$ . Similarly, it can be easily concluded that when  $b = 2a$  or  $a = 2b$ , possible logic functions can be uniformly distributed along the  $k$ -axis. Hence, when  $b = 2a$  or  $a = 2b$ , the logic values are clearly determined, and a confusion is less likely to occur. To simplify the problem and avoid some confusion,  $b = 2a$  will be used in this paper. Then, the value of  $I$  is simply  $I = a \cdot (I_0 + 2I_1)$ .

Figures 1(c)-1(d) show the judging method for the system output, where the logic value of the system is determined by a curve intersection method, for example, different points in these figures show different states of the system, and the

TABLE 2: All available logic gates for the system.

Region	$\beta$	$k/a$	Logic gate
I	$(0, \frac{1}{16}]$	$(-\infty, -\sqrt{\beta})$	1
		$(-\sqrt{\beta}, \sqrt{\beta})$	OR
		$(\sqrt{\beta}, \frac{1}{2} - \sqrt{\beta})$	1
		$(\frac{1}{2} - \sqrt{\beta}, \frac{1}{2} + \sqrt{\beta})$	$I_1 + I'_0$
		$(\frac{1}{2} + \sqrt{\beta}, 1 - \sqrt{\beta})$	1
		$(1 - \sqrt{\beta}, 1 + \sqrt{\beta})$	$I'_1 + I_0$
		$(1 + \sqrt{\beta}, \frac{3}{2} - \sqrt{\beta})$	1
		$(\frac{3}{2} - \sqrt{\beta}, \frac{3}{2} + \sqrt{\beta})$	NAND
II	$(\frac{1}{16}, \frac{1}{4}]$	$(\frac{3}{2} + \sqrt{\beta}, +\infty)$	1
		$(-\infty, -\sqrt{\beta})$	1
		$(-\sqrt{\beta}, \frac{1}{2} - \sqrt{\beta})$	OR
		$(\frac{1}{2} - \sqrt{\beta}, \sqrt{\beta})$	$I_1$
		$(\sqrt{\beta}, 1 - \sqrt{\beta})$	$I_1 + I'_0$
		$(1 - \sqrt{\beta}, \frac{1}{2} + \sqrt{\beta})$	XNOR
		$(\frac{1}{2} + \sqrt{\beta}, \frac{3}{2} - \sqrt{\beta})$	$I'_1 + I_0$
		$(\frac{3}{2} - \sqrt{\beta}, 1 + \sqrt{\beta})$	$I'_1$
III	$(\frac{1}{4}, \frac{9}{16}]$	$(1 + \sqrt{\beta}, \frac{2}{3} + \sqrt{\beta})$	NAND
		$(\frac{2}{3} + \sqrt{\beta}, +\infty)$	1
		$(-\infty, -\sqrt{\beta})$	1
		$(-\sqrt{\beta}, \frac{1}{2} - \sqrt{\beta})$	OR
		$(\frac{1}{2} - \sqrt{\beta}, 1 - \sqrt{\beta})$	$I_1$
		$(1 - \sqrt{\beta}, \sqrt{\beta})$	AND
		$(\sqrt{\beta}, \frac{3}{2} - \sqrt{\beta})$	XNOR
		$(\frac{3}{2} - \sqrt{\beta}, \frac{1}{2} + \sqrt{\beta})$	NOR
		$(\frac{1}{2} + \sqrt{\beta}, 1 + \sqrt{\beta})$	$I'_1$
		$(1 + \sqrt{\beta}, \frac{3}{2} + \sqrt{\beta})$	NAND
		$(\frac{3}{2} + \sqrt{\beta}, +\infty)$	1

TABLE 2: Continued.

Region	$\beta$	$k/a$	Logic gate
IV	$(\frac{9}{16}, +\infty)$	$(-\infty, -\sqrt{\beta})$	1
		$(-\sqrt{\beta}, \frac{1}{2} - \sqrt{\beta})$	OR
		$(\frac{1}{2} - \sqrt{\beta}, 1 - \sqrt{\beta})$	$I_1$
		$(1 - \sqrt{\beta}, \frac{3}{2} - \sqrt{\beta})$	AND
		$(\frac{3}{2} - \sqrt{\beta}, \sqrt{\beta})$	0
		$(\sqrt{\beta}, \frac{1}{2} + \sqrt{\beta})$	NOR
		$(\frac{1}{2} + \sqrt{\beta}, 1 + \sqrt{\beta})$	$I'_1$
		$(1 + \sqrt{\beta}, \frac{3}{2} + \sqrt{\beta})$	NAND
		$(\frac{3}{2} + \sqrt{\beta}, +\infty)$	1

functionality of the system can be altered by changing  $k$ . For each case of these four possible ranges of  $\beta$ , when  $k$  is known, the logic value can be determined. For example, when  $1/4 \leq \beta < 9/16$ , for  $\sqrt{\beta} < k < 2/3 - \sqrt{\beta}$  and  $1 - \sqrt{\beta} < k < \sqrt{\beta}$ , which are shown in Figures 1(c)-1(d), respectively. There are four intersection points between the straight line of  $k$  and these four curves. In Figure 1(c), since the values of point A and point B are higher than that of  $\beta$ , we get  $I_{\text{out}} = 1$  by (3); similarly, since the values of point C and point D are lower than that of  $\beta$ , we get  $I_{\text{out}} = 0$ . Hence, for inputs (0, 0) and (1, 1), the output is 1; while for inputs (0, 1) and (1, 0), the output is 0. The corresponding logic gate is an XNOR gate. Similarly, for Figure 1(d), the output for input (1, 1) is 1 and that for inputs (0, 0), (0, 1), and (1, 0), is 0. That is, the function of AND gate is achieved. It is worth noting that the transformation from XNOR gate to AND can be realized by only changing the control parameter  $k$ .

By a similar analytical method, all the logic gates can be achieved by the proposed scheme as summarized in Table 2. It is clearly seen that, by only altering the value of  $k$ , eight types of logic gates can be achieved. For example, when  $\beta \in (1/16, 1/4]$ , the possible logic functions that can be achieved are 1, OR,  $I_1$ ,  $I_1 + I'_0$ , XNOR,  $I'_1 + I_0$ ,  $I'_1$ , NAND.

**3.1. Analysis in the Presence of Noise.** In reality, noise is unavoidable. Generally, there are two types of noise: input noise and system noise. Figure 2(a) shows the output results of system without noise. When the system is added with input noise, then  $\dot{x} = -px + p(I + D\eta(t) - k)^2$ , and its steady state is

$$x = [I + D\eta(t) - k]^2, \quad (5)$$

where  $\eta(t)$  is the additive white Gaussian noise (AWGN) and  $D$  is its intensity. Figures 2(b)-2(c) show the simulation results

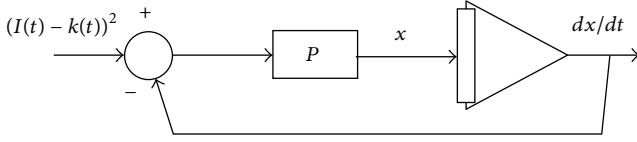


FIGURE 3: The system block diagram of a leaky integrator.

in the presence of input noise, where (b) the noise range is  $[-0.2, +0.2]$  V and (c) the noise range is  $[-0.5, +0.5]$  V. It can be clearly seen that when the input noise increases, the system becomes more fluctuating.

When the system is added with system noise, then  $\dot{x} = -px + p(I - k)^2 + D\eta(t)$ , and the steady state of the system is

$$x = [I - k]^2 + \frac{D\eta(t)}{p}. \quad (6)$$

Figures 2(d)-2(e) show the simulation results in the presence of system noise, where (d) the noise range is  $[-0.5, +0.5]$  V and (e) the noise range is  $[-10, +10]$  V. We can see from Figures 2(d)-2(e) that the system is strongly resistant to system noise which is one of its most important advantage. Therefore, if we want to build a robust logic gate, then we should put the best effort to minimize the input noise.

**3.2. Analysis of Delay.** The parameter  $p$  has an important influence on the response time of the system. The system equation  $\dot{x} = -px + p(I - k)^2$  can be rearranged into

$$\frac{1}{p} \cdot \frac{dx}{dt} = -x(t) + (I(t) - k(t))^2. \quad (7)$$

Hence, we can obtain a system of a leaky integrator whose block diagram is shown in Figure 3. It was proposed as a vital digital signal processing filter which has been very popular in different areas. It has been used to investigate biological and artificial learning processes. Moreover, its famous application in neuron network has made the computation much easier and more powerful [7]. The system here is applicable to study further details in timing and delays.

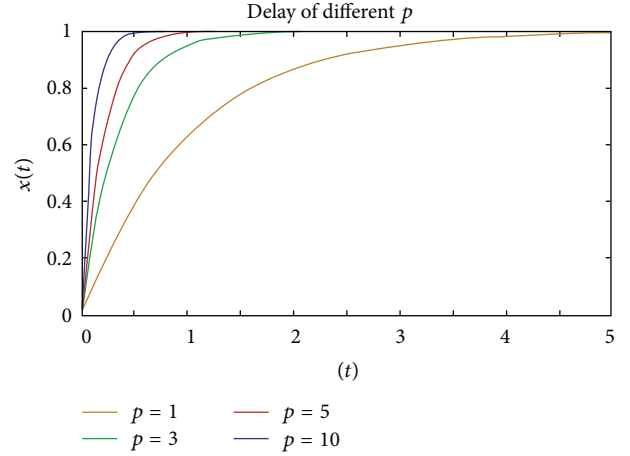
Note that  $1/p$  is the time constant of the system. Then, we get from (7)

$$x(t) = e^{-t/\tau} x(0) + p \int_0^t e^{-p(t-\tau)} (I(t-\tau) - k(t-\tau))^2 d\tau. \quad (8)$$

If  $(I(t) - k(t))^2$  is defined as a constant (e.g.,  $C$ ), then the relationship between  $p$  and  $x(t)$  is

$$x(t) = e^{-pt} x(0) + C(1 - e^{-pt}). \quad (9)$$

Figure 4 shows the evolution of  $x(t)$  as  $p = 1, 3, 5, 10$ . We can see from Figure 4 that the larger the value of  $p$  is, the shorter the time lag to reach a constant result is, or the more accurate the desired output is. If  $p$  is very small, the system may not fully response to an input and cannot reach a stable state before the next input starts. This indicates that

FIGURE 4: (Color online) the evolution of  $x(t)$  as  $p = 1, 3, 5, 10$ , respectively.

the response time of each transformation will be longer than the output intervals, and errors will occur. Therefore, we can say that larger  $p$  means a faster response time and a more accurate output. However, it is not the larger the better. In practice, larger  $p$  also means higher energy-consuming amplifier. Users should design a system based on specific applications to make the system work more effectively.

**3.3. Circuit Implementation.** The physical implementation of a logic cell is an important step for successful applications [8, 9]. Figure 5 shows the equivalent circuit of system (1) by simulation with multisim software.

In Figure 5, there are two parts which are the computation part and the judgment one serving for computing the solution of system (1) as well as judging whether the solution exceeds the threshold, respectively. The left part of Figure 5 corresponds to the computation part in which there are two subtractors, one multiplexer, one amplifier, and one integrator. The right part of Figure 5 corresponds to the judgment one in which there is an operational amplifier serving as the voltage comparator. For subtractor 1, the output is  $V_t = I_0 + 2I_1 - k$  and, for subtractor 2, the output is  $(I - k)^2 - x$ . For the voltage comparator, we can change the threshold by altering the value of the DC source.

By (1) and (3), all the parameters in the circuit of Figure 5 can be calculated. Therefore, certain circuits can be designed according to specific applications. For example, if all the parameters are set properly, then we can achieve an OR logic gate. Figure 6 gives the stream of input signals  $I_0$ ,  $I_1$  and the output  $I_{out}$  for the OR logic gate. The inputs  $I_0$  and  $I_1$  are square waves with 10 Vp amplitudes and 2 kHz and 4 kHz frequencies, respectively. The voltage values of  $I_0$ ,  $I_1$ , and  $I_{out}$  are shown in Figure 6 with 200 us/Div time base and 5 V/Div scale.

Similar results can be achieved as the frequencies of the inputs increases. When the frequencies of the inputs become large enough, the lag time must be taken into consideration. As discussed above, the increment of  $p$  leads to smaller lag



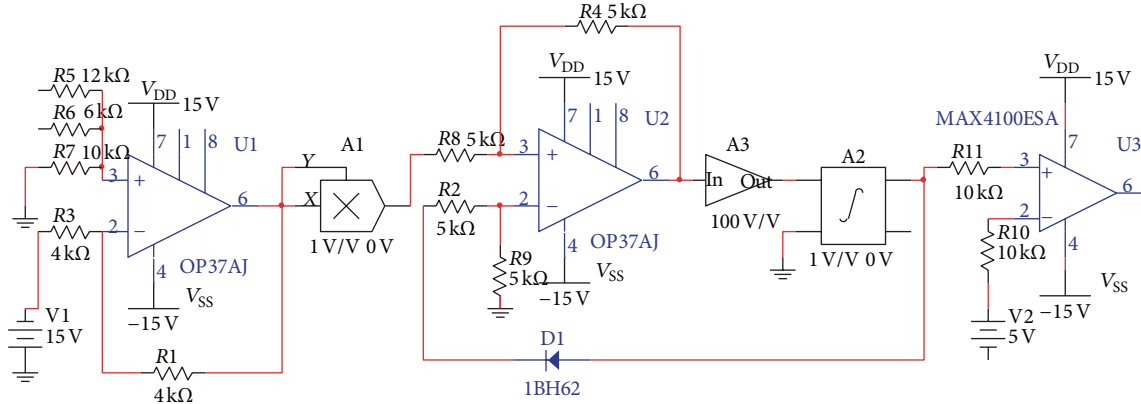


FIGURE 5: (Color online) the circuit diagram of the system (1).

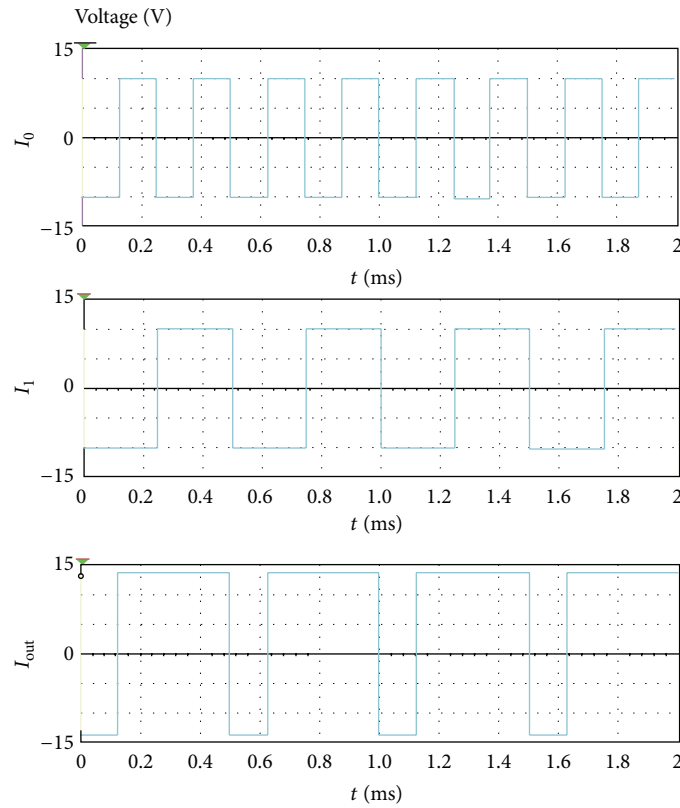


FIGURE 6: (Color online) simulation results of an OR gate.

time and faster convergence. This phenomenon is obvious for larger frequency inputs.

The proposed method can be used to other systems such as fractional oscillators [10, 11], and we may obtain some potential interesting results.

#### 4. Conclusion

To sum up, a scheme to realize a dynamic logic gate is introduced in this paper. Based on the proposed scheme, all available logics and its transformation method are discussed. Besides, the noise and lag characteristics of the system are

studied. We find that the system is resistant to system noise and its response time can be easily controlled. Finally, a circuit implementation for an OR logic gate is provided as an example. Other feasible logic gates can be achieved similarly. The scheme is both straightforward and robust which enables a strong flexible hardware implementation with very low cost. This dynamic logic gate can be applied as a universal basic hardware element to build various kinds of communication encoders and decoders, network coding routers, specific reconfigurable computer chips, graphics processor units, reconfigurable multimedia video cards, or specific systems that require frequent transformations between different

logics. Moreover, there are some further significant directions to be investigated such as all kinds of reconfigurable network coding routers and reconfigurable cyclic code encoder or decoder based on the proposed reconfigurable dynamic logic gate. Communication and computer hardware devices based on such dynamic logic scheme may be more flexible and robust than the existing statically wired hardware.

## Acknowledgments

The authors would like to thank the reviewers for their helpful advices. This paper is supported in part by the AoE grant E-02/08 from the University Grants Committee of the Hong Kong Special Administration Region, China, the Hong Kong Scholars Program (Grant no. HJ2012005), the China Postdoctoral Science Foundation Funded Project (Grant no. 2012T50209), the National Natural Science Foundation of China (Grant nos. 61070209, 61100204, 61272402), the Beijing Higher Education Young Elite Teacher Project, the Shenzhen Municipal Key Laboratory of Key Technology and Application (Grant no. C.02.12.00301) and the Fundamental Research Funding of Shenzhen, China (Grant no. C.02.13.00701).

## References

- [1] T. Munakata, S. Sinha, and W. L. Ditto, "Chaos computing: implementation of fundamental logical gates by chaotic elements," *IEEE Transactions on Circuits and Systems I*, vol. 49, no. 11, pp. 1629–1633, 2002.
- [2] S. Sinha and W. L. Ditto, "Dynamics based computation," *Physical Review Letters*, vol. 81, no. 10, pp. 2156–2159, 1998.
- [3] K. Murali and S. Sinha, "Using synchronization to obtain dynamic logic gates," *Physical Review E*, vol. 75, no. 2, Article ID 025201, 2007.
- [4] K. Murali, S. Sinha, W. L. Ditto, and A. R. Bulsara, "Reliable logic circuit elements that exploit nonlinearity in the presence of a noise floor," *Physical Review Letters*, vol. 102, no. 10, Article ID 104101, 2009.
- [5] H. Peng, F. Liu, L. Li, Y. Yang, and X. Wang, "Dynamic logic architecture based on piecewise-linear systems," *Physics Letters A*, vol. 374, no. 13-14, pp. 1450–1456, 2010.
- [6] D. Graham-Rowe, "How To Be Human: call centers might be able to teach "chat bots" a thing or two about passing the Turing Test," in MIT Technology Review Website, 2006.
- [7] D. Hansel, G. Mato, C. Meunier, and L. Neltner, "On numerical simulations of integrate-and-fire neural networks," *Neural Computation*, vol. 10, no. 2, pp. 467–483, 1998.
- [8] H. Peng, Y. Yang, L. Li, and H. Luo, "Harnessing piecewise-linear systems to construct dynamic logic architecture," *Chaos*, vol. 18, no. 3, Article ID 033101, 2008.
- [9] G. Taubes, "Computer design meets Darwin," *Science*, vol. 277, no. 5334, pp. 1931–1932, 1997.
- [10] M. Li, "Approximating ideal filters by systems of fractional order," *Computational and Mathematical Methods in Medicine*, vol. 2012, Article ID 365054, 6 pages, 2012.
- [11] M. Li, S. C. Lim, and S. Chen, "Exact solution of impulse response to a class of fractional oscillators and its stability," *Mathematical Problems in Engineering*, vol. 2011, Article ID 657839, 9 pages, 2011.

## Research Article

# Topology Identification of Complex Network via Chaotic Ant Swarm Algorithm

**Haipeng Peng,<sup>1</sup> Lixiang Li,<sup>1</sup> Jürgen Kurths,<sup>2</sup> Shudong Li,<sup>3</sup> and Yixian Yang<sup>1,4</sup>**

<sup>1</sup> Information Security Center, State Key Laboratory of Networking and Switching Technology,  
Beijing University of Posts and Telecommunications, Beijing 100876, China

<sup>2</sup> Potsdam Institute for Climate Impact Research, D14473 Potsdam, Germany

<sup>3</sup> College of Mathematics, Shandong Institute of Business and Technology, Yantai, Shandong 264005, China

<sup>4</sup> National Engineering Laboratory for Disaster Backup and Recovery, Beijing University of Posts and Telecommunications,  
Beijing 100876, China

Correspondence should be addressed to Lixiang Li; [li\\_lixiang2006@163.com](mailto:li_lixiang2006@163.com)

Received 18 July 2013; Accepted 22 August 2013

Academic Editor: Ming Li

Copyright © 2013 Haipeng Peng et al. This is an open access article distributed under the Creative Commons Attribution License, which permits unrestricted use, distribution, and reproduction in any medium, provided the original work is properly cited.

Nowadays, the topology of complex networks is essential in various fields as engineering, biology, physics, and other scientific fields. We know in some general cases that there may be some unknown structure parameters in a complex network. In order to identify those unknown structure parameters, a topology identification method is proposed based on a chaotic ant swarm algorithm in this paper. The problem of topology identification is converted into that of parameter optimization which can be solved by a chaotic ant algorithm. The proposed method enables us to identify the topology of the synchronization network effectively. Numerical simulations are also provided to show the effectiveness and feasibility of the proposed method.

## 1. Introduction

So far, most researches on complex networks are based on their exact structure dynamics. However, there is often various unknown or uncertain information in complex networks of the real world. This information including the topology connection of networks, and dynamical parameters of nodes, is always partially known and also changes continuously in many real complex networks such as gene networks, protein-DNA structure network, power grid networks, and biological neural networks [1–4]. Knowledge about the identification of the topology of complex networks is the prerequisite to analyze, control, and predict their dynamical behaviors. Therefore, this topic has drawn great attention of many researchers, since it is of great theoretical and practical significance to use the dynamics of observed nodes for the identification of the network structure [5–7].

The problem of topology identification can be formulated as a gray box model. From this viewpoint, a basic mathematical model of the topology for the complex network can be constructed, although its exact structure peculiarities are

not entirely known. In the model of a complex network, there are often some unknown structure parameters which can be completed via topology identification. Therefore, if the basic mathematical model of its topological structure is built, then we only need to identify the unknown structure parameters of this network. Recently, some research on topology identification of complex networks has emerged to identify some complex networks and some time-delay networks [8]. These researchers mainly used an adaptive feedback control algorithm to solve the problem of topological identification. But this algorithm may fail if the network is in a synchronous regime. In [9], an improved adaptive feedback control method was proposed to make it identifiable in synchronous complex networks. However, this improved method should change the coupling mode of its topology. In addition, to adapt this improved adaptive feedback control method, the dynamical parameter of each node must be observable, which is especially difficult to realize in most real networks such as metabolic networks and power grid networks.

In this paper, a method of topology identification for complex networks is proposed which is based on a chaotic ant swarm (CAS) algorithm. The problem of topology identification is converted into that of parameter optimization which could be solved by the CAS optimization algorithm [10]. The CAS algorithm was inspired by biological experiments of single ant's chaotic behavior. This CAS method is different from those of ant colony optimization (ACO), since the CAS algorithm combines chaotic and self-organizing behaviors of ants with the advantages of swarm-based algorithms. The CAS algorithm is a global optimization algorithm, and it can deal with topology identification of complex networks effectively when they are in a nonsynchronous and even when they are in a synchronous regime.

The remainder of this paper is organized as follows. In Section 2, the problem formulation of topology identification for complex networks is presented. In Section 3, the chaotic ant swarm algorithm is introduced. In Section 4, results of numerical simulations are given. Finally, some conclusions about the proposed method are drawn in Section 5.

## 2. Problem Formulation

To demonstrate the topology identification of complex networks, in this paper, we consider a general complex dynamical network as in [1] with each node being an  $n$ -dimensional dynamical system, and it is described by a differential equation of the following form

$$\dot{X}_i = F_i(X_i) + \sum_{j=1}^N c_{ij} H X_j, \quad i = 1, 2, \dots, N, \quad (1)$$

where  $N$  denotes the number of nodes in the dynamical network and  $X_i = (x_{i1}, x_{i2}, \dots, x_{in}) \in R_n$  is the state vector associated with the  $i$ th node. The function  $F_i$  is the corresponding nonlinear vector field.  $H$  is the inner-coupling matrix.  $C = (c_{ij})_{N \times N}$  is the coupling topology of the network. If there exists a coupling connection between node  $i$  and node  $j$  ( $i \neq j$ ),  $c_{ij} \neq 0$ ; otherwise,  $c_{ij} = 0$ . In this paper,  $C$  does not need to be symmetric or irreducible.

The coupling matrix  $C$  fully represents the topological information of the complex network. Consequently, the problem of topology identification for a complex network can be converted into that of identification of the unknown coupling matrix  $C$ . To identify the coupling matrix  $C$ , here, we assume that  $H$  and  $F_i$  can be experimentally measured in advance. Next, a drive-response network should be built. Equation (1) is taken as the driving network. Then, the response network can be designed as

$$\dot{\eta}_i = F_i(\eta_i) + \sum_{j=1}^N \hat{c}_{ij} H \eta_j, \quad (2)$$

where  $\hat{c}_{ij}$  is the estimated parameter of  $c_{ij}$ .  $\eta_i$  is obtained by simulating the network (1) with the estimated coupling matrix element  $\hat{c}_{ij}$ .

To identify the topology of the complex network, the following objective function is introduced as

$$V = \sum_{k=0}^M \sum_{i=1}^N \sum_{d=1}^D (x_{id}(k) - \eta_{id}(k))^2, \quad (3)$$

where  $M$  is the termination time of numerical simulation,  $N$  indicates the number of nodes,  $D$  denotes the dimensions of each node's dynamical system, and  $k$  is the discrete time.  $x_{ij}$  is the state vector of the driving network.  $\eta_{ij}$  is the state vector of the response network with initial value  $\eta_{ij} = x_{ij}$  and the estimated coupling matrix element  $\hat{c}_{ij}$ .

Hence, the problem of topology identification is converted into that of a parameter optimization by the search of the minimal value of  $V$ . The topology matrix  $C$  can be well identified through the method of objective function.

## 3. Chaotic Ant Swarm Algorithm

In recent years, a swarm intelligent optimization algorithm called chaotic ant swarm (CAS) algorithm is proposed to solve the optimization problem based on chaos theory [10]. The mathematical model of CAS algorithm is described as follows:

$$\begin{aligned} y_i(t) &= y_i(t-1)^{(1+r_i)}, \\ z_{id}(t) &= \Delta \exp((1 - \exp(-ay_i(t)))(3 - \Psi_d \Delta)) \\ &\quad - \frac{7.5}{\Psi_d \times V_i} + \exp(-2ay_i(t) + b) \\ &\quad \times (pbest_d(t-1) - z_{id}(t-1)), \end{aligned} \quad (4)$$

where  $y_i(t)$  is the organization variable of the CAS model and  $\Delta = z_{id}(t-1) + 7.5/(\Psi_d \times \phi_i)$ . It controls the chaotic behavior of an individual ant. In this paper,  $y_i(0) = 0.999$ .  $r_i$  is the organization parameter of individual ant which is a positive constant less than 1.  $a$  is a very large positive constant; here,  $a$  is set to be 200.  $b$  is a positive constant, where  $0 \leq b \leq 2/3$ .  $\Psi_i$  determines the searching range of the  $i$ th ant in  $d$ th dimension.  $\phi_i$  controls the moving proportion of the  $i$ th ant searching space.  $pbest(t-1)$  is the best position that the individual ant and its neighbors have ever found within  $t-1$  time steps. Here the neighbors are set to be global neighbors; that is, all the ants are the neighbors of each other.

The ants usually exchange information via certain direct or indirect communication methods. As a result of effective communication, the impact of the organization becomes stronger as time evolves. Finally, all the ants walk through the best path to forage food. Equation (4) shows the foraging process of CAS model. As time increases, the effect of the organization variable  $y_i(t)$  on the behavior of each ant is becoming stronger via the organization parameter  $r_i$ . Finally, by the effect of both  $pbest_d(t-1)$  and  $y_i(t)$ , the state of  $z_{id}(t)$  will converge to the best global position.

$r_i$  and  $\Psi_d$  are two important parameters.  $r_i$  has an effect on the converging speed of the CAS algorithm. If  $r_i$  is very large, then the converging speed of the CAS algorithm will be very fast so that the optimal solution might not be found. If  $r_i$  is

very small, then the converging speed of the CAS algorithm will be very slow and the runtime will be longer. If  $r_i$  is set to be zero, then the behavior of one ant will be chaotic all the time and the CAS algorithm cannot converge to a fixed position. Furthermore, since small changes of organization effect are desired,  $r_i$  is set to be  $0 \leq r_i \leq 0.5$ . The concrete formula of  $r_i$  depends on the specific problem as well as runtime. In order to enable each ant to have a different organization parameter, we set  $r_i = 0.1 + 0.2 \times \text{rand}$ , where  $\text{rand}$  is a uniformly distributed random number in the interval  $[0, 1]$ .  $\Psi_d$  has an effect on the searching range of the CAS algorithm. If the value of  $\Psi_d$  is very large, then the searching range will be small. If  $\Psi_d$  is very small, then the searching range will be very large. The searching range is set to be  $[-w_d/2, w_d/2]$ , and then  $w_d \approx 7.5/\Psi_d$ .

Based on the above discussions about the CAS algorithm, the detailed procedure for identifying the topology structure of a complex network is described as follows.

**Step 1.** To identify the topology parameter of a complex network, some important parameters of the CAS algorithm should be firstly initialized. In this paper, the positive constant  $a$  is set to be 200; the organization factor  $r_i$  of each node is set as  $r_i = 0.1 + 0.2 \times \text{rand}$ , where  $i$  is the  $i$ th ant in the whole  $Q$  ants;  $\phi_i$  is set properly to control the moving proportion. The organization variable of each node  $y_i$  is set to be 0.999.  $\Psi_d$  is set properly to control the searching range of  $z_{id}$ , where  $d$  is the  $d$ th dimension of the ant local position.

**Step 2.** Generate the initial position of the  $i$ th ant  $z_i(k=0) = (z_{i1}, z_{i2}, \dots, z_{id})^T$  randomly in the searching space.  $k = 0$  denotes the initial time point.

**Step 3.** By setting the initial time state vector  $x_i(0) = (x_{i1}, x_{i2}, \dots, x_{in})$ , the fourth-order Runge-Kutta algorithm is used in the driving network (1) to obtain a series of  $x_i(k)$ .

**Step 4.** By setting the initial time state vector  $\eta_i(0) = x_i(0)$ ,  $i = 1, 2, \dots, N$ , the well-known fourth-order Runge-Kutta algorithm is used in the response network (2) to obtain a series of  $\eta_i(k)$ ,  $i = 1, 2, \dots, N$ . The coupling matrix  $C$  can be estimated by the ant colony  $z_i(t)$ ,  $i = 1, 2, \dots, Q$ .

**Step 5.** Compute  $y_i$  for each ant. Then, update the position of each ant via (4).

**Step 6.** Compute the value of objective function for each ant  $z_i$ , and compare each value with previous  $fpbest$  of each ant. If the current value is smaller than the previous  $fpbest$ , then it is updated by the current value, and set the value of  $pbest$  to be the current individual location. Finally, compare each  $fpbest$  with  $fgbest$ . If the value of  $fpbest$  is smaller than  $fgbest$ , then  $fgbest$  is updated by  $fpbest$  of this ant. Then, the  $pgbest = (pgbest_1, pgbest_2, \dots, pgbest_d)$  is replaced by the current global best position.

**Step 7.** Go to Step 5 until the ending condition is satisfied. Then output the global best location of each ant, which means the coupling matrix  $C$  can be identified by the CAS algorithm.

## 4. Numerical Simulation

In this section, we present several numerical simulation results to illustrate the effectiveness of the proposed method. Lorenz chaotic equation is taken as the node dynamical system of the  $i$ th node, which is described as

$$\begin{aligned}\dot{x}_1 &= \theta_1 (x_2 - x_1), \\ \dot{x}_2 &= (\theta_2 - x_3) x_1 - x_2, \\ \dot{x}_3 &= x_1 x_2 - \theta_3 x_3,\end{aligned}\tag{5}$$

where  $x_1$ ,  $x_2$ , and  $x_3$  are the state variables;  $\theta_1 = 10$ ,  $\theta_2 = 28$ ,  $\theta_3 = 8/3$  are positive constants. For the CAS algorithm model (4), we set  $a = 200$ ,  $b = 2/3$ , and  $\phi_i = 0$ . To calculate the objective function  $V$ ,  $M = 20$  successive vectors are set in both driving and response networks. In order to show the effectiveness and feasibility of the proposed method, two examples are provided as follows to identify the topology structure of complex networks.

*Note.* There is an interesting phenomenon. Let  $\varphi$  be the golden ratio, which is approximately equal 1.618. Then,  $b$  approximately equals  $1/\varphi$ , and  $\theta_3$  approximately equals to  $\varphi^2$ . Why such an interesting phenomenon exist? We should give further study in our future work. The basic concept of the golden ratio is given in [11–13] and [14] for the spectra used in [11, 12].

**Example 1.** First of all, a nonsymmetric and non-synchronous diffusive network is considered, which includes three nodes with the topology matrix  $C$ . The elements of the topology matrix  $C$  are  $c_{1,2} = 4$ ,  $c_{2,1} = 5$ ,  $c_{2,3} = 3$ , and  $c_{3,2} = 2$ . The other elements are  $c_{i,j} = 0$  ( $i \neq j$ ) and  $c_{i,i} = -\sum c_{i,j}$ .  $H$  is an identical matrix  $I_3$ . Here, the initial state is set to be  $X(0) = [-6, 3, 7; -14, 3, -4; 5, -3, 4]$ . The population size is 40. The maximum time step is set as 200. Obviously, there are 6 independent variables, so the dimension of each ant position is set to be 6. We set  $\Psi_1 = \Psi_3 = 1.25$ ,  $\Psi_2 = 1$ ,  $\Psi_4 = 1.85$ , and  $\Psi_5 = \Psi_6 = 10$ .  $\eta_{id}$  is in the interval  $[0, 7.5]$ . The estimated process is shown as follows.

Figure 1 shows that the coupling matrix  $C$  can be well identified as the time increases. When the time step is approximately 200, the estimated coupling matrix converges to the true value where the population size is 40. To compare the CAS algorithm with the QPSO algorithm, we also use the definition of [15] to identify the topology of Example 1. Then, the evolution curve of the objective function against the time can be obtained, and their comparative result between these two algorithms is shown in Figure 2. We can see that the objective function  $V$  converges rapidly to the global optima as time evolves. Besides, the converging speed and the precision of the CAS algorithm are much better than those of the QPSO algorithm.

**Example 2.** In this example, a symmetric synchronous network is introduced to show the effectiveness of the proposed method. The parameters of the topology structure are set as  $c_{1,2} = c_{2,1} = 3$ ,  $c_{1,3} = c_{3,1} = 6$ ,  $c_{1,4} = c_{4,1} = 2$ ,  $c_{2,3} = c_{3,2} = 4$ ,



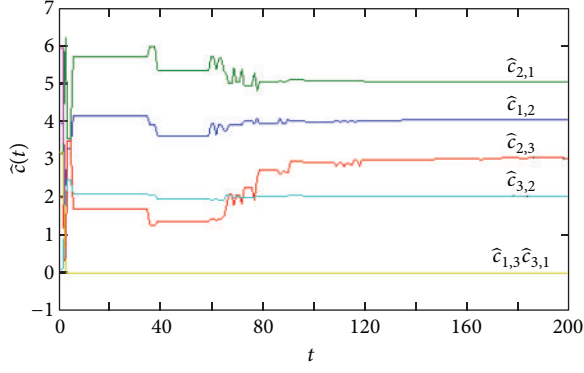


FIGURE 1: (Color online) Estimation of nonsynchronous network topology showing the value  $\hat{c}(t)$  against time step  $t$ .

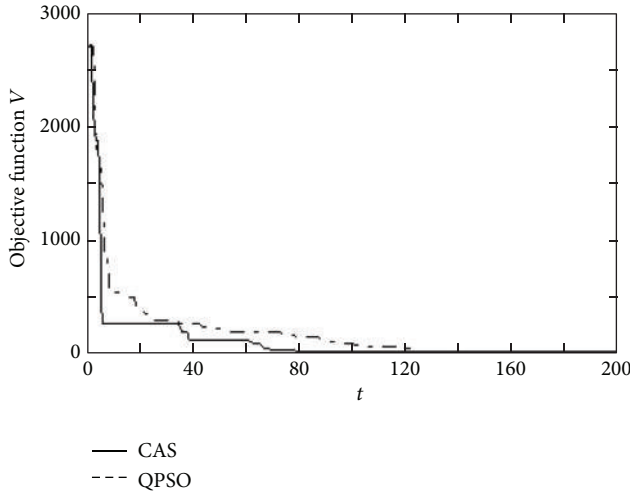


FIGURE 2: Estimation of nonsynchronous network topology showing the objective function value  $V$  against time step  $t$ .

$c_{3,4} = c_{4,3} = 5$ , and the other  $c_{i,j} = 0$  ( $i \neq j$ ) and  $c_{i,i} = -\sum c_{i,j}$ .  $H$  is an identical matrix  $I_3$ . Here, the initial state is  $X(0) = [-6, 3, 7; -14, 3, -4; -3, 4, 5; -5, 6, 1]$ . The population size is 30. The maximal time step is set as 300. Obviously, there are 6 independent variables, so the dimension of each ant position is set to be 6.  $\Psi_1$  is set to be 1.875.  $\Psi_2$  is set to be 0.75.  $\Psi_3$  is set to be 1.875.  $\Psi_4$  is set to be 1.25.  $\Psi_5$  is set to be 0.9375, and  $\Psi_6$  is set to be 10. Figure 3 shows the identification results.

We can see that the topology matrix  $C$  can be identified precisely as the time increases. To compare CAS algorithm with QPSO algorithm, we use the definition of [15] to identify the topology of Example 2. The comparative result is shown in Figure 4. From Figure 4 and Table 1, we can see that although the converging speed of QPSO algorithm is a little faster than that of CAS algorithm, the converging precision of QPSO is much less than that of CAS algorithm. Obviously, the CAS-based topology identification method is more effective than the QPSO-based topology identification method. Compared with the adaptive synchronization identification approach, the CAS algorithm does not need to change the coupling

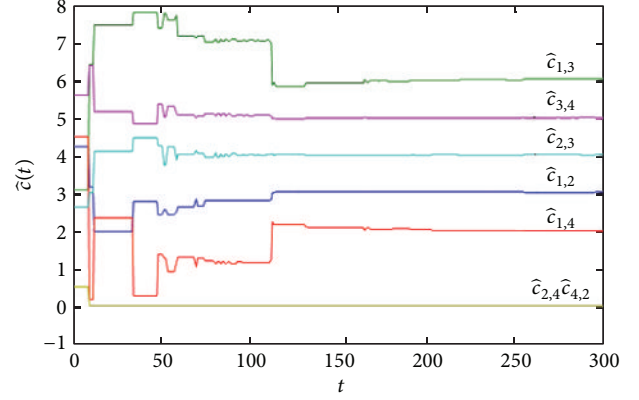


FIGURE 3: (Color online) Estimation of a synchronous network topology showing the value  $\hat{c}(t)$  against time step  $t$ .

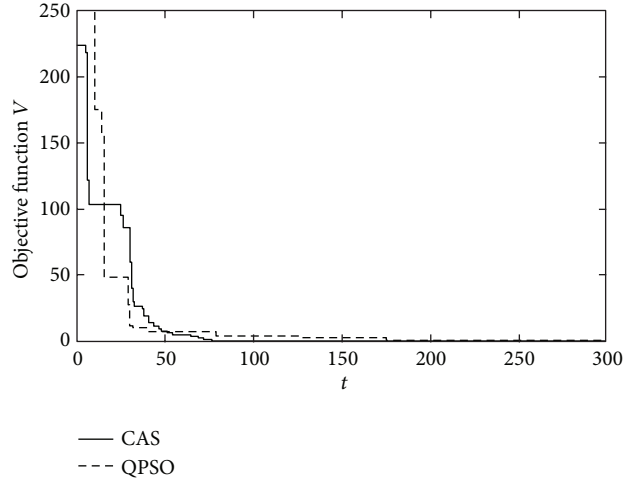


FIGURE 4: Estimation of nonsynchronous network topology showing the objective function value  $V$  against time step  $t$ .

TABLE 1: Comparison between two algorithms.

Algorithms	Objective value
CAS	0.317
QPSO	2.082

modes of the network topology, which has advantages in some real identification cases, for example, the biological neural network.

## 5. Conclusion

In this paper, a topology identification method is proposed based on the CAS algorithm. The problem of topology identification is converted into that of parameter optimization. Compared with the constraints of identifying synchronous complex networks via adaptive feedback control method and the relatively poorer converging precision via QPSO-based topology identification method, the proposed method based

on CAS algorithm can identify the topology structure of complex network effectively.

### Conflict of Interests

The authors declare that there is no conflict of interests regarding the publication of this paper.

### Acknowledgments

The authors would like to thank the editor and all the anonymous reviewers for their helpful advice. This work is supported by the Foundation for the Author of National Excellent Doctoral Dissertation of PR China (Grant no. 200951), the National Natural Science Foundation of China (Grant nos. 61170269, 61202362, and 61070209), the China Postdoctoral Science Foundation Funded Project (Grant no. 2013M540070), the Beijing Higher Education Young Elite Teacher Project, and the Asia Foresight Program under NSFC Grant (Grant no. 61161140320).

### References

- [1] A. E. Motter, C. Zhou, and J. Kurths, "Network synchronization, diffusion, and the paradox of heterogeneity," *Physical Review E*, vol. 71, no. 1, Article ID 016116, 2005.
- [2] Z. Aydin and Y. Altunbasak, "A signal processing application in genomic research: protein secondary structure prediction," *IEEE Signal Processing Magazine*, vol. 23, no. 4, pp. 128–131, 2006.
- [3] X. Zhu, W. Zhang, B. Yu, and W. Gong, "Identification of vulnerable lines in power grid based on complex network theory," in *Proceedings of the International Conference on Mechatronic Science, Electric Engineering and Computer (MEC '11)*, pp. 118–121, August 2011.
- [4] J. Zhou, W. Yu, X. Li, M. Small, and J.-A. Lu, "Identifying the topology of a coupled FitzHugh-Nagumo neurobiological network via a pinning mechanism," *IEEE Transactions on Neural Networks*, vol. 20, no. 10, pp. 1679–1684, 2009.
- [5] X. Wu, "Synchronization-based topology identification of weighted general complex dynamical networks with time-varying coupling delay," *Physica A*, vol. 387, no. 4, pp. 997–1008, 2008.
- [6] D. Yu, M. Righero, and L. Kocarev, "Estimating topology of networks," *Physical Review Letters*, vol. 97, no. 18, Article ID 188701, 2006.
- [7] W. K. S. Tang, M. Yu, and L. Kocarev, "Identification and monitoring of biological neural network," in *Proceedings of the IEEE International Symposium on Circuits and Systems (ISCAS '07)*, pp. 2646–2649, May 2007.
- [8] H. Liu, J.-A. Lu, J. Lü, and D. J. Hill, "Structure identification of uncertain general complex dynamical networks with time delay," *Automatica*, vol. 45, no. 8, pp. 1799–1807, 2009.
- [9] L. Chen, J. Lu, and C. K. Tse, "Synchronization: an obstructer in identifying network topology based on adaptive-feedback control algorithm," *IEEE Transactions on Circuits and Systems II*, vol. 56, p. 310, 2009.
- [10] H. Peng, L. Li, Y. Yang, and F. Liu, "Parameter estimation of dynamical systems via a chaotic ant swarm," *Physical Review E*, vol. 81, no. 1, Article ID 016207, 2010.
- [11] M. Li and W. Zhao, "Golden ratio phenomenon of random data obeying von Karman spectrum," *Mathematical Problems in Engineering*, vol. 2013, Article ID 130258, 6 pages, 2013.
- [12] M. Li and W. Zhao, "Essay on Kolmogorov law of minus 5 over 3, viewed with golden ratio," *Advances in High Energy Physics*, vol. 2013, Article ID 680678, 3 pages, 2013.
- [13] M. Livio, *The Golden Ratio*, Random House Inc., New York, NY, USA, 2003.
- [14] M. Li and W. Zhao, "On  $1/f$  noise," *Mathematical Problems in Engineering*, vol. 2012, Article ID 673648, 23 pages, 2012.
- [15] S.-X. Tang, L. Chen, and Y.-G. He, "Optimization-based topology identification of complex networks," *Chinese Physics B*, vol. 20, no. 11, Article ID 110502, 2011.

## Research Article

# Sensor Scheduling with Intelligent Optimization Algorithm Based on Quantum Theory

Zhiguo Chen,<sup>1</sup> Yi Fu,<sup>1,2</sup> and Wenbo Xu<sup>1</sup>

<sup>1</sup> Key Laboratory of Advanced Process Control for Light Industry, Ministry of Education, School of IoT Engineering, Jiangnan University, Wuxi 214122, China

<sup>2</sup> Research Centre of Environment Science and Engineering, Wuxi 214063, China

Correspondence should be addressed to Zhiguo Chen; [chenzg777@yahoo.com](mailto:chenzg777@yahoo.com)

Received 18 July 2013; Revised 3 September 2013; Accepted 4 September 2013

Academic Editor: Ming Li

Copyright © 2013 Zhiguo Chen et al. This is an open access article distributed under the Creative Commons Attribution License, which permits unrestricted use, distribution, and reproduction in any medium, provided the original work is properly cited.

The particle swarm optimization (PSO) algorithm superiority exists in convergence rate, but it tends to get stuck in local optima. An improved PSO algorithm is proposed using a best dimension mutation technique based on quantum theory, and it was applied to sensor scheduling problem for target tracking. The dynamics of the target are assumed as linear Gaussian model, and the sensor measurements show a linear correlation with the state of the target. This paper discusses the single target tracking problem with multiple sensors using the proposed best dimension mutation particle swarm optimization (BDMPSO) algorithm for various cases. Our experimental results verify that the proposed algorithm is able to track the target more reliably and accurately than previous ones.

## 1. Introduction

Nowadays, the optimization problems of real-world increase rapidly, and they are almost nonlinear and often have several local optima, so it is very hard to find the global optimal solution fast. For example in target tracking [1, 2] system, management of different kinds of sensors to get desired result within acceptable time is a very difficult task.

Heuristic search strategies can acquire faster solutions as they need not require the objective functions to be continuous or differentiable. For recent years the particle swarm optimization (PSO) algorithm in terms of social and cognitive behavior with heuristic search strategy has been successfully used in many real applications [3, 4] since it was proposed by Kennedy and Eberhart [5]. Like most biologically inspired algorithms, the PSO is population based, and the individuals which make up the population are referred to as particles. The main advantage of PSO algorithm is that it has fewer parameters to adjust, but when the search space is high its convergence speed will become very slow near the global optimum and get into local optima. PSO algorithm also shows poor quality results when it deals with large and complex data sets, and it often failed in searching for a global optimal solution

when the objective function has a large number of dimensions. The reason for this phenomenon is not only the existence of the local optimal solutions especially for some multimodal functions, but also the velocities of the particles sometimes lapsed into degeneracy, so that the successive range was restricted in the subplain of the whole search space [6].

Although it was confirmed that the PSO algorithm has potential to find global optimal solution on some benchmark functions [7], it could get stuck in local optima. So the issue of local optima in PSO algorithm has been studied widely and many different variants of PSO algorithm were proposed. For example, by dynamically adjusting the inertia weight  $w$  and acceleration weights  $c_1$ ,  $c_2$  in PSO algorithm, the convergence speed is increased and the swarm is encouraged to escape from local optimal [8]. Some other mutation techniques are used to mutate the positions of some particles in order to diverge the swarm [9]. However, it is still difficult for the modified methods above to find the global solutions for some complex applications. In this paper, a new mutation method called best dimension mutation (BDM) is proposed, and it enables the particles to converge to global optimum fast and easily escape from local optima. A new perturbation technique inspired by quantum mechanics is also introduced

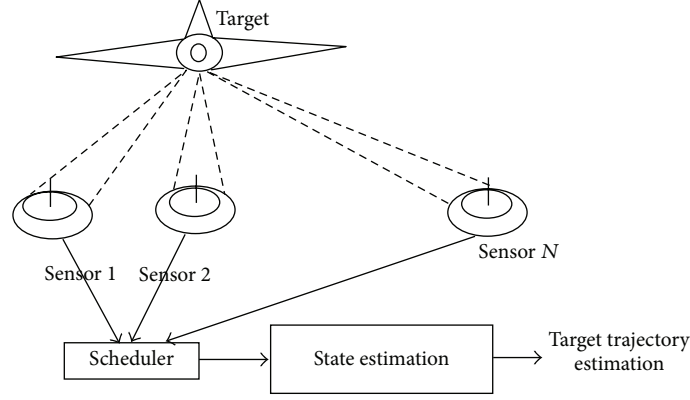


FIGURE 1: Single target tracking system with multiple sensors.

into original POS algorithm which is used to reinitialize the particles positions without distorting the ongoing search strategy when the particles are too close from each other. By combining the two proposed methodologies, the particles can escape from local optima more easily.

The rest of the paper is organized as follows. Section 2 discusses the tracking of single target using multiple noisy sensors. Section 3 presents the BDMPSO (best dimension mutated particle swarm optimization) algorithm. Section 4 shows our experimental results. Section 5 concludes the paper.

## 2. Sensor Scheduling for Target Tracking

Figure 1 illustrates such a scene where a single target moves across a geographical area and several sensors are used to track the target simultaneously. The target state  $X_k = [x_k \ \dot{x}_k \ y_k \ \dot{y}_k]'$  is unknown and the brief target model is considered as

$$X_{k+1} = AX_k + B\omega_k, \quad (1)$$

where  $\omega_k$  is white Gaussian process noise with covariance matrix  $Q$ . The target state kinematics equation is modeled by system matrix  $A$  and the noise intensity is determined by matrix  $B$ . The target state is observed by several sensors and the measurement results are impaired by Gaussian noise. At given time  $k$ , the measurement from the  $n$ th sensor is a column vector given by

$$Z_k^n = H^n X_k + v_k^n, \quad (2)$$

where  $v_k^n$  is the measurement noise of each sensor, which is assumed to be independent of other sensors and of the process noise. We make an assumption that covariance matrix  $R^n$  and observation matrix  $H^n$  are previously known, and the Kalman filtering techniques [10–13] are used to estimate the state of the target. For a given initial error covariance  $P_0$ , the estimated error covariance of the state is given by

$$P_{k|k} = P_{k|k-1} - P_{k|k-1} H'^n S_k^{-1} H^n P_{k|k-1}, \quad (3)$$

where

$$\begin{aligned} P_{k|k-1} &= AP_{k-1|k-1}A' + BQB', \\ S_k^n &= HP_{k|k-1}H' + R_n. \end{aligned} \quad (4)$$

The base station (BS), which schedules the sensors to be active or asleep, collects the latest information about the deleted and newly added sensors as soon as the parameters of the target have been obtained. In our work, we assume that only one sensor is scheduled to estimate the state of the target at any time. Therefore, there is only one sensor to be activated by the BS at a time. Let  $N$  describe the number of latest available sensors to take measurements and  $\mu(T) = \{u_1, u_2, \dots, u_T\}$  represent the sensor scheduling sequence for  $k = 1, 2, \dots, T$ , and let  $u_k \in \{1, \dots, N\}$  be the activated sensor at time step  $k$ . Our goal is to minimize the total estimated error of the target states given by the Kalman filter when  $k = 1$  to  $T$  and to weigh the total sensor usage cost. Calculating the trace of a matrix provides a cheaper and more effective means of defining a scaler based on the estimated error covariance than those of the other ways. Therefore, the trace of the error covariance matrix is considered as our scaler. By using a positive weighting factor  $w$ , we can weigh the cost between error and usage. If the cost function  $J_T$  is defined to measure the performance of the state's cumulative root mean square error and to weigh sensor usage cost for the time horizon  $\{1, 2, \dots, T\}$ , then

$$J_T = \sum_{k=1}^T \{P(u_k) + wc_k(u_k)\}, \quad (5)$$

where  $P(u_k) = \sqrt{\text{trace}(P_{k|k}(u_k))}$  represents the square root of the error covariance associated with the selected sensor  $u_k$  at instant time  $k$ . The  $n$ th sensor usage cost at  $k$ th instant time is  $c_k(n)$  and  $w \in R^+$  is a constant weight coefficient. Our objective is to find an optimal sensor sequence which can produce the minimum cost at the entire time horizon.

The optimal sensor sequence is described as  $\mu^*(T) = \{u_1^*, u_2^*, \dots, u_T^*\}$ :

$$\mu^*(T) = \arg \min_{\forall u_k} \left\{ \sum_{k=1}^T \{P(u_k) + wc_k(u_k)\} \right\}. \quad (6)$$

From (6), we can see that there are total  $N^T$  possible combinations to schedule the sensors. Up to now many optimal algorithms have been proposed to solve this sensor sequence problem. Dynamic programming (DP) and branch-and-bound (BB) were used to solve such problem, but the computational cost rose exponentially along with the increase in the number of sensors and the sequence length [14].

Rollout Algorithm (RA) is closely approximate to a dynamic programming method which can overcome the exponential computational cost problem [15], and it can produce attractive suboptimal results not worse than traditional heuristic methods.

Sliding Window (SW) is another suboptimal method and its window size will balance the computational cost and final results.

The PSO algorithm can be used to solve above target tracking problem [16], but the quality will dramatically decrease with the increment of the sensors. An improved PSO algorithm will be proposed in Section 3 and it will produce acceptable global optimization result.

### 3. Best Dimension Mutated Particle Swarm Optimization

**3.1. Best Dimension Mutation.** Our goal is to develop a methodology which is able to converge faster than PSO algorithm while ensuring the solution is near optimal. In GA (genetic algorithm) or any hybridized PSO algorithm, dimensions of particles are just selected by an assigned probability  $P$  for mutation. The performance of PSO algorithm varies with different values of  $P$  for different cases. High value of  $P$  may result in the swarm divergence and misleading results in some applications. Our methodology aims to speed up the searching process with simple and useful mutation ways. The proposed technique inspired from quantum theory is the key measure to improve the performance of PSO algorithm which can perturb the particles when they are too close from each other.

The PSO algorithm performs very rapid convergence rate at the beginning and will slow down during the remaining searching process [17], and sometimes the velocity of a particle will be zero at the end. This brings about the particles stagnated in local optima [18]. The new mutation technique will relocate the particles to new positions and keep moving around the searching space. The conventional mutation is carried out by selecting one or more dimensions of a particle probabilistically and then added a disturbance factor with special distribution [19, 20].

We developed a new mutation technique called best dimension mutation (BDM) which will find the best dimension to perform mutation at each iteration step, and the selected dimension will be replaced by a random value from the searching space as follows:

- (1) randomly select one particle  $X_i$  from the swarm population  $X_i = (X_i^1, X_i^2, \dots, X_i^D)$ ;
- (2) randomly select  $s$  number of dimensions in position vector of the selected particle and perform mutation for all selected dimensions separately. The mutated particles  $X_M$  are given by  $X_M = (X_{M_1}, X_{M_2}, \dots, X_{M_s})$ , where  $X_{M_m} = (X_i^1, \dots, X_i^{d-1}, r, X_i^{d+1}, \dots, X_i^D)$  and  $r = \text{rand}_i^d(\max X - \min X) + \min X$ ;
- (3) select the particle denoted by  $X_{M_m}^*$  with the best performance out of  $s$  number of mutated particles  $X_M$  and the parent particle  $X_i$ , considering problem  $X_{M_m}^* = \arg \min_{\forall X} f(X)$ ,  $X \in \{X_i, X_M\}$ ;
- (4) update position of the particle by the best mutated one. The velocity of the particle can be calculated as  $X_{i+1} = X_{M_m}^*$ ,  $v_{i+1} = X_{i+1} - X_i$ .

Figure 2 illustrates the flowchart of the proposed BDM procedure. It was observed that if more number of dimensions were selected at the beginning of the search process, the particles would find better solution in a short time period and the divergence of the swarm was more efficient. However, the computational complexity will increase with more dimensions. Therefore, we experimentally found that the performance and computational efficiency of the algorithm can be increased by selecting all of dimensions for a short period and gradually decreases toward the end of the search process. Figure 3 illustrates the selection of number of dimensions as number of iterations increase. The maximum number of iterations is denoted by  $IMAX$ . The mutation is carried out only for one particle in the swarm and it makes an additional  $s$  number of fitness evaluation at each iteration step.

**3.2. Refreshing Particles Based on Quantum Theory.** The performance of the BDM methodology above can be increased by selecting all of the dimensions for a short period of time at the beginning and gradually decreasing toward the end of the searching process. However, the problem of getting stuck in local optima would occur inevitably. Therefore, a perturbation technique is applied to the particles when they are too close from each other. The particle's position can be reinitialized with two different strategies as follows.

- (1) Use Gaussian distribution with the mean as global best solution  $G_t$  and the variance as  $L\%$  of the search space to generate the particles:

$$X_{i_t} \sim_{X_{i_t} \neq G_t} N(G_t, L). \quad (7)$$

- (2) Use the delta potential well distribution to generate the particles as used in [21]:

$$X_{i_t} \sim_{X_{i_t} \neq G_t} G_t \pm \frac{\lg(1/u)}{2g \ln \sqrt{2}} L, \quad (8)$$

where  $u$  is a random number in the range  $(0, 1]$  and  $g$  is a constant variable.



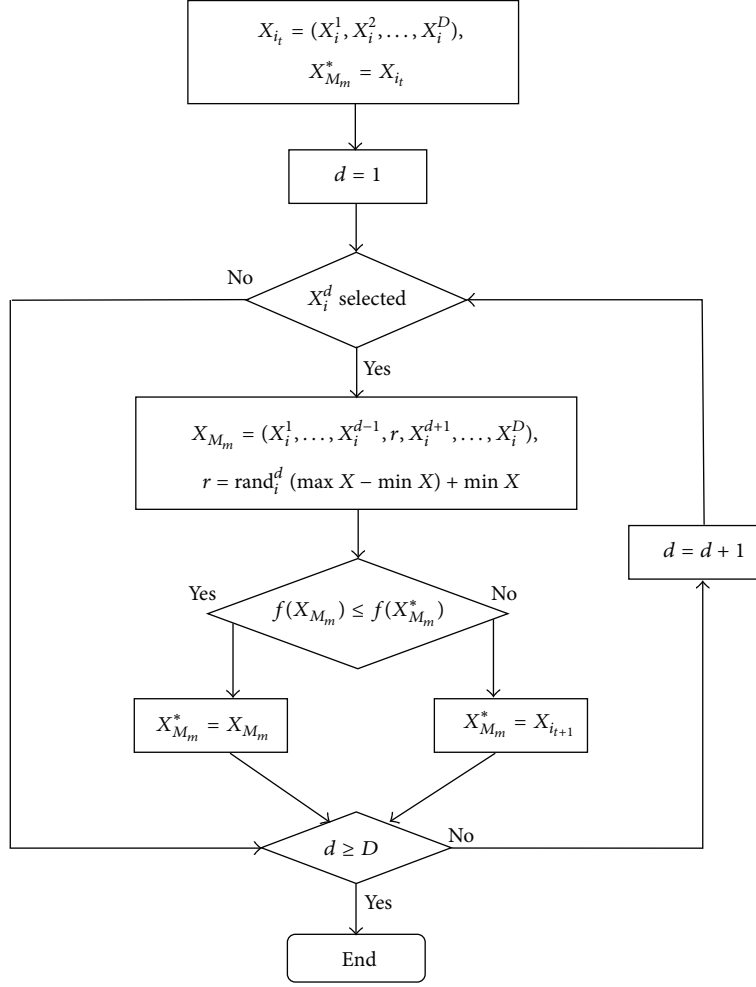


FIGURE 2: The flowchart of the proposed method of best dimension mutation (BDM).

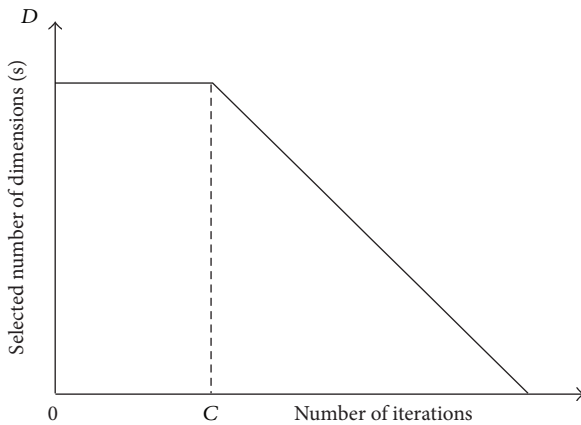


FIGURE 3: Selection of number of dimensions with number of iterations.

The particles generated by delta potential well distribution and Gaussian distribution are denoted by Qps and Gps, respectively, in Figure 4. Both quantum distribution (delta potential well) and Gaussian distribution have a great chances

to generate particles close to *gbest* (global best) position as shown in Figure 4. However, the delta potential distribution produces some particles significantly far away from *gbest* position. This is the tunneling effect; that is, particles have a great chance to reach the global optima even if the global optima should be far away from the local optima [21]. We tested the performance of the PSO algorithm with both particles generating techniques. We experimentally found that the particles generated with quantum based technique in PSO algorithm produce better results than those produced with Gaussian techniques. Therefore, we will use delta potential well to generate the particles when they are too close to each other in this paper.

The parameter  $L$  decides the position of the particles around *gbest* position. We can see from Figure 5 that the particles generated with larger  $L$  value are comparatively far away from *gbest* (where  $G_t = 0$ ). We assigned larger  $L$  from the start and linearly reduced it to zero with the increment of iterations to ensure the convergence of the particles. The algorithm will be very slow if the positions of the particles are calculated in each iteration, so we refresh the particles after  $t_{\text{cap}}$  predefined iterations. We investigated the impact of  $t_{\text{cap}}$  on final results and the value was chosen empirically.

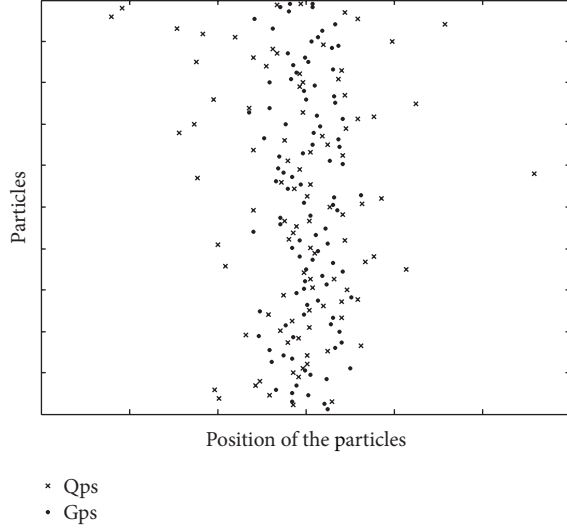


FIGURE 4: Particles generated with Gaussian distribution and Delta potential well distribution ( $L = 3$ ,  $G_t = 0$ , and  $g = 2.5$ ).

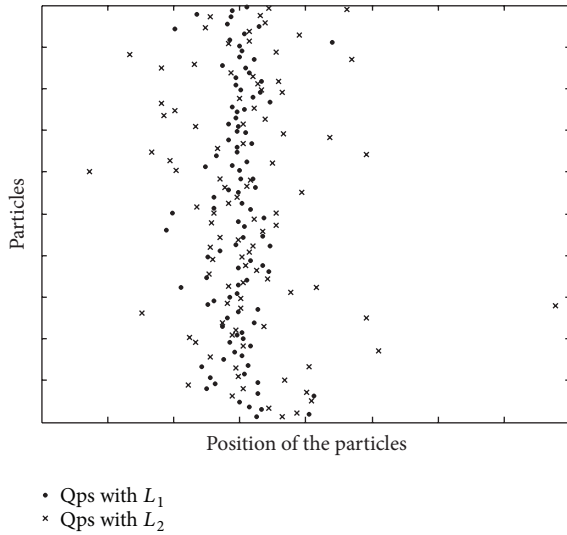


FIGURE 5: Particles generated with different  $L$  values ( $L_1 = 2$ ,  $L_2 = 5$ ,  $G_t = 0$ , and  $g = 2.5$ ).

**3.3. Sensor Scheduling by BDMP SO.** We assumed that we did not know the target parameters such as system matrix  $A$ , noise intensity  $B$ , and covariance matrix  $Q$  until the target appeared in the sensor field. Once the target has been detected the base station will awaken available sensors for target observing. After all information about the target and sensors has been collected, there will be a short period of time to schedule the sensor sequence. Therefore, the BDMP SO algorithm will be applied to produce optimal sensor sequence with the minimum iterations. As the number of sensors is discrete, we use rounding method to discretize the dimensions. Also the replacement mechanism is used when a particle goes beyond the search space as shown below:

$$X_{i_t}^d = \text{round} \left[ \text{rand}_i^d (\max X - \min X) + \min X \right]. \quad (9)$$

The flowchart of the proposed BDMP SO is illustrated in Figure 6.

The entire procedure of BDMP SO procedure for sensor scheduling can be described as below.

- (1) At  $t = 1$  randomly select particles from  $\{x_{i_1} \in \{u_1, u_2, \dots, u_T\}\}_{i=1}^{n_p}$ , and each of which indicates a corresponding feasible sensor sequence. Initialize velocity  $V_{i_0}$ , own best position  $p_{i_0}$ , and global best position  $G_0$ , and set  $\text{temp} = 0$ .
- (2) At iteration  $t$ , if  $\text{temp} = t_{\text{cap}}$  (a predefined number of iterations), refresh all the particles except the global best one using delta potential well distribution and set  $\text{temp} = 0$ ; else goto Step 3.
- (3) Randomly select a particle  $X_{i_t}$  from the swarm population and perform the BDM and go to Step 4.
- (4) Evaluate the fitness value and update the own best  $p_{i_t}$ , global best  $G_0$ , velocity  $V_{i_t}$ , and position  $X_{i_t}$  for all  $n_p$  particles. Increment  $\text{temp}$  by one and go to Step 5.
- (5) If  $t = I_{\text{MAX}}$  then go to Step 6; else increment  $t$  by one and go to Step 2.
- (6) The optimal sensor sequence of the problem is returned by the global best particle at the end of the  $\{u_1^*, u_2^*, \dots, u_T^*\} = G_{I_{\text{MAX}}}$ .

## 4. Simulation Results

In this section, we tested a single target tracking in a 2-dimensional Cartesian space, and the state of the target evolved with linear Gaussian dynamics. Our experiments used the constant velocity in target model. Therefore, the covariance matrix  $Q$  and system matrix  $A$  can be described as follows:

$$A = \begin{bmatrix} 1 & \Delta t & 0 & 0 \\ 0 & 1 & \Delta t & 0 \\ 0 & 0 & 1 & \Delta t \\ 0 & 0 & 0 & 1 \end{bmatrix}, \quad (10)$$

$$Q = q\Delta t = \begin{bmatrix} \frac{\Delta t^2}{4} & \frac{\Delta t}{2} & 0 & 0 \\ \frac{\Delta t}{2} & 1 & \frac{\Delta t}{2} & 0 \\ 0 & 0 & \frac{\Delta t^2}{4} & \frac{\Delta t}{2} \\ 0 & 0 & \frac{\Delta t}{2} & 1 \end{bmatrix},$$

where the scalar quantity  $q$  dominates the intensity of system noise and the state updates with time step  $\Delta t$ . We assigned  $q = 20$  and  $\Delta t = 1$  for all of the experiments. The sensor measurement showed a linear correlation of the target state and was impaired by white Gaussian noise in (2). All of the sensors are homogeneous, and the error covariances and usage costs differ from one another. The observation matrix  $H$  is a unit matrix with 4 by 4 for all sensors. There are 24 sensors used

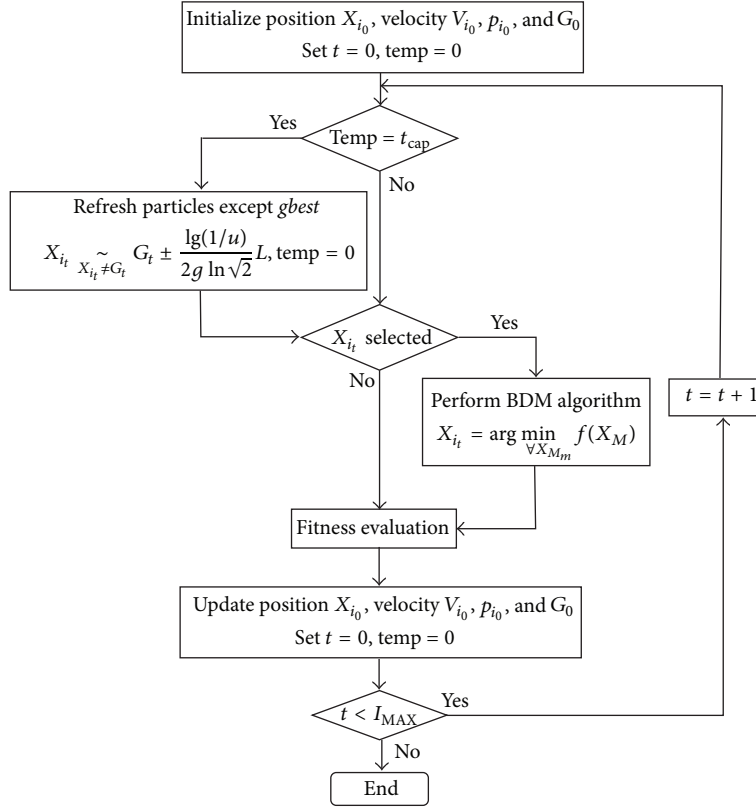


FIGURE 6: The flowchart of the proposed procedure for the BDMPSO algorithm.

for the experiments all together and the error covariances of which can be described as follows:

$$\begin{aligned}
 R_1 &= 10^3 \begin{bmatrix} 2 & 0 & 0 & 0 \\ 0 & 1.5 & 0 & 0 \\ 0 & 0 & 200 & 0 \\ 0 & 0 & 0 & 1.5 \end{bmatrix}, \\
 R_2 &= 10^3 \begin{bmatrix} 2.5 & 0 & 0 & 0 \\ 0 & 0.5 & 0 & 0 \\ 0 & 0 & 100 & 0 \\ 0 & 0 & 0 & 0.5 \end{bmatrix}, \\
 R_3 &= 10^3 \begin{bmatrix} 150 & 0 & 0 & 0 \\ 0 & 0.5 & 0 & 0 \\ 0 & 0 & 1.5 & 0 \\ 0 & 0 & 0 & 1.5 \end{bmatrix}, \\
 R_4 &= 10^3 \begin{bmatrix} 200 & 0 & 0 & 0 \\ 0 & 1.5 & 0 & 0 \\ 0 & 0 & 200 & 0 \\ 0 & 0 & 0 & 1.5 \end{bmatrix},
 \end{aligned} \tag{11}$$

where the other sensors' error covariance eigenvalues are larger than  $R_4$ . Among the entire time horizon, the usage costs are defined as  $c(1) = 65$ ,  $c(2) = 25$ ,  $c(3) = 40$ , and  $c(n) = 60$ , for all  $n \geq 4$ . Therefore, the optimal solution including  $R_1$ ,  $R_2$ ,  $R_3$ , and  $R_4$  produced by sensors such that  $n > 4$  should be the same as that produced by four sensors only. The intention in generating these covariances is to change the

landscape of the problem with the global solution unchanged. For all experiments the weighting factor  $w$  in (5) is assigned 1. We have measured the performance of the proposed method in contrast to PSO with time varying parameters (PSO-tp), Comprehensive Learning PSO [22] (CLPSO), Rollout Algorithm using PSO (RA1), Rollout Algorithm using one step-look-ahead (RA2), and Sliding Window (SW) approach. The set values of BDMPSO are  $t_{\text{cap}} = 30$ ,  $L = 2\%$ ,  $c = 40$ , and  $n_p = 30$  and the rest parameters are the same as in [23].

Firstly, we tested the ability of proposed algorithms with the length of the sensor scheduling sequences varying. Table 1 shows the average results over 30 independent runs for all six different methods in different time horizons (the best costs are highlighted). For the algorithms above, the maximum fitness evaluation (FE) is 20000 with the exception of BDMPSO, being 15000. We can see from Table 1 that the performances of the RA2, SW, and PSO-tp decrease with the sequence length increasing. However, the performances of BDMPSO will not be affected by the increasing number of dimensions. By combining best dimension mutation and new refreshment technology, the performance of the BDMPSO algorithm makes a much more enhancement than others.

Secondly, we analyzed the performance of the PSOs (PSO algorithms) by varying numbers of sensors. Table 2 shows the average results over 30 independent runs for (the best costs are highlighted) all six different methods. The fitness evaluations (FEs) are assigned to 20000 for all the PSOs. As the SW and RA2 are deterministic means, the results are the same for different cases. The performances of RA2 and

TABLE 1: Comparison of cumulative cost for different time horizons.

$T$	SW ( $10^3$ )	RA1 ( $10^3$ )	RA2 ( $10^3$ )	PSO-tp ( $10^3$ )	CLPSO ( $10^3$ )	BDMPSO ( $10^3$ )
30	2.576	2.641	2.498	2.479	2.542	<b>2.396</b>
40	3.295	3.592	3.426	3.192	3.252	<b>3.159</b>
50	4.315	3.971	4.201	3.859	3.883	<b>3.736</b>
60	4.855	4.732	5.076	4.621	4.597	<b>4.527</b>
70	5.662	5.319	6.125	5.302	5.304	<b>5.204</b>
80	6.174	6.201	6.823	6.343	5.902	<b>5.842</b>
90	6.822	6.924	7.418	6.912	6.721	<b>6.587</b>
100	7.252	7.427	8.421	7.724	7.403	<b>7.196</b>
110	8.961	8.093	9.381	8.581	8.067	<b>8.036</b>
120	9.382	8.801	10.24	9.304	8.812	<b>8.512</b>

TABLE 2: Comparison of cumulative cost for different numbers of sensors.

$N$	SW ( $10^3$ )	RA1 ( $10^3$ )	RA2 ( $10^3$ )	PSO-tp ( $10^3$ )	CLPSO ( $10^3$ )	BDMPSO ( $10^3$ )
3	7.476	7.324	7.389	7.395	7.557	<b>7.242</b>
6	7.476	7.406	<b>7.389</b>	7.413	7.562	7.392
9	7.476	7.364	7.389	7.630	7.642	<b>7.331</b>
12	7.476	7.426	7.389	7.598	7.585	<b>7.329</b>
15	7.476	7.524	7.389	7.621	7.612	<b>7.326</b>
18	7.476	7.631	7.389	7.655	7.620	<b>7.346</b>
21	7.476	7.630	7.389	7.623	7.632	<b>7.363</b>
24	7.476	7.762	7.389	7.692	7.593	<b>7.379</b>

BDMPSO are better than the others'. However, it can be seen from Table 2 that the performances of PSO-tp and CLPSO decrease when the number of sensors increases, and easily get stuck in local optima. The BDMPSO produces the better results for all of the cases.

Thirdly, we compared the performance of PSOs with different numbers of FEs. The parameters were assigned to the same numbers except for the FEs which varied from 10000 to 40000. Table 3 shows the average results over 30 independent runs for (the best costs are highlighted) all six different methods with sequence length of 100 units. It can be seen from Table 3 that the proposed BDMPSO achieves better result than other variant PSO algorithms and it converges to desired results in fewer iterations, but other PSOs will need considerably more numbers of FEs to achieve comparative result. Therefore, the proposed BDMPSO algorithm is more suitable for nearly linear problems in less time.

## 5. Conclusions

We have presented an improved PSO algorithm and applied it to the target tracking problem. The best dimension mutation method with quantum based reinitialization technique makes the particles escape from the local optima correspondingly easier and accelerates the convergence rate. Relatively this

TABLE 3: Comparison of cumulative cost for different FEs.

FEs	PSO-tp ( $10^3$ )	CLPSO ( $10^3$ )	BDMPSO ( $10^3$ )
Number of sensors $N = 3$			
10000	7.812	7.509	<b>7.348</b>
15000	7.712	7.496	<b>7.337</b>
20000	7.712	7.400	<b>7.315</b>
30000	7.702	7.327	<b>7.298</b>
40000	7.642	7.307	<b>7.297</b>
Number of sensors $N = 6$			
10000	7.713	8.904	<b>7.405</b>
15000	7.532	7.987	<b>7.359</b>
20000	7.501	7.640	<b>7.313</b>
30000	7.487	7.462	<b>7.297</b>
40000	7.486	7.462	<b>7.297</b>
Number of sensors $N = 9$			
10000	9.387	9.846	<b>7.409</b>
15000	9.346	9.105	<b>7.412</b>
20000	8.615	8.510	<b>7.406</b>
30000	8.559	7.559	<b>7.413</b>
40000	8.578	7.542	<b>7.357</b>
Number of sensors $N = 12$			
10000	11.762	10.824	<b>7.768</b>
15000	11.516	9.637	<b>7.422</b>
20000	11.327	9.120	<b>7.425</b>
30000	10.678	8.249	<b>7.516</b>
40000	10.519	<b>7.348</b>	7.496
Number of sensors $N = 15$			
10000	12.513	11.305	<b>8.098</b>
15000	12.249	10.190	<b>7.416</b>
20000	12.301	9.598	<b>7.387</b>
30000	12.209	8.315	<b>7.375</b>
40000	11.879	7.627	<b>7.375</b>
Number of sensors $N = 18$			
10000	14.138	11.467	<b>8.304</b>
15000	14.030	10.654	<b>7.412</b>
20000	13.975	10.213	<b>7.327</b>
30000	13.567	8.649	<b>7.310</b>
40000	13.439	7.781	<b>7.309</b>
Number of sensors $N = 21$			
10000	14.725	11.496	<b>8.398</b>
15000	14.098	10.912	<b>7.406</b>
20000	14.134	10.146	<b>7.378</b>
30000	13.320	8.697	<b>7.294</b>
40000	13.140	8.416	<b>7.292</b>
Number of sensors $N = 24$			
10000	15.412	11.849	<b>8.792</b>
15000	14.678	11.102	<b>7.509</b>
20000	14.355	10.534	<b>7.376</b>
30000	14.297	8.912	<b>7.324</b>
40000	14.295	8.246	<b>7.324</b>

methodology does not increase the computational cost significantly compared with the original PSO algorithm and also it is more easily to implement. To sum up, the proposed BDMPSO algorithm shows better performance and achieves the results faster than other existing ones for target tracking problem. We plan to focus on shortening the convergence time of BDMPSO algorithm in further work.

## Acknowledgments

This work was supported in part by the Fundamental Research Funds for the Central Universities under Grant no. JUSRP111A46 and the National Natural Science Foundation of China under Grant no. 61170119.

## References

- [1] H. S. Meyerhoff, F. Papenmeier, and M. Huff, "Object-based integration of motion information during attentive tracking," *Perception*, vol. 42, pp. 119–121, 2013.
- [2] G. Jahn, J. Wendt, M. Lotze, F. Papenmeier, and M. Huff, "Brain activation during spatial updating and attentive tracking of moving targets," *Brain and Cognition*, vol. 78, no. 2, pp. 105–113, 2012.
- [3] S. Rana, S. Jasola, and R. Kumar, "A review on particle swarm optimization algorithms and their applications to data clustering," *Artificial Intelligence Review*, vol. 35, no. 3, pp. 211–222, 2011.
- [4] A. A. A. Esmin and S. Matwin, "HPSOM: a hybrid particle swarm optimization algorithm with genetic mutation," *International Journal of Innovative Computing, Information and Control*, vol. 9, no. 5, pp. 1919–1934, 2013.
- [5] J. Kennedy and R. Eberhart, "Particle swarm optimization," in *Proceedings of the 1995 IEEE International Conference on Neural Networks*, pp. 1942–1948, December 1995.
- [6] R. Thangaraj, M. Pant, A. Abraham, and V. Snasel, "Modified particle swarm optimization with timevarying velocity vector," *International Journal of Innovative Computing, Information and Control*, vol. 8, no. 1, pp. 201–218, 2012.
- [7] S. Baskar and P. N. Suganthan, "A novel concurrent particle swarm optimization," in *Proceedings of the Congress on Evolutionary Computation (CEC '04)*, vol. 1, pp. 792–796, June 2004.
- [8] Y. V. Pehlivanoglu, "A new particle swarm optimization method enhanced with a periodic mutation strategy and neural networks," *IEEE Transactions on Evolutionary Computation*, vol. 17, no. 3, pp. 436–452, 2013.
- [9] Y. Zhang and L. Wu, "A hybrid TS-PSO optimization algorithm," *Journal of Convergence Information Technology*, vol. 6, no. 5, pp. 169–174, 2011.
- [10] R. E. Kalman, "A new approach to linear filtering and prediction problems," *Transactions of the ASME*, vol. 82, no. 1, pp. 35–45, 1960.
- [11] L. Xie, P. Yang, T. Yang, and M. Li, "Dual-EKF-based real-time celestial navigation for lunar rover," *Mathematical Problems in Engineering*, vol. 2012, Article ID 578719, 16 pages, 2012.
- [12] M. Li, "Approximating ideal filters by systems of fractional order," *Computational and Mathematical Methods in Medicine*, vol. 2012, Article ID 365054, 6 pages, 2012.
- [13] M. Li, S. C. Lim, and S. Chen, "Exact solution of impulse response to a class of fractional oscillators and its stability," *Mathematical Problems in Engineering*, vol. 2011, Article ID 657839, 9 pages, 2011.
- [14] A. C. Nearchou, "Solving the single machine total weighted tardiness scheduling problem using a hybrid simulated annealing algorithm," in *Proceedings of the 2nd IEEE International Conference on Industrial Informatics (INDIN '04)*, pp. 513–516, June 2004.
- [15] D. P. Bertsekas, *Dynamic Programming and Optimal Control. Volume 1*, Athena Scientific, Nashua, NH, USA, 3rd edition, 2005.
- [16] H. T. Yao, H. Q. Chen, and T. F. Qin, "Niche PSO particle filter with particles fusion for target tracking," *Applied Mechanics and Materials*, vol. 239, pp. 1368–1372, 2013.
- [17] M. J. A. Hasan and S. Ramakrishnan, "A survey: hybrid evolutionary algorithms for cluster analysis," *Artificial Intelligence Review*, vol. 36, no. 3, pp. 179–204, 2011.
- [18] F. S. Levin, *An Introduction to Quantum Theory*, Cambridge University Press, New York, NY, USA, 2002.
- [19] Z. Chen, Y. Bo, P. Wu, and W. Zhou, "A new particle filter based on organizational adjustment particle swarm optimization," *Applied Mathematics & Information Sciences*, vol. 7, no. 1, pp. 179–186, 2013.
- [20] Y. Bo, Z. Chen, J. Zhang, and J. Zhu, "New clone particle swarm optimization-based particle filter algorithm and its application," *Applied Mathematics & Information Sciences*, vol. 7, no. 1, pp. 171–177, 2013.
- [21] S. M. Mikki and A. A. Kishk, "Quantum particle swarm optimization for electromagnetics," *IEEE Transactions on Antennas and Propagation*, vol. 54, no. 10, pp. 2764–2775, 2006.
- [22] J. J. Liang, A. K. Qin, P. N. Suganthan, and S. Baskar, "Comprehensive learning particle swarm optimizer for global optimization of multimodal functions," *IEEE Transactions on Evolutionary Computation*, vol. 10, no. 3, pp. 281–295, 2006.
- [23] A. Ratnaweera, S. K. Halgamuge, and H. C. Watson, "Self-organizing hierarchical particle swarm optimizer with time-varying acceleration coefficients," *IEEE Transactions on Evolutionary Computation*, vol. 8, no. 3, pp. 240–255, 2004.

## Research Article

# First-Order ARMA Type Fuzzy Time Series Method Based on Fuzzy Logic Relation Tables

**Cem Kocak**

*School of Health, Hitit University, 19000 Corum, Turkey*

Correspondence should be addressed to Cem Kocak; [cemkocak@hotmail.com](mailto:cemkocak@hotmail.com)

Received 2 July 2013; Revised 1 August 2013; Accepted 3 August 2013

Academic Editor: Ming Li

Copyright © 2013 Cem Kocak. This is an open access article distributed under the Creative Commons Attribution License, which permits unrestricted use, distribution, and reproduction in any medium, provided the original work is properly cited.

Fuzzy time series approaches have an important deficiency according to classical time series approaches. This deficiency comes from the fact that all of the fuzzy time series models developed in the literature use autoregressive (AR) variables, without any studies that also make use of moving averages (MAs) variables with the exception of only one study (Egrioglu et al. (2013)). In order to eliminate this deficiency, it is necessary to have many of daily life time series be expressed with Autoregressive Moving Averages (ARMAs) models that are based not only on the lagged values of the time series (AR variables) but also on the lagged values of the error series (MA variables). To that end, a new first-order fuzzy ARMA(1,1) time series forecasting method solution algorithm based on fuzzy logic group relation tables has been developed. The new method proposed has been compared against some methods in the literature by applying them on Istanbul Stock Exchange national 100 index (IMKB) and Gold Prices time series in regards to forecasting performance.

## 1. Introduction

Fuzzy time series approaches not necessitating many of the limitations seen in classical time series approaches such as linearity, stationarity, and number of observations have increased the interest towards these approaches. Fuzzy time series concept first mentioned in the literature by Song and Chissom [1] was based on the fuzzy set theory of Zadeh [2]. Song and Chissom [3, 4] divided fuzzy time series into two groups, namely, time variant and time invariant. A vast majority of the studies in the literature are methods proposed for solving time invariant fuzzy time series. Because models are significantly effective on the forecasting performances during the determination of fuzzy relations stage, different approaches have been proposed in the literature. In the studies of Song and Chissom [1, 3, 4], relations are determined with complex matrix operations. In order to eliminate this complexity, a new first-order fuzzy time series model has been proposed where fuzzy logic group relation tables are used in Chen's [5] study with simplified operations not necessitating complex matrix processes. This approach of Chen [5] is used in many studies due to its positive effect

on forecasting performance. Therefore, Chen [6] developed a new approach by using the fuzzy logic relation tables also in high-order fuzzy time series models. Because the methods proposed in the studies of Chen [5, 6] necessitate obtaining of many fuzzy logic group relation tables, they require numerous operations. Thus, studies where fuzzy relations are determined with artificial neural networks are commonly seen. Some studies where artificial neural networks are used for determining fuzzy relations may be listed as the studies of Huarng and Yu [7], Aladag et al. [8], Yu and Huarng [9], and Yolcu et al. [10].

In majority of the studies in the literature, interval lengths are specified intuitively. In his study, Huarng [11] has proposed two separate approaches based on average and distribution to specify optimal interval length. The optimal interval lengths determined by the approach of Huarng [11] may be obtained to be very large values. Thus, Egrioglu et al. [12] proposed approaches based on the optimisation of interval length. Different from these studies, Huarng and Yu [13] proposed an approach based on ratio with interval length varying exponentially instead of determining a fixed interval length in the solution of first-order fuzzy time series.



Determining the ratio in the study of Huarng and Yu [13] requires many complex calculations. Therefore, Yolcu et al. [14] proposed a new approach that improves the approach of Huarng and Yu [13], based on the optimisation of ratio.

There are 3 most commonly used models in the analysis of single variable time series in classical time series approach. These are autoregressive (AR), moving averages (MAs), and mixed autoregressive moving averages (ARMAs) models. However, fuzzy time series methods developed in the literature focus on the AR model of the classical time series theory, without any study conducted on the utilisation of MA and ARMA models except Uslu et al. [15], Alpaslan et al. [16], and Aladag et al. [17]. These studies [15–17] on the other hand are methods that have been proposed for the solution of seasonal time series. No study has been made on the inclusion of error variable to the model for nonseasonal fuzzy time series with the exception of Egrioglu et al. [18] study. This study [18] is the first study developed as first order fuzzy ARMA type model based on particle swarm optimization for the solution of nonseasonal time series in the literature. All of the models in the literature have mentioned issues such as the use of universe of discourse partitioning, membership order, model order, and artificial intelligence approaches. However, the fuzzy time series models proposed in the literature only including AR variables which may lead to a model specification error. In many modelling of the real life time series, MA variables are also required. In this sense, use of only AR variables for the solution of fuzzy time series requiring also MA variables for modelling becomes insufficient regarding the forecasting performance.

For the purpose of eliminating the adverse effects mentioned, a solution algorithm for a new first-order fuzzy ARMA(1,1) time series forecast model where fuzzy relations are determined based on fuzzy logic group relations has been proposed in this study. The logic for determining fuzzy relations in the proposed method is an approach similar to that of the study of Chen [5], aiming to show that the forecasting performance can be significantly improved when the model specification error in the method of Chen [5], accepted as a fundamental approach in literature, is eliminated. For many real life time series, performance can be increased through the use of high-order fuzzy time series models due to the ability to realise solution with more information. However, because the proposed fuzzy ARMA(1,1) model uses a second variable (error variable), it utilises more information to the extent it eliminates the model error, and although just a first order model, it occurs to have a better forecasting performance than that of high order fuzzy time series methods.

In this paper, the time series which were used in application are examined according to long-range dependence. Time series can be classified short range or long-range dependence time series. Many time series have long-range dependence. The long-range dependence time series are forecasted different methods like autoregressive fractionally integrated moving average (ARFIMA). ARFIMA models have fractionally differencing parameter. First studies were concerned with estimation of fractional differencing parameter in fractional white noise processes.  $R/S$  statistic was proposed in Hurst [19]. The other important studies about fractional differenced

processes are Li and Zhao [20, 21], Li [22], Stanley et al. [23], Werner [24], Beran [25], Ivanov et al. [26], Podobnik et al. [27], Zevallos and Palma [28], and Bhansali and Kokoszka [29].

In the second section of the study, basic definitions regarding fuzzy time series have been provided. In the third section, the proposed fuzzy time series forecasting model has been defined and the solution algorithm has been provided. In the fourth section, the proposed method has been applied to Istanbul Stock Exchange (IMKB) national 100 index time series and gold prices in 2009 taken from Turkish Republic Central Bank (TCMB) website, comparing it to some other methods in the literature regarding forecasting performance. An in-depth comparison has been made in this section. In the fifth section, the study has been summed up by discussing the results obtained.

## 2. Definition of Fuzzy Time Series

Fuzzy time series concepts and definitions have been developed in accordance to the lagged variables of times series (AR, autoregressive) in all studies conducted in the literature. Main time series definitions developed using AR variables are listed below.

*Definition 1.* Let  $X(t)$  ( $t = \dots, 0, 1, 2, \dots$ ), a subset of real numbers, be the universe of discourse on which fuzzy sets  $f_j(t)$  are defined. If  $F(t)$  is a collection of  $f_1(t), f_2(t), \dots$  then  $F(t)$  is called a fuzzy time series defined on  $X(t)$  [1, 3, 4].

*Definition 2.* Let us consider the fuzzy relation between  $R(t, t-1)$ ,  $F(t-1)$ , and  $F(t)$ . For any  $t$  value, if  $R(t, t-1)$  is independent from  $t$ , then  $R(t, t-1) = R(t-1, t-2)$ . In this case,  $F(t)$  is called the time invariant fuzzy time series, while otherwise called as time variant fuzzy time series [1].

*Definition 3.* If the  $F(t)$  fuzzy time series is only affected by one lagged  $F(t-1)$  fuzzy time series, then the fuzzy relation between  $F(t-1)$  and  $F(t)$  is expressed as

$$F(t-1) \longrightarrow F(t). \quad (1)$$

This is called as a first-order fuzzy time series forecasting model. Then this relation can be expressed as

$$F(t) = F(t-1) \circ R(t, t-1). \quad (2)$$

The “ $\circ$ ” operator in (2) had been determined as the max-min operator by Song and Chissom [1, 3, 4].

*Definition 4.* If  $F(t)$  fuzzy time series is affected by the lagged fuzzy time series of  $F(t-1), F(t-2), \dots, F(t-p)$ , then the fuzzy relation between  $F(t)$  fuzzy time series and  $F(t-1), F(t-2), \dots, F(t-p)$  fuzzy time series may be expressed as

$$F(t-p), \dots, F(t-2), F(t-1) \longrightarrow F(t) \quad (3)$$

and is called the  $p$ th order fuzzy time series forecasting model [6].

### 3. The Proposed Method

Based on the definition of fuzzy AR(1) given in Definition 3, the definition of the main fuzzy time series to represent the fuzzy ARMA(1,1) model is expressed as follows.

**Definition 5.** Let  $F(t)$  be a fuzzy time series and let  $\varepsilon(t)$  be the fuzzy error series obtained from  $F(t)$  fuzzy time series. If  $F(t)$  is affected by one lagged  $F(t-1)$  and one lagged  $\varepsilon(t-1)$  fuzzy time series, then the relationship can be expressed as

$$F(t-1), \varepsilon(t-1) \longrightarrow F(t). \quad (4)$$

This is called as first-order fuzzy autoregressive moving averages (ARMA(1,1)) time series forecasting model [18].

In this study, an algorithm has been proposed for solving the ARMA(1,1) fuzzy time series forecasting model defined in (4). In the algorithm proposed, initially the AR(1) fuzzy time series model defined in (1) is estimated. Later on, errors are calculated by taking the differences between the observed values of the times series and the forecasts obtained through the solution of fuzzy AR(1). By using these errors, the fuzzy ARMA(1,1) model defined in (4) is estimated. The algorithm of the proposed approach is given below.

**Algorithm 6.** The proposed method's algorithm.

**Step 1** (the universe of discourse ( $U$ ) and subintervals ( $u_i$ ,  $i = 1, 2, \dots, b$ ) are defined). The beginning and the ending points of the universe of discourse for time series are determined. Then  $U$  is divided into subintervals according to appropriate interval length. Definition of interval length is up to the researcher. It should not be forgotten that the interval length to be determined affects the number of subintervals. If the smallest value of the time series is taken as  $X_{\min}$ , the largest value as  $X_{\max}$ , and two arbitrary values as  $D_1$  and  $D_2$ , the universal set may be defined as the closed interval of

$$U = [X_{\min} - D_1, X_{\max} + D_2]. \quad (5)$$

$u_i$  subintervals determined for  $i = 1, 2, \dots, b$  are the subintervals of the universal set  $U$ , which is defined as

$$U = \{u_1, u_2, \dots, u_b\}. \quad (6)$$

For example, for  $X_{\min} = 43$  and  $X_{\max} = 96$  when  $U$  is selected as  $[40, 100]$  and interval length is selected as 10, subintervals are specified as  $u_1 = [40, 50]$ ,  $u_2 = [50, 60]$ ,  $u_3 = [60, 70]$ ,  $u_4 = [70, 80]$ ,  $u_5 = [80, 90]$ , and  $u_6 = [90, 100]$ .

**Step 2.** For the time series, fuzzy sets are defined according to the universal set ( $U$ ) and the divisions of ( $u_i$ ). These fuzzy sets are expressed as

$$A_i = \frac{f_{A_i}(u_1)}{u_1} + \frac{f_{A_i}(u_2)}{u_2} + \dots + \frac{f_{A_i}(u_b)}{u_b}, \quad (7)$$

for  $i = 1, 2, \dots, b$ .

For  $i = 1, 2, \dots, b$ ,

$$f_{A_i}(u_i) = \begin{cases} 1, & k = i \\ 0.5, & k = i-1, i+1 \\ 0, & \text{otherwise.} \end{cases} \quad (8)$$

For example, according to (7) and (8), the fuzzy set of  $A_3$  can be expressed as  $0/u_1 + 0.5/u_2 + 1/u_3 + 0.5/u_4 + 0/u_5 + 0/u_6$ .

**Step 3** (observations are fuzzified). Subintervals ( $u_i$ ) where each observation occurs are defined. Then the fuzzy set  $A_i$  where the defined sub-interval has the highest membership value is determined. The fuzzy value of the observation is this  $A_i$  fuzzy set defined.

**Step 4.** For the purpose of determining fuzzy relations, fuzzy logic relations are identified and a fuzzy logic group relation table is formed.

For example, where the fuzzy logic relations are as  $A_2 \rightarrow A_3$ ,  $A_2 \rightarrow A_5$ , according to Chen method [5], the fuzzy logic group relation for  $A_2$  fuzzy value is as  $A_2 \rightarrow A_3, A_5$ . In the proposed method, this relation occurs to be as  $A_2 \rightarrow A_3, A_3, A_5$ . Thus, a little improvement has been realised in the fuzzy AR(1) model of Chen [5] with the proposed method.

**Step 5** (fuzzy forecasts are obtained). As  $F(t-1) = A_j$  and  $F(t) = A_j$ , 3 possible situations regarding forecast obtainment are as follows.

**Situation 1.** If a relation of  $A_i \rightarrow A_j, \dots, A_j$  is valid on the fuzzy group relation table where  $A_i$  affects only  $a$  pieces of  $A_j$ , then the fuzzy forecast is  $A_j$ . For example, if the group relation for  $A_1$  is as  $A_1 \rightarrow A_2$  that this relation is repeated a few times in the time series, then the fuzzy forecast is specified as  $A_2$ .

**Situation 2.** If a relation of  $A_i \rightarrow A_j, \dots, A_j, A_k, \dots, A_k, A_l, \dots, A_l$  is valid on the fuzzy group relation table where  $A_i$  affects  $a$  pieces of  $A_j$ ,  $b$  pieces  $A_k$  and  $c$  pieces  $A_l$ , then the fuzzy forecast is  $A_j, \dots, A_j, A_k, \dots, A_k, A_l, \dots, A_l$ , comprising of  $a + b + c$  pieces of fuzzy values. For example; if the group relation for  $A_2$  is as  $A_2 \rightarrow A_2, A_3, A_3, A_5, A_5, A_5$ , then the fuzzy forecast is specified as  $A_2, A_3, A_3, A_5, A_5, A_5$ .

**Situation 3.** If  $A_i \rightarrow \text{empty}$  on the fuzzy group relation table, the fuzzy forecast occurs to be  $A_i$ . For example, if the group relation for  $A_3$  is  $A_3 \rightarrow \text{empty}$ , then the fuzzy forecast is  $A_3$ .

**Step 6** (defuzzification process is executed). In this step, centralisation method is used. When the fuzzy forecast for Situation 1 and Situation 3 defined in Step 5 is  $A_j$ , then the defuzzy forecast should be the middle point of the  $u_j$  sub-interval that has the highest membership value within the fuzzy set  $A_j$ . For Situation 2, the defuzzy forecast is calculated with the weighted average formula below, by using the middle points ( $m_j, m_k, \dots, m_l$ ) of the  $u_j, u_k, \dots, u_l$  intervals that have

TABLE 1: An example to the fuzzy AR(1) solution of the proposed method.

Years	Data	Fuzzy value	Fuzzy forecast	Defuzzy forecast
2001	43	$A_1$	—	—
2002	47	$A_1$	$A_1, A_1, A_1, A_2$	47.5
2003	45	$A_1$	$A_1, A_1, A_1, A_2$	47.5
2004	46	$A_1$	$A_1, A_1, A_1, A_2$	47.5
2005	53	$A_2$	$A_1, A_1, A_1, A_2$	47.5
2006	65	$A_3$	$A_3, A_3$	65
2007	57	$A_2$	$A_2, A_2$	55
2008	62	$A_3$	$A_3, A_3$	65
2009	51	$A_2$	$A_2, A_2$	55

the highest membership value of each of the  $A_j, A_k, \dots, A_l$  fuzzy sets. Consider

$$\hat{x}(t) = \frac{a \times m_j + b \times m_k + c \times m_l}{a + b + c}. \quad (9)$$

On an example time series, when solutions are made according to the proposed method from Step 1 to Step 6 as per the determined subintervals of  $u_1 = [40, 50]$ ,  $u_2 = [50, 60]$ , and  $u_3 = [60, 70]$ , the solutions displayed in Table 1 are obtained.

*Step 7.* Errors are calculated by taking the differences between the observed time series values and the defuzzified forecast values obtained in Step 6. Real values of the time series are  $x(t)$  and the defuzzified forecast values obtained in Step 6 are  $\hat{x}(t)$ ; the error series  $e(t)$  is calculated as follows:

$$e(t) = x(t) - \hat{x}(t). \quad (10)$$

*Step 8.* For the errors, the universe of discourse set is defined as  $(V)$  and subintervals are defined as  $(v_i, i = 1, 2, \dots, b)$ .

The same partition of the universe of discourse processes done in Step 1 is made for the error series.

*Step 9.* Fuzzy sets based on the universal set  $(V)$  and partitions  $(v_i)$  are defined for the errors. The fuzzy sets are expressed as

$$B_j = \frac{f_{B_j}(v_1)}{v_1} + \frac{f_{B_j}(v_2)}{v_2} + \dots + \frac{f_{B_j}(v_c)}{v_c}, \quad (11)$$

for  $j = 1, 2, \dots, c$ .

For  $j = 1, 2, \dots, c$ ,

$$f_{B_j}(v_j) = \begin{cases} 1, & k = j \\ 0.5, & k = j - 1, j + 1 \\ 0, & \text{otherwise.} \end{cases} \quad (12)$$

For example, according to (11) and (12), the fuzzy set of  $B_3$  can be specified as  $0/v_1 + 0.5/v_2 + 1/v_3 + 0.5/v_4 + 0.5/v_5$ .

*Step 10* (error series  $e(t)$  is fuzzified). Subintervals  $(v_j)$  for each observation are determined. Then the fuzzy set  $B_j$  where the determined sub-interval has the highest membership value is defined. The fuzzy value of the observation is this fuzzy set  $B_j$ .

*Step 11* (fuzzy relations are determined and fuzzy logic group relation table is formed). The fuzzy value  $A_i$  of the fuzzy relations time series and the fuzzy value  $B_j$  of the error series are determined by taking the fuzzy values into consideration together. For the one lagged fuzzy value of the  $t$ th observation being  $F(t-1) = A_i$ , one lagged error value being  $\varepsilon(t-1) = B_j$ , and the fuzzy value being  $F(t) = A_k$ , the fuzzy relation given in (4) occurs to be  $(A_i, B_j) \rightarrow A_k$ . Thus, the fuzzy values are formed of  $(A_i, B_j)$  ordered pairs, and a relation in the manner of one lagged time series and error affecting the time series is mentionable. For example, when the fuzzy logic relations are as  $(A_2, B_3) \rightarrow A_2$ ,  $(A_2, B_3) \rightarrow A_2$ ,  $(A_2, B_3) \rightarrow A_4$ , the fuzzy logic group relation for  $(A_2, B_3)$  fuzzy value occurs to be  $(A_2, B_3) \rightarrow A_2, A_2, A_4$ .

*Step 12* (fuzzy forecasts are obtained). As  $F(t-1) = A_i$  ve  $\varepsilon(t-1) = B_j$  and  $F(t) = A_k$ , 3 possible situations regarding forecast obtainment are as follows.

*Situation 1.* If a relation of  $(A_i, B_j) \rightarrow A_k, \dots, A_k$  is valid on the fuzzy group relation table where  $(A_i, B_j)$  affects only  $a$  pieces of  $A_k$ , then the fuzzy forecast is  $A_k$ . For example, if the group relation for  $(A_1, B_2)$  is as  $(A_1, B_2) \rightarrow A_2$  that this relation is repeated within a few times in the time series, then the fuzzy forecast is determined as  $A_2$ .

*Situation 2.* If a relation of  $(A_i, B_j) \rightarrow A_k, \dots, A_k, A_l, \dots, A_l, A_m, \dots, A_m$  is valid on the fuzzy group relation table where  $(A_i, B_j)$  affects  $a$  pieces of  $A_k$ ,  $b$  pieces  $A_l$  and  $c$  pieces  $A_m$ , then the fuzzy forecast is  $A_k, \dots, A_k, A_l, \dots, A_l, A_m, \dots, A_m$ , comprising of  $a + b + c$  pieces of fuzzy values. For example, if the group relation for  $(A_1, B_2)$  is as  $(A_1, B_2) \rightarrow A_2, A_3, A_3, A_5, A_5, A_5$ , then the fuzzy forecast is determined as  $A_2, A_3, A_3, A_5, A_5, A_5$ .

*Situation 3.* If  $(A_i, B_j) \rightarrow \text{empty}$  on the fuzzy group relation table, the fuzzy forecast occurs to be  $A_i$ . For example, if the group relation for  $(A_1, B_2)$  is  $(A_1, B_2) \rightarrow \text{empty}$ , then the fuzzy forecast is  $A_1$ .

*Step 13* (defuzzification process is made). In this step, centralisation method is used. When the fuzzy forecast for Situation 1 and Situation 3 defined in Step 5 is  $A_j$ , then the defuzzy forecast should be the middle point of the  $u_j$  sub-interval that has the highest membership value within the fuzzy set

TABLE 2: An application of the proposed method on an example time series.

Years	Data	Error	Fuzzy value	Fuzzy forecast	Defuzzy forecast
2001	43	0	$(A_1, B_2)$	—	—
2002	47	−0.5	$(A_1, B_1)$	$A_1$	45
2003	45	−2.5	$(A_1, B_1)$	$A_1, A_1, A_2$	48.33
2004	46	−1.5	$(A_1, B_1)$	$A_1, A_1, A_2$	48.33
2005	53	5.5	$(A_2, B_3)$	$A_1, A_1, A_2$	48.33
2006	65	0	$(A_3, B_2)$	$A_3$	65
2007	57	2	$(A_2, B_2)$	$A_2$	55
2008	62	−3	$(A_3, B_1)$	$A_3$	65
2009	51	−4	$(A_2, B_1)$	$A_2$	55

$A_j$ . For Situation 2, the defuzzy forecast is calculated with the weighted average formula given in (9).

On an example time series, when solutions are made according to the proposed method as per the determined time series subintervals of  $u_1 = [40, 50]$ ,  $u_2 = [50, 60]$ , and  $u_3 = [60, 70]$  and error series subintervals of  $v_1 = [-5, 0]$ ,  $v_2 = [0, 5]$ , and  $v_3 = [5, 10]$ , solutions displayed in Table 2 are obtained.

#### 4. Application

The performance indicators of the root mean square error (RMSE), mean average percentage error (MAPE), and direction accuracy (DA) values used for comparison of the results obtained are as follows:

$$\begin{aligned}
 \text{RMSE} &= \sqrt{\frac{\sum_{t=1}^n (Y_t - \hat{Y}_t)^2}{n}}, \\
 \text{MAPE} &= \frac{1}{n} \sum_{t=1}^n \left| \frac{Y_t - \hat{Y}_t}{Y_t} \right|, \\
 \text{DA} &= \frac{1}{n-1} \sum_{t=1}^{n-1} \begin{cases} 1, & (Y_{t+1} - Y_t)(\hat{Y}_{t+1} - Y_t) > 0, \\ 0, & \text{otherwise.} \end{cases}
 \end{aligned} \quad (13)$$

Data is divided into two within the applications, assigning the first part as training set and the second part as test set obtained through taking the last observations into consideration of which number was predetermined. By looking up the fuzzy relation table obtained for the training set as per the Steps 5 and 12 of the proposed method, the fuzzy forecast of the test set and from there the defuzzy forecasts of the test set are calculated by utilizing Steps 6 and 13. After, the RMSE, MAPE, and DA values for the test set are calculated. Therefore, the future performances of the methods are determined. As the forecasts with the lowest RMSE value calculated for the test set provide the best result of the used method, the future performances of the forecasts are obtained along with the aid of MAPE and DA values.

Solution of vast majority of some fuzzy forecasting methods in the literature is realised according to the specified number of fuzzy sets, and some are realised according to interval lengths. For the purpose of maintaining consistency

during the comparison of forecast performances, the interval length to be used at fuzzification stage is determined as to have the number of fuzzy sets 5 as the lowest and 35 as the highest for each application data and for all methods. Therefore, in case the universal set division is realised in accordance to interval length, the interval lengths to be tried have been specified by calculation with the formula below:

$$\text{Interval Length} = \frac{\max(\text{data}) - \min(\text{data})}{\text{Number of Fuzzy Sets}}. \quad (14)$$

The operations below have been realised when making solution via the proposed method.

- (i) The last  $k$  number of data has been specified as test set, aiming to increase the future performances.
- (ii) During the fuzzification of time series stage of the proposed method, different time series interval lengths for the division of universal set  $U$  have been tried. Data have been solved from Step 1 to Step 6 according to these intervals lengths. And so, a lot of forecasts have been obtained. The test set forecast with the smallest RMSE value among these forecasts has been determined as the best result of the fuzzy AR(1) model.
- (iii) The error value of the first observation of data has been assumed as 0, while the error values of other observations have been calculated with the formula (9) by using the training set and test set forecasts obtained through the best result of the fuzzy AR(1) model. Thus the error series has been obtained.
- (iv) Different time series interval lengths and different error series interval lengths have been tried by solving data from Step 1 to Step 13. Among these trials, the test set forecast with the smallest RMSE value has been determined as the best result of the fuzzy ARMA(1,1) model.

For the purpose of comparing the proposed method with the other fuzzy time series methods in the literature, 2 different data sets comprising of less observations (smaller sample size) and more observations (larger sample size) have been used. One of these data sets is the IMKB time series seen in Figure 1 comprising of 53 observations between





FIGURE 1: Graph of IMKB time series.

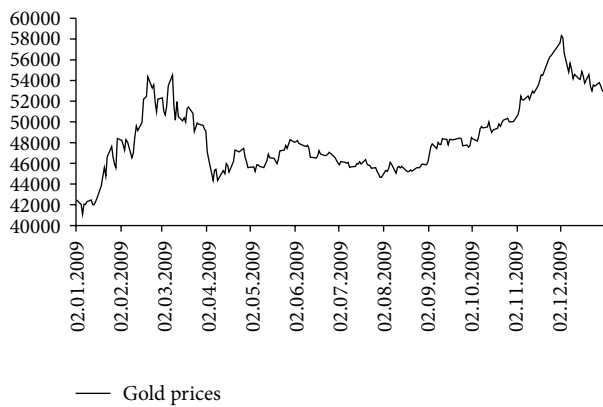


FIGURE 2: Graph of gold prices.

the dates of 01.10.2010 and 23.12.2010. The second data set is the gold prices time series seen in Figure 2 comprising of 248 observations received from Turkish Republic Central Bank (TCMB) website between the dates of 02.01.2009 and 31.12.2009.

In the solution of the IMKB data given in Figure 1 via the methods in the literature by taking the last 7 observations and the last 15 observations as test set, one has the following.

- (i) During the fuzzification stage of the Song and Chissom [1] first-order fuzzy time series method, among the 31 different results obtained from increasing the fuzzy set number between 5 and 35, the test set forecast that has the minimum RMSE value has been determined as the best result of the method from this results.
- (ii) For each of the 2nd-, 3rd-, 4th-, and 5th-order models of Chen [5] first-order fuzzy time series forecast method, Chen [6] high order fuzzy time series forecast method, and Aladag et al. [8] high order fuzzy time series forecast method, the RMSE values have been found for different intervals lengths being increased 100 units between 300 and 2300. The test set forecasts that have the minimum RMSE values among these 21 trials have been determined as the best results of the methods.

- (iii) By using the optimal interval lengths calculated with the distribution-based approach of Huarng [11] and the average-based approaches, solution has been executed as per the first-order fuzzy time series forecast method of Chen [5]. Thus, the best results of the test set from the distribution based approach and the average-based approaches have been obtained via a single trial.
- (iv) In the application of the ratio-based approach of Huarng and Yu [13], alpha parameter has been taken as 0.50, obtaining the best result for the test set of the method in one trial.

In the solution of the IMKB time series seen in Figure 1 via the proposed method by taking the number of test sets 7 and 15, one has the following.

- (i) The division of universal set  $U$  have been taken different values as increasing the interval length between 300 and 2300 by 100 units and different forecasts have been obtained by solving from Step 1 to Step 6. The test set forecast with the smallest RMSE value among these forecasts has been determined as the best result of the fuzzy AR(1) model. The best fuzzy AR(1) results have been obtained when the interval length is 300 for 7 as the number of test sets and when the interval length is 900 for 15 as the number of test sets.
- (ii) The error value of the first observation of data has been assumed as 0, while the error values of other observations have been calculated via the formula (9) by utilising data and forecasts obtained through the best result of the fuzzy AR(1) model. Thus the error series has been obtained for 53 observations.
- (iii) Different trials have been made by increasing the interval length between 300 and 2300 by 100 units for the time series and by increasing the interval length between 300 and 2100 by 100 units for the error series by solving from Step 1 to Step 13. Among these trials, the test set forecast with the smallest RMSE value has been determined as the best result of the fuzzy ARMA(1,1) model.

During the application of the proposed method and the methods in the literature on IMKB time series, the parameters with which the forecasts with the best test set performance for 7 and 15 numbers of test sets occurred to be

- (i) for the application of Song and Chissom [1] method, when the number of fuzzy sets is 9 for 7 and 20 for 15,
- (ii) for the application of Chen [5] method, when the interval length is 300 for 7 and 900 for 15,
- (iii) for the application of distribution-based Huarng [11] approach, when the interval length is 1000, and for the application of average based approach, when the interval length is 200,
- (iv) for the application of ratio-based Huarng and Yu [13] approach, when the sample percentile  $\alpha = 0.5$ ,

TABLE 3: The best results obtained for 7-observation test set of IMKB data.

Date	Test set	Song and Chissom [1]	Chen [5]	Chen [6]	Huarng [11] distribution-based method	Huarng [11] average-based method	Huarng and Yu [13] rational-based method	Aladag et al. [8]	Proposed method*
15.12.2010	65499	65356	66550	65900.0	67400	66500	66784.7	67300	66266.7
16.12.2010	64429	65356	66250	65900.0	65400	66300	66178.0	64900	63700.0
17.12.2010	63524	65975	64450	64800.0	65900	64500	65878.7	64900	63700.0
20.12.2010	63502	64737	63550	64066.7	64900	63500	63514.3	64300	63700.0
21.12.2010	64820	64737	63550	63700.0	64900	63500	63514.3	63700	65900.0
22.12.2010	65440	65975	65800	64800.0	65900	65500	65878.7	65500	65900.0
23.12.2010	66219	65356	66250	65900.0	65400	66300	66178.0	66700	66266.7
	RMSE	1161.91	1001.70	928.70	1365.14	1014.73	1317.77	1034.06	606.07
	MAPE	0.01387	0.01217	0.01283	0.01773	0.01175	0.01593	0.01350	0.00762
	DA	0.50000	0.50000	0.33333	0.50000	0.50000	0.66667	0.66667	0.83333

\*The best situation.

(v) for the application of Chen [6] method, when the interval length is 2200 in 3rd-order model for 7 and 1400 in 2nd-order model for 15,

(vi) For the application of Aladag et al. [8] method, when the interval length is 600 on 2nd-degree model and unit number of artificial neural network hidden layers is 5 for 7, and when the interval length is 1500 on 2nd-degree model and unit number of artificial neural network hidden layers is 6 for 15,

(vii) For the application of the proposed fuzzy ARMA(1,1) method, when the interval length of time series is 2200 and the interval length of error series is 1400 for 7, and when the interval length of time series is 1400 and the interval length of error series is 400 for 15.

Best forecasts and forecast performances of all methods in result of IMKB time series solution for 7 observation test set are summarised in Table 3.

When Table 3 is analyzed, it is seen in result of the solution of IMKB time series for 7 observation test set that the proposed method produced the best forecasting performance with a minimum RMSE value of 606.07, minimum MAPE value of 0.762%, and maximum direction accuracy of 83.33%. The graphs of the last 7 observations of IMKB time series along with the 7-observation test set forecasts obtained with the proposed method are shown together in Figure 3.

Best forecasts and forecast performances of all methods in result of IMKB time series solution for 15-observation test set are summarised in Table 4.

When Table 4 is analyzed, it is seen that the proposed method produced the best forecasting performance with a minimum RMSE value of 865.28, minimum MAPE value of 1.029%, and maximum direction accuracy of 71.43% in result of the solution of IMKB time series for 15-observation test set. The graphs of the last 15 observations of IMKB time series along with the 15-observation test set forecasts obtained with the proposed method are shown together in Figure 4.

In result of the solutions of IMKB time series, it has been observed that the proposed method significantly increased

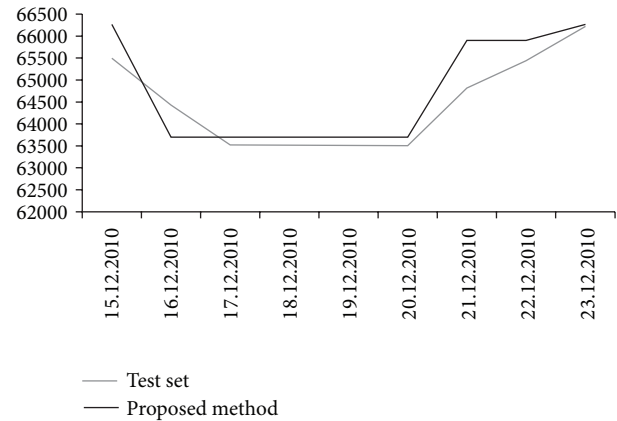


FIGURE 3: The graphs of the 7-observation test set of IMKB data and the forecasts of the test set obtained with the proposed method.

the future forecasting performance compared to other methods. Also in the graphs within Figures 3 and 4, the results of the proposed method are seen to be considerably similar to the test set values.

In the solution of the gold prices data given in Figure 2 via the methods in the literature by taking the last 30 observations and the last 45 observations as test set, one has the following.

- Gold prices solution of Song and Chissom [1], Huarng [11], and Huarng and Yu [13] methods has been conducted just as previously done on the abovementioned IMKB time series.
- For each of the 2nd-, 3rd-, 4th-, and 5th-order models of Chen [5] first-order fuzzy time series forecast method, Chen [6] high-order fuzzy time series forecast method, and Aladag et al. [8] high order fuzzy time series forecast method, the RMSE values have been found for different lengths being increased 100 units between 500 and 3500. The test set forecasts



TABLE 4: The best results obtained for 15-observation test set of IMKB data.

Date	Test set	Song and Chissom [1]	Chen [5]	Chen [6]	Huarng [11] distribution-based method	Huarng [11] average-based method	Huarng and Yu [13] rational-based method	Aladag et al. [8]	Proposed method*
01.12.2010	66156	65695.5	66250	64833.3	65900.0	65300	66328.8	65650	66000
02.12.2010	66939	66438.2	65800	66700.0	65566.7	64100	66164.2	67150	67633
03.12.2010	66860	67088.0	67450	66700.0	67233.3	66700	67143.8	67150	66700
08.12.2010	67705	67088.0	67450	66700.0	67233.3	66700	67143.8	67150	66700
09.12.2010	65914	66252.5	66250	67633.3	65900.0	67700	66328.8	67150	68100
10.12.2010	64759	65695.5	65800	66233.3	65566.7	65900	65791.4	64150	65300
13.12.2010	66380	65695.5	65350	66700.0	65900.0	64700	65258.3	65650	65300
14.12.2010	66510	66438.2	65800	66700.0	65566.7	67100	66164.2	65650	66700
15.12.2010	65499	66438.2	65800	66700.0	67233.3	66500	66164.2	67150	66700
16.12.2010	64429	65695.5	66250	65766.7	65566.7	66300	66328.8	64150	65300
17.12.2010	63524	65695.5	65350	64366.7	65900.0	64500	65258.3	65650	63900
20.12.2010	63502	65138.5	63550	63900.0	64900.0	63500	63684.8	65650	63900
21.12.2010	64820	65138.5	63550	63900.0	64900.0	63500	63684.8	65650	63900
22.12.2010	65440	65695.5	65350	64833.3	65900.0	65500	65258.3	65650	65300
23.12.2010	66219	65695.5	66250	66700.0	65566.7	66300	66328.8	65650	66000
RMSE		919.47	925.42	954.17	1052.90	1283.18	896.96	1060.12	865.28
MAPE		0.01124	0.01081	0.01245	0.01285	0.01558	0.01085	0.01312	0.01029
DA		0.71429	0.57143	0.64286	0.50000	0.57143	0.64286	0.64286	0.71429

\*The best result.

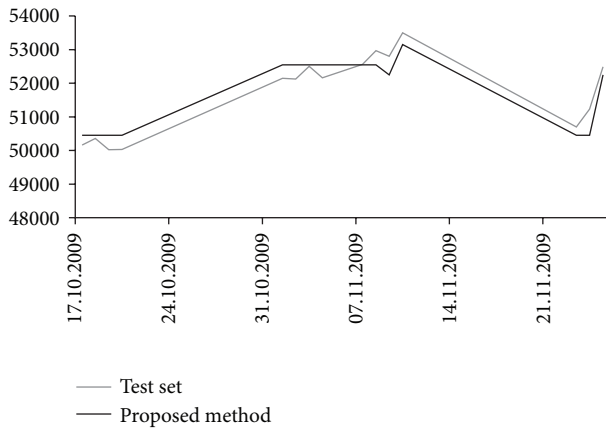


FIGURE 4: The graphs of the 15-observation test set of IMKB data and forecasts of the test set obtained with the proposed method.

that have the minimum RMSE values among these 31 trials have been determined as the best results of the methods.

In the solution of the gold prices data given in Figure 2 via the proposed method by taking the last 30 observations and the last 45 observations as test set, one has the following.

- (i) During the fuzzification of time series of the proposed method, interval lengths of  $U$  have been tried as increasing the interval length between 500 and 3500 by 100 units by solving from Steps 1 and 6. The test set

forecast with the smallest RMSE value among these forecasts has been determined as the best result of the fuzzy AR(1) model.

- (ii) The error series have been obtained via the formula (9) for 248 observations with the same calculation made previously in the application of IMKB data.
- (iii) Different trials have been made by increasing the interval length between 500 and 3500 by 100 units for the time series and by increasing the interval length between 100 and 1100 by 50 units for the error series by solving from Step 1 to Step 13. Among these trials, the test set forecast with the smallest RMSE value has been determined as the best result of the fuzzy ARMA(1,1) model.

During the application of the proposed method and the methods in the literature on gold prices time series, the parameters with which the forecasts with the best test set performance for 30 and 45 test sets occurred to be the following:

- (i) for the application of Song and Chissom [1] method, when the number of fuzzy sets is 10 for both 30 and 45 test sets,
- (ii) for the application of Chen [5] method, when the interval length is 600 for 30 and 1700 for 45,
- (iii) for the application of distribution-based Huarnng approach [11], when the interval length is 400, and for the application of average based approach, when the interval length is 200,

TABLE 5: The best results obtained for 30-observation test set of gold prices.

Date	Test set	Song and Chissom [1]	Chen [5]	Chen [6]	Huarng [11] distribution-based method	Huarng [11] average-based method	Huarng and Yu [13] rational-based method	Aladag et al. [8]	Proposed method*
17.11.2009	53935	53157	53300	53000.0	53200	53200	53356.4	53300	53400
18.11.2009	54550	53157	53900	53666.7	54000	53900	53894.0	53900	54200
19.11.2009	54495	53157	52400	54066.7	52400	51500	51715.7	54500	54200
20.11.2009	54830	53157	52400	54200.0	52400	51500	51715.7	53900	54200
23.11.2009	55950	53157	55100	54600.0	54800	54900	55017.3	54500	55000
24.11.2009	56285	52294	55700	55266.7	56000	55900	55779.2	55100	55800
25.11.2009	56430	52294	56300	56066.7	56400	56300	56164.1	55700	56600
01.12.2009	57635	52294	56300	56466.7	56400	56500	56551.6	55100	56600
02.12.2009	58330	53157	57500	57000.0	57600	57700	57730.3	55700	57400
03.12.2009	58150	53157	58100	57666.7	58400	58300	58529.8	56300	58200
04.12.2009	56630	53157	58100	58066.7	58000	58100	58128.7	56300	58200
07.12.2009	54820	53157	56900	57400.0	56800	56700	56551.6	55100	56600
08.12.2009	55660	53157	55100	56066.7	54800	54900	51715.7	55100	55000
09.12.2009	55110	52294	55700	55666.7	55600	55700	55779.2	55100	55800
10.12.2009	54180	52294	55100	55266.7	55200	55100	55017.3	54500	55000
11.12.2009	54580	53157	53900	54733.3	54000	54100	53157.9	53900	54200
14.12.2009	54190	53157	52400	54333.3	52400	51500	51715.7	54500	54200
15.12.2009	54120	53157	53900	54200.0	54000	54100	53157.9	53300	54200
16.12.2009	54855	53157	53900	54200.0	54000	54100	53157.9	53900	54200
17.12.2009	54430	53157	55100	54600.0	54800	54900	55017.3	54500	55000
18.12.2009	53750	53157	52400	54466.7	52400	51500	53157.9	54500	54200
21.12.2009	54570	53157	53900	53933.3	53200	53700	53894.0	53300	53400
22.12.2009	53400	53157	52400	53933.3	52400	51500	51715.7	54500	54200
23.12.2009	52990	53157	53300	53666.7	53200	53200	53356.4	53300	53400
24.12.2009	53575	52294	53150	53133.3	53200	53200	53524.7	52700	53400
25.12.2009	53450	53157	53300	53133.3	53200	53200	53356.4	53300	53400
28.12.2009	53795	53157	53300	53266.7	53200	53200	53356.4	53300	53400
29.12.2009	53515	53157	53900	53400.0	53200	53700	53894.0	53900	53400
30.12.2009	53095	53157	53300	53400.0	53200	53200	53356.4	52700	53400
31.12.2009	52920	52294	53300	53400.0	53600	53100	53524.7	53300	53400
RMSE		2410.96	1031.12	857.34	1045.23	1288.80	1412.66	1003.50	707.71
MAPE		0.03339	0.01512	0.01245	0.01530	0.01713	0.01935	0.01382	0.01028
DA		0.55172	0.55172	0.51724	0.55172	0.62069	0.55172	0.48276	0.62069

\*The best result.

- (iv) for the application of ratio-based Huarng and Yu [13] approach, when the sample percentile  $\alpha = 0.5$ ,
- (v) for the application of Chen method [6], when the interval length is 1900 in 5th order model for 30 and 800 in 3rd-order model for 45,
- (vi) for the application of Aladag et al. [8], when the interval length is 600 on 5th-degree model and unit number of artificial neural network hidden layers is 5 for 30, and when the interval length is 800 on 3rd degree model and unit number of artificial neural network hidden layers is 4 for 45,

- (vii) for the application of the proposed fuzzy ARMA(1,1) method, when the interval length of time series is 800 and the interval length of error series is 2500 for 30, and when the interval length of time series is 900 and the interval length of error series is 1000 for 45.

Best forecasts and forecast performances of all methods in result of gold prices time series solution for 30-observation test set are summarised in Table 5.

When Table 5 is observed, it is seen in result of the solution of gold prices time series for 30 observation test set

TABLE 6: The best results obtained for 45-observation test set of gold prices.

Date	Test set	Song and Chissom [1]	Chen [5]	Chen [6]	Huarng [11] distribution-based method	Huarng [11] average-based method	Huarng and Yu [13] rational-based method	Aladag et al. [8]	Proposed method*
17.10.2009	50162	50568	50350	49933.3	50800.0	50420.0	50829.1	50200	50450
18.10.2009	50355	50568	50350	50066.7	50800.0	51100.0	50829.1	50200	50450
19.10.2009	50020	50568	50350	50120.0	50000.0	49900.0	50051.5	50200	50450
20.10.2009	50030	50568	50350	51000.0	50800.0	51100.0	50829.1	50200	50450
23.11.2009	50700	50568	50350	51000.0	50800.0	51100.0	50829.1	50200	50450
24.11.2009	51230	50568	50350	51800.0	51066.7	51500.0	50824.1	51000	50450
25.11.2009	52490	50568	52050	50866.7	51200.0	51500.0	51128.5	51000	52250
01.11.2009	52150	52294	52050	51800.0	52666.7	54300.0	54499.6	52600	52550
02.11.2009	52125	52294	52050	51933.3	50600.0	52100.0	51916.0	51800	52550
03.11.2009	52500	52294	52050	51933.3	50600.0	52100.0	51916.0	51800	52550
04.11.2009	52165	52294	52050	52200.0	52666.7	54300.0	54499.6	52600	52550
07.11.2009	52560	52294	52050	52066.7	50600.0	52100.0	51916.0	51800	52550
08.11.2009	52972	52294	52050	52333.3	52666.7	54300.0	54499.6	52600	52550
09.11.2009	52800	52294	52900	52466.7	52800.0	52900.0	52867.3	52600	52250
10.11.2009	53500	52294	52050	54200.0	52800.0	52900.0	52867.3	52600	53150
17.11.2009	53935	53157	52900	53000.0	53200.0	53200.0	53205.5	53400	54950
18.11.2009	54550	53157	52900	53666.7	54000.0	53900.0	53840.7	53400	54050
19.11.2009	54495	53157	52900	54066.7	52400.0	51500.0	52393.3	54200	54950
20.11.2009	54830	53157	52900	54200.0	52400.0	51500.0	52393.3	54200	54050
23.11.2009	55950	53157	55450	54600.0	54800.0	54900.0	54832.0	54200	54950
24.11.2009	56285	52294	55450	55266.7	56000.0	55900.0	55841.6	54200	55850
25.11.2009	56430	52294	55450	56066.7	56400.0	56300.0	56182.2	55000	55850
01.12.2009	57635	52294	57150	56466.7	56400.0	56500.0	56524.9	55000	56750
02.12.2009	58330	53157	57150	57000.0	57600.0	57700.0	57565.6	55000	57650
03.12.2009	58150	53157	58850	57666.7	58400.0	58300.0	58270.1	55000	58550
04.12.2009	56630	53157	58850	58066.7	58000.0	58100.0	58270.1	55800	58550
07.12.2009	54820	53157	57150	57400.0	56800.0	56700.0	56524.9	55800	56750
08.12.2009	55660	53157	55450	56066.7	54800.0	54900.0	54832.0	55000	54950
09.12.2009	55110	52294	55450	55666.7	55600.0	55700.0	55503.0	54200	55850
10.12.2009	54180	52294	55450	55266.7	55200.0	55100.0	55166.5	54200	54950
11.12.2009	54580	53157	52900	54733.3	54000.0	54100.0	54169.1	54200	54050
14.12.2009	54190	53157	52900	54333.3	52400.0	51500.0	52393.3	54200	54950
15.12.2009	54120	53157	52900	54200.0	54000.0	54100.0	54169.1	54200	54050
16.12.2009	54855	53157	52900	54200.0	54000.0	54100.0	54169.1	54200	54050
17.12.2009	54430	53157	55450	54600.0	54800.0	54900.0	54832.0	54200	54950
18.12.2009	53750	53157	52900	54466.7	52400.0	51500.0	52393.3	54200	54050
21.12.2009	54570	53157	52900	53933.3	53200.0	53700.0	53840.7	53400	54050
22.12.2009	53400	53157	52900	53933.3	52400.0	51500.0	52393.3	53400	54950
23.12.2009	52990	53157	52900	53666.7	53200.0	53200.0	53205.5	53400	53150
24.12.2009	53575	52294	52900	53133.3	52800.0	52900.0	52867.3	52600	53150
25.12.2009	53450	53157	52900	53133.3	53200.0	53200.0	53205.5	53400	52250
28.12.2009	53795	53157	52900	53266.7	53200.0	53200.0	53205.5	53400	53150
29.12.2009	53515	53157	52900	53400.0	53200.0	53700.0	53840.7	53400	54050
30.12.2009	53095	53157	52900	53400.0	53200.0	53200.0	53205.5	53400	53150
31.12.2009	52920	52294	52900	53400.0	53600.0	53100.0	53514.3	53400	53150
RMSE		2009.32	1028.39	787.71	1022.13	1200.24	1041.74	1068.71	719.69
MAPE		0.02556	0.01499	0.01146	0.01499	0.01628	0.01517	0.01328	0.01072
DA		0.54545	0.52273	0.54545	0.52273	0.61364	0.59091	0.54545	0.50000

\*The best result.

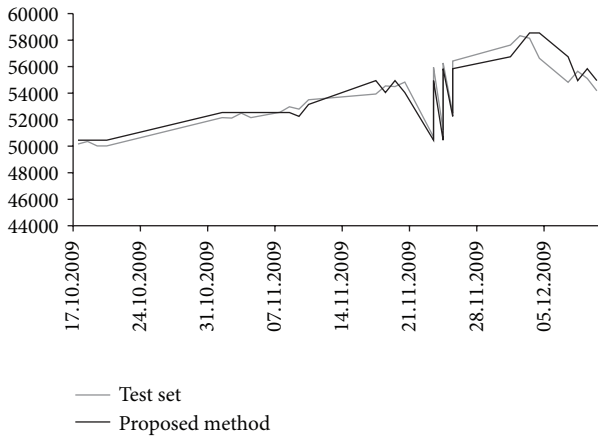


FIGURE 5: The graphs of the 30-observation test set of gold prices and forecasts of the test set obtained with the proposed method.

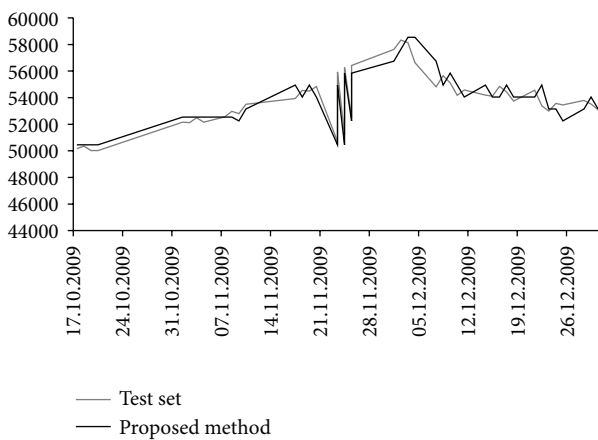


FIGURE 6: The graphs of the 45-observation test set of gold prices and forecasts of the test set obtained with the proposed method.

that the proposed method produced the best forecasting performance with a minimum RMSE value of 707.71, minimum MAPE value of 1.028%, and maximum direction accuracy of 62.07%. The graphs of the last 30 observations of gold prices time series along with the 30-observation test set forecasts obtained with the proposed method are shown together in Figure 5.

Best forecasts and forecast performances of all methods in result of gold prices time series solution for 45-observation test set are summarised in Table 6. Furthermore, the graphs of the last 45 observations of gold prices time series along with the 45-observation test set forecasts obtained with the proposed method are shown together in Figure 6.

When Table 6 is evaluated, it is seen in result of the solution of gold prices time series for 45 observation test set that the proposed method produced the best forecasting performance with a minimum RMSE value of 719.69, minimum MAPE value of 1.072%.

In result of the solutions of gold prices time series, it has been observed that the proposed method significantly increased the future forecasting performance compared to

TABLE 7:  $R/S$  test results.

Data	$R/S$ statistics	$P < 0.01$
IMKB	1.6523	No
Gold price	1.9560	No

other methods. Also in the graphs within Figures 5 and 6, the results of the proposed method are seen to be considerably similar to the test set values.

## 5. Discussion and Conclusion

MA variables are not included in the fuzzy time series forecast models proposed in the literature whereas real life time series are also influenced from MA variables in addition to AR variables. Therefore, redefining fuzzy times series methods as models including also MA variables are a more realistic act. In this study, a solution algorithm for a new first-order fuzzy ARMA(1,1) time series forecast model containing not only AR but also MA variables is proposed based on group relation tables. The method proposed is a basic algorithm similar to Chen [5] approach, aiming at eliminating the model specification error formed due to the exclusion of MA variables. In conclusion of the applications, it has been observed that the proposed method has higher forecasting performance than many of the fuzzy time series forecasting methods commonly used in the literature. It is an important finding that although the proposed method is a basic method based on group relation tables, it may have a higher forecasting performance even than the high order fuzzy time series methods based on artificial neural networks. Therefore, it is obvious that forecasting performance is going to increase significantly when fuzzy ARMA models are developed where fuzzy relations are specified with artificial neural networks and artificial intelligence methods or where membership values are used for specification of fuzzy relations. Thus, the proposed method may be provided with a more systematic structure and higher forecasting performance with improvements that may be done on various stages of the method during future studies. Moreover, there is no linear model assumption in the proposed fuzzy time series method. Thus, the proposed method and other fuzzy time series methods can be applied to nonlinear time series. In the application, proposed method is applied to short range dependent time series. In the future studies, it will be researched about the performance of the proposed method for long range dependent time series.

## Appendix

The  $R/S$  test was applied to two time series which are used in the application.  $R/S$  test was applied by using "FinMetrics module of S-PLUS package program". The obtained results are shown in Table 7. It is obtained that both of time series have short range dependence.

## References

- [1] Q. Song and B. S. Chissom, "Fuzzy time series and its models," *Fuzzy Sets and Systems*, vol. 54, no. 3, pp. 269–277, 1993.
- [2] L. A. Zadeh, "Fuzzy sets," *Information and Computation*, vol. 8, pp. 338–353, 1965.
- [3] Q. Song and B. S. Chissom, "Forecasting enrollments with fuzzy time series. Part I," *Fuzzy Sets and Systems*, vol. 54, pp. 1–10, 1993.
- [4] Q. Song and B. S. Chissom, "Forecasting enrollments with fuzzy time series. Part II," *Fuzzy Sets and Systems*, vol. 62, no. 1, pp. 1–8, 1994.
- [5] S.-M. Chen, "Forecasting enrollments based on fuzzy time series," *Fuzzy Sets and Systems*, vol. 81, no. 3, pp. 311–319, 1996.
- [6] S.-M. Chen, "Forecasting enrollments based on high-order fuzzy time series," *Cybernetics and Systems*, vol. 33, no. 1, pp. 1–16, 2002.
- [7] K. Huarng and H.-K. Yu, "The application of neural networks to forecast fuzzy time series," *Physica A*, vol. 363, no. 2, pp. 481–491, 2006.
- [8] C. H. Aladag, M. A. Basaran, E. Egrioglu, U. Yolcu, and V. R. Uslu, "Forecasting in high order fuzzy times series by using neural networks to define fuzzy relations," *Expert Systems with Applications*, vol. 36, no. 3, pp. 4228–4231, 2009.
- [9] T. H.-K. Yu and K.-H. Huarng, "A neural network-based fuzzy time series model to improve forecasting," *Expert Systems with Applications*, vol. 37, no. 4, pp. 3366–3372, 2010.
- [10] U. Yolcu, C. H. Aladag, E. Egrioglu, and V. R. Uslu, "Time series forecasting with a novel fuzzy time series approach: an example for Istanbul stock market," *Journal of Statistical Computation and Simulation*, vol. 83, no. 4, pp. 599–612, 2013.
- [11] K. Huarng, "Effective lengths of intervals to improve forecasting in fuzzy time series," *Fuzzy Sets and Systems*, vol. 123, no. 3, pp. 387–394, 2001.
- [12] E. Egrioglu, C. H. Aladag, U. Yolcu, V. R. Uslu, and M. A. Basaran, "Finding an optimal interval length in high order fuzzy time series," *Expert Systems with Applications*, vol. 37, no. 7, pp. 5052–5055, 2010.
- [13] K. Huarng and T. H.-K. Yu, "Ratio-based lengths of intervals to improve fuzzy time series forecasting," *IEEE Transactions on Systems, Man, and Cybernetics B*, vol. 36, no. 2, pp. 328–340, 2006.
- [14] U. Yolcu, E. Egrioglu, V. R. Uslu, M. A. Basaran, and C. H. Aladag, "A new approach for determining the length of intervals for fuzzy time series," *Applied Soft Computing Journal*, vol. 9, no. 2, pp. 647–651, 2009.
- [15] V. R. Uslu, C. H. Aladag, U. Yolcu, and E. Egrioglu, "A new hybrid approach for forecasting a seasonal fuzzy time series," in *Proceedings of the International Symposium Computing Science and Engineering Proceeding Book*, pp. 1152–1158, 2010.
- [16] F. Alpaslan, O. Cagcag, C. H. Aladag, U. Yolcu, and E. Egrioglu, "A novel seasonal fuzzy time series method," *Hacettepe Journal of Mathematics and Statistics*, vol. 41, no. 3, pp. 375–385, 2012.
- [17] S. Aladag, C. H. Aladag, T. Menten, and E. Egrioglu, "A new seasonal fuzzy time series method based on the multiplicative neuron model and SARIMA," *Hacettepe Journal of Mathematics and Statistics*, vol. 41, no. 3, pp. 337–345, 2012.
- [18] E. Egrioglu, U. Yolcu, C. H. Aladag, and C. Kocak, "An ARMA type fuzzy time series forecasting method based on particle swarm optimization," *Mathematical Problems in Engineering*, vol. 2013, Article ID 935815, 12 pages, 2013.
- [19] H. E. Hurst, "Long-term storage capacity of reservoirs," *Transactions of the American Society of Civil Engineers*, vol. 116, pp. 770–779, 1951.
- [20] M. Li and W. Zhao, "On  $1/f$  noise," *Mathematical Problems in Engineering*, vol. 2012, Article ID 673648, 22 pages, 2012.
- [21] M. Li and W. Zhao, "Visiting power laws in cyber-physical networking systems," *Mathematical Problems in Engineering*, vol. 2012, Article ID 302786, 13 pages, 2012.
- [22] M. Li, "Fractal time series: a tutorial review," *Mathematical Problems in Engineering*, vol. 2010, Article ID 157264, 26 pages, 2010.
- [23] H. E. Stanley, S. V. Buldyrev, A. L. Goldberger, S. Havlin, C.-K. Peng, and M. Simons, "Long-range power-law correlations in condensed matter physics and biophysics," *Physica A*, vol. 200, no. 14, pp. 4–24, 1993.
- [24] G. Werner, "Fractals in the nervous system: conceptual implications for theoretical neuroscience," *Frontiers in Fractal Physiology*, vol. 1, article 15, 28 pages, 2010.
- [25] J. Beran, "Statistical methods for data with long-range dependence," *Statistica Science*, vol. 7, no. 4, pp. 404–416, 1992.
- [26] P. C. Ivanov, L. A. Nunes Amaral, A. L. Goldberger et al., "From  $1/f$  noise to multifractal cascades in heartbeat dynamics," *Chaos*, vol. 11, no. 3, pp. 641–652, 2001.
- [27] B. Podobnik, D. Horvatic, A. L. Ng, H. E. Stanley, and P. Ch. Ivanov, "Modeling long-range cross-correlations in two-component ARFIMA and FIARCH processes," *Physica A*, vol. 387, no. 15, pp. 3954–3959, 2008.
- [28] M. Zevallos and W. Palma, "Minimum distance estimation of ARFIMA processes," *Computational Statistics & Data Analysis*, vol. 58, pp. 242–256, 2013.
- [29] R. J. Bhansali and P. S. Kokoszka, "Prediction of long-memory time series: a tutorial review," in *Processes With Long-Range Correlations*, vol. 621 of *Lecture Notes in Physics*, pp. 3–21, 2003.



## Research Article

# Residual ISI Obtained by Nonblind Adaptive Equalizers and Fractional Noise

**Monika Pinchas**

*Department of Electrical and Electronic Engineering, Ariel University, 40700 Ariel, Israel*

Correspondence should be addressed to Monika Pinchas; [monika.pinchas@gmail.com](mailto:monika.pinchas@gmail.com)

Received 18 July 2013; Accepted 29 August 2013

Academic Editor: Ming Li

Copyright © 2013 Monika Pinchas. This is an open access article distributed under the Creative Commons Attribution License, which permits unrestricted use, distribution, and reproduction in any medium, provided the original work is properly cited.

Recently, a closed-form approximated expression was derived by the same author for the achievable residual intersymbol interference (ISI) case that depends on the step-size parameter, equalizer's tap length, input signal statistics, signal to noise ratio (SNR), and channel power and is valid for fractional Gaussian noise (fGn) input where the Hurst exponent is in the region of  $0.5 \leq H < 1$ . But this expression was obtained for the blind adaptive case and cannot be applied to the nonblind adaptive version. Up to now, the achievable residual ISI for the non-blind adaptive case could be obtained only via simulation. In this paper, we derive a closed-form approximated expression (or an upper limit) for the residual ISI obtained by non-blind adaptive equalizers valid for fractional Gaussian noise (fGn) input where the Hurst exponent is in the region of  $0.5 \leq H < 1$ . This new obtained expression depends on the step-size parameter, equalizer's tap length, input signal statistics, SNR, channel power, and the Hurst exponent parameter. Simulation results indicate that there is a high correlation between the calculated results (obtained from the new obtained expression for the residual ISI) and those obtained from simulating the system.

## 1. Introduction

We consider a nonblind deconvolution problem in which we observe the output of an unknown, possibly nonminimum phase, linear system (single-input-single-output (SISO) FIR system) from which we want to recover its input (source) using an adjustable linear filter (equalizer) and training symbols. During transmission, a source signal undergoes a convolutive distortion between its symbols and the channel impulse response. This distortion is referred to as ISI [1, 2]. It is well known that ISI is a limiting factor in many communication environments where it causes an irreducible degradation of the bit error rate thus imposing an upper limit on the data symbol rate. In order to overcome the ISI problem, an equalizer is implemented in those systems [1–12].

In this paper, we consider the nonblind adaptive equalizer where training sequences are needed to generate the error that is fed into the adaptive mechanism which updates the equalizer's taps [9–12]. The nonblind adaptive approach yields in most cases a better equalization performance considering convergence speed and equalization quality compared with the blind adaptive version [6]. In addition, the blind adaptive

version has a higher computational cost compared with its nonblind approach [6].

The equalization performance from the residual ISI point of view depends on the channel characteristics, on the added noise, on the step-size parameter used in the adaptation process, on the equalizer's tap length and on the input signal statistics [13, 14]. Fast convergence speed and reaching a residual ISI where the eye diagram is considered to be open (for the communication case) are the main requirements from a blind or nonblind equalizer. Fast convergence speed may be obtained by increasing the step-size parameter. But, increasing the step-size parameter may lead to a higher residual ISI which might not meet the system's requirements any more. Recently [2], a closed-form approximated expression was derived for the achievable residual ISI case that depends on the step-size parameter, equalizer's tap length, input signal statistics, SNR, Hurst exponent, and channel power. But this expression is valid only for the blind adaptive case and cannot be used for the nonblind version.

Up to now, the achievable residual ISI for the nonblind adaptive case (for the noisy or noiseless case) could be obtained only via simulation. Thus, the system designer had



to spend a lot of time in simulating the whole system in order to find the best values for the step-size parameter and equalizer's tap length that meet the system's requirements from the residual ISI point of view. In this paper, we derive a closed-form approximated expression (or an upper limit) for the residual ISI obtained by nonblind adaptive equalizers that depends on the step-size parameter, equalizer's tap length, input signal statistics, SNR, channel power, and Hurst exponent parameter. This expression is valid for fGn input where the Hurst exponent is in the region of  $0.5 \leq H < 1$ . Please note,  $H = 1$  is the limit case, which does not have much practical sense [15–17]. It should be pointed out that a white Gaussian process is a special case ( $H = 0.5$ ) of the fractional Gaussian noise (fGn) model [18]. FGn with  $H \in (0.5, 1)$  corresponds to the case of long-range dependency (LRD) [18]. Thus, the new obtained expression for the achievable residual ISI is not only valid for the special case of white Gaussian process but also covers those cases that correspond to the case of LRD.

The paper is organized as follows. After having described the system under consideration in Section 2, the closed-form approximated expression (or upper limit) for the residual ISI is introduced in Section 3. In Section 4, simulation results are presented, and the conclusion is given in Section 5.

## 2. System Description

The system under consideration is illustrated in Figure 1, where we make the following assumptions.

- (1) The input sequence  $x[n]$  belongs to a two independent quadrature carriers case constellation input with variance  $\sigma_x^2$ , where  $x_r[n]$  and  $x_i[n]$  are the real and imaginary parts of  $x[n]$ , respectively, and  $\sigma_{x_r}^2$  is the variance of  $x_r[n]$ .
- (2) The unknown channel  $h[n]$  is a possibly nonminimum phase linear time-invariant filter in which the transfer function has no “deep zeros”; namely, the zeros lie sufficiently far from the unit circle.
- (3) The equalizer  $c[n]$  is a tap-delay line.
- (4) The noise  $w[n]$  consists of  $w[n] = w_r[n] + jw_i[n]$ , where  $w_r[n]$  and  $w_i[n]$  are the real and imaginary parts of  $w[n]$ , respectively, and  $w_r[n]$  and  $w_i[n]$  are independent. Both  $w_r[n]$  and  $w_i[n]$  are fractional Gaussian noises (fGn) with zero mean. Note that  $\sigma_{w_r}^2 = E[w_r^2[n]]$ ,  $\sigma_{w_i}^2 = E[w_i^2[n]]$ , for  $m \neq k$ :  $E[w_r[n-k]w_r[n-m]] = (\sigma_{w_r}^2/2)[(|m-k|-1)^{2H} - 2(|m-k|)^{2H} + (|m-k|+1)^{2H}]$  and  $E[w_i[n-k]w_i[n-m]] = (\sigma_{w_i}^2/2)[(|m-k|-1)^{2H} - 2(|m-k|)^{2H} + (|m-k|+1)^{2H}]$ , where  $E[\cdot]$  denotes the expectation operator on  $(\cdot)$  and  $H$  is the Hurst exponent.
- (5) The variance of  $w[n]$  is denoted as  $E[w[n]w^*[n]] = \sigma_w^2$ , where  $\sigma_w^2 = 2\sigma_{w_i}^2 = 2\sigma_{w_r}^2$  and  $(\cdot)^*$  is the conjugate operation on  $(\cdot)$ .

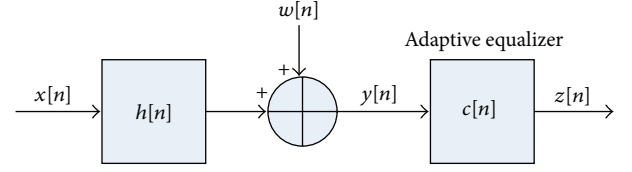


FIGURE 1: Block diagram of a baseband communication system.

The transmitted sequence  $x[n]$  is sent through the channel  $h[n]$  and is corrupted with noise  $w[n]$ . Therefore, the equalizer's input sequence  $y[n]$  may be written as

$$y[n] = x[n] * h[n] + w[n], \quad (1)$$

where “ $*$ ” denotes the convolution operation. The equalized output signal can be written as

$$z[n] = x[n] + p[n] + \tilde{w}[n], \quad (2)$$

where  $p[n]$  is the convolutional noise, namely, the residual intersymbol interference (ISI) arising from the difference between the ideal equalizer's coefficients and those chosen in the system and  $\tilde{w}[n] = w[n] * c[n]$ . The ISI is often used as a measure of performance in equalizers' applications, defined by

$$\text{ISI} = \frac{\sum_{\tilde{m}} |\tilde{s}_{\tilde{m}}|^2 - |\tilde{s}|_{\max}^2}{|\tilde{s}|_{\max}^2}, \quad (3)$$

where  $|\tilde{s}|_{\max}$  is the component of  $\tilde{s}$ , given in (4), having the maximal absolute value. Consider that

$$\tilde{s}[n] = c[n] * h[n] = \delta[n] + \zeta[n], \quad (4)$$

where  $\delta$  is the Kronecker delta function and  $\zeta[n]$  stands for the difference (error) between the ideal and the actual value used for  $c[n]$ .

Next, we turn to the adaptation mechanism of the equalizer which is based on training symbols [9–12, 19]:

$$\underline{c}_{\text{eq}}[n+1] = \underline{c}_{\text{eq}}[n] - \mu(z[n] - x[n])\underline{y}^*[n], \quad (5)$$

where  $\mu$  is the step-size parameter,  $\underline{c}_{\text{eq}}[n]$  is the equalizer vector where the input vector is  $\underline{y}[n] = [y[n] \cdots y[n-N+1]]^T$ , and  $N$  is the equalizer's tap length. The operator  $(\cdot)^T$  denotes for transpose of the function  $(\cdot)$ . Please note that for the nonblind adaptive case, during the training period, a known data sequence is transmitted. A replica of this sequence is made available at the receiver in proper synchronism with the transmitter, thereby making it possible for adjustments to be made to the equalizer coefficients in accordance with the adaptive filtering algorithm employed in the equalizer design [19].

## 3. Residual ISI for Fractional Gaussian Noise Input

In this section, a closed-form approximated expression (or an upper limit) is derived for the residual ISI valid for the fGn input case.

**Theorem 1.** *Noted the following assumptions.*

- (1) *The convolutional noise  $p[n]$  is a zero mean, white Gaussian process with variance  $\sigma_p^2 = E[p[n]p^*[n]]$ . The real part of  $p[n]$  is denoted as  $p_r[n]$  and  $E[p_r^2[n]] = m_p$ .*
- (2) *The source signal  $x[n]$  is a rectangular Quadrature Amplitude Modulation (QAM) signal (where the real part of  $x[n]$  is independent of the imaginary part of  $x[n]$ ) with known variance and higher moments.*
- (3) *The convolutional noise  $p[n]$  and the source signal are independent.*
- (4) *The gain between the source and equalized output signal is equal to one.*
- (5) *The convolutional noise  $p[n]$  is independent of  $\tilde{w}[n]$ .*
- (6) *The added noise is fGn with zero mean.*
- (7) *The channel  $h[n]$  has real coefficients.*
- (8) *The Hurst exponent is in the range of  $0.5 \leq H < 1$ .*

The residual ISI expressed in dB units may be defined as

$$\text{ISI} = 10 \log_{10}(m_p) - 10 \log_{10}(\sigma_{x_r}^2), \quad (6)$$

where  $m_p$  is defined by

$$\begin{aligned} m_p &= \sigma_{\tilde{w}_r}^2 \left( \mu \left( N\sigma_x^2 \sum_{k=0}^{R-1} h_k^2[n] + \frac{N\sigma_x^2}{\text{SNR}} \right)^2 \right. \\ &\quad \times \left( 2 \left( N\sigma_x^2 \sum_{k=0}^{R-1} h_k^2[n] + \frac{N\sigma_x^2}{\text{SNR}} \right) \right. \\ &\quad \left. \left. - \mu \left( N\sigma_x^2 \sum_{k=0}^{R-1} h_k^2[n] + \frac{N\sigma_x^2}{\text{SNR}} \right)^2 \right)^{-1} \right) \\ &= \sigma_{\tilde{w}_r}^2 \frac{\mu \left( N\sigma_x^2 \sum_{k=0}^{R-1} h_k^2[n] + \frac{N\sigma_x^2}{\text{SNR}} \right)}{2 - \mu \left( N\sigma_x^2 \sum_{k=0}^{R-1} h_k^2[n] + \frac{N\sigma_x^2}{\text{SNR}} \right)}, \\ \sigma_{\tilde{w}_r}^2 &\cong \frac{\sigma_{x_r}^2}{\text{SNR} \sum_{k=0}^{R-1} h_k^2[n]} \left[ 1 + \sqrt{(N-1)H(2H-1)} \right], \end{aligned} \quad (7)$$

and  $R$  is the channel length,  $\sigma_{\tilde{w}_r}^2$  is the variance of  $\tilde{w}_r[n]$  ( $\tilde{w}_r[n]$  is the real part of  $\tilde{w}[n]$ ), and SNR is given by  $\text{SNR} = \sigma_{x_r}^2 / \sigma_{\tilde{w}_r}^2 = \sigma_x^2 / \sigma_w^2$ .

*Comments.* It should be pointed out that assumptions (1)–(5) from above are precisely the same assumptions made in [2, 14].

*Proof.* Let us first recall the expression for the adaptation mechanism of the equalizer given in (5). Then, we substitute (2) into (5) and obtain

$$\underline{c}_{\text{eq}}[n+1] = \underline{c}_{\text{eq}}[n] - \mu (p[n] + \tilde{w}[n]) \underline{y}^*[n]. \quad (8)$$

Next, we recall from [14] the expression for  $E[\Delta(p_r^2)]$ , where  $p_r$  is the real part of  $p[n]$  and  $\Delta(p_r^2) = p_r^2[n+1] - p_r^2[n]$ :

$$\begin{aligned} E[\Delta(p_r^2)] &\cong -2E \left[ p_r \left( \mu P_r(z) \sum_{m=0}^{m=N-1} y[n-m] y^*[n-m] \right) \right] \\ &\quad + E \left[ \left( -\mu P_r(z) \sum_{m=0}^{m=N-1} y[n-m] y^*[n-m] \right)^2 \right], \end{aligned} \quad (9)$$

where  $P_r(z)$  is the real part of  $P(z)$  and is given in our case as

$$P(z) = z[n] - x[n] = p[n] + \tilde{w}[n] \implies P_r(z) = p_r + \tilde{w}_r[n]. \quad (10)$$

According to [13, 14], when the equalizer has converged, we may assume that  $E[\Delta(p_r^2)] \cong 0$ . Therefore, by setting  $E[\Delta(p_r^2)] = 0$  into (9), we obtain

$$\begin{aligned} &-2\mu m_p E \left[ \sum_{m=0}^{m=N-1} y[n-m] y^*[n-m] \right] \\ &\quad + \mu^2 (m_p + \sigma_{\tilde{w}_r}^2) \\ &\quad \times E \left[ \left( \sum_{m=0}^{m=N-1} y[n-m] y^*[n-m] \right)^2 \right] = 0 \\ &\quad \Downarrow \\ m_p &= \sigma_{\tilde{w}_r}^2 \left( \mu E \left[ \left( \sum_{m=0}^{m=N-1} y[n-m] y^*[n-m] \right)^2 \right] \right. \\ &\quad \times \left( 2E \left[ \sum_{m=0}^{m=N-1} y[n-m] y^*[n-m] \right] - \mu E \right. \\ &\quad \left. \left. \times \left[ \left( \sum_{m=0}^{m=N-1} y[n-m] y^*[n-m] \right)^2 \right] \right)^{-1} \right) \right). \end{aligned} \quad (11)$$

In [13], the expression  $E[(\sum_{m=0}^{m=N-1} y[n-m] y^*[n-m])^2]$  was approximated as  $(E[\sum_{m=0}^{m=N-1} y[n-m] y^*[n-m]])^2$ . It should be pointed out that this approximation fits the MPSK case where QPSK is a special case of it. However, satisfying results were obtained in [13] for the 16QAM and 64QAM cases in spite of the fact that the above mentioned approximation was applied. Thus, it makes sense to use the same approximation also here for our case. The expression  $E[\sum_{m=0}^{m=N-1} y[n-m] y^*[n-m]]$  may be written as

$$E \left[ \sum_{m=0}^{m=N-1} y[n-m] y^*[n-m] \right] = N\sigma_x^2 \sum_{k=0}^{k=R-1} h_k^2[n] + \frac{N\sigma_x^2}{\text{SNR}}. \quad (12)$$

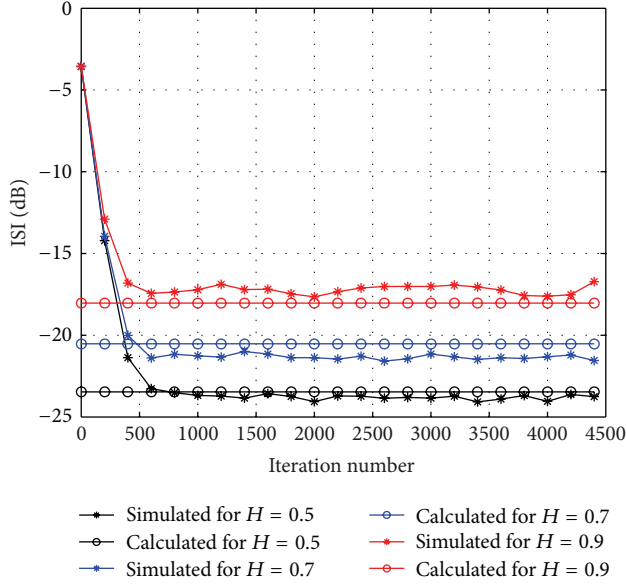


FIGURE 2: A comparison between the simulated and calculated residual ISI for the 16QAM source input going through channel1 for SNR = 10 [dB]. The averaged results were obtained in 100 Monte Carlo trials. The equalizer's tap length and step-size parameter were set to 13 and 0.0006 respectively.

Next, we turn to find a closed-form approximated expression for  $\sigma_{\tilde{w}_r}^2$ . The real part of  $\tilde{w}[n]$ , namely,  $\tilde{w}_r[n]$ , may be expressed as

$$\tilde{w}_r[n] = \sum_{k=0}^{N-1} c_k[n] w_r[n-k]. \quad (13)$$

Thus, the variance of  $\tilde{w}_r[n]$  is given by:

$$\begin{aligned} \sigma_{\tilde{w}_r}^2 &= E \left[ \sum_{k=0}^{N-1} c_k[n] w_r[n-k] \sum_{m=0}^{N-1} c_m[n] w_r[n-m] \right] \\ &= \sum_{k=0}^{N-1} \sum_{m=0}^{N-1} c_k[n] c_m[n] E[w_r[n-k] w_r[n-m]], \end{aligned} \quad (14)$$

which can be also written as

$$\begin{aligned} \sigma_{\tilde{w}_r}^2 &= \sigma_{w_r}^2 \sum_{k=0}^{N-1} c_k^2[n] \\ &\quad + \sum_{k=0, k \neq m}^{N-1} \sum_{m=0, k \neq m}^{N-1} c_k[n] c_m[n] E[w_r[n-k] w_r[n-m]]. \end{aligned} \quad (15)$$

According to [2], expression (15) can be approximately written as

$$\sigma_{\tilde{w}_r}^2 \cong \frac{\sigma_{x_r}^2}{\text{SNR} \sum_{k=0}^{N-1} h_k^2[n]} \left[ 1 + \sqrt{N-1} H(2H-1) \right], \quad (16)$$

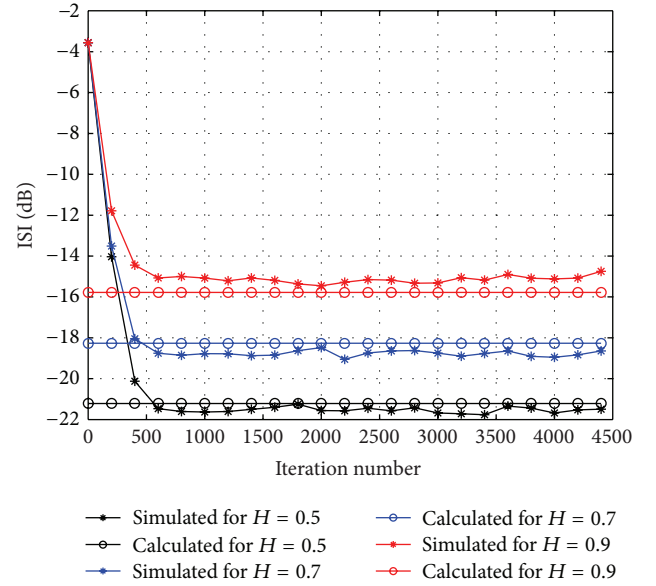


FIGURE 3: A comparison between the simulated and calculated residual ISI for the 16QAM source input going through channel1 for SNR = 8 [dB]. The averaged results were obtained in 100 Monte Carlo trials. The equalizer's tap length and step-size parameter were set to 13 and 0.0006 respectively.

by using assumption (4) from the system description section, assumptions (4) and (6)–(8) from this section, the Holder inequality [20], and the following approximation [21]:

$$\begin{aligned} &0.5 \left[ (|m-k|-1)^{2H} - 2(|m-k|)^{2H} + (|m-k|+1)^{2H} \right] \\ &\simeq H(2H-1) |m-k|^{2H-2}. \end{aligned} \quad (17)$$

Now, by substituting (12) and (16) into (11) we obtain (7). This completes our proof.  $\square$

#### 4. Simulation

In this section, we test our new proposed expression for the residual ISI for the 16QAM case (a modulation using  $\pm\{1, 3\}$  levels for in-phase and quadrature components) with the algorithm described in (5) for different SNR, step-size, and equalizer's tap length values and for two different channel types. The following two channels were considered. *Channel1* (initial ISI = 0.44): the channel parameters were determined according to [22]

$$\begin{aligned} h_n &= \begin{cases} 0 & \text{for } n < 0; \\ -0.4 & \text{for } n = 0 \\ \times 0.84 \cdot 0.4^{n-1} & \text{for } n > 0 \end{cases} \end{aligned} \quad (18)$$

*Channel2* (initial ISI = 0.88) the channel parameters were determined according to

$$h_n = (0.4851, -0.72765, -0.4851). \quad (19)$$

The equalizer was initialized by setting the center tap equal to one and all others to zero.

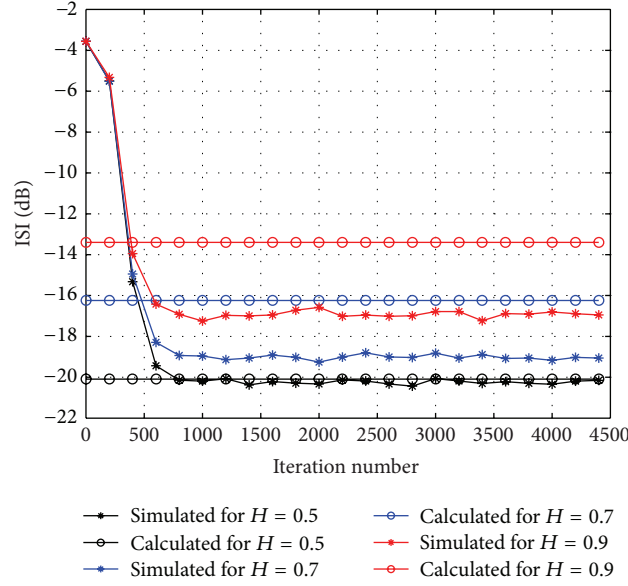


FIGURE 4: A comparison between the simulated and calculated residual ISI for the 16QAM source input going through channel1 for SNR = 10 [dB]. The averaged results were obtained in 100 Monte Carlo trials. The equalizer's tap length and step-size parameter were set to 27 and 0.0006 respectively.

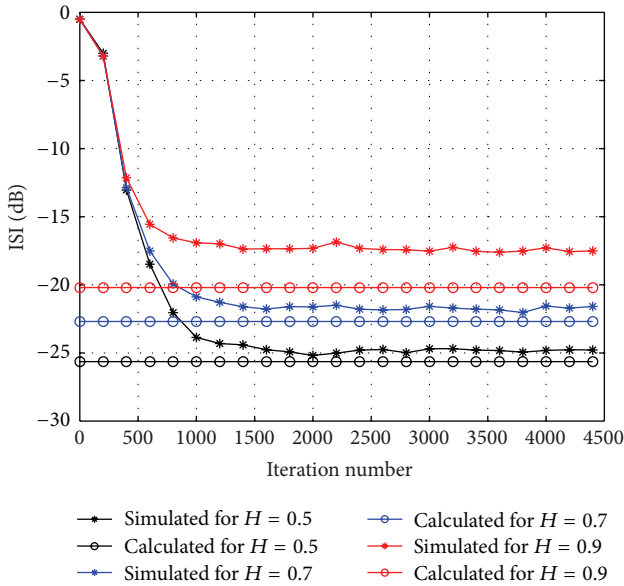


FIGURE 5: A comparison between the simulated and calculated residual ISI for the 16QAM source input going through channel2 for SNR = 12 [dB]. The averaged results were obtained in 100 Monte Carlo trials. The equalizer's tap length and step-size parameter were set to 13 and 0.0006 respectively.

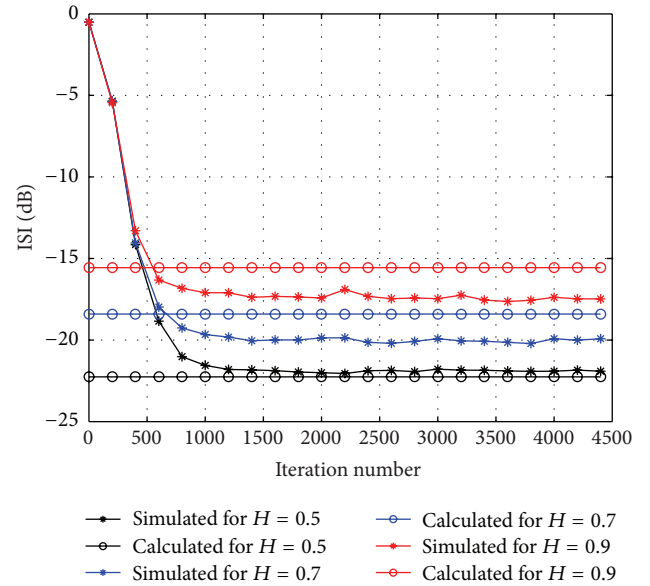


FIGURE 6: A comparison between the simulated and calculated residual ISI for the 16QAM source input going through channel2 for SNR = 12 [dB]. The averaged results were obtained in 100 Monte Carlo trials. The equalizer's tap length and step-size parameter were set to 27 and 0.0006 respectively.

In the following, we denote the residual ISI performance according to (6) with (7) as “Calculated ISI.” Figure 2 to Figure 8 show the ISI performance as a function of the iteration number of our proposed expression (6) with (7) for the achievable residual ISI compared with the simulated results for two different channels and equalizer's tap length

and various values for  $H$ , SNR and step-size parameter. According to Figures 2, 3, 5, 6, 7, and 8, a high correlation is observed between the simulated and calculated results even for  $H = 0.9$ . According to Figure 4, the calculated ISI may be considered as an upper limit for the simulated results for  $H > 0.5$ .

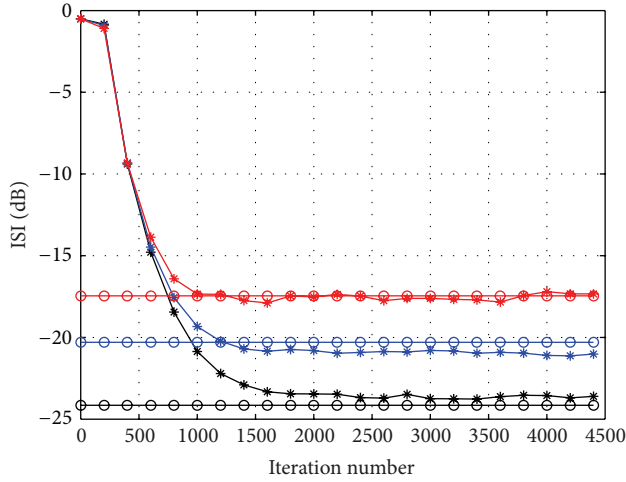


FIGURE 7: A comparison between the simulated and calculated residual ISI for the 16QAM source input going through channel2 for SNR = 12 [dB]. The averaged results were obtained in 100 Monte Carlo trials. The equalizer's tap length and step-size parameter were set to 27 and 0.0004 respectively.

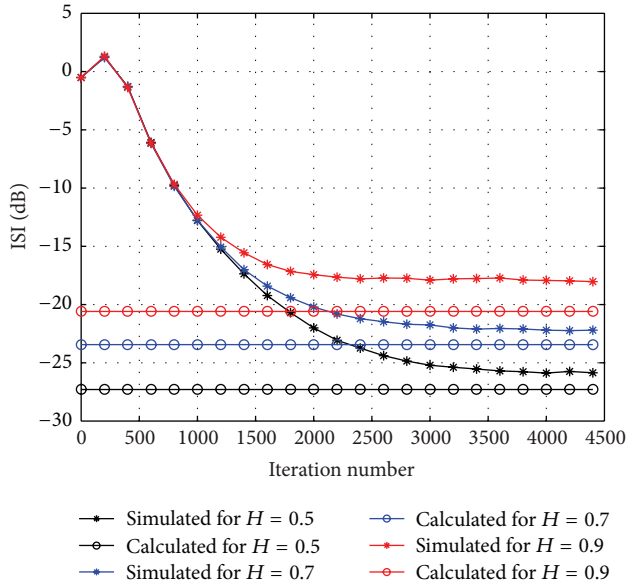


FIGURE 8: A comparison between the simulated and calculated residual ISI for the 16QAM source input going through channel2 for SNR = 12 [dB]. The averaged results were obtained in 100 Monte Carlo trials. The equalizer's tap length and step-size parameter were set to 27 and 0.0002 respectively.

## 5. Conclusion

In this paper, we proposed a closed-form approximated expression (or an upper limit) for the residual ISI obtained by nonblind adaptive equalizers valid for the fGn input case where the Hurst exponent is in the region of  $0.5 \leq H < 1$ . This new obtained expression depends on the step-size parameter, equalizer's tap length, input signal statistics, SNR, channel power, and the Hurst exponent parameter. According

to simulation results, a high correlation is obtained between the calculated and simulated results for the residual ISI for some cases, while for others the new obtained expression is a relative tight upper limit for the averaged residual ISI results.

## References

- [1] M. Pinchas, "Two blind adaptive equalizers connected in series for equalization performance improvement," *Journal of Signal and Information Processing*, vol. 4, no. 1, pp. 64–71, 2013.
- [2] M. Pinchas, "Residual ISI obtained by blind adaptive equalizers and fractional noise," *Mathematical Problems in Engineering*, vol. 2013, Article ID 972174, 11 pages, 2013.
- [3] M. Pinchas and B. Z. Bobrovsky, "A maximum entropy approach for blind deconvolution," *Signal Processing*, vol. 86, no. 10, pp. 2913–2931, 2006.
- [4] M. Pinchas and B. Z. Bobrovsky, "A novel HOS approach for blind channel equalization," *IEEE Transactions on Wireless Communications*, vol. 6, no. 3, pp. 875–886, 2007.
- [5] M. Pinchas, *Blind Equalizers by Techniques of Optimal Non-Linear Filtering Theory*, VDM Verlagsservice Gesellschaft mbH, 2009.
- [6] M. Pinchas, *The Whole Story Behind Blind Adaptive Equalizers/Blind Deconvolution*, Bentham Science Publishers, 2012.
- [7] G. H. Im, C. J. Park, and H. C. Won, "A blind equalization with the sign algorithm for broadband access," *IEEE Communications Letters*, vol. 5, no. 2, pp. 70–72, 2001.
- [8] D. N. Godard, "Self recovering equalization and carrier tracking in two-dimensional data communication system," *IEEE Transactions on Communications Systems*, vol. 28, no. 11, pp. 1867–1875, 1980.
- [9] M. Reuter and J. R. Zeidler, "Nonlinear effects in LMS adaptive equalizers," *IEEE Transactions on Signal Processing*, vol. 47, no. 6, pp. 1570–1579, 1999.
- [10] A. H. I. Makki, A. K. Dey, and M. A. Khan, "Comparative study on LMS and CMA channel equalization," in *Proceedings of the International Conference on Information Society (i-Society '10)*, pp. 487–489, June 2010.
- [11] E. Tucu, F. Akir, and A. Zen, "New step size control technique for blind and non-blind equalization algorithms," *Radioengineering*, vol. 22, no. 1, p. 44, 2013.
- [12] <http://www.academypublisher.com/proc/iscsct10/papers/iscsct10p256.pdf>.
- [13] M. Pinchas, "A closed approximated formed expression for the achievable residual intersymbol interference obtained by blind equalizers," *Signal Processing*, vol. 90, no. 6, pp. 1940–1962, 2010.
- [14] M. Pinchas, "A new closed approximated formed expression for the achievable residual ISI obtained by adaptive blind equalizers for the noisy case," in *Proceedings of the IEEE International Conference on Wireless Communications, Networking and Information Security (WCNIS '10)*, pp. 26–30, Beijing, China, June 2010.
- [15] J. Beran, *Statistics for Long-Memory Processes*, vol. 61 of *Mono-graphs on Statistics and Applied Probability*, Chapman and Hall, New York, NY, USA, 1994.
- [16] M. Li and W. Zhao, "On  $1/f$  noise," *Mathematical Problems in Engineering*, vol. 2012, Article ID 673648, 23 pages, 2012.
- [17] M. Li, "Fractal time series—a tutorial review," *Mathematical Problems in Engineering*, vol. 2010, Article ID 157264, 26 pages, 2010.



- [18] M. Li and W. Zhao, "Quantitatively investigating locally weak stationarity of modified multifractional Gaussian noise," *Physica A*, vol. 391, no. 24, pp. 6268–6278, 2012.
- [19] G. Malik and A. S. Sappal, "Adaptive equalization algorithms: an overview," *International Journal of Advanced Computer Science and Applications*, vol. 2, no. 3, 2011.
- [20] M. R. Spiegel, *Mathematical Handbook of Formulas and Tables*, Schaum's Outline Series, McGraw-Hill, New York, NY, USA, 1968.
- [21] M. Li and W. Zhao, "On bandlimitedness and lag-limitedness of fractional Gaussian noise," *Physica A*, vol. 392, no. 9, pp. 1955–1961, 2013.
- [22] O. Shalvi and E. Weinstein, "New criteria for blind deconvolution of nonminimum phase systems (channels)," *IEEE Transactions on Information Theory*, vol. 36, no. 2, pp. 312–321, 1990.

## Research Article

# Wild Fluctuations of Random Functions with the Pareto Distribution

Ming Li<sup>1</sup> and Wei Zhao<sup>2</sup>

<sup>1</sup> School of Information Science & Technology, East China Normal University, No. 500 Dong-Chuan Road, Shanghai 200241, China

<sup>2</sup> Department of Computer and Information Science, University of Macau, Padre Tomas Pereira Avenue, Taipa 1356, Macau

Correspondence should be addressed to Ming Li; [ming\\_lihk@yahoo.com](mailto:ming_lihk@yahoo.com)

Received 15 July 2013; Accepted 2 August 2013

Academic Editor: Massimo Scalia

Copyright © 2013 M. Li and W. Zhao. This is an open access article distributed under the Creative Commons Attribution License, which permits unrestricted use, distribution, and reproduction in any medium, provided the original work is properly cited.

This paper provides the fluctuation analysis of random functions with the Pareto distribution. By the introduced concept of wild fluctuations, we give an alternative way to classify the fluctuations from those with light-tailed distributions. Moreover, the suggested term wildest fluctuation may be used to classify random functions with infinite variance from those with finite variances.

## 1. Introduction

The Pareto distribution is typically a type of heavy-tailed distributions gaining research interests and applications in many fields of sciences and technologies, ranging from financial engineering to geosciences; see, for example, [1–9]. By heavy tail of a probability distribution density (PDF) function, we mean that the PDF is in the form of a certain power function instead of exponential functions, such as the Poisson distribution and Gaussian distribution. The subject of heavy-tailed PDFs, including the Pareto one, may be in the field of power laws, which has been attracted by researchers in various fields; see, for example, [10–16].

Though Pareto reported his distribution in 1895 [17, 18] from a view of economics, its applications to the other fields are widely reported from a view of fractals in particular. Due to the fact that the Pareto distribution plays a role in so many areas, we give an introductive description about it from a view of its fluctuations in comparison with some common PDFs, such as Gaussian distribution.

The remainder of this paper is organized as follows. Section 2 briefs the study background. The wild fluctuations of random functions with the Pareto distribution are discussed in Section 3. Conclusions are given in Section 4.

## 2. Background

Denote by  $p(x)$  the PDF of a second-order random function (random function for short)  $x(t)$ . Then, its mean, that is, its first moment, and its variance, that is, its second central moment, play a role in characterizing  $x(t)$ .

Without generality losing in the discussions, we assume that  $x(t)$  is stationary. Let  $\mu$  and  $\sigma^2$  be the mean and the variance of  $x(t)$ . Then,  $\mu$  and  $\sigma^2$  are expressed by (1) and (2), respectively;

$$\mu = E[x(t)] = \int_{-\infty}^{\infty} xp(x)dx, \quad (1)$$

$$\sigma^2 = E\{[x(t) - \mu]^2\} = \int_{-\infty}^{\infty} [x(t) - \mu]^2 p(x)dx. \quad (2)$$

Note that  $\mu$  represents the average value around which  $x(t)$  fluctuates. On the other side,  $\sigma^2$  is a parameter for measuring the dispersion or fluctuation of  $x(t)$  around  $\mu$ . Two parameters are essential. For instance, in the field of measurements, an accurate measurement implies that the variance of that measurement should be small [19–21].

Now, we consider two random functions  $x(t)$  and  $y(t)$ . Suppose that their means are equal. Denote by  $\sigma_x^2$  and  $\sigma_y^2$  the

variances of  $x(t)$  and  $y(t)$ , respectively. Then, in engineering, one may say that  $x(t)$  is more random than  $y(t)$  if

$$\sigma_x^2 > \sigma_y^2. \quad (3)$$

In other words, one may also say that  $x(t)$  is more diverse than  $y(t)$  if (3) holds [21, 22]. Using the term fluctuation, one may say that the fluctuation range of  $x(t)$  is larger than that of  $y(t)$  when (3) holds. As a matter of fact, variance analysis plays a role in statistics [23, 24].

Note that if  $x(t)$  is Gaussian, its PDF is uniquely determined by its  $\mu$  and  $\sigma^2$  because

$$p(x) = \frac{1}{\sqrt{2\pi}\sigma} \exp\left[-\frac{(x-\mu)^2}{2\sigma^2}\right], \quad -\infty < x < \infty. \quad (4)$$

The particularly useful result by using  $\sigma^2$  can be explained as follows. Though  $-\infty < x < \infty$  in general, the fluctuation of a Gaussian random function  $x(t)$  can be simply determined with a certain probability. For example, it is well known that, with probability 95%, the fluctuation interval of  $x(t)$  is given by

$$-(\mu - 3\sigma) < x < \mu + 3\sigma. \quad (5)$$

It is obvious that the tool of variance analysis may work if variances to be studied exist. In fact, one may use (3) to identify whether the fluctuation of  $x(t)$  is more severe than that of  $y(t)$  if both variances of  $x(t)$  and  $y(t)$  exist.

### 3. Fluctuation Analysis of Random Function with the Pareto PDF

Recall that the necessary and sufficient condition for a function  $p(x)$  to be a PDF is  $p(x) \geq 0$  and

$$\int_{-\infty}^{\infty} p(x) dx = 1. \quad (6)$$

Denote by  $p_{\text{Pareto}}(x)$  the PDF of the Pareto distribution. Then,

$$p_{\text{Pareto}}(x) = \begin{cases} \frac{ab^a}{x^{a+1}}, & x \geq b, \\ 0, & \text{otherwise.} \end{cases} \quad (7)$$

In the above,  $a$  and  $b$  are positive parameters (<http://math-world.wolfram.com/ParetoDistribution.html>).

*Note 1* (heavy tail). The function  $p_{\text{Pareto}}(x)$  decays hyperbolically. Hence, heavy tail is compared to PDFs that are exponentially decayed.

The mean and variance of  $x(t)$  that follows  $p_{\text{Pareto}}(x)$  are, respectively, given by

$$\mu_{\text{Pareto}} = \int_b^{\infty} x p_{\text{Pareto}}(x) dx = \frac{ab}{a-1}, \quad (8)$$

$$\text{Var}(x)_{\text{Pareto}} = \frac{ab^2}{(a-1)^2(a-2)}. \quad (9)$$

*Note 2* (infinite variance). If  $a \rightarrow 1$  or  $a \rightarrow 2$ ,  $\text{Var}(x)_{\text{Pareto}} \rightarrow \infty$  as can be seen from (9).

Since the heavy tails of random functions imply their larger fluctuation ranges than those with light tails, that is, exponential type distributions, such as the Gaussian or Poisson distribution, we specifically, though informal, introduce a term “wild fluctuation,” in comparison with those with light tails. In addition, because infinite invariance implies that the fluctuation range of a random function is infinite, we, though informal again, introduce another term “wildest fluctuation,” in comparison with those with finite variances.

*Remark 1* (wildest fluctuation). The fluctuation of a random function  $x(t)$  that follows  $p_{\text{Pareto}}(x)$  may be wildest if  $a \rightarrow 1$  or  $a \rightarrow 2$ .

*Case Study 1.* Suppose that there are two different random functions  $x(t)$  and  $y(t)$ . Both obey the Pareto distribution. When  $x(t)$  is with  $a = 1$  while  $y(t)$  is with  $a = 2$ , we have  $\text{Var}(x) \rightarrow \infty$  and  $\text{Var}(y) \rightarrow \infty$ . In this case, one may fail to identify whether the fluctuation of  $x(t)$  is more severe than that of  $y(t)$  based on the tool of variance analysis. More precisely, variance analysis that plays a role in conventional statistics fails to be used for the fluctuation analysis of random functions with infinite variance.

## 4. Conclusions

We have explained our introduction of the term wild fluctuation and wildest one by using the Pareto distributions. Though the present analysis is based on the Pareto distribution, it may yet be an alternative material to shortly describe the fact that caution should be paid to variance analysis of a random function with a heavy-tailed distribution unless its variance exists.

## Acknowledgments

This work was supported in part by the 973 plan under the Project Grant no. 2011CB302800 and by the National Natural Science Foundation of China under the Project Grant nos. 61272402, 61070214, and 60873264.

## References

- [1] V. Pisarenko and M. Rodkin, *Heavy-Tailed Distributions in Disaster Analysis*, Springer, New York, NY, USA, 2010.
- [2] S. I. Resnick, *Heavy-Tail Phenomena Probabilistic and Statistical Modeling*, Springer Series in Operations Research and Financial Engineering, Springer, New York, NY, USA, 2007.
- [3] R. J. Adler, R. E. Feldman, and M. S. Taqqu, Eds., *A Practical Guide to Heavy Tails: Statistical Techniques and Applications*, Birkhäuser, Boston, Mass, USA, 1998.
- [4] W. Hürlimann, “From the general affine transform family to a Pareto type IV model,” *Journal of Probability and Statistics*, vol. 2009, Article ID 364901, 10 pages, 2009.
- [5] A. Adler, “Limit theorems for randomly selected adjacent order statistics from a Pareto distribution,” *International Journal of*

- Mathematics and Mathematical Sciences*, no. 21, pp. 3427–3441, 2005.
- [6] C. Cattani, “Fractals and hidden symmetries in DNA,” *Mathematical Problems in Engineering*, vol. 2010, Article ID 507056, 31 pages, 2010.
  - [7] C. Cattani, E. Laserra, and I. Bochicchio, “Simplicial approach to fractal structures,” *Mathematical Problems in Engineering*, vol. 2012, Article ID 958101, 21 pages, 2012.
  - [8] C. Cattani, “On the existence of wavelet symmetries in archaea DNA,” *Computational and Mathematical Methods in Medicine*, vol. 2012, Article ID 673934, 21 pages, 2012.
  - [9] V. Paxson and S. Floyd, “Wide area traffic: the failure of Poisson modeling,” *IEEE/ACM Transactions on Networking*, vol. 3, no. 3, pp. 226–244, 1995.
  - [10] H. E. Stanley, “Power laws and universality,” *Nature*, vol. 378, no. 6557, p. 554, 1995.
  - [11] F. Angeletti, E. Bertin, and P. Abry, “Critical moment definition and estimation, for finite size observation of log-exponential-power law random variables,” *Signal Processing*, vol. 92, no. 12, pp. 2848–2865, 2012.
  - [12] M. C. Bowers, W. W. Tung, and J. B. Gao, “On the distributions of seasonal river flows: lognormal or power law?” *Water Resources Research*, vol. 48, no. 5, 12 pages, 2012.
  - [13] I. Eliazar and J. Klafter, “A probabilistic walk up power laws,” *Physics Reports*, vol. 511, no. 3, pp. 143–175, 2012.
  - [14] N. Jakšić, “Power law damping parameter identification,” *Journal of Sound and Vibration*, vol. 330, no. 24, pp. 5878–5893, 2011.
  - [15] A. R. Bansal, G. Gabriel, and V. P. Dimri, “Power law distribution of susceptibility and density and its relation to seismic properties: an example from the German Continental Deep Drilling Program (KTB),” *Journal of Applied Geophysics*, vol. 72, no. 2, pp. 123–128, 2010.
  - [16] S. Milojević, “Power law distributions in information science: making the case for logarithmic binning,” *Journal of the American Society for Information Science and Technology*, vol. 61, no. 12, pp. 2417–2425, 2010.
  - [17] V. Pareto, “La legge della domanda,” *Giornale Degli Economisti*, vol. 10, pp. 59–68, 1895, English translation in *Rivista di Politica Economica*, vol. 87, pp. 691–700, 1997.
  - [18] V. Pareto, “La Courbe de la Repartition de la Richesse,” in *Oevres Completes De Vilfredo Pareto*, G. Busino, Ed., pp. 1–5, Librairie Droz, Geneva, Switzerland, 1965, Originally published in 1896.
  - [19] J. S. Bendat and A. G. Piersol, *Piersol, Random Data: Analysis and Measurement Procedure*, Wiley Series in Probability and Statistics, John Wiley & Sons Inc., Hoboken, NJ, USA, 3rd edition, 2010.
  - [20] R. A. Bailey, *Design of Comparative Experiments*, Cambridge Series in Statistical and Probabilistic Mathematics, Cambridge University Press, Cambridge, UK, 2008.
  - [21] ASME, *Measurement Uncertainty Part 1, Instruments and Apparatus*, Supplement to ASME, Performance Test Codes, ASME, New York, NY, USA, 1986.
  - [22] D. Sheskin, *Statistical Tests and Experimental Design: A Guidebook*, Gardner Press, New York, NY, USA, 1984.
  - [23] A. Gelman, “Analysis of variance? why it is more important than ever,” *The Annals of Statistics*, vol. 33, no. 1, pp. 1–53, 2005.
  - [24] D. A. Freedman, *Statistical Models: Theory and Practice*, Cambridge University Press, Cambridge, UK, 2005.

## Research Article

# Set Pair Analysis Based on Phase Space Reconstruction Model and Its Application in Forecasting Extreme Temperature

Yin Zhang,<sup>1</sup> Xiao-hua Yang,<sup>2</sup> Ling Zhang,<sup>3</sup> Wan-ying Ma,<sup>1</sup> and Ling-xia Qiao<sup>1</sup>

<sup>1</sup> School of Mathematical Sciences, Beijing Normal University, Beijing 100875, China

<sup>2</sup> State Key Laboratory of Water Environment Simulation, School of Environment, Beijing Normal University, Beijing 100875, China

<sup>3</sup> Department of Mathematics and Statistics, Auburn University, Auburn, AL 36832, USA

Correspondence should be addressed to Xiao-hua Yang; [xiaohuayang@bnu.edu.cn](mailto:xiaohuayang@bnu.edu.cn)

Received 3 June 2013; Revised 16 July 2013; Accepted 19 July 2013

Academic Editor: Ming Li

Copyright © 2013 Yin Zhang et al. This is an open access article distributed under the Creative Commons Attribution License, which permits unrestricted use, distribution, and reproduction in any medium, provided the original work is properly cited.

In order to improve the precision of forecasting a time series, set pair analysis based on phase space reconstruction (SPA-PSR) model is established. In the new model, by using chaos analysis, we reconstruct the phase space with delay time and embedding dimension. Based on it, we rebuilt history sets and current sets in the SPA-PSR model. Two cases of forecasting extreme temperature in Mount Wutai and Datong are taken to examine the performance of SPA-PSR model. The results indicate that the mean relative error (MRE) of SPA-PSR model has decreased by 65.97%, 59.32%, and 7.79% in the case of Mount Wutai and 29.11%, 32.82%, and 9.03% in the case of Datong, respectively, compared with autoregression (AR) model, rank set pair analysis (R-SPA) model, and Back-Propagation (BP) neural network model. It gives a theoretical support for set pair analysis and improves precision of numerical forecasting.

## 1. Introduction

The global and regional climates have already begun changing [1], and as the important factor of climate change, temperature plays a significant role in human's daily life [2, 3]. It is important to forecast extreme temperature accurately [4]. Temperature change process is usually nonlinear, complex, and dynamic, so the accurate prediction of extreme temperature is faced with a high degree of scientific uncertainty, which traditional deterministic mathematical model cannot solve perfectly. And numerical simulation method can solve the problem better [4–6].

Auto regression (AR) model is the traditional method used to deal with the time series forecasting [7]; for example, Bańbura et al. used Bayesian vector autoregressions for commercial forecasting [8]. In recent years, artificial neural network (ANN) algorithms are widely used to deal with forecasting meteorological objects [9]. Based on the genetic algorithm (GA) and particle swarm algorithm, Yang designed the Back-Propagation (BP) neural networks to establish the multifactor time series forecasting model [10]. At the same

time, set pair analysis (SPA) model which is easy to operate and gives good prediction results is also popular in meteorological forecast field [5, 6]. Yang et al. gave the set pair analysis based on similarity forecast (SPA-SF) model for forecasting water resources changing process, and the application results showed that the statistic and physical concepts of SPA-SF were distinct and its precision was high [9]. Recently, Mei et al. used SPA to find an optimal choice of Bioretention media [11] and Guo et al. employed it to assess the ecoenvironment quality for uncertain problems [12]. Because SPA model does not provide a unified standard of quantifying the set element symbols, the rank set pair analysis (R-SPA) model is presented by using the rank set pair analysis [5, 9, 10], and the results are proved to be better.

However, for SPA (including R-SPA) [5, 9], there is no accurate method to determine the dimension of history sets and current sets, which is used to calculate the connection degree and affects prediction results. And by finding the most similar history set, SPA model uses subsequent value as the forecasting value of current set, while it does not give a satisfying theoretical proof. Phase space



reconstruction, based on chaos time series analysis, is the newest development to deal with nonlinear time series [13–17]. It has an excellent description of the system's dynamic behavior by applying the nonlinear dynamics theory and fractal theory. In particular chaos systems are dynamical systems that defy synchronization. They are ubiquitous in nature, and most of them do not have an explicit dynamical equation and can be only understood through the available time series [18]. Under some circumstances, such processes can create time series that appear to be completely random—the corollary of this is that some seemingly random series are in fact chaotic and thus to a certain extent predictable [14]. In 2012, Khatibi et al. studied the chaos in river time series [16] and Di et al. discussed the chaos control and synchronization of a nonlinear system [17]. Based on multiple criteria decision making (MCDM), Yang et al. presented using the chaotic Bayesian method for forecasting nonlinear hydrological time series [19]. Compared with the results of the add-weighted one-rank local-region method (AOLM), the method can improve the forecast accuracy of daily runoffs. And by analyzing the chaos of time series, She and Yang also used the new adaptive local linear prediction in hydrological time [20].

As discussed above, to have a more accurate numerical forecasting of extreme temperature, by using chaos time series analysis, a set pair analysis based on phase space reconstruction (SPA-PSR) model is proposed in the paper: we use the Takens embedding theory [21] to embed the rebuilt history sets and current sets in SPA so that the parameter (dimension of history sets) can be calculated and both kinds of sets have theoretical meanings for prediction. Two cases of forecasting extreme temperature in Mount Wutai and Datong stations are taken to examine the efficiency of SPA-PSR model.

## 2. The Method of Phase Space Reconstruction (PSR)

For a scalar time series,  $x_1, x_2, \dots, x_n$ , according to Takens embedding theory [21], the phase space can be reconstructed to a multidimensional space and the coordinate delay method is commonly used. The constructed  $m$  dimension state vector  $Y_i$  is

$$Y_i = (x_i, x_{i+\tau}, \dots, x_{i+(m-1)\tau}), \quad (1)$$

where  $n$  is the length of time series,  $\tau$  is the delay time and  $m$  is the embedding dimension  $i = 1, 2, \dots, M$ ,  $M$  is the total points number of the phase-space, and  $M = n - (m - 1)\tau$ .

**2.1. The Determination of Delay Time.** In this study, we use the autocorrelation function to determine the delay time  $\tau$  [22–24]. As for time series  $x_1, x_2, \dots, x_n$ , the autocorrelation coefficient function with the lag time  $t$  is [20, 25, 26]

$$C(t) = \frac{1}{n-t} \frac{\sum_{i=1}^{n-t} (x_i - \mu)(x_{i+t} - \mu)}{\sigma^2(x)}, \quad (2)$$

where  $\mu$  and  $\sigma$  are the mean and standard variation of the time series respectively. Drawing the plot of  $t - C(t)$ , the delay

time  $\tau$  is selected when the autocorrelation coefficient has dropped to  $(1 - 1/e)$  [22] of its initial value ( $e$  is the base of natural logarithm).

**2.2. The Determination of Embedding Dimension.** There are also many ways to decide the embedding dimension [27–31]. In order to have a good predicting result, we choose the minimum prediction error method [27] to assure embedding dimension.

For a scalar time series  $x_1, x_2, \dots, x_n$ , reconstruct it with (1). According to Takens embedding theory, when  $\tau$  and  $m$  are the best delay time and best embedding dimension, respectively, there is a mapping that existed:  $F : R^m \rightarrow R^m$ , such that

$$Y_{i+1} = F(Y_i). \quad (3)$$

At this time, the average prediction error (also can be the maximum prediction error, or other prediction errors):

$$E(m, \tau) = \frac{1}{M-1} \sum_{i=1}^{M-1} |x_{i+1+(m-1)\tau} - x_{\eta(i)+1+(m-1)\tau}| \quad (4)$$

should be the minimum. In formula (4),  $\eta(i)$  is assured by finding the nearest neighbor spot  $Y_{\eta(i)}$  of  $Y_i$ , and the way is shown as follows:

$$\|Y_{\eta(i)} - Y_i\| = \min_{j=1,2,\dots,M; j \neq i} \|Y_j - Y_i\|, \quad (5)$$

where  $\|Y_{\eta(i)} - Y_i\|$  means the Euclidian distance (the norm in certain space) between  $Y_{\eta(i)}$  and  $Y_i$ , and we take the norm of  $L_\infty$  space:

$$\begin{aligned} \|Y_{\eta(i)} - Y_i\| &= \min_{j=1,2,\dots,M; j \neq i} \|Y_j - Y_i\| \\ &= \min_{j=1,2,\dots,M; j \neq i} \max_{1 \leq l \leq m-1} |x_{j+l\tau} - x_{i+l\tau}|. \end{aligned} \quad (6)$$

According to the existence of the largest Lyapunov exponents and noise, with embedding dimension  $m$  increasing, the value of  $E(m, \tau)$  will be heavily influenced. So we make  $m$  increase from two, taking the first minimum point in  $E(m, \tau) - m$  curve as the best embedding dimension [27].

The PSR algorithm is shown as follows.

- (1) For a scalar time series  $x_1, x_2, \dots, x_n$ , first, take a smaller value of embedding dimension  $m = 2$ ; then the corresponding phase space reconstruction state vectors are

$$Y_i = (x_i, x_{i+\tau}, \dots, x_{i+(m-1)\tau}) \quad i = 1, 2, \dots \quad (7)$$

- (2) Using formula (5) to find the  $Y_i$ 's nearest neighbor spot,  $Y_{\eta(i)}$ ,  $i = 1, 2, \dots, N$ , and then taking them into formula (4), calculate the corresponding value of  $E(m, \tau)$ .
- (3) Increase the embedding dimension, take  $m + 1 \rightarrow m$ , and repeat Steps 1 and 2.
- (4) Find the first minimum value of  $E(m, \tau)$ , and the corresponding value of  $m$  is the embedding dimension.

**2.3. Verification of the Chaos of Time Series.** In order to verify whether time series is chaotic, we calculate the largest Lyapunov exponent of our studied time series by using the delay time and embedding dimension above [22]. The largest Lyapunov exponent is defined by the value of its nearest neighbor divergence rate on average

$$\ln D_i(k) = \ln C_i + \lambda \cdot (k \cdot \Delta t), \quad (8)$$

where  $D_i(k)$  represents the distance between  $i$ th point and its nearest neighbor after  $k$  time units, and

$$D_i(0) = \min_j \|Y_i - Y_j\|, \quad (9)$$

where  $|i - j| > w$  and  $C_i$  is the initial distance. So the slope  $\lambda$  can represent the largest Lyapunov exponent, which can be calculated by using the least square method.

If the largest Lyapunov exponent  $\lambda$  is greater than 0, the time series is chaotic. If not, the Takens embedding theory is not tenable, and the set pair analysis based on phase space reconstruction model (SPA-PSR) model could not be used.

### 3. Set Pair Analysis Based on Phase Space Reconstruction (SPA-PSR) Model

By analyzing the chaotic time series, the reconstructed phase space is applied to set pair analysis. The set pair analysis based on phase space reconstruction (SPA-PSR) model is shown as follows.

**Step 1** (the phase space reconstruction). According to the methods mentioned in Section 2, the reconstructed phase space is established, and the corresponding state vector  $Y_i$  is

$$Y_i = (x_i, x_{i+\tau}, \dots, x_{i+(m-1)\tau}) \quad (10)$$

according to Takens embedding theory: when  $\tau$  and  $m$  are the best delay time and best embedding dimension, respectively; another corresponding smooth function existed,  $F_1: R^m \rightarrow R$ :

$$x_{i+1+(m-1)\tau} = F_1(Y_i), \quad (11)$$

where  $F_1$  represents the state transformation of studied time series in  $m$  dimension space.

**Step 2** (rebuilt set pair  $(A_i, B)$ ). According to the similarity for development theory, the SPA model uses the history sets' subsequent value to predict future values. So based on the phase space reconstruction with delay time  $\tau$  and embedding dimension  $m$  in Step 1, we can obtain the dimension  $T$  and rebuilt history sets and the current set: the dimension  $T = m$ , the history set  $A_i$  is  $Y_i = (x_i, x_{i+\tau}, \dots, x_{i+(m-1)\tau})$ ,  $i = 1, 2, \dots, N$ , current set  $B = (x_i, x_{i+\tau}, \dots, x_{i+(m-1)\tau})$ , and all are shown in Table 1.

Then, we got the rank transformation of the rebuilt sets  $A_1, A_2, \dots, A_{M-1}$ . If some elements have the same rank, we mark them according to their average rank and round off the value. We could obtain the rank set  $A'_1, A'_2, \dots, A'_{M-1}$ .

By combining the set  $B'$  with  $M - 1$  set  $A'_i$  separately, we get the rank set pair  $(A'_i, B')$ . The sets  $(A'_i, B')$  are the rebuilt set pair in constructed phase space. Simply, we make  $(A_i, B)$  represent  $(A'_i, B')$ .

**Step 3** (the calculation of connection degree). According to the connection degree formula of  $A_i, B$  [5, 9],

$$U_{A_i-B} = \frac{S}{N} + \frac{F}{N}i + \frac{P}{N}j, \quad (12)$$

where  $N$  is the number of elements in set  $A_i$  or  $B$ ,  $S$  represents the number of identical elements,  $P$  represents the number of contrary elements,  $F$  represents the number of discrepant elements,  $i$  and  $j$  represent discrepancy degree and contrary degree, respectively.

Use  $d(a_k, b_k) = |a_k - b_k|$ ,  $(a_k, b_k) \in (A_i, B)$  to describe differences between sets  $(A_i, B)$ , and the codomain of  $d(a_k, b_k)$  is  $[0, M - 1]$ . So the  $U_{A_i-B}$  is calculated as follows.

- (1) When  $d(a_k, b_k) = 0$ , add 1 to the element number in set  $S$ .
- (2) When  $0 < d(a_k, b_k) \leq (M - 2)$ , add 1 to the element number in set  $F$ .
- (3) When  $d(a_k, b_k) = M - 1$ , add 1 to the element number in set  $P$ .

According to the three principle above, take  $N = m$ ; using formula (12), the  $U_{A_i-B}$  can be obtained.

**Step 4** (the determination of similar set and prediction). According to the connection degree maximum principle [5, 9], some  $A_k$  similar to  $B$  are chosen from all the history sets. Thus, the forecast value of  $x_{M+(m-1)\tau}$ , namely, the  $x_{n+1}$ , is  $\hat{x}_{n+1}$  as follows:

$$\hat{x}_{n+1} = \frac{1}{m} \sum_{k=1}^m w_k x_{k+(m-1)\tau+1}, \quad (13)$$

where  $w_k$  denotes the ratio of mean of elements in  $B$  to mean of elements in  $A_k$ .

## 4. Applications in Extreme Temperature

### 4.1. Case 1

**(1) Study Area and Data Description.** The SPA-PSR model is applied to the highest temperature prediction of Mount Wutai in July 1956~2010, which is relatively more accurate in measurement, easy to get, and useful in practice [32, 33].

We use the temperatures in 1956~1999 as known data and thus obtain the time series  $x_1, x_2, \dots, x_{44}$ . Then we will forecast the highest temperature of Mount Wutai in July 2000~2010.

**(2) The Phase Space Reconstruction.** For the scalar time series of the highest temperature prediction of Mount Wutai in July  $x_1, x_2, \dots, x_{44}$ , we use the autocorrelation method and minimum prediction error method to calculate Mount Wutai highest temperature in July's corresponding delay time and embedding dimension, which is shown in Figure 1.

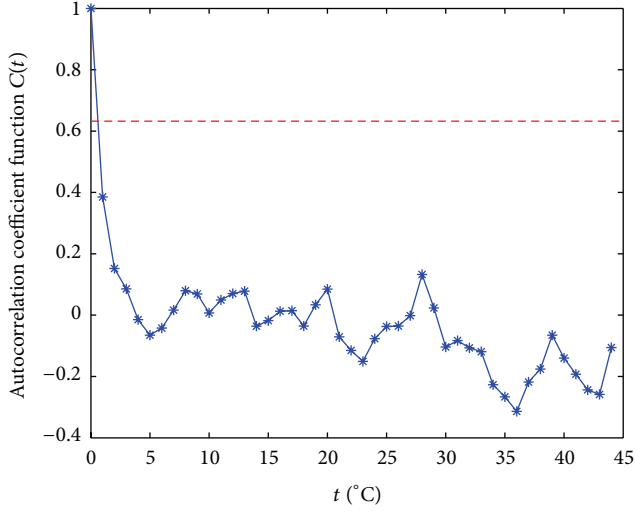


FIGURE 1: Autocorrelation coefficient in Case 1 (the dash line presents the situation where the autocorrelation function value is  $(1 - 1/e)$  of its initial value).

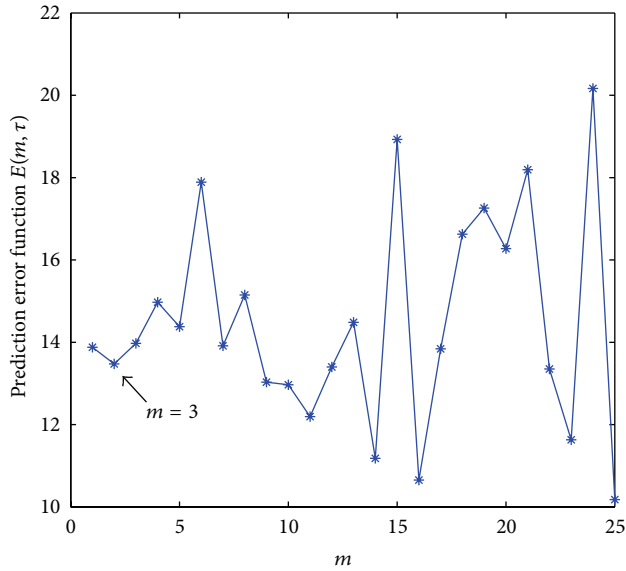


FIGURE 2: The corresponding prediction error function, when delay time  $\tau = 1$ .

In Figure 1, we calculate the autocorrelation of the highest temperature in July of Mount Wutai. When the autocorrelation coefficient has dropped to  $(1 - 1/e)$  of its initial value, the corresponding  $t < 1$ , it indicates that the best delay time is less than 1. However, in reality, the highest temperature in July appears in every other year, which means that  $\tau \geq 1$ ; thus, we take the nearest time to be the delay time, which is  $\tau = 1$ .

From Figure 2, it is obvious that when  $\tau = 1$ ,  $m = 3$ , the prediction error function  $E(m, \tau)$  attains its first minimum point, which indicates that  $m = 3$  is the best embedding dimension for the reconstruction of phase space. Taking  $w = 2$ , with the largest Lyapunov exponent  $\lambda = 0.00086 > 0$ ,

TABLE 1: The rebuilt history sets  $A_i$  and the current set  $B$ .

Sets	Elements in $A_i, B$				Subsequent value
$A_1$	$x_1$	$x_{1+\tau}$	$\cdots$	$x_{1+(m-1)\tau}$	$x_{1+(m-1)\tau+1}$
$A_2$	$x_2$	$x_{2+\tau}$	$\cdots$	$x_{2+(m-1)\tau}$	$x_{2+(m-1)\tau+1}$
$\cdots$	$\cdots$	$\cdots$	$\cdots$	$\cdots$	$\cdots$
$A_i$	$x_i$	$x_{i+\tau}$	$\cdots$	$x_{i+(m-1)\tau}$	$x_{i+(m-1)\tau+1}$
$\cdots$	$\cdots$	$\cdots$	$\cdots$	$\cdots$	$\cdots$
$A_{M-1}$	$x_{M-1}$	$x_{M-1+\tau}$	$\cdots$	$x_{M-1+(m-1)\tau}$	$x_{i+(m-1)\tau+1}$
$B$	$x_M$	$x_{M+\tau}$	$\cdots$	$x_{M+(m-1)\tau}$	$x_{M+(m-1)\tau+1}$

which indicates that the time series of Mount Wutai is chaotic and satisfies the Takens embedding series.

In sum, with the delay time  $\tau = 1$  and embedding dimension  $m = 3$ , the phase space of the highest temperature in July of Mount Wutai is reconstructed, and the corresponding state vector  $Y_i = (x_i, x_{i+1}, x_{i+2})$ .

(3) *Set Pair Analysis Based on Phase Space Reconstruction (SPA-PSR)*. Based on the reconstruction of phase space in formula (1), the number of reconstructed spots  $M = n - (m - 1) \cdot \tau = 44 - 2 = 42$  and the rebuilt set pairs of  $(A_i, B)$  of the highest temperature of Mount Wutai in July time series  $x_1, x_2, \dots, x_{44}$  is shown as follows:

$$\begin{aligned}
 A_1 &= (x_1, x_2, x_3), \\
 A_2 &= (x_2, x_3, x_4), \\
 &\vdots \\
 A_{41} &= (x_{41}, x_{42}, x_{43}),
 \end{aligned}
 \tag{14}$$

and the corresponding current set  $B$  is

$$B = (x_{42}, x_{43}, x_{44}) \tag{15}$$

then using the method mentioned in Section 3, We can have the  $x_{45}$  value, namely, the prediction of the highest temperature of Mount Wutai in July 2000.

(4) *The Prediction Results and Analysis*. Prediction results of the highest temperature (P) in Mount Wutai in July 2000~2010 and the corresponding relative error (RE) are shown in Table 1.

Moreover, to verify the prediction effect of SPA-PSR model, we take R-SPA model, AR model, and BP model to make comparisons. To be the same, in AR model [7], it uses the temperatures in 1946~1999 in every 6 years to obtain the regression linear equation of Mount Wutai, and by using the equation, we can predict the corresponding data in 2000~2010; in BP model [10], the temperatures in 1956~1999 are used as trained sets, and the data in 2000~2010 are tested sets, with 500 trained times and the study rate 0.3; in R-SPA model [9], it uses the pervious 6 years as the history sets to predict the temperatures in 2000~2010.

Compared with the results of AR model, R-SPA model, and BP model, SPA-PSR model has the smallest deviation (RE) with the measured value in those 11 years in general as

TABLE 2: Prediction results and the corresponding relative errors (REs).

Year	Measured value (0.1/°C)	AR model		BP model		R-SPA model		SPA-PSR model	
		P (0.1/°C)	RE (%)	P (0.1/°C)	RE (%)	P (0.1/°C)	RE (%)	P (0.1/°C)	RE (%)
2000	250	177.91	28.84	172.66	30.94	220.89	11.64	208.91	16.43
2001	239	182.30	23.72	182.74	23.54	208.08	12.94	258.14	8.01
2002	241	183.82	23.73	183.67	23.79	212.71	11.74	239.92	0.45
2003	233	173.99	25.33	202.02	13.30	236.92	1.68	254.56	9.25
2004	216	173.07	19.88	184.38	14.64	242.55	12.29	244.02	12.97
2005	241	178.01	26.14	210.23	12.77	253.00	4.98	228.12	5.35
2006	227	179.06	21.12	192.55	15.17	243.40	7.23	248.73	9.57
2007	234	173.69	25.77	192.24	17.85	247.74	5.87	214.79	8.21
2008	232	181.48	21.78	184.54	20.46	247.80	6.81	243.74	5.06
2009	236	178.04	24.56	179.79	23.82	274.66	16.38	234.01	0.84
2010	286	176.15	38.41	179.06	37.39	253.15	11.48	232.09	18.85

TABLE 3: The error analysis in four models.

Models	AR model	BP model	R-SPA model	SPA-PSR model
MRE (%)	25.39	21.24	9.37	8.64
MAE	61.59	51.92	22.57	21.12

shown in Table 2. AR model and R-SPA model does not have the prediction in which relative errors are below 10%, while in R-SPA model and SPA-PSR model are 5 and 8, respectively. According to those points, SPA-PSR model has a better forecasting result.

To make it clear, the precision of prediction is evaluated by two measurement indices in this paper, namely, the mean relative error (MRE) and Mean absolute error (MAE). The results are calculated in Table 3.

In Table 3, we can find that AR model and BP model do not have good forecasting results of Mount Wutai, for that their MREs are all above 20%, and MAEs are above 50, while for R-SPA and SPA-PSR, the prediction error is reduced a lot. Compared with AR model, BP model, and R-SPA model, the MRE of SPA-PSR model is relatively decreased by 65.97%, 59.32%, and 7.79%, respectively, and the MAE is also the lowest, which relatively decreased by 65.71%, 59.32%, and 6.42%. The two measurement indices both indicate that SPA-PSR model has the best forecasting results.

#### 4.2. Case 2

(1) *Study Area and Data Description.* We also apply SPA-PSR model to predict results of the highest temperature in Datong in July 2000~2010, known data in 1955~2010.

(2) *The Phase Space Reconstruction.* For the scalar time series of the highest temperature prediction of Mount Wutai in July  $x_1, x_2, \dots, x_{45}$ , the same methods are used to reconstruct phase space. The corresponding delay time and embedding dimension are shown in Figures 3 and 4.

From Figure 3, we find that similar to Mount Wutai, the Datong corresponding autocorrelation coefficient sharpen decreased from  $t = 0$ ; when it has dropped to  $(1 - 1/e)$  of

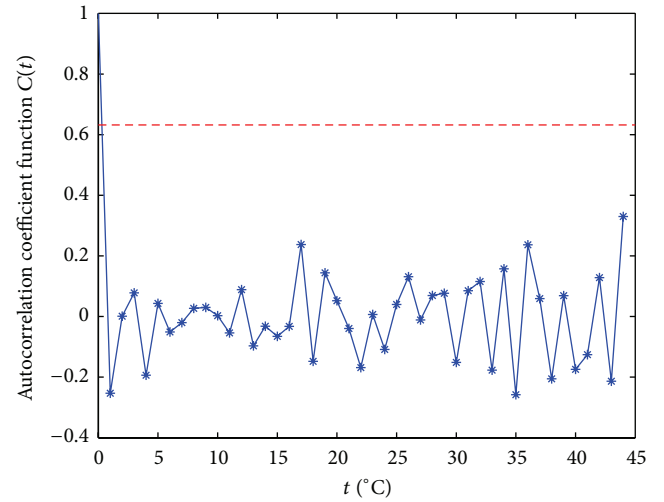


FIGURE 3: The autocorrelation coefficient in Case 2 (the dash line presents the situation where the autocorrelation function value is  $(1 - 1/e)$  of its initial value).

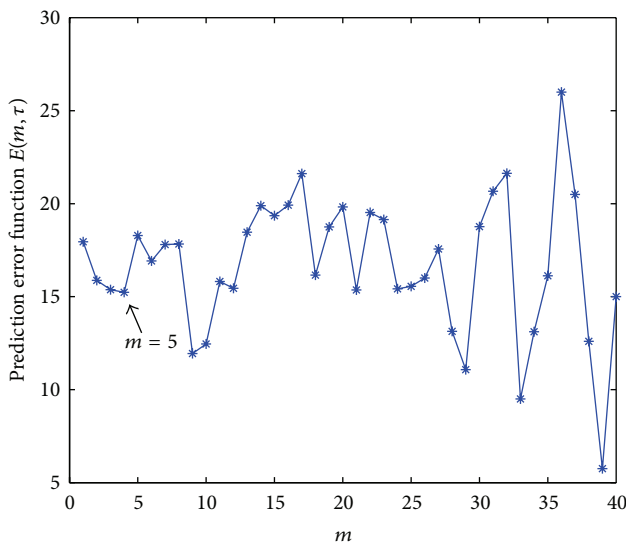
its initial value, the corresponding  $t < 1$ , in the same way, we take  $\tau = 1$  as the delay time. In Figure 4, when  $\tau = 1$  and  $m = 5$ , the prediction error function  $E(m, \tau)$  attains its first minimum point, so the best embedding dimension for Datong is  $m = 5$ . And taking  $w = 2$ , the largest Lyapunov exponent  $\lambda = 0.00024 > 0$ , which indicates that the Datong's time series is chaotic and satisfies the Takens embedding series.

In sum, with the delay time  $\tau = 1$  and embedding dimension  $m = 5$ , the phase space of the highest temperature in July of Datong is reconstructed, and the corresponding state vector is  $Y_i = (x_i, x_{i+1}, x_{i+2}, x_{i+3}, x_{i+4})$ . Being similar to Mount Wutai, the set pairs are rebuilt according to phase space reconstruction and used to forecast the highest temperature of Datong in July 2000~2010.

(3) *The Prediction Results and Analysis.* Prediction results of the highest temperature (P) in Datong in July 2000~2010 and the corresponding relative error (RE) are shown in Table 4.

TABLE 4: Prediction results and the corresponding relative errors (REs).

Year	Measured value (0.1/°C)	AR model		BP model		R-SPA model		SPA-PSR model	
		P (0.1/°C)	RE (%)	P (0.1/°C)	RE (%)	P (0.1/°C)	RE (%)	P (0.1/°C)	RE (%)
2000	361	325.44	9.85	338.18	6.32	313.79	13.08	331.21	8.25
2001	355	310.31	12.59	312.06	12.10	334.54	5.76	317.05	10.69
2002	357	320.83	10.13	324.77	9.03	338.44	5.20	354.39	0.73
2003	324	310.33	4.22	278.54	14.03	350.04	8.04	345.62	6.67
2004	333	323.09	2.98	323.39	2.89	351.28	5.49	345.68	3.81
2005	341	325.48	4.55	280.00	17.89	365.02	7.05	335.29	1.67
2006	335	320.68	4.27	322.46	3.74	327.98	2.10	344.97	2.98
2007	345	328.86	4.68	346.26	0.37	343.53	0.43	367.30	6.46
2008	379	327.16	13.68	321.26	15.23	328.10	13.43	336.75	11.15
2009	360	310.04	13.88	332.43	7.66	347.50	3.47	326.48	9.31
2010	392	310.39	20.82	321.35	18.02	332.37	15.21	351.54	10.32

FIGURE 4: The corresponding prediction error function, when delay time  $\tau = 1$ .

The computational methods of the other three models are similar to Case 1.

Compared with the results of AR model, R-SPA model, and BP model, SPA-PSR model has the smallest deviation (RE) with the measured value in those 11 years in general. The numbers of relative errors below 10% in three models are, respectively, 6, 6, 8, and 8. And the majority of forecasting results in SPA-PSR model is below 5%. According to those points, SPA-PSR model is better to be used to forecast.

In Table 5, it indicates that AR model and BP model have better forecasting results for Datong than for Mount Wutai, due to that the corresponding MRE is within 10% and the MAE is also decreased. What is more, the BP model is not better than AR model; the reason is likely to be train function or other factors. At the same time, the two indices all indicate that SPA-PSR model has the best forecasting results. Compared with AR model, BP model, and R-SPA model, the MRE of SPA-PSR model is relatively decreased by 29.11%, 32.82%, and 9.03%, respectively, and the MAE is relatively decreased by 29.93%, 32.56%, and 9.53%.

TABLE 5: The error analysis in four models.

Models	AR model	BP model	R-SPA model	SPA-PSR model
MRE (%)	9.24	9.75	7.20	6.55
MAE	33.58	34.89	26.01	23.53

## 5. Conclusions

To obtain the optimum prediction results, set pair analysis based on phase space reconstruction (SPA-PSR) model is proposed, in which the phase space with embedding dimension and the delay time is reconstructed and prediction results are gotten by combining SPA and phase space reconstruct methods. Two cases of forecasting the highest temperature in July of Mount Wutai and Datong stations are studied by using the new model. The main conclusions are shown as follows.

- (1) By combining the chaotic time series analysis and SPA analysis in the SPA-PSR model, we have a more clearly depiction of the complexity nonlinear dynamical behavior of original forecasting system of extreme temperature, which is a good foundation to make nonlinear forecasting.
- (2) Cases applications indicate that the SPA-PSR model can have a better result for forecasting the highest temperature in July of Mount Wutai and Datong stations. In two cases, compared with AR model, BP model, and R-SPA model, the MRE of SPA-PSR model is relatively decreased by 65.97%, 59.32%, and 7.79% in the case of Mount Wutai and 29.11%, 32.82%, and 9.03% in the case of Datong, respectively, and the MAE is relatively decreased by 65.71%, 59.32%, and 6.42% in the case of Mount Wutai and 29.93%, 32.56%, and 9.53% in the case of Datong, respectively. The results indicate that SPA-PSR model has the better forecasting values.
- (3) Due to the widely use of SPA [5, 6] and ubiquity of chaotic time series [18], the SPA-PSR model can also be used in predicting other nonlinear time series in the future and it will be further studied.



## Acknowledgments

This work was supported by the Project of National Basic Research Program of China (no. 2010CB951104), the National Natural Foundation of China (no. 50939001, 51379013), the Funds for Creative Research Groups of China (no. 51121003), the Specialized Research Fund for the Doctoral Program of Higher Education (no. 20100003110024), and the Program for Changjiang Scholars and Innovative Research Team in University (no. IRT0809).

## References

- [1] G. B. Sahoo and S. G. Schladow, "Impacts of climate change on lakes and reservoirs dynamics and restoration policies," *Sustainability Science*, vol. 3, no. 2, pp. 189–199, 2008.
- [2] B. Bošnjaković, "Geopolitics of climate change: a review," *Thermal Science*, vol. 16, no. 3, pp. 629–654, 2012.
- [3] B. Matic, J. Tepić, S. Sremac et al., "Development and evaluation of the model for the surface pavement temperature prediction," *Metalurgija*, vol. 51, no. 3, pp. 329–332, 2012.
- [4] H. S. Hippert, C. E. Pedreira, and R. C. Souza, "Combining neural networks and ARIMA models for hourly temperature forecast," in *Proceedings of the International Joint Conference on Neural Networks (IJCNN '00)*, vol. 4, pp. 414–419, July 2000.
- [5] F. G. Liu and Y. Zuo, "The application of rank set pair analysis similar prediction model in futures price forecasting," in *Proceedings of the International Conference*, pp. 240–243, Beijing, China, 2009.
- [6] W. Li, L. Qiu, X. Chen, and Q. Huang, "Assessment model for river ecology health based on set pair analysis and variable fuzzy set," *Journal of Hydraulic Engineering*, vol. 42, no. 7, pp. 775–782, 2011.
- [7] K. Holden, "Vector auto regression modeling and forecasting," *Journal of Forecasting*, vol. 14, no. 3, pp. 159–166, 1995.
- [8] M. Bańbura, D. Giannone, and L. Reichlin, "Large Bayesian vector auto regressions," *Journal of Applied Econometrics*, vol. 25, no. 1, pp. 71–92, 2010.
- [9] S. S. Yang, X. H. Hua, R. Jiang, and Y. C. Zhang, "New optimal weight combination model for forecasting precipitation," *Mathematical Problems in Engineering*, vol. 2012, Article ID 376010, 13 pages, 2012.
- [10] S. Yang, "Neural network forecast under the organic hybrid model of genetic algorithm and particle swarm algorithm," in *Proceedings of the International Conference on Wavelet Analysis and Pattern Recognition (ICWAPR '08)*, vol. 1, 2, pp. 254–258, August 2008.
- [11] Y. Mei, X. H. Yang, C. C. Chang et al., "Set pair analysis for optimal selection of bioretention media," *Advanced Science Letters*, vol. 10, no. 1, pp. 687–689, 2012.
- [12] T. N. Guo, X. H. Yang, Y. Mei et al., "Set pair analysis of eco-environment quality using maximum entropy," *Advanced Science Letters*, vol. 10, no. 1, pp. 640–643, 2012.
- [13] L. Cao, Y. Hong, H. Fang, and G. He, "Predicting chaotic time series with wavelet networks," *Physica D*, vol. 85, no. 1–2, pp. 225–238, 1995.
- [14] J. D. Farmer and J. J. Sidorowich, "Predicting chaotic time series," *Physical Review Letters*, vol. 59, no. 8, pp. 845–848, 1987.
- [15] D. I. Jeong and Y. Kim, "Combining single-value streamflow forecasts—a review and guidelines for selecting techniques," *Journal of Hydrology*, vol. 377, no. 3–4, pp. 284–299, 2009.
- [16] R. Khatibi, B. Sivakumar, M. A. Ghorbani, O. Kisi, K. Koçak, and D. Farsadi Zadeh, "Investigating chaos in river stage and discharge time series," *Journal of Hydrology*, vol. 414–415, pp. 108–117, 2012.
- [17] C. L. Di, X. H. Yang, D. W. Huang et al., "Chaos control and synchronization of a nonlinear system," *Nonlinear Science Letters C*, vol. 2, no. 2, pp. 47–54, 2012.
- [18] Z. Liu, "Chaotic time series analysis," *Mathematical Problems in Engineering*, vol. 2010, Article ID 720190, 31 pages, 2010.
- [19] X. H. Yang, D. X. She, Z. F. Yang, Q. H. Tang, and J. Q. Li, "Chaotic bayesian method based on multiple criteria decision making (MCDM) for forecasting nonlinear hydrological time series," *International Journal of Nonlinear Sciences and Numerical Simulation*, vol. 10, no. 11–12, pp. 1595–1610, 2009.
- [20] D. She and X. Yang, "A new adaptive local linear prediction method and its application in hydrological time series," *Mathematical Problems in Engineering*, vol. 2010, Article ID 205438, 15 pages, 2010.
- [21] F. Takens, "Detecting strange attractors in turbulence," in *Dynamical Systems and Turbulence*, D. A. Rand and L. S. Young, Eds., vol. 898 of *Lecture Notes in Mathematics*, pp. 366–381, Springer, Berlin, Germany, 1981.
- [22] M. T. Rosenstein, J. J. Collins, and C. J. De Luca, "A practical method for calculating largest Lyapunov exponents from small data sets," *Physica D*, vol. 65, no. 1–2, pp. 117–134, 1993.
- [23] A. M. Fraser and H. L. Swinney, "Independent coordinates for strange attractors from mutual information," *Physical Review A*, vol. 33, no. 2, pp. 1134–1140, 1985.
- [24] M. T. Rosenstein, J. J. Collins, and C. J. De Luca, "Reconstruction expansion as a geometry-based framework for choosing proper delay times," *Physica D*, vol. 73, no. 1, pp. 82–98, 1994.
- [25] M. Li and W. Zhao, "Smoothing the sample autocorrelation of long-range dependent traffic," *Mathematical Problems in Engineering*, vol. 2013, Article ID 631498, 10 pages, 2013.
- [26] M. Li and W. Zhao, "Quantitatively investigating locally weak stationarity of modified multifractional Gaussian noise," *Physica A*, vol. 391, no. 24, pp. 6268–6278, 2012.
- [27] Y. Lai and D. Lerner, "Effective scaling regime for computing the correlation dimension from chaotic time series," *Physica D*, vol. 115, no. 1–2, pp. 1–18, 1998.
- [28] P. Grassberger and I. Procaccia, "Measuring the strangeness of strange attractors," *Physica D*, vol. 9, no. 1, pp. 189–208, 1983.
- [29] M. B. Kennel, R. Brown, and H. D. I. Abarbanel, "Determining embedding dimension for phase-space reconstruction using a geometrical construction," *Physical Review A*, vol. 45, no. 6, pp. 3403–3411, 1992.
- [30] H. D. I. Abarbanel, R. Brown, J. J. Sidorowich, and L. S. Tsimring, "The analysis of observed chaotic data in physical systems," *Reviews of Modern Physics*, vol. 65, no. 4, pp. 1331–1392, 1993.
- [31] L. Cao, "Practical method for determining the minimum embedding dimension of a scalar time series," *Physica D*, vol. 110, no. 1, pp. 43–50, 1997.
- [32] J. C. Price, "Land surface temperature measurements from the split window channels of the NOAA 7 advanced very high resolution radiometer," *Journal of Geophysical Research D*, vol. 89, no. 5, pp. 7231–7237, 1984.
- [33] D. R. Easterling, G. A. Meehl, C. Parmesan, S. A. Changnon, T. R. Karl, and L. O. Mearns, "Climate extremes: observations, modeling, and impacts," *Science*, vol. 289, no. 5487, pp. 2068–2074, 2000.

## Research Article

# Symbol Error Rate as a Function of the Residual ISI Obtained by Blind Adaptive Equalizers for the SIMO and Fractional Gaussian Noise Case

**Monika Pinchas**

*Department of Electrical and Electronic Engineering, Ariel University, 40700 Ariel, Israel*

Correspondence should be addressed to Monika Pinchas; [monika.pinchas@gmail.com](mailto:monika.pinchas@gmail.com)

Received 26 May 2013; Accepted 26 June 2013

Academic Editor: Ming Li

Copyright © 2013 Monika Pinchas. This is an open access article distributed under the Creative Commons Attribution License, which permits unrestricted use, distribution, and reproduction in any medium, provided the original work is properly cited.

A nonzero residual intersymbol interference (ISI) causes the symbol error rate (SER) to increase where the achievable SER may not answer any more on the system's requirements. In the literature, we may find for the single-input-single-output (SISO) case a closed-form approximated expression for the SER that takes into account the achievable performance of the chosen blind adaptive equalizer from the residual ISI point of view and a closed-form approximated expression for the residual ISI valid for the single-input-multiple-output (SIMO) case. Both expressions were obtained by assuming that the input noise is a white Gaussian process where the Hurst exponent ( $H$ ) is equal to 0.5. In this paper, we derive a closed-form approximated expression for the residual ISI obtained by blind adaptive equalizers for the SIMO case, valid for fractional Gaussian noise (fGn) input where the Hurst exponent is in the region of  $0.5 \leq H < 1$ . Based on this new expression for the residual ISI, a closed-form approximated expression is obtained for the SER valid for the SIMO and fGn case. In this paper, we show via simulation results that the SER might get improved for increasing values of  $H$ .

## 1. Introduction

We consider a blind deconvolution problem in which we observe the multiple output of a finite impulse-response (FIR) single-input multiple-output (SIMO) channel from which we want to recover its input using adjustable linear filters (equalizers). In the field of communication, SIMO channels appear either when the signal is oversampled at the receiver or from the use of an array of antennas in the receiver [1–5]. It should be pointed out that for the SIMO case, the same information is transmitted through different subchannels, and all received sequences will be distinctly distorted versions of the same message, which accounts for a certain signal diversity [6]. Therefore, it is reasonable to assume that more information about the transmitted signal will be available at the receiver end [6]. SIMO transmission is widely replacing single-input-single-output (SISO) approach to enhance the performance via diversity combining [7]. It is well known that intersymbol interference (ISI) is a limiting factor in many communication environments where it causes

an irreducible degradation of the bit error rate (BER) and symbol error rate (SER) thus imposing an upper limit on the data symbol rate [1]. In order to overcome the ISI problem, an equalizer is implemented in those systems. Recently [1], a closed-form approximated expression was derived for the achievable residual ISI obtained by blind adaptive equalizers in a SIMO system where the error that is fed into the adaptive mechanism which updates the equalizer's taps is expressed as a polynomial function of order three of the equalized output. But, this expression was obtained by assuming that the input noise is a white Gaussian process where the Hurst exponent ( $H$ ) is equal to 0.5. A white Gaussian process is a special case ( $H = 0.5$ ) of the fractional Gaussian noise (fGn) model [8]. fGn with  $H \in (0.5, 1)$  corresponds to the case of long-range dependency (LRD) [8]. As stated in [9], LRD implies heavy-tailed probability density functions, which in general imply more random; see [10–13]. This point of view was recently detailed by [14, 15]. In the literature, we may also find a closed-form approximated expression for the SER valid for the SISO case [16] that takes into account the performance

of the chosen blind adaptive equalizer from the residual ISI point of view. But, this expression is not valid for the SIMO case and is based again on the assumption that the input noise is a white Gaussian process where the Hurst exponent ( $H$ ) is equal to 0.5. Up to now, there is no closed-form approximated expression for the SER valid for the SIMO and fGn input case where the Hurst exponent is in the region of  $0.5 \leq H < 1$  that takes into account the performance of the chosen blind adaptive equalizer from the residual ISI point of view. Thus, the system designer still has to carry out many simulations in order to find those system parameters such as the equalizer's tap length and step-size parameter that will lead the system to the required SER.

In this paper, we propose for the real and two independent quadrature carriers case, a closed-form approximated expression for the achievable residual ISI obtained by blind adaptive equalizers for the SIMO and fGn input case that depends on the step-size parameter, equalizer's tap length, input constellation statistics, channel power, and the number of receive antennas used in the SIMO system and on  $H$ . The new closed-form approximated expression is applicable for type of blind adaptive equalizers used in a SIMO FIR channel where the error that is fed into the adaptive mechanism which updates the equalizer's taps can be expressed as a polynomial function of order three of the equalized output. Based on this new expression for the residual ISI, a closed-form approximated expression is obtained for the SER valid for the SIMO and fGn case. As already mentioned, fGn with  $H \in (0.5, 1)$  corresponds to the case of LRD. Thus, it could be thought that the SER might increase as the value for  $H$  increases due to the noise dependency from the different receive paths. But, according to simulation results, improved SER performance is seen for higher values of  $H$ .

The paper is organized as follows. After having described the system under consideration in Section 2, the closed-form approximated expressions for the residual ISI and SER are introduced in Section 3. In Section 4, simulation results are presented, and the conclusion is given in Section 5.

## 2. System Description

The system under consideration, illustrated in Figure 1, is the same system described in [1] (except for the input noise issue which will be discussed later on in this paper). In this paper, we make the following assumptions.

- (1) The source sequence  $x[n]$  belongs to a real or two independent quadrature carriers case constellation input with variance  $\sigma_x^2$ , where  $x_r[n]$  and  $x_i[n]$  are the real and imaginary parts of  $x[n]$ , respectively.
- (2) The unknown subchannel  $h^{(m)}[n]$  ( $m = 1, 2, 3, \dots, M$  where  $M$  is the number of subchannels) is a possibly nonminimum phase linear time-invariant filter. There is no common zero among all the subchannels.
- (3) Each equalizer  $c^{(m)}[n]$  ( $m = 1, 2, 3, \dots, M$ ) is a tap-delay line.
- (4) The noise  $w^{(m)}[n]$  ( $m = 1, 2, 3, \dots, M$ ) consists of  $w^{(m)}[n] = w_r^{(m)}[n] + jw_i^{(m)}[n]$ , where  $w_r^{(m)}[n]$

and  $w_i^{(m)}[n]$  are the real and imaginary parts of  $w^{(m)}[n]$ , respectively, and  $w_r^{(m)}[n]$  and  $w_i^{(m)}[n]$  are independent. Both  $w_r^{(m)}[n]$  and  $w_i^{(m)}[n]$  are fractional Gaussian noises (fGn) with zero mean. For  $m = k$ , we have  $E[w_r^{(m)}[n]w_r^{(k)}[\tilde{n}]] = \sigma_{w_r}^2 \delta[n - \tilde{n}]$  and  $E[w_i^{(m)}[n]w_i^{(k)}[\tilde{n}]] = \sigma_{w_i}^2 \delta[n - \tilde{n}]$ . For  $m \neq k$ , we have  $E[w_r^{(m)}[n]w_r^{(k)}[\tilde{n}]] = (\sigma_{w_r}^2/2)[(|m-k|-1)^{2H} - 2(|m-k|)^{2H} + (|m-k|+1)^{2H}]\delta[n - \tilde{n}]$  and  $E[w_i^{(m)}[n]w_i^{(k)}[\tilde{n}]] = (\sigma_{w_i}^2/2)[(|m-k|-1)^{2H} - 2(|m-k|)^{2H} + (|m-k|+1)^{2H}]\delta[n - \tilde{n}]$ , where  $E[\cdot]$  denotes the expectation operator on  $(\cdot)$ ,  $\delta$  is the Kronecker delta function, and  $H$  is the Hurst exponent. In the following, we assume that  $\sigma_{w_i}^2 = \sigma_{w_r}^2$ .

According to Figure 1, the  $m$ th observation  $y^{(m)}[n]$  ( $y^{(m)}[n] = x[n] * h^{(m)}[n] + w^{(m)}[n]$ ) is the result of a linear convolution between the source signal  $x[n]$  and the corresponding channel response  $h^{(m)}[n]$ , corrupted by noise  $w^{(m)}[n]$ , where “ $*$ ” denotes the convolution operation. The equalizer's output  $z[n]$  is derived as follows:

$$\begin{aligned} z[n] &= \sum_{m=1}^{m=M} z^{(m)}[n] = \sum_{m=1}^{m=M} y^{(m)}[n] * c^{(m)}[n] \\ &= \sum_{m=1}^{m=M} (x[n] * h^{(m)}[n] * c^{(m)}[n] + w^{(m)}[n] * c^{(m)}[n]) \\ &= x[n] + p[n] + \tilde{w}[n], \end{aligned} \quad (1)$$

where  $p[n]$  is the convolutional noise ( $p[n] = x[n] * \xi[n]$ ),  $\xi[n] = \sum_{m=1}^{m=M} h^{(m)}[n] * c^{(m)}[n] - \delta[n]$ , and  $\tilde{w}[n] = \sum_{m=1}^{m=M} w^{(m)}[n] * c^{(m)}[n]$ . Next, we turn to the adaptation mechanism of the equalizer in each subchannel which is based on a predefined cost function  $F[n]$  that characterizes the intersymbol interference; see, for example, [17–23]:

$$\underline{c}^{(m)}[n+1] = \underline{c}^{(m)}[n] - \mu^{(m)} \frac{\partial F[n]}{\partial \underline{z}[n]} \underline{y}^{(m)*}[n], \quad (2)$$

where  $\mu^{(m)}$  is the step-size parameter in the subchannel,  $\underline{c}^{(m)}[n]$  is the equalizer vector, where the input vector is  $\underline{y}^{(m)}[n] = [y^{(m)}[n] \dots y^{(m)}[n - N + 1]]^T$ , and  $N$  is the equalizer's tap length. The operator  $(\cdot)^T$  and  $(\cdot)^*$  denote for transpose and conjugate of the function  $(\cdot)$ , respectively. Recently [1], a closed-form approximated expression was derived for the achievable residual ISI, valid for the SIMO case that depends on the step-size parameter, equalizer's tap length, input signal statistics, SNR, number of receive antennas, and channel power and is given in (dB) units by [1]:

$$\text{ISI} \cong 10 \log_{10}(m_p) - 10 \log_{10}(\sigma_{x_r}^2), \quad (3)$$

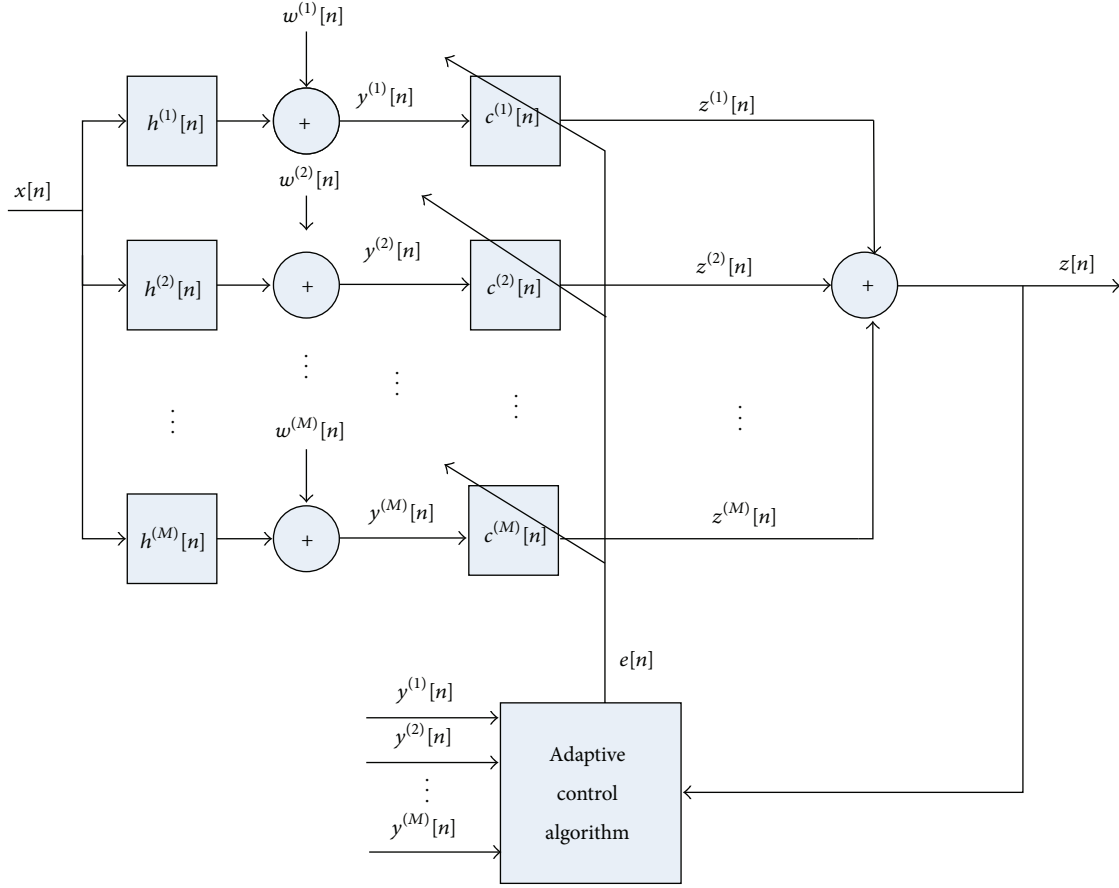


FIGURE 1: Block diagram of a baseband SIMO communication system.

where

$$m_p = \min [\text{Sol}_1^{mp_1}, \text{Sol}_2^{mp_1}] \quad \text{for } \text{Sol}_1^{mp_1} > 0, \text{Sol}_2^{mp_1} > 0$$

$$\text{or } m_p = \max [\text{Sol}_1^{mp_1}, \text{Sol}_2^{mp_1}] \quad \text{for } \text{Sol}_1^{mp_1} \cdot \text{Sol}_2^{mp_1} < 0,$$

$$\text{where } \text{Sol}_1^{mp_1} = \frac{-B_1 + \sqrt{B_1^2 - 4A_1C_1B}}{2A_1};$$

$$\text{Sol}_2^{mp_1} = \frac{-B_1 - \sqrt{B_1^2 - 4A_1C_1B}}{2A_1}, \quad (4)$$

$$A_1 = (B(45\sigma_{x_r}^2 a_3^2 + 18\sigma_{x_r}^2 a_3 a_{12} + 6a_1 a_3 + 9\sigma_{x_r}^2 a_{12}^2 + 2a_1 a_{12}) - 2(3a_3 + a_{12})) + B(45a_3^2 + 18a_3 a_{12} + 9a_{12}^2) \sigma_{\bar{w}_r}^2, \quad (5)$$

$$B_1 = (B(12(\sigma_{x_r}^2)^2 a_3 a_{12} + 6(\sigma_{x_r}^2)^2 a_{12}^2 + 12\sigma_{x_r}^2 a_1 a_3 + 4\sigma_{x_r}^2 a_1 a_{12} + a_1^2 + 15\mathbf{E}[x_r^4] a_3^2 + 2\mathbf{E}[x_r^4] a_3 a_{12} + \mathbf{E}[x_r^4] a_{12}^2)$$

$$-2(a_1 + 3\sigma_{x_r}^2 a_3 + \sigma_{x_r}^2 a_{12})) + B(45a_3^2 + 16a_3 a_{12} + 9a_{12}^2) \sigma_{\bar{w}_r}^4 + (B(90a_3^2 \sigma_{x_r}^2 + 36a_3 a_{12} \sigma_{x_r}^2 + 12a_1 a_3 + 18a_{12}^2 \sigma_{x_r}^2 + 4a_1 a_{12}) - 2a_{12} - 6a_3) \sigma_{\bar{w}_r}^2, \quad (6)$$

$$B = N\sigma_{x_r}^2 \sum_{m=1}^M \mu^m \left( \sum_{k=0}^{k=R-1} |h_k^{(m)}[n]|^2 + \frac{1}{\text{SNR}} \right), \quad (7)$$

$$C_1 = (2(\sigma_{x_r}^2)^2 a_1 a_{12} + \sigma_{x_r}^2 a_1^2 + 2\mathbf{E}[x_r^4] \sigma_{x_r}^2 a_3 a_{12} + \mathbf{E}[x_r^4] \sigma_{x_r}^2 a_{12}^2 + 2\mathbf{E}[x_r^4] a_1 a_3 + \mathbf{E}[x_r^6] a_3^2) + (15a_3^2 + 6a_3 a_{12} + 3a_{12}^2) \sigma_{\bar{w}_r}^6 + (45a_3^2 \sigma_{x_r}^2 + 18a_3 a_{12} \sigma_{x_r}^2 + 6a_1 a_3 + 9a_{12}^2 \sigma_{x_r}^2 + 2a_1 a_{12}) \sigma_{\bar{w}_r}^4 + (a_1^2 + 12a_1 a_3 \sigma_{x_r}^2 + 4a_1 a_{12} \sigma_{x_r}^2 + 15a_3^2 \mathbf{E}[x_r^4]$$

$$\begin{aligned}
& + 12a_3a_{12}(\sigma_{x_r}^2)^2 + 2a_3a_{12}\mathbf{E}[x_r^4] \\
& + a_{12}^2\mathbf{E}[x_r^4] + 6a_{12}(\sigma_{x_r}^2)^2\sigma_{\bar{w}_r}^2,
\end{aligned} \tag{8}$$

where  $h_k^{(m)}[n]$  denotes the  $k$ th tap of the  $m$ th subchannel at time index  $n$ ,  $R$  is the subchannel length, and

$$\sigma_{\bar{w}_r}^2 \cong \sum_{m=1}^{m=M} \frac{\sigma_{x_r}^2}{M^2 \text{SNR} \sum_{k=0}^{k=R-1} |h_k^{(m)}[n]|^2}, \tag{9}$$

where  $\text{SNR} = \sigma_x^2/\sigma_w^2$  and  $a_1, a_{12}$ , and  $a_3$  are properties of the chosen equalizer and found by

$$\begin{aligned}
& \Re\left(\frac{\partial F[n]}{\partial z[n]}\right) \\
& = \left(a_1(z_r[n]) + a_3(z_r[n])^3 + a_{12}(z_r[n])(z_i[n])^2\right),
\end{aligned} \tag{10}$$

where  $\Re(\cdot)$  is the real part of  $(\cdot)$  and  $z_r, z_i$  are the real and imaginary parts of the equalized output  $z[n]$ , respectively.

As it was already implied earlier in this paper, the closed-form approximated expression for the residual ISI [1] was obtained by assuming that the noise  $w^{(m)}[n]$  is an additive Gaussian white noise ( $H = 0.5$ ). Thus, it is not applicable for the fGn case (for  $0.5 \leq H < 1$ ). Therefore, in order to derive the expression for the SER applicable for the SIMO and fGn ( $0.5 \leq H < 1$ ) case, a new expression for the achievable residual ISI is needed.

### 3. Residual ISI and SER for the SIMO and Fractional Gaussian Noise Case

In this section, a closed-form approximated expression is derived for the residual ISI valid for the SIMO and fGn case. Based on this new expression, the SER is obtained.

#### 3.1. Derivation of the Residual ISI

**Theorem 1.** Consider the following assumptions.

- (1) The convolutional noise  $p[n]$  is a zero mean, white Gaussian process with variance  $\sigma_p^2 = E[p[n]p^*[n]]$ . The real part of  $p[n]$  is denoted as  $p_r[n]$  and  $E[p_r^2[n]] = m_p$ .
- (2) The source signal  $x[n]$  is a rectangular quadrature amplitude modulation (QAM) signal (where the real part of  $x[n]$  is independent with the imaginary part of  $x[n]$ ) with known variance and higher moments.
- (3) The convolutional noise  $p[n]$  and the source signal are independent.

(4)  $\partial F[n]/\partial z[n]$  can be expressed as a polynomial function of the equalized output of order three.

(5) The gain between the source and equalized output signal is equal to one.

(6) The convolutional noise  $p[n]$  is independent with  $\bar{w}[n]$ .

(7) The added noise is fGn as defined in the previous section in assumption (4).

(8) The Hurst exponent is in the range of  $0.5 \leq H < 1$ .

The residual ISI expressed in (dB) units may be defined as (3), (4), (5), (6), (7), and (8), where  $\text{SNR} = \sigma_x^2/\sigma_w^2$ ,  $a_1, a_{12}, a_3$  are properties of the chosen equalizer and found by (10) and

$$\sigma_{\bar{w}_r}^2 \cong \sum_{m=1}^M \frac{\sigma_{x_r}^2}{M^2 \text{SNR} \sum_{k=0}^{k=R-1} |h_k^{(m)}[n]|^2} (1 + H(2H - 1)(M - 1)). \tag{11}$$

*Comments.* Please note that for  $H = 0.5$  (Gaussian white noise case), the expressions for  $\sigma_{\bar{w}_r}^2$  given in (11) and (9) are equivalent. By repeating the steps in [1] for the calculation of the expression of the residual ISI the only place where the difference between the assumption of  $w_r(n)$  and  $w_i(n)$  being Gaussian white noises or fractional Gaussian noises has a major role on the total result of the approximated derived expression for the residual ISI, is in the calculation of  $\sigma_{\bar{w}_r}^2$ . Thus, we bring here only the various steps that led to (11).

It should be pointed out that assumptions (1)–(6) from above, are precisely the same assumptions made in [1].

*Proof.* The real part of  $\bar{w}[n]$ , namely,  $\bar{w}_r[n]$  may be expressed as follows:

$$\begin{aligned}
& \bar{w}_r[n] \\
& = \sum_{m=1}^M \sum_{k=0}^{k=N-1} \left( c_r^{(m)}[k] w_r^{(m)}[n-k] - c_i^{(m)}[k] w_i^{(m)}[n-k] \right),
\end{aligned} \tag{12}$$

where  $c_r^{(m)}[k]$  and  $c_i^{(m)}[k]$  are the real and imaginary parts of  $c^{(m)}[k]$ , respectively. The variance of  $\bar{w}_r[n]$  may be expressed by

$$\begin{aligned}
\sigma_{\bar{w}_r}^2 = E & \left[ \sum_{m=1}^M \sum_{k=0}^{k=N-1} \left( c_r^{(m)}[k] w_r^{(m)}[n-k] - c_i^{(m)}[k] w_i^{(m)}[n-k] \right) \right. \\
& \cdot \sum_{p=1}^M \sum_{kk=0}^{kk=N-1} \left( c_r^{(p)}[kk] w_r^{(p)}[n-kk] \right. \\
& \left. \left. - c_i^{(p)}[kk] w_i^{(p)}[n-kk] \right) \right]
\end{aligned} \tag{13}$$



which can be also written as follows:

$$\begin{aligned} \sigma_{\bar{w}_r}^2 &= \sum_{m=1}^M \sigma_{w_r}^2 \sum_{k=0}^{k=N-1} |c^{(m)}[k]|^2 \\ &+ \sum_{m=1, m \neq p}^M \sum_{p=1, p \neq m}^M \sum_{k=0}^{k=N-1} E [c_r^{(m)}[k] c_r^{(p)}[k] \\ &\quad \cdot w_r^{(m)}[n-k] w_r^{(p)}[n-k] \\ &\quad + c_i^{(m)}[k] c_i^{(p)}[k] \\ &\quad \cdot w_i^{(m)}[n-k] w_i^{(p)}[n-k]] \end{aligned} \quad (14)$$

or by

$$\begin{aligned} \sigma_{\bar{w}_r}^2 &= \sum_{m=1}^M \sigma_{w_r}^2 \sum_{k=0}^{k=N-1} |c^{(m)}[k]|^2 \\ &+ \sum_{m=1, m \neq p}^M \sum_{p=1, p \neq m}^M \frac{\sigma_{w_r}^2}{2} [ (|m-p|-1)^{2H} - 2(|m-p|)^{2H} \\ &\quad + (|m-p|+1)^{2H} ] \\ &\quad \cdot \sum_{k=0}^{k=N-1} [c_r^{(m)}[k] c_r^{(p)}[k] + c_i^{(m)}[k] c_i^{(p)}[k]]. \end{aligned} \quad (15)$$

According to [24],

$$\begin{aligned} &0.5 [ (|m-p|-1)^{2H} - 2(|m-p|)^{2H} + (|m-p|+1)^{2H} ] \\ &\simeq H(2H-1) |m-p|^{2H-2}. \end{aligned} \quad (16)$$

Thus, substituting (16) into (15) yields to

$$\begin{aligned} \sigma_{\bar{w}_r}^2 &\cong \sum_{m=1}^M \sigma_{w_r}^2 \sum_{k=0}^{k=N-1} |c^{(m)}[k]|^2 \\ &+ \sigma_{w_r}^2 H(2H-1) \sum_{m=1, m \neq p}^M \sum_{p=1, p \neq m}^M |m-p|^{2H-2} \\ &\quad \times \sum_{k=0}^{k=N-1} [c_r^{(m)}[k] c_r^{(p)}[k] + c_i^{(m)}[k] c_i^{(p)}[k]]. \end{aligned} \quad (17)$$

This expression (17) can be upper limited by

$$\begin{aligned} \sigma_{\bar{w}_r}^2 &\leq \sum_{m=1}^M \sigma_{w_r}^2 \sum_{k=0}^{k=N-1} |c^{(m)}[k]|^2 \\ &+ \sigma_{w_r}^2 H(2H-1) \max_{p \neq m, p, m=1:M} [|m-p|^{2H-2}] \\ &\quad \times \left| \sum_{m=1, m \neq p}^M \sum_{p=1, p \neq m}^M \sum_{k=0}^{k=N-1} [c_r^{(m)}[k] c_r^{(p)}[k] \right. \\ &\quad \left. + c_i^{(m)}[k] c_i^{(p)}[k]] \right|. \end{aligned} \quad (18)$$

According to the triangle inequality [25], we have

$$\begin{aligned} &\left| \sum_{m=1, m \neq p}^M \sum_{p=1, p \neq m}^M \sum_{k=0}^{k=N-1} [c_r^{(m)}[k] c_r^{(p)}[k] + c_i^{(m)}[k] c_i^{(p)}[k]] \right| \\ &\leq \left| \sum_{m=1, m \neq p}^M \sum_{p=1, p \neq m}^M \sum_{k=0}^{k=N-1} [c_r^{(m)}[k] c_r^{(p)}[k]] \right| \\ &\quad + \left| \sum_{m=1, m \neq p}^M \sum_{p=1, p \neq m}^M \sum_{k=0}^{k=N-1} [c_i^{(m)}[k] c_i^{(p)}[k]] \right|. \end{aligned} \quad (19)$$

According to the holder inequality [25], we may write

$$\begin{aligned} &\left| \sum_{m=1, m \neq p}^M \sum_{p=1, p \neq m}^M c_r^{(m)}[k] c_r^{(p)}[k] \right| \leq (M-1) \sum_{m=1}^M (c_r^{(m)}[k])^2, \\ &\left| \sum_{m=1, m \neq p}^M \sum_{p=1, p \neq m}^M c_i^{(m)}[k] c_i^{(p)}[k] \right| \leq (M-1) \sum_{m=1}^M (c_i^{(m)}[k])^2. \end{aligned} \quad (20)$$

By taking into account that  $\max_{p \neq m, p, m=1:M} |m-p|^{2H-2} = 1$  for  $0.5 \leq H < 1$ , we may write with the help of (18), (19), and (20) as follows:

$$\sigma_{\bar{w}_r}^2 \leq \sum_{m=1}^M \sigma_{w_r}^2 \sum_{k=0}^{k=N-1} |c^{(m)}[k]|^2 (1 + H(2H-1)(M-1)). \quad (21)$$

As already mentioned in the system description section,  $\sum_{m=1}^M h^{(m)}[n] * c^{(m)}[n] = \xi[n] + \delta[n]$ , where  $\xi[n]$  stands for the error not having perfect equalization. Therefore, the expression  $h^{(m)}[n] * c^{(m)}[n]$  could have been written as  $h^{(m)}[n] * c^{(m)}[n] = \delta[n]/M + \tilde{\xi}^{(m)}[n]$ , where  $\xi[n] = \sum_{m=1}^M \tilde{\xi}^{(m)}[n]$ . Thus, for the case where the variance of  $\tilde{\xi}^{(m)}[n]$  can be considered as very small we may write

$$\sum_{k=0}^{k=N-1} |c^{(m)}[k]|^2 \cong \frac{1}{M^2 \sum_{k=0}^{k=R-1} |h_k^{(m)}[n]|^2}. \quad (22)$$

Now, substituting (22) into (21) yields to

$$\sigma_{\bar{w}_r}^2 \leq \sum_{m=1}^M \frac{\sigma_{x_r}^2}{M^2 \text{SNR} \sum_{k=0}^{k=R-1} |h_k^{(m)}[n]|^2} (1 + H(2H-1)(M-1)). \quad (23)$$

In practice, the variance of  $\tilde{\xi}^{(m)}[n]$  is not so small. Thus, the expression for  $\sum_{k=0}^{k=N-1} |c^{(m)}[k]|^2$  is higher than that given in (22). Therefore, we may define  $\sigma_{\bar{w}_r}^2$  as given in (11). This completes our proof.  $\square$

**3.2. Derivation of the SER for the SIMO Case.** In this subsection, we derive the SER for a source signal  $x[n]$  belonging to a rectangular QAM constellation, applicable for the SIMO and fGn case.

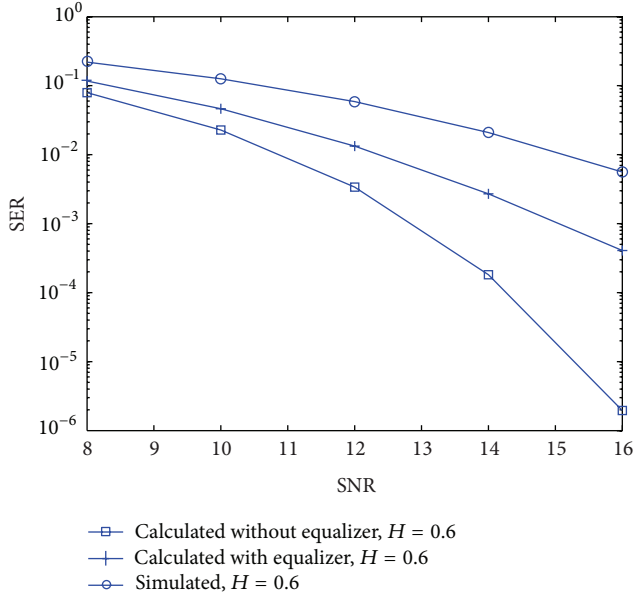


FIGURE 2: SER comparison with the following parameters:  $d = 1$ , the step-size parameter  $\mu = 0.000005$ ,  $N = 17$ , and  $H = 0.6$ , channel case A; the results were obtained for 1600000 symbols.

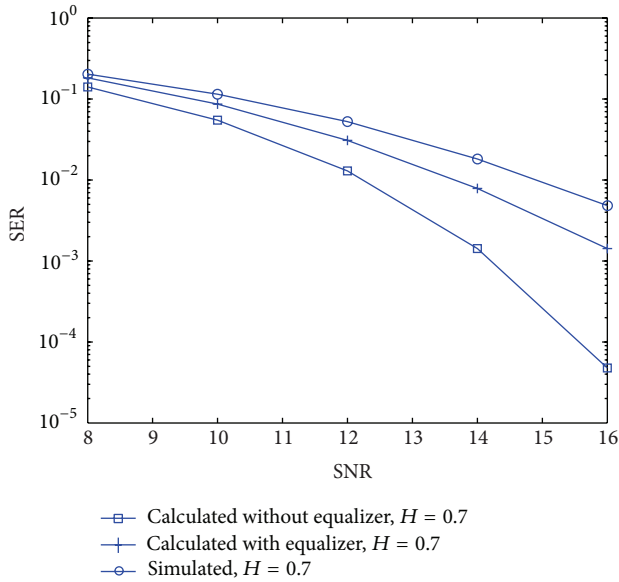


FIGURE 3: SER comparison with the following parameters:  $d = 1$ , the step-size parameter  $\mu = 0.000005$ ,  $N = 17$ , and  $H = 0.7$ , channel case A; the results were obtained for 1600000 symbols.

**Theorem 2.** Based on the assumptions given in the previous subsection, the SER for the SIMO and fGn case may be defined as follows:

$$SER_{QAM} = 4 \frac{\bar{M} - 1}{\bar{M}} Q\left(\frac{d}{\sigma_T}\right) \left(1 - \frac{\bar{M} - 1}{\bar{M}} Q\left(\frac{d}{\sigma_T}\right)\right), \quad (24)$$

where  $\bar{M} = \sqrt{M_{QAM}}$  and  $M_{QAM}$  is the number of signal points for a  $M_{QAM}$ -ary QAM constellation,  $d$  is half the distance

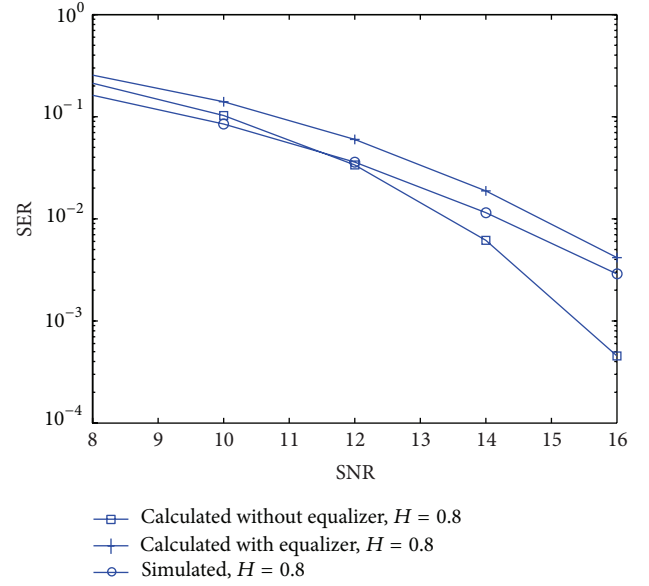


FIGURE 4: SER comparison with the following parameters:  $d = 1$ , the step-size parameter  $\mu = 0.000005$ ,  $N = 17$ , and  $H = 0.8$ , channel case A; the results were obtained for 1600000 symbols.

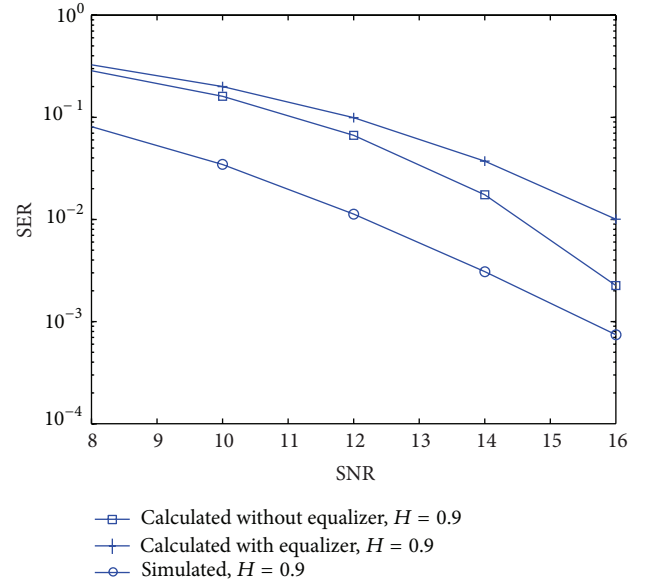


FIGURE 5: SER comparison with the following parameters:  $d = 1$ , the step-size parameter  $\mu = 0.000005$ ,  $N = 17$ , and  $H = 0.9$ , channel case A; the results were obtained for 1600000 symbols.

between adjacent  $\sqrt{M_{QAM}}$ -ary pulse amplitude modulation (PAM) signals:

$$\sigma_T = \sqrt{m_p + \sigma_{\bar{w}_r}^2}; \quad Q\left(\frac{d}{\sigma_T}\right) = \frac{1}{\sqrt{2\pi}} \int_{d/\sigma_T}^{\infty} e^{-u^2/2} du, \quad (25)$$

and  $m_p$ ,  $\sigma_{\bar{w}_r}^2$  are according to (4) and (11), respectively.

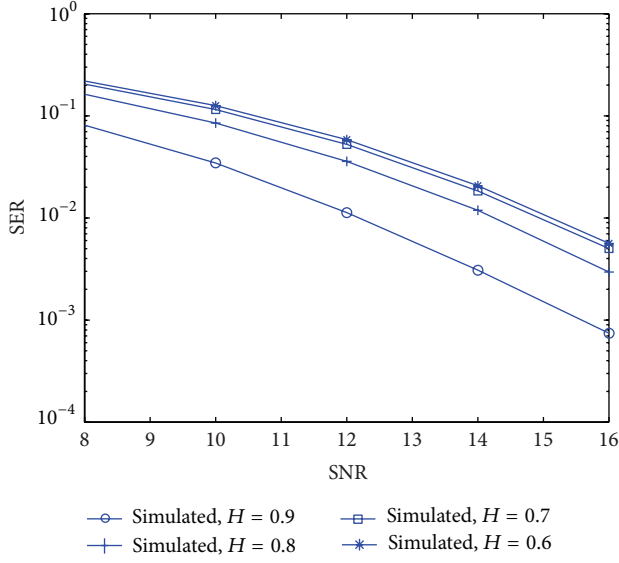


FIGURE 6: SER comparison with the following parameters:  $d = 1$ , the step-size parameter  $\mu = 0.000005$ ,  $N = 17$ , and  $H = 0.9, 0.8, 0.7, 0.6$ , channel case A; the results were obtained for 1600000 symbols.

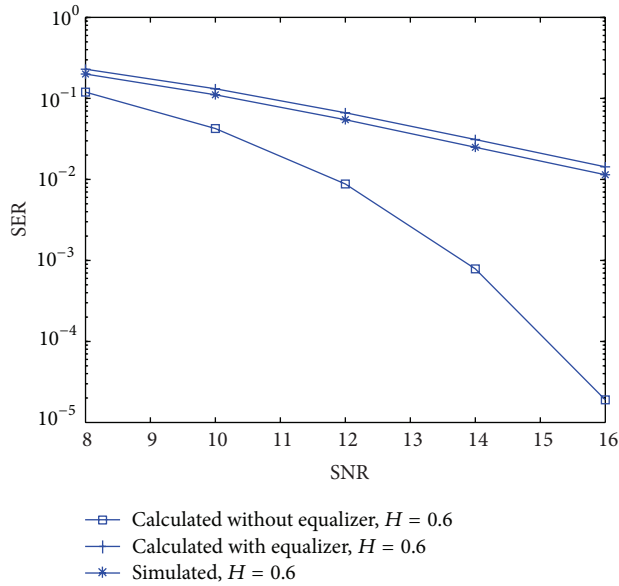


FIGURE 7: SER comparison with the following parameters:  $d = 1$ , the step-size parameter  $\mu = 0.00002$ ,  $N = 13$ , and  $H = 0.6$ , channel case B; the results were obtained for 1600000 symbols.

*Proof.* According to (1), the equalized output is given by  $z[n] = x[n] + p[n] + \bar{w}[n]$ . The expression for the equalized output for the SISO and white Gaussian case (case one) looks quite similar to the expression for the equalized output for the SIMO and fGn case (case two). The difference between the two cases (case one and case two) lies in the fact that the variance of  $p[n]$  and  $\bar{w}[n]$  is very different. For each case, the expressions for the variance of the real part of  $p[n]$  (named in this paper as  $m_p$ ) and  $\sigma_{\bar{w}_r}^2$  are different. Recently [16],

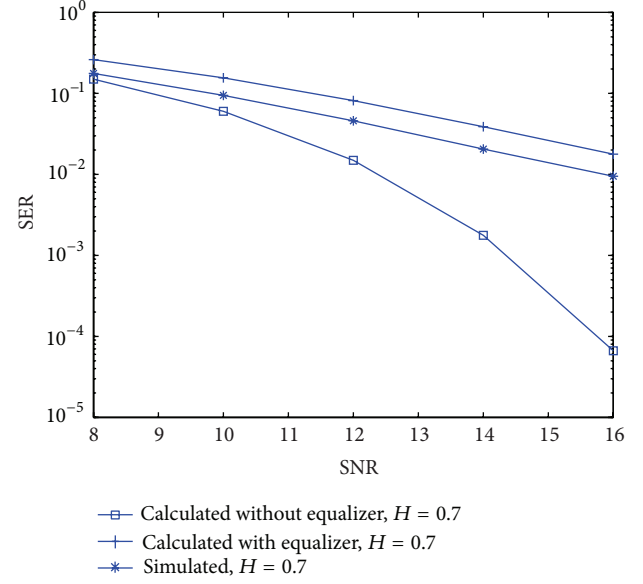


FIGURE 8: SER comparison with the following parameters:  $d = 1$ , the step-size parameter  $\mu = 0.00002$ ,  $N = 13$ , and  $H = 0.7$ , channel case B; the results were obtained for 1600000 symbols.

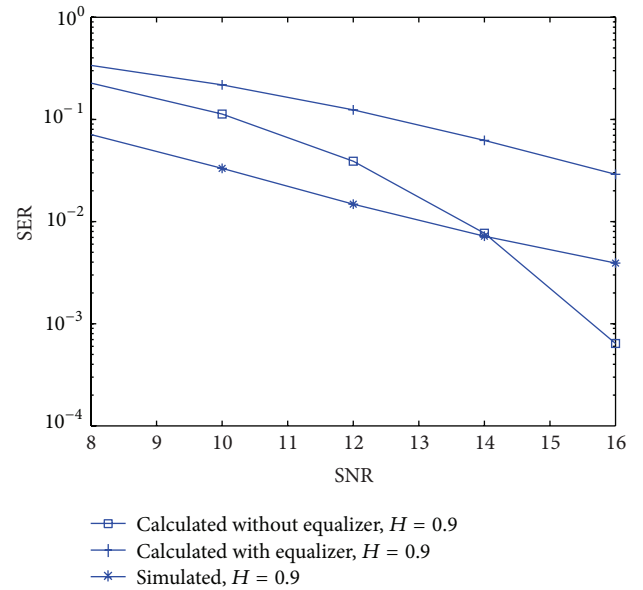


FIGURE 9: SER comparison with the following parameters:  $d = 1$ , the step-size parameter  $\mu = 0.00002$ ,  $N = 13$ , and  $H = 0.9$ , channel case B; the results were obtained for 1600000 symbols.

a closed-form approximated expression was obtained for the SER, based on  $z[n] = x[n] + p[n] + \bar{w}[n]$ , valid for the SISO and white Gaussian ( $H = 0.5$ ) case. The recently obtained expression for the SER [16] is recalled in (24), (25), where  $m_p$  and  $\sigma_{\bar{w}_r}^2$  were taken for the SISO and white Gaussian case. In order to obtain a closed-form approximated expression for the SER valid for the SIMO and fGn case, the recently obtained expression for the SER [16] was used with  $m_p$  and

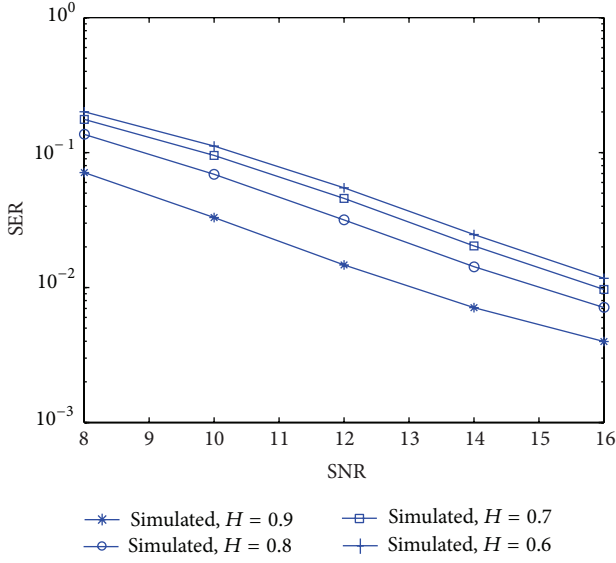


FIGURE 10: SER comparison with the following parameters:  $d = 1$ , the step-size parameter  $\mu = 0.00002$ ,  $N = 13$ , and  $H = 0.9, 0.8, 0.7, 0.6$ , channel case B; the results were obtained for 1600000 symbols.

$\sigma_{\bar{w}_r}^2$  valid for the SIMO and fGn case. This completes our proof.  $\square$

$$\begin{aligned}
 h_1 &= [-0.0318 + j0.2330 \quad 0.3128 - j0.3693 \quad -0.3609 + j0.3810 \quad 0.6490 \quad -0.1110 + j0.0396], \\
 h_2 &= [0.3005 - j0.0247 \quad 0.6784 \quad 0.6248 - j0.1316 \quad 0.1282 - j0.1411 \quad -0.0590 - j0.0366], \\
 h_3 &= [-0.1351 - j0.2061 \quad -0.1274 + j0.5876 \quad 0.6401 \quad -0.1818 - j0.3354 \quad 0.0871 - j0.1216], \\
 h_4 &= [0.2835 + j0.0204 \quad 0.6799 \quad 0.5936 + j0.0986 \quad 0.1938 + j0.2101 \quad -0.0333 + j0.1095].
 \end{aligned} \tag{28}$$

#### 4. Simulation

In this section, we test our new proposed expression for the SER for the 16 QAM case (a modulation using  $\pm\{1, 3\}$  levels for in-phase and quadrature components) with Godard's algorithm [17] for different values of SNR and equalizer's tap length and for two different channel cases. The equalizer taps for Godard's algorithm [17] were updated according to the following:

$$c_m[n+1] = c_m[n] - \mu_G \left( |z[n]|^2 - \frac{E[|x[n]|^4]}{E[|x[n]|^2]} \right) \times z[n] y^*[n-m], \tag{26}$$

where  $\mu_G$  is the step size. The values for  $a_1$ ,  $a_{12}$ , and  $a_3$  corresponding to Godard's [17] algorithm are given by

$$a_1 = -\frac{E[|x[n]|^4]}{E[|x[n]|^2]}; \quad a_{12} = 1; \quad a_3 = 1. \tag{27}$$

In the following, we consider two channel cases. *Channel case A* which is a four-channel model with channel coefficients determined according to the following:

*Channel case B* which is a two-channel model with channel coefficients determined according to the following:

$$\begin{aligned}
 h_1 &= [-0.4000 \quad 0.8000 \quad 0.3200 \quad 0.1280 \quad 0.0512 \quad 0.0205 \quad 0.0082 \quad 0.0033 \quad 0.0013 \\
 &\quad 0.0005 \quad 0.0002 \quad 0.0001 \quad 0.0000], \\
 h_2 &= [1.3000 \quad 0.6000 - j0.6364 \quad 0 \quad 0 \quad 0 \quad 0 \quad 0 \quad 0 \quad 0 \quad 0 \quad 0 \quad 0].
 \end{aligned} \tag{29}$$

Please note that channel case B was also used in [1]. The equalizer was initialized by setting the center tap equal to one and all others to zero.

In the following, we denote the SER performance according to (24) as "calculated with equalizer." In addition, we wish to show the SER performance for the case where the residual ISI is not taken into account. Therefore, we denote in the following the SER performance that does not take into account the residual ISI as "calculated without equalizer."

Figures 2, 3, 4, and 5 and Figures 7, 8, and 9 show the SER performance for different values of  $H$  as a function of SNR of our proposed expression (24) compared with the simulated results and with those calculated results that do not take into account the residual ISI. According to Figure 2 to Figure 5 and Figure 7 to Figure 9, a high correlation is observed between the simulated and calculated results (24), while the opposite is seen by comparing the simulated and those calculated results that do not take into account the

residual ISI. Figures 6 and 10 show the SER performance for different values of  $H$  in the range of  $0.5 < H < 1$  as a function of SNR for channel cases A and B, respectively. It is reasonable to think that the SER might increase as the value for  $H$  increases due to the noise dependency from the different receive paths. But, according to simulation results (Figures 6 and 10), improved SER performance is seen for higher values of  $H$ .

## 5. Conclusion

In this paper, we proposed for the real and two independent quadrature carrier cases, a closed-form approximated expression for the SER that takes into account the residual ISI obtained by blind adaptive equalizers and is applicable for the SIMO and fGn ( $0.5 \leq H < 1$ ) input case. This new expression is applicable for the type of blind adaptive equalizers used in a SIMO FIR channel where the error that is fed into the adaptive mechanism which updates the equalizer's taps can be expressed as a polynomial function of order three of the equalized output. The expression for the SER depends on the system's parameters (step-size parameter, equalizer's tap length, input constellation statistics, channel power, and number of receive antennas used in the SIMO system and on  $H$ ). Thus, there is no need anymore to carry out any simulation in order to find those system's parameters that will lead to the required SER performance. According to the simulation results, a high correlation is obtained between the calculated and simulated results for the SER. FGn with  $H \in (0.5, 1)$  corresponds to the case of LRD. Thus, it could be thought that the SER might increase as the value for  $H$  increases due to the noise dependency from the different receive paths. But, according to the simulation results, improved SER performance is seen for higher values of  $H$ .

## References

- [1] M. Pinchas, "A closed-form approximated expression for the achievable residual ISI obtained by blind adaptive equalizers in a SIMO FIR channel," in *Proceedings of the IEEE 27th Convention of Electrical and Electronics Engineers in Israel*, Hilton Queen of Sheba, Eilat, Israel, November 2012.
- [2] I. Moazzen, A. M. Doost-Hoseini, and M. J. Omid, "A novel blind frequency domain equalizer for SIMO systems," in *Proceedings of the International Conference on Wireless Communications and Signal Processing (WCSP '09)*, pp. 1–6, Nanjing, China, November 2009.
- [3] D. Peng, Y. Xiang, Z. Yi, and S. Yu, "CM-based blind equalization of time-varying SIMO-FIR channel with single pulsation estimation," *IEEE Transactions on Vehicular Technology*, vol. 60, no. 5, pp. 2410–2415, 2011.
- [4] A. Coskun and I. Kale, "Blind multidimensional matched filtering techniques for single input multiple output communications," *IEEE Transactions on Instrumentation and Measurement*, vol. 59, no. 5, pp. 1056–1064, 2010.
- [5] S. Van Vaerenbergh, J. Via, and I. Santamaria, "Blind identification of SIMO wiener systems based on kernel canonical correlation analysis," *IEEE Transactions on Signal Processing*, vol. 61, no. 9, pp. 2219–2230, 2013.
- [6] <http://books.google.co.il/books?id=bimBH2czOZ0C>.
- [7] S. Chen, A. Wolfgang, and L. Hanzo, "Constant modulus algorithm aided soft decision directed scheme for blind space-time equalisation of SIMO channels," *Signal Processing*, vol. 87, no. 11, pp. 2587–2599, 2007.
- [8] M. Li and W. Zhao, "Quantitatively investigating locally weak stationarity of modified multifractional Gaussian noise," *Physica A*, vol. 391, no. 24, pp. 6268–6278, 2012.
- [9] M. Pinchas, "Residual ISI obtained by blind adaptive equalizers and fractional noise," *Mathematical Problems in Engineering*, vol. 2013, Article ID 972174, 11 pages, 2013.
- [10] B. B. Mandelbrot, *Multifractals and 1/f noise*, Springer, New York, NY, USA, 1999.
- [11] B. B. Mandelbrot and J. R. Wallis, "Noah, Joseph, and operational hydrology," *Water Resources Research*, vol. 4, no. 5, pp. 909–918, 1968.
- [12] R. J. Adler, E. Raissa Feldman, and M. S. Taqqu, Eds., *A Practical Guide to Heavy Tails: Statistical Techniques and Applications*, Birkhäuser, Boston, Mass, USA, 1998.
- [13] A. Mura, M. S. Taqqu, and F. Mainardi, "Non-Markovian diffusion equations and processes: analysis and simulations," *Physica A*, vol. 387, no. 21, pp. 5033–5064, 2008.
- [14] M. Li and W. Zhao, "On  $1/f$  noise," *Mathematical Problems in Engineering*, vol. 2012, Article ID 673648, 23 pages, 2012.
- [15] M. Li and W. Zhao, "Visiting power laws in cyber-physical networking systems," *Mathematical Problems in Engineering*, vol. 2012, Article ID 302786, 13 pages, 2012.
- [16] M. Pinchas, "Symbol error rate as a function of the residual ISI obtained by blind adaptive equalizers," in *Proceedings of the Pervasive and Embedded Computing and Communication Systems (PECCS '13)*, Barcelona, Spain, February 2013.
- [17] D. N. Godard, "Self-recovering equalization and carrier tracking in two-dimensional data communication systems," *IEEE Transactions on Communications Systems*, vol. 28, no. 11, pp. 1867–1875, 1980.
- [18] S. Haykin, "Blind deconvolution," in *Adaptive Filter Theory*, S. Haykin, Ed., Chapter 20, Prentice-Hall, Englewood Cliffs, NJ, USA, 1991.
- [19] M. Pinchas, "A MSE optimized polynomial equalizer for 16QAM and 64QAM constellation," *Signal, Image and Video Processing*, vol. 5, no. 1, pp. 29–37, 2011.
- [20] O. Shalvi and E. Weinstein, "New criteria for blind deconvolution of nonminimum phase systems (channels)," *IEEE Transactions on Information Theory*, vol. 36, no. 2, pp. 312–321, 1990.
- [21] M. Pinchas, *The Whole Story Behind Blind Adaptive Equalizers/Blind Deconvolution*, e-books Publications Department Bentham Science Publishers.
- [22] M. Pinchas and B. Z. Bobrovsky, "A maximum entropy approach for blind deconvolution," *Signal Processing*, vol. 86, no. 10, pp. 2913–2931, 2006.
- [23] M. Pinchas, "What are the analytical conditions for which a blind equalizer will loose the convergence state?" *Signal, Image and Video Processing*, vol. 6, no. 2, pp. 325–340, 2012.
- [24] M. Li and W. Zhao, "On bandlimitedness and lag-limitedness of fractional Gaussian noise," *Physica A*, vol. 392, no. 9, pp. 1955–1961, 2013.
- [25] M. R. Spiegel, *Mathematical Handbook of Formulas and Tables*, SCHAU'S Outline Series, McGRAW-HILL, New York, NY, USA, 1968.



## Research Article

# An ARMA Type Fuzzy Time Series Forecasting Method Based on Particle Swarm Optimization

Erol Egrioglu,<sup>1</sup> Ufuk Yolcu,<sup>2</sup> Cagdas Hakan Aladag,<sup>3</sup> and Cem Kocak<sup>4</sup>

<sup>1</sup> Department of Statistics, Ondokuz Mayıs University, 55139 Samsun, Turkey

<sup>2</sup> Department of Statistics, Ankara University, 06100 Ankara, Turkey

<sup>3</sup> Department of Statistics, Hacettepe University, 06100 Ankara, Turkey

<sup>4</sup> Medical High School, Hitit University, 19000 Çorum, Turkey

Correspondence should be addressed to Erol Egrioglu; [erole@omu.edu.tr](mailto:erole@omu.edu.tr)

Received 18 April 2013; Revised 21 June 2013; Accepted 22 June 2013

Academic Editor: Ming Li

Copyright © 2013 Erol Egrioglu et al. This is an open access article distributed under the Creative Commons Attribution License, which permits unrestricted use, distribution, and reproduction in any medium, provided the original work is properly cited.

In the literature, fuzzy time series forecasting models generally include fuzzy lagged variables. Thus, these fuzzy time series models have only autoregressive structure. Using such fuzzy time series models can cause modeling error and bad forecasting performance like in conventional time series analysis. To overcome these problems, a new first-order fuzzy time series which forecasting approach including both autoregressive and moving average structures is proposed in this study. Also, the proposed model is a time invariant model and based on particle swarm optimization heuristic. To show the applicability of the proposed approach, some methods were applied to five time series which were also forecasted using the proposed method. Then, the obtained results were compared to those obtained from other methods available in the literature. It was observed that the most accurate forecast was obtained when the proposed approach was employed.

## 1. Introduction

Fuzzy time series firstly proposed by Song and Chissom [1] can be divided into two subclasses time variant and time invariant. Fuzzy time series method generally embodies three stages such as fuzzification, determination of fuzzy relations, and defuzzification stages. In the fuzzification stage, observations of time series are fuzzified. Fuzzy relations between the observations are defined in the stage of determination of fuzzy relations. Finally, the calculated fuzzy forecasts are defuzzified in the defuzzification phase. If one or more of these stages can be improved, the performance of the method will increase. Therefore, new fuzzy time series approaches have been proposed by making contributions to these stages in the literature.

In the literature, various methods have been proposed to fuzzify observations. While fixed interval lengths are used in Song and Chissom [1–3], Chen [4], Huarng [5], Chen [6], Tsaur et al. [7], Singh [8], and Egrioglu et al. [9, 10], dynamic length of interval lengths is employed in Huarng and Yu [11], Davari et al. [12], Yolcu et al. [13], Kuo et al. [14, 15], Park et al.

[16], Hsu et al. [17], and Huang et al. [18] in order to partition the universe of discourse. Also, Cheng et al. [19], Li et al. [20], Egrioglu et al. [21], Chen and Tanuwijaya [22], and Bang and Lee [23] used some methods based on clustering algorithms.

Song and Chissom [3] exploited feed forward neural networks to defuzzify fuzzy forecasts. Chen [4], Huarng [5], and Huarng and Yu [11] utilized centroid method in the defuzzification stage. Besides, Cheng et al. [24] and Aladag et al. [25] used a different technique based on adaptive expectation and centroid methods for fuzzification.

Establishing fuzzy relations plays important role in the forecasting performance of the method. In this phase, Song and Chissom [1] utilized fuzzy relationship matrix, and Sullivan and Woodall [26] used transition matrices based on Markov chain instead of fuzzy relationship matrix. Chen [4] suggested an approach in which fuzzy logic group relationship tables are employed to define fuzzy relations, and Cheng et al. [24], Huarng [5], Huarng and Yu [11], Yu [27], and Egrioglu et al. [21] also used fuzzy logic group relationship tables. Huarng and Yu [28] and Aladag et al. [29] preferred to utilize feed forward artificial neural networks in this stage.

Aladag et al. [30] used a different type of artificial neural networks which is Elman recurrent neural networks. In the determination of fuzzy relations, Yu and Huarng [31] and Yolcu et al. [32] proposed different approaches in which feed forward artificial neural networks using membership values are used. Eğrioglu [33] utilized genetic algorithms to define fuzzy relations. Moreover, many soft computing techniques have been used for forecasting in the literature. Yang et al. [34], and Yang et al. [35], and Yang et al. [36] are some of them.

In all of the studies mentioned previously, fuzzy time series forecasting models have autoregressive (AR) structure. However, many real life fuzzy time series can contain both autoregressive and moving average (MA) structures. Using forecasting models that have only AR structure for these time series can produce insufficient results. To analyze such time series, it is needed to use an ARMA type fuzzy time series forecasting model that includes both AR and MA structures. In this study, a novel fuzzy time series forecasting approach based on ARMA type fuzzy time series forecasting model is proposed to increase forecasting accuracy. Some fuzzy time series approaches in which fuzzy logic group relationship tables are employed disregard the fuzzy set theory since fuzzy sets' elements whose membership value is 1 are only taken into account in the fuzzification phase. Therefore, information loss occurs, and it is expected to decrease the explanation power of the model. In order to overcome these problems, the particle swarm optimization method is employed in the proposed approach to establish fuzzy relations. In addition, the computational cost of the proposed approach is very reasonable since it does not need to perform complex matrix operations when the particle swarm optimization method is used. Another advantage of the proposed method is that it uses the fuzzy  $c$ -means clustering method in the fuzzification phase. In the fuzzification phase of the fuzzy time series approach, there are some common problems such as the decision of the number of intervals, arbitrary determination of interval length, and arbitrary choice of degrees of membership. Since the fuzzy  $c$ -means clustering technique is employed in the proposed approach, it works in a systematic way.

In the real life, some time series have long-range dependence. Long-range-dependent time series is forecasted by using special linear models. ARFIMA models, which are used to forecast long-range-dependent time series, were firstly introduced by Granger and Joyeux [37]. General properties of ARFIMA models were given by Hosking [38, 39] and Beran [40]. First studies are concerned with estimation of fractional differencing parameter in fractional white noise processes.  $R/S$  statistic was proposed in Hurst [41]. Eğrioglu and Gunay [42], and Li [43], Li and Zhao [44] are important papers about fractional processes. In this study, time series are examined by using  $R/S$  hypothesis test to determine long-range dependence in the application. The performance of proposed method is examined according to long-range dependence.

The next section presents basic definitions of fuzzy time series and fuzzy- $c$  means clustering method. In Section 3, the modified particle swarm optimization algorithm is given.

Section 4 introduces the proposed approach based on ARMA type fuzzy time series forecasting model and particle swarm optimization. The implementation is given in Section 5. Finally, the last section concludes the paper.

## 2. Fuzzy Time Series Basic Definitions and Fuzzy C-Means Clustering

The fuzzy time series was firstly introduced by Song and Chissom [1]. The fundamental definitions of fuzzy time series, time variant, and time invariant fuzzy time series definitions are presented in what follows.

*Definition 1.* Let  $Y(t)$  ( $t = \dots, 0, 1, 2, \dots$ ), a subset of real numbers, be the universe of discourse on which fuzzy sets  $f_j(t)$  are defined. If  $F(t)$  is a collection of  $f_1(t), f_2(t), \dots$ , then  $F(t)$  is called a fuzzy time series defined on  $Y(t)$ .

*Definition 2.* Suppose that  $F(t)$  is caused by  $F(t-1)$  only; that is,  $F(t-1) \rightarrow F(t)$ . Then, this relation can be expressed as  $F(t) = F(t-1) \circ R(t, t-1)$ , where  $R(t, t-1)$  is the fuzzy relationship between  $F(t-1)$  and  $F(t)$  and  $F(t) = F(t-1) \circ R(t, t-1)$  is called the first-order model of  $F(t)$ . " $\circ$ " represents max-min composition of fuzzy sets.

*Definition 3.* Suppose that  $R(t, t-1)$  is a first-order model of  $F(t)$ . If for any  $t$ ,  $R(t, t-1)$  is independent of  $t$ ; that is, for any  $t$ ,  $R(t, t-1) = R(t-1, t-2)$ ; then  $F(t)$  is called a time invariant fuzzy time series; otherwise, it is called a time variant fuzzy time series.

Song and Chissom [2] firstly introduced an algorithm based on the first-order model for forecasting time invariant  $F(t)$ . In Song and Chissom [2], the fuzzy relationship matrix  $R(t, t-1) = R$  is obtained by many matrix operations. The fuzzy forecasts are obtained based on max-min composition as in what follows:

$$F(t) = F(t-1) \circ R. \quad (1)$$

The dimension of  $R$  matrix depends on the number of fuzzy sets. The number of fuzzy sets equals the number of intervals that is composed of universe of discourse. The more fuzzy sets are used, the more matrix operations are needed to obtain  $R$  matrix. When the number of fuzzy set is high, using the method proposed by Song and Chissom [2] considerably increases the computational cost.

For fuzzification, partition of universe of discourse method is used in the method proposed by Song and Chissom [1]. However, there are several problems related to the decomposition of universe of discourse. These problems are the determination of the number of intervals, arbitrarily choice of interval length, and membership degrees. In order to deal with these problems, Cheng et al. [19] and Li et al. [20] used fuzzy  $c$ -means clustering method for fuzzification. The fuzzy  $c$ -means clustering method was firstly introduced by Bezdek [45]. This clustering method is the most widely used one. In this method, fuzzy clustering is conducted by minimizing the least squared errors within groups. Let  $u_{ij}$  be the membership values,  $v_i$  the center of cluster,  $n$  the number

of variables, and  $c$  the number of clusters. Then, the objective function, which is minimized in fuzzy clustering, is

$$J_\beta(X, V, U) = \sum_{i=1}^c \sum_{j=1}^n u_{ij}^\beta d^2(x_j, v_i), \quad (2)$$

where  $\beta$  is a constant ( $\beta > 1$ ) and called the fuzzy index.  $d(x_j, v_i)$  is a similarity measure between an observation and the center of corresponding fuzzy cluster. The objective function  $J_\beta$  is minimized subject to constraints given in what follows:

$$\begin{aligned} 0 &\leq u_{ij} \leq 1, \quad \forall i, j, \\ 0 &< \sum_{j=1}^n u_{ij} \leq n, \quad \forall i, \\ \sum_{i=1}^c u_{ij} &= 1, \quad \forall j. \end{aligned} \quad (3)$$

In fuzzy  $c$ -means clustering method, to solve the minimization problem given previously, an iterative algorithm is used. In each iteration, the values of  $v_i$  and  $u_{ij}$  are updated by using the formulas given in (4) and (5), respectively:

$$v_i = \frac{\sum_{j=1}^n u_{ij}^\beta x_j}{\sum_{j=1}^n u_{ij}^\beta}, \quad (4)$$

$$u_{ij} = \frac{1}{\sum_{k=1}^c (d(x_j, v_i) / d(x_j, v_k))^{2/(\beta-1)}}. \quad (5)$$

### 3. The Particle Swarm Optimization

Particle swarm optimization, which is a population-based heuristic algorithm, was firstly proposed by Kennedy and Eberhart [46]. Distinguishing feature of this heuristic algorithm is that it simultaneously examines different points in different regions of the solution space to find the global optimum solution. Local optimum traps can be avoided because of this feature.

In a few fuzzy time series studies, particle swarm optimization method has been exploited in fuzzification phase. While the particle swarm optimization method was employed by Davari et al. [12] for fuzzification in the first-order fuzzy time series forecasting model, Kuo et al. [14] utilized the method in high-order models. In the fuzzification phase, Kuo et al. [15] utilized the particle swarm optimization method in both the first- and the high-order models. Park et al. [16] used the same method for fuzzification in a two-factor high-order model. However, the particle swarm optimization method has never been used to establish fuzzy logic relations in the literature. In time variant fuzzy time series forecasting method proposed in this study, the modified particle swarm optimization whose algorithm is given later is exploited. The modified particle swarm optimization algorithm has time varying inertia weight like in Shi and Eberhart [47]. In a similar way, this algorithm also has time varying acceleration coefficient like in Ma et al. [48].

*Algorithm 4.* The algorithm of the modified particle swarm optimization.

*Step 1.* Positions of each  $k$ th ( $k = 1, 2, \dots, pn$ ) particles' positions are randomly determined and kept in a vector  $X_k$  given as follows:

$$X_k = \{x_{k,1}, x_{k,2}, \dots, x_{k,d}\}, \quad k = 1, 2, \dots, pn, \quad (6)$$

where  $x_i^k$  ( $i = 1, 2, \dots, d$ ) represents  $i$ th position of  $k$ th particle.  $pn$  and  $d$  represent the number of particles in a swarm and positions, respectively.

*Step 2.* Velocities are randomly determined and stored in a vector  $V_k$  given in what follows:

$$V_k = \{v_{k,1}, v_{k,2}, \dots, v_{k,d}\}, \quad k = 1, 2, \dots, pn. \quad (7)$$

*Step 3.* According to the evaluation function,  $Pbest$  and  $Gbest$  particles given in (8) and (9), respectively, are determined:

$$Pbest_k = (p_{k,1}, p_{k,2}, \dots, p_{k,d}), \quad k = 1, 2, \dots, pn, \quad (8)$$

$$Gbest = (p_{g,1}, p_{g,2}, \dots, p_{g,d}), \quad (9)$$

where  $Pbest_k$  is a vector that stores the positions corresponding to the  $k$ th particle's best individual performance and  $Gbest$  represents the best particle, which has the best evaluation function value, found so far.

*Step 4.* Let  $c_1$  and  $c_2$  represent cognitive and social coefficients, respectively, and  $w$  is the inertia parameter. Let  $(c_{1i}, c_{1f})$ ,  $(c_{2i}, c_{2f})$ , and  $(w_1, w_2)$  be the intervals which include possible values for  $c_1$ ,  $c_2$ , and  $w$ , respectively. At each iteration, these parameters are calculated by using the formulas given in (10):

$$\begin{aligned} c_1 &= (c_{1f} - c_{1i}) \frac{t}{\max t} + c_{1i}, \\ c_2 &= (c_{2f} - c_{2i}) \frac{t}{\max t} + c_{2i}, \\ w &= (w_2 - w_1) \frac{\max t - t}{\max t} + w_1, \end{aligned} \quad (10)$$

where  $\max t$  and  $t$  represent maximum iteration number and current iteration number, respectively.

*Step 5.* Values of velocities and positions are updated by using the formulas given in (11) and (12), respectively.

$$\begin{aligned} v_{i,d}^{t+1} &= [w \times v_{i,d}^t + c_1 \times \text{rand}_1 \times (p_{i,d} - x_{i,d}) \\ &\quad + c_2 \times \text{rand}_2 \times (p_{g,d} - x_{i,d})], \end{aligned} \quad (11)$$

$$x_{i,d}^{t+1} = x_{i,d}^t + v_{i,d}^{t+1}, \quad (12)$$

where  $\text{rand}_1$  and  $\text{rand}_2$  are random values from the interval  $[0, 1]$ .

*Step 6.* Steps 3 to 5 are repeated until a predetermined maximum iteration number ( $\max t$ ) is reached.

We would like to note that the aim of this study is not to propose a new particle swarm optimization algorithm. In the literature, it was shown that using some time varying parameters can increase the convergence speed of the algorithm (Shi and Eberhart [47]; Ma et al. [48]). Therefore, we just used both the time varying acceleration coefficient (Ma et al. [48]) and the time varying inertia weight (Shi and Eberhart [47]) in the standard particle swarm optimization as mentioned previously. Then, this modified particle swarm optimization method was utilized to calculate membership values in the fuzzy relationship matrix as addressed in the next section. It is not claimed in the paper that a better particle swarm optimization algorithm was improved.

#### 4. The Proposed Approach

The fuzzy time series forecasting methods in the literature have only AR structure that includes lagged fuzzy variables. On the other hand, it will be wiser to use a model which includes both AR and MA structures in order to forecast real life time series that contain both structures. In the literature, we firstly define a new model which includes both AR and MA terms in Definition 5.

**Definition 5.** Let fuzzy time series  $F(t)$  be caused by lagged fuzzy time series  $F(t-1)$  and lagged absolute fuzzy error series  $\varepsilon(t-1)$ ; then the relationship can be expressed as

$$F(t-1), \quad \varepsilon(t-1) \longrightarrow F(t). \quad (13)$$

This model given in (13) is called an ARMA(1,1) fuzzy time series forecasting model. Thus, definition of fuzzy relations for this model is presented in Definition 6.

**Definition 6.** Suppose that  $F(t)$  is caused by only  $F(t-1)$  and  $\varepsilon(t-1)$ ; that is,  $F(t-1), \varepsilon(t-1) \rightarrow F(t)$ . Then, this relation can be expressed as

$$F(t) = (F(t-1) \circ R_1(t, t-1)) \cap (\varepsilon(t-1) \circ R_2(t, t-1)), \quad (14)$$

where  $R_1(t, t-1)$  ( $R_1 = [r_{ij1}]$ ,  $i = 1, 2, \dots, c$ ,  $j = 1, 2, \dots, c$ ) is the fuzzy relationship matrix between  $F(t-1)$  and  $F(t)$  and  $R_2(t, t-1)$  ( $R_2 = [r_{ij2}]$ ,  $i = 1, 2, \dots, c$ ,  $j = 1, 2, \dots, c$ ) is the fuzzy relationship matrix between  $\varepsilon(t-1)$  and  $F(t)$ .

In this study, a new fuzzy time series forecasting approach is suggested to forecast ARMA(1,1) fuzzy time series forecasting model in (13). The proposed approach provides some advantages which can be given as follows.

- (i) Since the model given in (13) is employed in the proposed approach, it is more proper to use this method for forecasting real life time series that contain both AR and MA structures.
- (ii) Since fuzzy  $c$ -means clustering method is utilized for fuzzification in the proposed approach, the number of intervals, the interval length, and the degrees of memberships is not arbitrarily determined in the fuzzification phase, so the proposed approach is a systematic method.

- (iii) The methods in the literature that exploit fuzzy logic group relationship tables disregard the fuzzy set theory since only some elements of fuzzy sets are taken into account in the fuzzification phase. Thus, information loss occurs and it is expected to decrease the explanation power of the model. However, in the proposed method, particle swarm optimization method is used to calculate membership values in the fuzzy relationship matrix, so information loss and decrease in explanatory power of the model are prevented.
- (iv) In the proposed method, instead of using centroid method, a method which considers all membership degrees is employed. Therefore, information loss that occurs in the defuzzification stage is avoided.
- (v) Since the proposed approach provides the advantages given previously, it is expected that the suggested method has high forecasting accuracy.

The algorithm of the proposed method is given later step by step.

**Algorithm 7.** The proposed method's algorithm.

**Step 1.** Fuzzify time series by using the fuzzy  $c$ -means clustering, and define fuzzy sets for absolute values of errors.

Let  $c$  be the number of fuzzy set, such that  $2 \leq c \leq n$ . The fuzzy  $c$ -means clustering algorithm in which the number of fuzzy sets is  $c$  is applied to the time series which consists of crisp values. After this application, the center of each fuzzy set is determined. Then, the degrees for each observation, which denote a degree of belonging to a fuzzy set for that observation, are calculated with respect to the obtained values of center of fuzzy sets. Finally, ordered fuzzy sets,  $L_r$  ( $r = 1, 2, \dots, c$ ), are obtained according to the ascending ordered centers, which are denoted by  $v_r$  ( $r = 1, 2, \dots, c$ ).

Fuzzy sets for absolute values of errors are defined in accordance with predetermined length of interval. Subintervals that contain absolute values of errors are generated. The number of clusters is taken as  $c$  which equals the number of cluster of time series. Thus, the number of subintervals is  $c$ . The upper bound of the last subinterval is always open. While the first subinterval has the minimum absolute error, the subsequent subintervals have comparatively greater absolute errors. Generally, subintervals can be defined by

$$u_1 = [0, la], \quad (15)$$

$$u_2 = [la, 2 \times la], \dots, u_c = [(c-1) \times la, \infty],$$

where  $la$  represents the length of interval. In accordance with these subintervals, fuzzy sets for absolute errors are defined as follows:

$$\begin{aligned} A_1 &= \frac{1}{u_1} + \frac{0.5}{u_2}, & A_2 &= \frac{0.5}{u_1} + \frac{1}{u_2} + \frac{0.5}{u_3}, \\ A_{c-1} &= \frac{0.5}{u_{c-2}} + \frac{1}{u_{c-1}} + \frac{0.5}{u_c}, & A_c &= \frac{0.5}{u_{c-1}} + \frac{1}{u_c}. \end{aligned} \quad (16)$$



TABLE 1: An example time series  $X_t$ .

Date	$X_t$	Membership values				
		$v_1 = 13000$	$v_2 = 13500$	$v_3 = 14000$	$v_4 = 14500$	$v_5 = 15000$
1971	13055	0.7	0.2	0.1	0	0
1972	13563	0.2	0.7	0.1	0	0
1973	13867	0.1	0.4	0.5	0	0

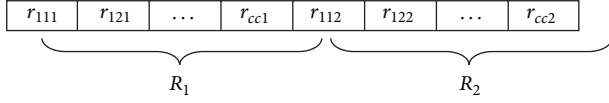


FIGURE 1: The structure of a particle.

**Step 2.** Determine the parameters of particle swarm optimization.

Some parameters of particle swarm optimization are possible intervals for social coefficient ( $c_{1i}, c_{1f}$ ), cognitive coefficient ( $c_{2i}, c_{2f}$ ), and inertia weight ( $w_1, w_2$ ). The other parameters are swarm size ( $pn$ ) and maximum iteration number ( $\max t$ ). Evaluation function is RMSE criterion which is computing as in what follows:

$$\text{RMSE} = \sqrt{\frac{\sum_{t=1}^n (x_t - \hat{x}_t)^2}{n}}, \quad (17)$$

where  $x_t$  is crisp time series,  $\hat{x}_t$  is defuzzified forecasts, and  $n$  is the number of forecasts.

**Step 3.** Generate a random initial population.

Elements of each particle are elements of  $R_1$  and  $R_2$  fuzzy relation matrices given in Definition 6. Since both  $R_1$  and  $R_2$  matrices consist of  $c^2$  elements ( $R_k = [r_{ijk}]$ ,  $i = 1, 2, \dots, c$ ,  $j = 1, 2, \dots, c$ ,  $k = 1, 2$ ), the number of elements in a particle equals to  $2c^2$ . For the number of fuzzy sets  $c$ , representation of a particle is illustrated in Figure 1.

In this step,  $r_{ij}$  ( $i, j = 1, 2, \dots, c$ ) values of all particles are randomly generated from the interval  $[0, 1]$  to generate a random initial population.

**Step 4.** Calculate the evaluation function values of all particles in the current swarm.

The method for calculating RMSE for any particle is given in Steps 4.1, 4.2, and 4.3.

**Step 4.1.**  $R_1$  and  $R_2$  fuzzy relation matrices are designed from positions of particles. Each  $c$  position sets are the rows of  $R_1$  and  $R_2$  matrices.

**Step 4.2.** Fuzzy forecasts are calculated by using (14). After  $R_1$  and  $R_2$  relation matrices are estimated, fuzzy forecasts can be obtained by using fuzzy errors and fuzzy observations. When the first forecast is calculated, it is assumed that the error equals to zero since this assumption is also valid in conventional time series analysis.

For instance, some observations of a time series  $X_t$ , corresponding membership values of these observations, and the center values ( $v_i$ ,  $i = 1, 2, 3, 4, 5$ ) for each fuzzy set are given in Table 1.

Let the relations matrices be as follows:

$$R_1 = \begin{bmatrix} 1 & 0.5 & 0 & 0 & 0 \\ 0 & 0 & 1 & 0 & 0 \\ 0 & 0 & 0 & 0.5 & 0 \\ 0 & 0 & 0 & 0 & 0 \\ 1 & 0 & 0 & 0 & 0 \end{bmatrix}, \quad R_2 = \begin{bmatrix} 1 & 0.5 & 0 & 0 & 0 \\ 0.5 & 0 & 1 & 0 & 0 \\ 0.3 & 0 & 0 & 0.05 & 0 \\ 0 & 0 & 0 & 0 & 0 \\ 1 & 0 & 0 & 0 & 0 \end{bmatrix}. \quad (18)$$

Thus, fuzzy forecast for 1972 can be calculated as follows:

$$\begin{aligned} \hat{F}(1972) &= F(1971) \circ R_1 \cap \varepsilon(1971) \circ R_2 \\ &= [0.7 \ 0.5 \ 0.2 \ 0 \ 0] \\ &= [0.7 \ 0.2 \ 0.1 \ 0 \ 0] \circ \begin{bmatrix} 1 & 0.5 & 0 & 0 & 0 \\ 0 & 0 & 1 & 0 & 0 \\ 0 & 0 & 0 & 0.5 & 0 \\ 0 & 0 & 0 & 0 & 0 \\ 1 & 0 & 0 & 0 & 0 \end{bmatrix} \\ &\quad \cap [1 \ 0.5 \ 0 \ 0 \ 0] \circ \begin{bmatrix} 1 & 0.5 & 0 & 0 & 0 \\ 0.5 & 0 & 1 & 0 & 0 \\ 0.3 & 0 & 0 & 0.05 & 0 \\ 0 & 0 & 0 & 0 & 0 \\ 1 & 0 & 0 & 0 & 0 \end{bmatrix}. \end{aligned} \quad (19)$$

After this procedure, fuzzy forecasts are defuzzified by using the rules given in what follows.

- (i) If the memberships of fuzzy forecast have only one maximum, then select the center of this cluster as the defuzzified forecasted value.
- (ii) If memberships of fuzzy forecast have two or more consecutive maximums, then select arithmetic mean of centers of corresponding clusters as the defuzzified forecasted value.
- (iii) Otherwise, standardize the fuzzy output, and use the center of the fuzzy sets as the forecasted value.

For example, defuzzified forecast for 1972 can be calculated as follows. Since the memberships of fuzzy forecast have only one maximum, defuzzified forecast value is taken as the center value ( $v_1 = 13000$ ) of the first fuzzy set which has the maximum membership value. This can be expressed by

$$\hat{X}_{1972} = \text{Def}(\hat{F}(1972)) = 13000. \quad (20)$$



Then, absolute error value for 1972 is calculated given as follows:

$$E_{1972} = |X_{1972} - \hat{X}_{1972}| = |13055 - 13000| = 55. \quad (21)$$

Absolute error value is fuzzified by using corresponding fuzzy set which has the maximum membership value for the interval which includes this absolute error value. For instance, for the time series given in Table 1, when the interval length of absolute error is taken as 50, 5 subintervals are as follows:

$$\begin{aligned} u_1 &= [0, 50], & u_2 &= [50, 100], & u_3 &= [100, 150], \\ u_4 &= [150, 200], & u_5 &= [200, \infty). \end{aligned} \quad (22)$$

Since the absolute error value 55 is in the second interval  $u_2$ , defuzzified absolute error is  $A_2$ . Thus, for 1972, the absolute error is obtained given as follows:

$$\varepsilon(1972) = [0.5 \ 1 \ 0.5 \ 0 \ 0]. \quad (23)$$

Then, the forecast for 1973 can be calculated as follows:

$$\hat{F}(1973) = F(1972) \circ R_1 \cap \varepsilon(1972) \circ R_2. \quad (24)$$

In the same way, other forecasts for other years can be obtained.

*Step 4.3.* RMSE is computed using the formula given in (17).

*Step 5.* Update cognitive coefficient  $c_1$ , social coefficient  $c_2$ , and inertia parameter  $w$  at each iteration by using formulas in (10).

*Step 6.* New positions of the particles are calculated by using the formulas given in (11) and (12).

*Step 7.* Repeat Steps 4 to 7 until maximum iteration bound ( $\max t$ ) is reached.

## 5. Application of the Proposed Method

Firstly, the proposed method was applied to Alabama University enrollment data (1971–1992) that is well-known data in the literature. The enrollment data is presented in Table 2.

The algorithm of the proposed method was coded in MATLAB 7.9 version. In the application of the proposed method, we used seven fuzzy sets ( $c = 7$ ) in Step 1 since the same number has been employed in other studies available in the literature (Cheng et al., 2008). The centers of clusters and the membership values which are obtained from FCM algorithm in Step 1 are given in Tables 3 and 4, respectively. In the fuzzification process of the absolute error, if the interval length is too small, aggregation will arise in the last fuzzy set. If it is too big, aggregation will occur in the first fuzzy set. Therefore, the length of interval for absolute error is picked

TABLE 2: The enrollment data.

Years	Actual	Years	Actual
1971	13055	1982	15433
1972	13563	1983	15497
1973	13867	1984	15145
1974	14696	1985	15163
1975	15460	1986	15984
1976	15311	1987	16859
1977	15603	1988	18150
1978	15861	1989	18970
1979	16807	1990	19328
1980	16919	1991	19337
1981	16388	1992	18876

TABLE 3: The centers of clusters obtained from FCM algorithm in Step 1.

$v_1$	$v_2$	$v_3$	$v_4$	$v_5$	$v_6$	$v_7$
13458.81	14700.56	15379.31	15904.31	16412.94	16889.11	19075.31

as 300. Then, 7 fuzzy sets for absolute errors can be defined as follows:

$$\begin{aligned} u_1 &= [0, 300], & u_2 &= [300, 600], & u_3 &= [600, 900], \\ u_4 &= [900, 1200], & u_5 &= [1200, 1500], \\ u_6 &= [1500, 1800], & u_7 &= [1800, \infty). \end{aligned} \quad (25)$$

In the literature, there are no general rules to determine parameter values of particle swarm optimization. Parameter values for this method have been generally specified intuitively due to the data in most of the applications. Therefore, the parameters of particle swarm optimization used in this study were intuitively determined like in other studies available in the literature (Ma et al., 2006). The parameters of the modified particle swarm optimization are determined according to trial and error method. The different values of the parameters were employed. The best parameters of the modified particle swarm optimization are determined as follows:  $(c_{1i}, c_{1f}) = (2, 3)$ ,  $(c_{2i}, c_{2f}) = (2, 3)$ ,  $(w_1, w_1) = (1, 2)$ ,  $pn = 30$ , and  $\max t = 200$ . The optimal  $R_1$  and  $R_2$  matrices obtained from our methods are given later. The fuzzy and defuzzified forecasts of the proposed method are given in Table 5:

$$R_1 = \begin{bmatrix} 1.0000 & 0.0000 & 1.0000 & 0.0000 & 1.0000 & 0.0000 & 0.4540 \\ 0.0000 & 0.7525 & 0.0000 & 0.0458 & 0.0000 & 0.0000 & 0.0000 \\ 0.3374 & 1.0000 & 1.0000 & 1.0000 & 1.0000 & 0.7000 & 1.0000 \\ 1.0000 & 0.0000 & 1.0000 & 1.0000 & 0.8283 & 0.0000 & 0.0000 \\ 0.4271 & 0.0000 & 1.0000 & 0.3627 & 0.0000 & 0.0000 & 1.0000 \\ 0.0000 & 1.0000 & 1.0000 & 1.0000 & 0.1443 & 1.0000 & 0.4579 \\ 0.0000 & 0.0000 & 1.0000 & 0.0000 & 1.0000 & 0.4002 & 0.0000 \end{bmatrix}, \quad (26)$$

TABLE 4: The memberships of the observations obtained from FCM algorithm in Step 1.

Years	Cluster 1	Cluster 2	Cluster 3	Cluster 4	Cluster 5	Cluster 6	Cluster 7
1971	0.8768	0.0528	0.0265	0.0176	0.0127	0.0097	0.0039
1972	0.9839	0.0083	0.0032	0.0019	0.0013	0.0010	0.0004
1973	0.7128	0.1709	0.0519	0.0286	0.0183	0.0130	0.0044
1974	0.0000	0.9999	0.0000	0.0000	0.0000	0.0000	0.0000
1975	0.0015	0.0107	0.9463	0.0312	0.0068	0.0030	0.0005
1976	0.0013	0.0121	0.9679	0.0128	0.0037	0.0018	0.0003
1977	0.0063	0.0354	0.5767	0.3178	0.0440	0.0174	0.0024
1978	0.0003	0.0014	0.0079	0.9824	0.0060	0.0017	0.0002
1979	0.0006	0.0014	0.0031	0.0078	0.0410	0.9448	0.0012
1980	0.0001	0.0002	0.0004	0.0009	0.0035	0.9948	0.0002
1981	0.0001	0.0002	0.0006	0.0026	0.9939	0.0025	0.0001
1982	0.0007	0.0052	0.9769	0.0127	0.0029	0.0013	0.0002
1983	0.0029	0.0193	0.8823	0.0737	0.0146	0.0063	0.0010
1984	0.0133	0.1919	0.6905	0.0658	0.0236	0.0125	0.0025
1985	0.0118	0.1599	0.7306	0.0622	0.0219	0.0115	0.0022
1986	0.0009	0.0036	0.0163	0.9388	0.0324	0.0073	0.0006
1987	0.0001	0.0002	0.0004	0.0010	0.0045	0.9936	0.0002
1988	0.0176	0.0325	0.0504	0.0767	0.1281	0.2432	0.4516
1989	0.0004	0.0006	0.0009	0.0012	0.0017	0.0025	0.9928
1990	0.0018	0.0029	0.0040	0.0053	0.0073	0.0104	0.9684
1991	0.0019	0.0031	0.0042	0.0056	0.0077	0.0110	0.9664
1992	0.0013	0.0022	0.0032	0.0044	0.0064	0.0098	0.9728

TABLE 5: The forecasts produced by the proposed methods.

Years	Fuzzy forecasts							Defuzzified forecasts
1972	0.8768	0.5000	0.1475	0.0458	0.5824	0.0000	0.4540	13458.81
1973	0.9839	0.5000	0.1475	0.0458	0.5824	0.0000	0.4540	13458.81
1974	0.5000	0.7128	0.1709	0.1709	0.5000	0.5000	0.5000	14700.56
1975	0.9999	0.2359	0.9999	0.0458	0.4169	0.0000	0.4540	15395.91
1976	0.7084	0.3526	0.9463	0.0458	0.0312	0.0000	0.4540	15379.31
1977	0.7084	0.3526	0.9679	0.0458	0.0128	0.0000	0.4540	15379.31
1978	0.5767	0.3526	0.5767	0.0458	0.3178	0.0000	0.4540	15673.54
1979	0.5122	0.5000	0.7212	0.0079	0.9824	0.0000	0.4540	16412.94
1980	0.0078	0.0410	0.2108	0.0031	0.5000	0.0078	0.5000	17217.39
1981	0.0009	0.0035	0.2108	0.0004	0.9019	0.0000	0.4540	16412.94
1982	0.0026	0.5000	0.9939	0.0006	0.1144	0.0000	0.0026	15379.31
1983	0.7084	0.3526	0.9769	0.0458	0.0127	0.0000	0.4540	15379.31
1984	0.7084	0.3526	0.8823	0.0458	0.0737	0.0000	0.4540	15379.31
1985	0.6905	0.3526	0.6905	0.0458	0.1919	0.0000	0.4540	15517.4
1986	0.5000	0.3526	0.5000	0.5000	0.1599	0.5000	0.5000	15987.15
1987	0.5122	0.5000	0.7212	0.0163	0.9388	0.0000	0.4540	16412.94
1988	0.0010	0.0045	0.2108	0.0004	0.5000	0.0010	0.5000	17318.67
1989	0.3198	0.1281	0.2108	0.0504	0.2432	0.0767	0.4516	19075.31
1990	0.3198	0.0017	0.1446	0.0009	0.0025	0.0000	0.4540	19075.31
1991	0.3198	0.0073	0.1446	0.0040	0.0104	0.0000	0.4540	19075.31
1992	0.3198	0.0077	0.1446	0.0042	0.0110	0.0000	0.4540	19075.31

TABLE 6: The obtained results for the enrollment data.

Method	MSE
[2]	412499
[26]	386055
[4]	407507
[49] ( $w = 2$ )	333274
[49] (1998) ( $w = 3$ )	299634
[49] (1998) ( $w = 4$ )	321418
[7]	134923
[8]	133700
[19]	228918
[24]	192086
The proposed method	85089

$$R_2 = \begin{bmatrix} 1.0000 & 1.0000 & 0.1475 & 0.1273 & 0.5824 & 1.0000 & 1.0000 \\ 1.0000 & 0.2359 & 1.0000 & 0.6483 & 0.4169 & 0.2619 & 1.0000 \\ 0.7084 & 0.3526 & 1.0000 & 1.0000 & 0.0000 & 1.0000 & 1.0000 \\ 0.5122 & 1.0000 & 0.7212 & 0.0000 & 1.0000 & 1.0000 & 0.8676 \\ 0.0000 & 1.0000 & 1.0000 & 0.0000 & 0.1144 & 0.0000 & 0.0000 \\ 0.0000 & 0.0000 & 0.2108 & 0.0000 & 0.9019 & 0.0000 & 1.0000 \\ 0.3198 & 0.0000 & 0.1446 & 0.0000 & 0.0000 & 0.0000 & 0.6737 \end{bmatrix}. \quad (27)$$

The mean square error (MSE) value of the proposed method is given in Table 6. For comparison, the forecasting results of some other well-known fuzzy time series forecasting approaches are also presented in Table 6. When Table 6 was examined, it is seen that the proposed method gives the most accurate forecasts in terms of MSE criterion.

Secondly, to examine the forecasting performance of the proposed approach on test set, it was also applied to four different data sets. The first data set is index 100 in stocks and bonds exchange market of İstanbul (ISBEMI) whose daily observations are between May 20, 2008 and September 29, 2008. This data is called ISBEMI Set 1. The second data is index 100 in stocks and bonds exchange market of İstanbul (ISBEMI) whose daily observations are between October 3, 2008 and December 31, 2008. The second data is called ISBEMI Set 2. The third one is ISBEMI Set 3, and its daily observations are from October 01, 2009 to December 31 2009. ISBEMI Set 1, ISBEMI Set 2, and ISBEMI Set 3 have 95, 59, and 63 observations, respectively. For comparison, these time series were also forecasted using other well-known fuzzy time series method proposed by Song and Chissom [2], Chen [4], Chen [6], Huarng [5], Huarng and Yu [11], and Aladag et al. [29]. In the implementation, the last 15 of ISBEMI Set 1, 7 observations of ISBEMI Set 2, and 7 observations and 15 observations of ISBEMI Set 3 were used for test sets.

It is a well-known fact that there are no general rules to determine the parameters such as the length of interval or the number of fuzzy sets for some methods used in the implementation. Thus, related parameters were determined using trial and error method like in other studies available in the literature. To find the best length of interval for the methods introduced in [4], Chen [6], and Aladag et al. [29], the values between 200 and 2500 were examined with

increment 100. The interval lengths in the methods given in Huarng [5] and Huarng and Yu [11] were determined when the methods were progressing because of the nature of these methods. The number of fuzzy sets was experienced between 5 and 25 for the proposed approach and Song and Chissom [2]. When the methods proposed by Chen [5] and Aladag et al. [29] were employed, models order 2, 3, 4, and 5 were examined since time series have daily observations. Finally, the number of neurons in hidden layer was changed from 1 to 10 when the approach proposed by Aladag et al. [29] was applied. After practicing, the forecasts obtained from the case where we have got the best result for the test data and the error criteria related to those forecasts are presented in Tables 7 and 8 for ISBEMI Sets 1 and 2, respectively.

For Table 7, the cases in which the superlative results were obtained are

- (i) the number of the fuzzy sets was 12 for the Song-Chissom method [2];
- (ii) the interval length was 1200 for the Chen method [4];
- (iii) the interval length was 800 for the Huarng distribution-based method [5];
- (iv) the interval length was 200 for the Huarng average-based method [5];
- (v) the ratio sample percentile was 0.5 for the Huarng and Yu ratio-based method [11];
- (vi) the number of the fuzzy sets was five for the Cheng et al. method [19];
- (vii) the number of the fuzzy sets was 11 and the number of the neurons in the hidden layer was five for Yolcu et al. [32];
- (viii) the number of the fuzzy sets was 5 in the proposed method.

For Table 8, the cases in which the superlative results were obtained are

- (i) when the number of fuzzy sets is 12, for the method of Song and Chissom [2];
- (ii) when the length of interval is 1900 for the method of [4];
- (iii) when the length of interval is 2200 and the model order is 2 for the method of Chen [6];
- (iv) when the length of interval is 800 for the method of Huarng distribution based [5];
- (v) when the length of interval is 200 for the method of Huarng average based [5];
- (vi) when the ratio sample percentile is 0.5 for the method of Huarng and Yu ratio based [11];
- (vii) when the length of interval is 1000, the model order is 2, and number of neurons in hidden layer is 7 for the method proposed by Aladag et al. [29];
- (viii) when the number of fuzzy sets is 5 in the proposed method.

TABLE 7: The obtained results for ISBEMI Set 1.

Date	The test data	[2]	[4]	[5] distribution-based method	[5] average-based method	[11]	[32]	The proposed method
23.12.2008	26294	26410	26400	26200	26100	26091	26274	26 343
24.12.2008	26055	26410	26400	26200	26367	26091	26273	26 292
25.12.2008	26059	26410	26400	26200	26100	26091	26339	25 983
26.12.2008	26499	26410	26400	26200	26100	26091	26337	26 255
29.12.2008	26424	26410	26400	26200	26500	26608	26565	26 513
30.12.2008	26411	26410	26400	26200	26500	26608	26429	26 192
31.12.2008	26864	26410	26400	26200	26500	26091	26460	26 513
RMSE		261.0109	259.7625	310.4688	251.2390	354.7194	219.2734	207.91
MAPE		0.0075	0.0075	0.0096	0.0080	0.0098	0.0067	0.0067
DA		0.6667	0.6667	0.8333	0.5000	0.5000	0.6667	0.6667

TABLE 8: The obtained results for ISBEMI Set 2.

Date	The test data	[2]	[4]	[6]	[5] distribution-based method	[5] average-based method	[11]	[29]	The proposed method
09.09.2008	40124.6	39958.4	40550	39700	40000	39967	40547	40500	40457.3
10.09.2008	39295.0	40294.2	40550	37500	40000	39800	40126	39500	40457.3
11.09.2008	37388.1	39431.8	38650	37500	40000	39100	39603	39500	39335.3
12.09.2008	37033.9	37656.1	36750	37500	37200	37500	37602	38500	39335.3
15.09.2008	35081.4	37272.4	36750	37500	37200	37100	36955	37500	36339.1
16.09.2008	33736.4	35024.0	34850	35300	34533	34700	34881	35500	33234.8
17.09.2008	32727.6	33954.4	33900	33100	34400	33700	34037	33500	33234.8
18.09.2008	32216.4	33638.4	33900	33100	32400	32700	32266	32500	33234.8
19.09.2008	36370.2	37746.4	33900	35300	32400	32300	32221	35500	36339.1
22.09.2008	36183.6	36450.8	36750	35300	36800	37700	36711	35500	36339.1
23.09.2008	35454.2	36166.4	36750	35300	36800	36100	35225	35500	36339.1
24.09.2008	35177.1	35072.6	34850	35300	35600	35100	35634	35500	33234.8
25.09.2008	36361.8	35024.0	34850	35300	34533	34700	34881	35500	36339.1
26.09.2008	36556.6	36450.8	36750	35300	36800	37700	36711	37500	36339.1
29.09.2008	36051.3	36450.8	36750	37500	36800	35900	36711	35500	36339.1
RMSE		1155.3	1229.7	1143.6	1579.1	1483.0	1484.9	1145.9	1107.2
MAPE		0.0268	0.0299	0.0261	0.0327	0.0308	0.0298	0.0255	0.0233
DA		0.4286	0.5000	0.5714	0.4286	0.7143	0.4286	0.6429	0.5714

TABLE 9: The obtained results (last 7 observations are test set) for ISBEMI Set 3.

Date	The test data	[2]	[4]	[5] distribution-based method	[5] average-based method	[11]	[32]	The proposed method
23.12.2009	51162	51137	52150	51900	51573	51033	51317	51684
24.12.2009	51461	51137	50850	50700	50373	51033	51317	51109
25.12.2009	51661	51137	50850	50700	51240	51033	51317	51684
28.12.2009	51619	51137	52150	51900	51573	51033	51317	51684
29.12.2009	51786	51137	52150	51900	51573	51033	51317	51684
30.12.2009	51668	51137	52150	51900	51773	52004	51317	51684
31.12.2009	52825	51137	52150	51900	51573	51033	51317	51684
RMSE		771.0155	666.5039	659.9450	671.4803	830.4429	640.4131	494.5180
MAPE		0.0116	0.0123	0.0111	0.0097	0.0128	0.0090	0.0061
DA		0.3333	0.3333	0.3333	0.3333	0.1667	0.5000	0.6667

TABLE 10: The obtained results (last 15 observations are test set) for ISBEMI Set 3.

Date	The test data	[2]	[4]	[5] distribution-based method	[5] average-based method	[11]	[32]	The proposed method
11.12.2009	49386	49872	50250	49500	49100	49748	49516	49982.39
14.12.2009	50198	48606	48750	49500	49300	49316	50064	49982.39
15.12.2009	50450	49872	50250	49900	50500	50405	50942	50833.82
16.12.2009	50817	50294	50250	49900	48900	48886	50217	50833.82
17.12.2009	49963	50294	50250	50300	50900	48886	49641	50833.82
18.12.2009	50138	49872	50250	49900	49900	49748	49619	49613.83
21.12.2009	51281	49872	50250	49900	50500	50405	50932	51390.68
22.12.2009	51533	51137	51000	50300	50967	50625	50817	51390.68
23.12.2009	51162	51137	51000	51900	51500	51065	51100	51390.68
24.12.2009	51461	51137	51000	50300	50550	50625	50646	51390.68
25.12.2009	51661	51137	51000	50300	51500	51065	51073	51390.68
28.12.2009	51619	51137	51000	51900	51700	51065	51117	51390.68
29.12.2009	51786	51137	51000	51900	51700	51065	51114	51390.68
30.12.2009	51668	51137	51000	51900	51700	51963	51119	51390.68
31.12.2009	52825	51137	51000	51900	51700	51065	51117	51390.68
RMSE		810.8493	820.5748	815.9879	760.7710	917.1070	662.3497	522.0852
MAPE		0.0128	0.0133	0.0134	0.0110	0.0147	0.0106	0.0075
DA		0.2857	0.5000	0.2857	0.5000	0.3571	0.5000	0.6429

The best cases for the results given in Table 9 resulted when

- (i) Song-Chissom method [2] was applied with nine fuzzy sets;
- (ii) interval length was 1300 for the Chen method [4];
- (iii) interval length was 800 for the Huarng distribution-based method [5];
- (iv) interval length was 200 for the Huarng average-based method [5];
- (v) ratio sample percentile was 0.50 for the Huarng and Yu ratio-based method [11];
- (vi) the number of the fuzzy sets was 13 and the number of the neurons in the hidden layer was seven for Yolcu et al. [32];
- (vii) when the number of fuzzy sets is 5 in the proposed method.

The best cases for the results given in Table 10 resulted when

- (i) Song-Chissom [2] method was applied with nine fuzzy sets;
- (ii) interval length was 1500 for the Chen method [4];
- (iii) interval length was 800 for the Huarng distribution-based method [5];
- (iv) interval length was 200 for the Huarng average-based method [5];
- (v) ratio sample percentile was 0.50 for the Huarng and Yu ratio-based method [11];

(vi) the number of the fuzzy sets was seven and the number of the neurons in the hidden layer was three for Yolcu et al. [32];

(vii) the number of the fuzzy sets was five in the proposed method.

When Tables 6–10 are examined, it is obvious that the most accurate forecasts are obtained for all data sets when the proposed forecasting approach is used.

## 6. Conclusion and Discussion

In this study, an ARMA type fuzzy time series forecasting model is firstly introduced in the literature. In addition, to analyze this model, a novel approach based on fuzzy *c*-means and particle swarm optimization methods is suggested in this study. To show the forecasting performance of the proposed forecasting approach, the enrollments of Alabama University are applied to a well-known data and obtained forecasting results are compared to those produced by other fuzzy time series forecasting methods available in the literature. In addition, to evaluate the forecasting performance of the proposed forecasting approach on test set, two different time series are forecasted by utilizing the proposed method and other approaches available in the literature. As a result of the comparison, it is observed that the proposed approach gives the most accurate forecasts.

In the literature, the proposed method is the first method based on a fuzzy time series forecasting model which contains both AR and MA terms. In the linear stochastic ARMA models, the AR( $\infty$ ) model is equal to MA(1) model. But this result is only valid for linear ARMA models. There is no such



TABLE 11: Results of R/S test.

Data	R/S statistics	$P < 0.01$
ISBEMI Set 1	1.2966	No
ISBEMI Set 2	1.5937	No
ISBEMI Set 3	1.6523	No
Enrollment data	1.0969	No

kind of result for fuzzy time series model, artificial neural network model, and nonlinear stochastic models. Because of this, adding MA terms to fuzzy time series forecasting model is really important. Also, in the proposed method, particle swarm optimization method is used to calculate membership values in the fuzzy relationship matrix, so information loss and decrease in explanatory power of the model are prevented. Besides, since fuzzy  $c$ -means clustering method is employed in the fuzzification process, the number of intervals, the interval length, and the degrees of memberships are not arbitrarily determined, so the proposed approach works in a systematic way. In addition, information loss which occurs in the defuzzification stage is avoided by using a method which takes all membership degrees into account instead of using centroid method. Therefore, the proposed method has high forecasting accuracy.

Moreover, long-range dependence was determined for all time series by using R/S tests, and results are given in the appendix. All of the time series are short-range dependent. In the future studies, the performance of the proposed method will be able to research for long-range time series. But in the proposed fuzzy time series method, any linear model was not used. Fuzzy time series methods can be used to forecast nonlinear time series. In the fuzzy time series methods, the relations are employed instead of functions.

The proposed forecasting approach is suggested to forecast a first-order model including both AR and MA terms. In future studies, high-order models can be defined. Then, it is possible to extend the proposed approach to forecast high order models.

## Appendix

R/S test was applied to five time series to determine long-range dependence. The test results are given in Table 11. As a result of hypotheses tests, all data sets are short-range dependent. The tests were applied in S-PLUS package program.

## Acknowledgments

The authors would like to thank the reviewers for their helpful comments and opinions. This work was supported by "The Scientific and Technological Research Council of Turkey (TUBITAK)," Turkey, under Project no. 210T150.

## References

- [1] Q. Song and B. S. Chissom, "Fuzzy time series and its models," *Fuzzy Sets and Systems*, vol. 54, no. 3, pp. 269–277, 1993.

- [2] Q. Song and B. S. Chissom, "Forecasting enrollments with fuzzy time series—part I," *Fuzzy Sets and Systems*, vol. 54, pp. 1–10, 1993.
- [3] Q. Song and B. S. Chissom, "Forecasting enrollments with fuzzy time series—part II," *Fuzzy Sets and Systems*, vol. 62, no. 1, pp. 1–8, 1994.
- [4] S. M. Chen, "Forecasting enrollments based on fuzzy time series," *Fuzzy Sets and Systems*, vol. 81, no. 3, pp. 311–319, 1996.
- [5] K. Huarng, "Effective lengths of intervals to improve forecasting in fuzzy time series," *Fuzzy Sets and Systems*, vol. 123, no. 3, pp. 387–394, 2001.
- [6] S. Chen, "Forecasting enrollments based on high-order fuzzy time series," *Cybernetics and Systems*, vol. 33, no. 1, pp. 1–16, 2002.
- [7] R.-C. Tsaur, J. C. O. Yang, and H.-F. Wang, "Fuzzy relation analysis in fuzzy time series model," *Computers & Mathematics with Applications*, vol. 49, no. 4, pp. 539–548, 2005.
- [8] S. R. Singh, "A simple method of forecasting based on fuzzy time series," *Applied Mathematics and Computation*, vol. 186, no. 1, pp. 330–339, 2007.
- [9] E. Egrioglu, C. H. Aladag, U. Yolcu, V. R. Uslu, and M. A. Basaran, "Finding an optimal interval length in high order fuzzy time series," *Expert Systems with Applications*, vol. 37, no. 7, pp. 5052–5055, 2010.
- [10] E. Egrioglu, C. H. Aladag, M. A. Basaran, U. Yolcu, and V. R. Uslu, "A new approach based on the optimization of the length of intervals in fuzzy time series," *Journal of Intelligent and Fuzzy Systems*, vol. 22, no. 1, pp. 15–19, 2011.
- [11] K. Huarng and T. H. Yu, "Ratio-based lengths of intervals to improve fuzzy time series forecasting," *IEEE Transactions on Systems, Man, and Cybernetics B*, vol. 36, no. 2, pp. 328–340, 2006.
- [12] S. Davari, M. H. F. Zarandi, and I. B. Turksen, "An improved fuzzy time series forecasting model based on particle swarm intervalization," in *Proceedings of the Annual Meeting of the North American Fuzzy Information Processing Society (NAFIPS '09)*, Cincinnati, Ohio, USA, June 2009.
- [13] U. Yolcu, E. Egrioglu, V. R. Uslu, M. A. Basaran, and C. H. Aladag, "A new approach for determining the length of intervals for fuzzy time series," *Applied Soft Computing Journal*, vol. 9, no. 2, pp. 647–651, 2009.
- [14] I. H. Kuo, S. J. Horng, T. W. Kao, T. L. Lin, C. L. Lee, and Y. Pan, "An improved method for forecasting enrollments based on fuzzy time series and particle swarm optimization," *Expert Systems with Applications*, vol. 36, no. 3, pp. 6108–6117, 2009.
- [15] I. H. Kuo, S. J. Horng, Y. H. Chen et al., "Forecasting TAIEX based on fuzzy time series and particle swarm optimization," *Expert Systems with Applications*, vol. 37, no. 2, pp. 1494–1502, 2010.
- [16] J. Park, D. Lee, C. Song, and M. Chun, "TAIEX and KOSPI 200 forecasting based on two-factors high-order fuzzy time series and particle swarm optimization," *Expert Systems with Applications*, vol. 37, no. 2, pp. 959–967, 2010.
- [17] L. Hsu, S. Horng, T. Kao et al., "Temperature prediction and TAIEX forecasting based on fuzzy relationships and MTPSO techniques," *Expert Systems with Applications*, vol. 37, no. 4, pp. 2756–2770, 2010.
- [18] Y. Huang, S. Horng, T. Kao et al., "An improved forecasting model based on the weighted fuzzy relationship matrix combined with a PSO adaptation for enrollments," *International Journal of Innovative Computing, Information and Control*, vol. 7, no. 7A, pp. 4027–4046, 2011.

- [19] C. Cheng, G. Cheng, and J. Wang, "Multi-attribute fuzzy time series method based on fuzzy clustering," *Expert Systems with Applications*, vol. 34, no. 2, pp. 1235–1242, 2008.
- [20] S.-T. Li, Y.-C. Cheng, and S.-Y. Lin, "A FCM-based deterministic forecasting model for fuzzy time series," *Computers & Mathematics with Applications*, vol. 56, no. 12, pp. 3052–3063, 2008.
- [21] E. Egrioglu, C. H. Aladag, U. Yolcu, V. R. Uslu, and N. A. Erilli, "Fuzzy time series forecasting method based on Gustafson-Kessel fuzzy clustering," *Expert Systems with Applications*, vol. 38, no. 8, pp. 10355–10357, 2011.
- [22] S. Chen and K. Tanuwijaya, "Fuzzy forecasting based on high-order fuzzy logical relationships and automatic clustering techniques," *Expert Systems with Applications*, vol. 38, no. 12, pp. 15425–15437, 2011.
- [23] Y. Bang and C. Lee, "Fuzzy time series prediction using hierarchical clustering algorithms," *Expert Systems with Applications*, vol. 38, no. 4, pp. 4312–4325, 2011.
- [24] C. Cheng, T. Chen, H. J. Teoh, and C. Chiang, "Fuzzy time-series based on adaptive expectation model for TAIEX forecasting," *Expert Systems with Applications*, vol. 34, no. 2, pp. 1126–1132, 2008.
- [25] C. H. Aladag, U. Yolcu, and E. Egrioglu, "A high order fuzzy time series forecasting model based on adaptive expectation and artificial neural networks," *Mathematics and Computers in Simulation*, vol. 81, no. 4, pp. 875–882, 2010.
- [26] J. Sullivan and W. H. Woodall, "A comparison of fuzzy forecasting and Markov modeling," *Fuzzy Sets and Systems*, vol. 64, no. 3, pp. 279–293, 1994.
- [27] H. Yu, "Weighted fuzzy time series models for TAIEX forecasting," *Physica A*, vol. 349, no. 3–4, pp. 609–624, 2005.
- [28] K. Huarng and T. H. Yu, "The application of neural networks to forecast fuzzy time series," *Physica A*, vol. 363, no. 2, pp. 481–491, 2006.
- [29] C. H. Aladag, M. A. Basaran, E. Egrioglu, U. Yolcu, and V. R. Uslu, "Forecasting in high order fuzzy times series by using neural networks to define fuzzy relations," *Expert Systems with Applications*, vol. 36, no. 3, pp. 4228–4231, 2009.
- [30] C. H. Aladag, E. Egrioglu, S. Gunay, and U. Yolcu, "High order fuzzy time series model and stock exchange application," *Anadolu Üni., Anadolu Üniversitesi Bilim ve Teknoloji Dergisi*, vol. 11, no. 2, pp. 95–101, 2010.
- [31] T. H. Yu and K. Huarng, "A neural network-based fuzzy time series model to improve forecasting," *Expert Systems with Applications*, vol. 37, no. 4, pp. 3366–3372, 2010.
- [32] U. Yolcu, C. H. Aladag, E. Egrioglu, and V. R. Uslu, "Time series forecasting with a novel fuzzy time series approach: an example for Istanbul stock market," *Journal of Statistical Computation and Simulation*, vol. 83, no. 4, 2013.
- [33] E. Egrioglu, "A new time-invariant fuzzy time series forecasting method based on genetic algorithm," *Advances in Fuzzy Systems*, vol. 2012, Article ID 785709, 6 pages, 2012.
- [34] X. H. Yang, Z. F. Yang, and Z. Y. Shen, "GHHAGA for environmental systems optimization," *Journal of Environmental Informatics*, vol. 5, no. 1, pp. 36–41, 2005.
- [35] X. Yang, Z. Yang, X. Yin, and J. Li, "Chaos gray-coded genetic algorithm and its application for pollution source identifications in convection-diffusion equation," *Communications in Nonlinear Science and Numerical Simulation*, vol. 13, no. 8, pp. 1676–1688, 2008.
- [36] X. H. Yang, D. X. She, Z. F. Yang, Q. H. Tang, and J. Q. Li, "Chaotic bayesian method based on multiple criteria decision making (MCDM) for forecasting nonlinear hydrological time series," *International Journal of Nonlinear Sciences and Numerical Simulation*, vol. 10, no. 11–12, pp. 1595–1610, 2009.
- [37] C. W. J. Granger and R. Joyeux, "An introduction to long-memory time series models and fractional differencing," *Journal of Time Series Analysis*, vol. 1, no. 1, pp. 15–29, 1980.
- [38] J. R. M. Hosking, "Fractional differencing," *Biometrika*, vol. 68, no. 1, pp. 165–176, 1981.
- [39] J. R. M. Hosking, "Modeling persistence in hydrological time series using fractional differencing," *Water Resources Research*, vol. 20, no. 12, pp. 1898–1908, 1984.
- [40] J. Beran, *Statistics for Long-Memory Processes*, vol. 61, Chapman and Hall, New York, NY, USA, 1994.
- [41] H. E. Hurst, "Long-term storage capacity of reservoirs," *Transactions of the American Society of Civil Engineers*, vol. 116, pp. 770–779, 1951.
- [42] E. Egrioglu and S. Gunay, "Two new Mmethods for bayesian model selection in ARFIMA models," *Expert Systems with Applications*, vol. 37, pp. 8359–8364, 2010.
- [43] M. Li, "Fractal time series—a tutorial review," *Mathematical Problems in Engineering*, vol. 2010, Article ID 157264, 26 pages, 2010.
- [44] M. Li and W. Zhao, "On  $1/f$  noise," *Mathematical Problems in Engineering*, vol. 2012, Article ID 673648, 23 pages, 2012.
- [45] J. C. Bezdek, *Pattern Recognition with Fuzzy Objective Function Algorithms*, Plenum Press, New York, NY, USA, 1981.
- [46] J. Kennedy and R. Eberhart, "Particle swarm optimization," in *Proceedings of the IEEE International Conference on Neural Networks*, pp. 1942–1948, IEEE Press, Piscataway, NJ, USA, December 1995.
- [47] Y. Shi and R. C. Eberhart, "Empirical study of particle swarm optimization," in *Proceedings of the Congress on Evolutionary Computation (CEC '99)*, vol. 3, pp. 1950–1945, 1999.
- [48] Y. Ma, C. Jiang, Z. Hou, and C. Wang, "The formulation of the optimal strategies for the electricity producers based on the particle swarm optimization algorithm," *IEEE Transactions on Power Systems*, vol. 21, no. 4, pp. 1663–1671, 2006.
- [49] J. Hwang, S. Chen, and C. Lee, "Handling forecasting problems using fuzzy time series," *Fuzzy Sets and Systems*, vol. 100, no. 1–3, pp. 217–228, 1998.

## Research Article

# Convergence of Sample Autocorrelation of Long-Range Dependent Traffic

Ming Li<sup>1</sup> and Wei Zhao<sup>2</sup>

<sup>1</sup> School of Information Science & Technology, East China Normal University, No. 500, Dongchuan Road, Shanghai 200241, China

<sup>2</sup> Department of Computer and Information Science, University of Macau, Avenida Padre Tomas Pereira, Taipa 1356, Macau

Correspondence should be addressed to Ming Li; [ming\\_lihk@yahoo.com](mailto:ming_lihk@yahoo.com)

Received 28 May 2013; Accepted 30 June 2013

Academic Editor: Carlo Cattani

Copyright © 2013 M. Li and W. Zhao. This is an open access article distributed under the Creative Commons Attribution License, which permits unrestricted use, distribution, and reproduction in any medium, provided the original work is properly cited.

We depict our work on a fundamental issue in the theory of long-range dependent traffic in the aspect of the convergence of sample autocorrelation function (ACF) of real traffic. The present results suggest that the sample ACF of traffic is convergent. In addition, we show that the sample size has considerable effects in estimating the sample ACF of traffic. More precisely, a sample ACF of traffic tends to be smoother when the sample size increases.

## 1. Introduction

Start with the meaning of the convergence of a sample autocorrelation function (ACF) of a stationary random function  $x(t)$  for  $t \in (0, \infty)$ . Denote by  $x_T(t)$  a sample record of  $x(t)$  with length  $T$ , that is,  $x_T(t) = x(t)$  for  $t \in (0, T)$ . Let  $r_T(\tau)$  be the ACF of  $x_T(t)$ , meaning  $r_T(\tau) = E[x_T(t)x_T(t + \tau)]$  for  $t, t + \tau \in (0, T)$ . Then, we say that  $r_T(\tau)$  is convergent if  $\lim_{T \rightarrow \infty} r_T(\tau) = r(\tau)$  exists, where  $r(\tau)$  is the ACF of  $x(t)$ . Otherwise,  $r_T(\tau)$  is divergent or does not exist. In the discrete case,  $x(t)$  is replaced by  $x(i)$  ( $i = 0, \dots, \infty$ ),  $x_T(t)$  is substituted by  $x_I(i)$  for  $i = 0, \dots, I - 1$ , and  $r_T(\tau)$  is replaced with  $r_I(k)$  ( $k = 0, \dots, I - 1$ ). When  $\lim_{I \rightarrow \infty} r_I(k) = r(k)$  exists, where  $r(k)$  is the ACF of  $x(i)$ , we say that  $r_I(k)$  is convergent. That is the meaning of the convergence or existence of a sample ACF of a random function.

The issue described above may be unnecessary to treat in the field of conventional second-order random functions because an ACF of a conventional 2-order random function generally exists [1–6]. However, the issue whether a sample ACF of teletraffic (traffic for short) time series with long-range dependence is convergent or not is worth discussing.

The research by Resnick et al. [7] stated that the sample ACF of stable random functions with infinite variance may be random when the sample size approaches infinity instead of being convergent. The example of such a type of random functions includes  $\alpha$ -stable processes with infinite variance [7, Page 798]. Recall that traffic modeling using  $\alpha$ -stable processes was described by reports, such as Karasaridis and Hatzinakos [8], Barbe and McCormick [9]. On the other side, the reports by Field et al. [10, 11] discussed the traffic modeling using the standard Cauchy distribution, which implied that traffic is of infinite variance because variance of a random function obeying the Cauchy distribution is infinite [2–4]. Therefore, a sample ACF of traffic may be divergent if it is of infinite variance. Nonetheless, correlations of traffic play a role in practice; see, for example [12–22], just to cite a few. Consequently, the answer to the question whether a sample ACF of traffic is convergent or not is desired from the point of view of the theory of traffic. This paper aims at exhibiting that sample ACFs of real-traffic data are convergent.

The rest of the paper is organized as follows. Problem statement is described in Section 2. Results are explained in Section 3. Discussions are given in Section 4, which is followed by conclusions.

## 2. Problem Statement

In what follows, we assume that traffic  $x(i)$  is causal. By causal, we mean that  $x(i)$  is defined for  $i \geq 0$  and  $x(i) = 0$  if  $i < 0$ . In the interval  $[0, I]$ , the sample ACF of  $x_I(i)$  is given by

$$r_I(k) = \frac{1}{I} \sum_{i=0}^{I-1} x(i) x(i+k). \quad (1)$$

For  $I_l \neq I_m$ , assuming  $I_l < I_m$ , we have,

$$r_{I_l}(k) \neq r_{I_m}(k), \quad k = 0, \dots, I_l - 1. \quad (2)$$

What is previously mentioned may be expressed by

$$r_{I_l}(k) + \Delta_{I_l}(k) = r_{I_m}(k), \quad k = 0, \dots, I_l - 1, \quad (3)$$

where  $\Delta_{I_l}(k)$  is a fluctuation noise. Further, For  $I_l \neq I_m \neq I_n$ , assuming  $I_l < I_m < I_n$ , we have

$$r_{I_m}(k) + \Delta_{I_m}(k) = r_{I_n}(k), \quad k = 0, \dots, I_l - 1. \quad (4)$$

In general, if  $r_I(k)$  is convergent, we have

$$\sum_{k=0}^{I_l-1} |\Delta_{I_m}(k)| \leq \sum_{k=0}^{I_l-1} |\Delta_{I_l}(k)|. \quad (5)$$

More precisely, in the case of  $r_I(k)$  being convergent, we have

$$\lim_{I_l \rightarrow \infty} r_{I_l}(k) = \lim_{I_m \rightarrow \infty} r_{I_m}(k) = r(k). \quad (6)$$

Consequently, the above means that

$$\lim_{I_l \rightarrow \infty} \Delta_{I_l}(k) = 0. \quad (7)$$

Since a real-traffic data series is always of finite length and because the true ACF of  $x(i)$  is never achieved, the issue we treat in this research is to investigate whether  $r_I(k)$  tends smoother when  $I$  becomes larger. If that is so, we infer that  $r_I(k)$  is convergent. If not, it is divergent.

## 3. Results

Before showing the results, we brief the real-traffic data used in this section. Let  $x(t(i))$  be a sample record of traffic, where  $t(i)$  is the series of timestamps, indicating the timestamp of the  $i$ th packet arriving at a server. Thus,  $x(t(i))$  represents the packet size of the  $i$ th packet recorded at time  $t(i)$ . Note that the pattern of  $x(t(i))$  is consistent with that of  $x(i)$  that represents the size of the  $i$ th packet on a packet-by-packet basis.

We use two real-traffic traces. One is named BC-pOct89 that contains 1,000,000 packets. It was recorded on an Ethernet at the Bellcore Morristown Research and Engineering Facility [23], which is now Telcordia Technologies ([http://en.wikipedia.org/wiki/Telcordia\\_Technologies](http://en.wikipedia.org/wiki/Telcordia_Technologies)), made by Will Leland and Dan Wilson. The other is DEC-PKT-1 with 3.3 million packets. It was made by Jeff Mogul of Digital's Western Research Lab [24]. The former was used in the pioneering research of the fractal statistics of

traffic in [25, 26]. The latter was utilized by Paxson and Floyd in [27]. We cite relatively recent articles [28–30] for the nice description of the basic statistics of traffic.

Figure 1 is the plot of the first 2048 data points of traffic trace BC-pOct89. Figure 2 indicates the plots of sample ACFs of BC-pOct89 with different sample sizes as follows.

- (i) Figure 2(a): sample ACF of BC-pOct89 with the sample size  $I = 2^{11} = 2048$ .
- (ii) Figure 2(b): sample ACF of BC-pOct89 with the sample size  $I = 2^{12} = 4096$ .
- (iii) Figure 2(c): sample ACF of BC-pOct89 with the sample size  $I = 2^{13} = 8192$ .
- (iv) Figure 2(d): sample ACF of BC-pOct89 with the sample size  $I = 2^{14} = 16384$ .
- (v) Figure 2(e): sample ACF of BC-pOct89 with the sample size  $I = 2^{15} = 32768$ .
- (vi) Figure 2(f): sample ACF of BC-pOct89 with the sample size  $I = 2^{16} = 65536$ .
- (vii) Figure 2(g): sample ACF of BC-pOct89 with the sample size  $I = 2^{17} = 131072$ .

From Figure 2, we obtain the following observations.

*Observation 1.* The sample ACF of BC-pOct89 with different sample sizes obeys a certain deterministic function.

*Observation 2.* The fluctuation of a sample ACF of BC-pOct89 decreases as the sample size increases.

In order to refine Observation 2, we demonstrate the first 1024 points of the sample ACFs in the sense of zoom as shown in Figure 3. Thus, comes the following consequence.

*Consequence 1.* The sample ACF of BC-pOct89 is convergent.

The demonstrations of the sample ACF of DEC-PKT-1 are given in the appendix.

## 4. Discussions

The modeling of the sample ACF of BC-pOct89 may be fractional Gaussian noise (fGn), which is appropriate when the time scaling is large [31, 32], or the generalized fGn [33]. Both BC-pOct89 and DEC-PKT-1 may be well described by the generalized Cauchy (GC) correlation structure [34]. The theme of this research is the convergence of sample ACF of traffic instead of correlation modeling of traffic. From the present results, nevertheless, one may infer that (5), (6), and (7) hold.

The data used on this research were measured in the last century, more precisely, BC-pOct89 in 1989 and DEC-PKT-1 in 1995. However, the research by Borgnat et al. [35] suggested that statistics of traffic remain identical from the early age of the Internet to today. Therefore, we infer that sample ACF of traffic today may be convergent.

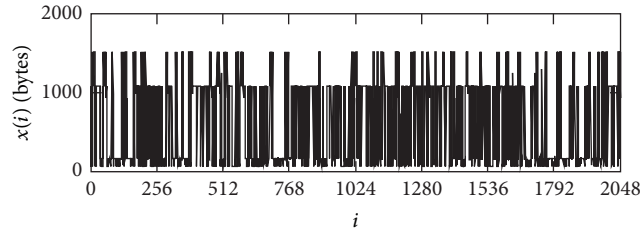


FIGURE 1: Plot of packet-size series of traffic trace BC-pOct89 on a packet-by-packet basis.

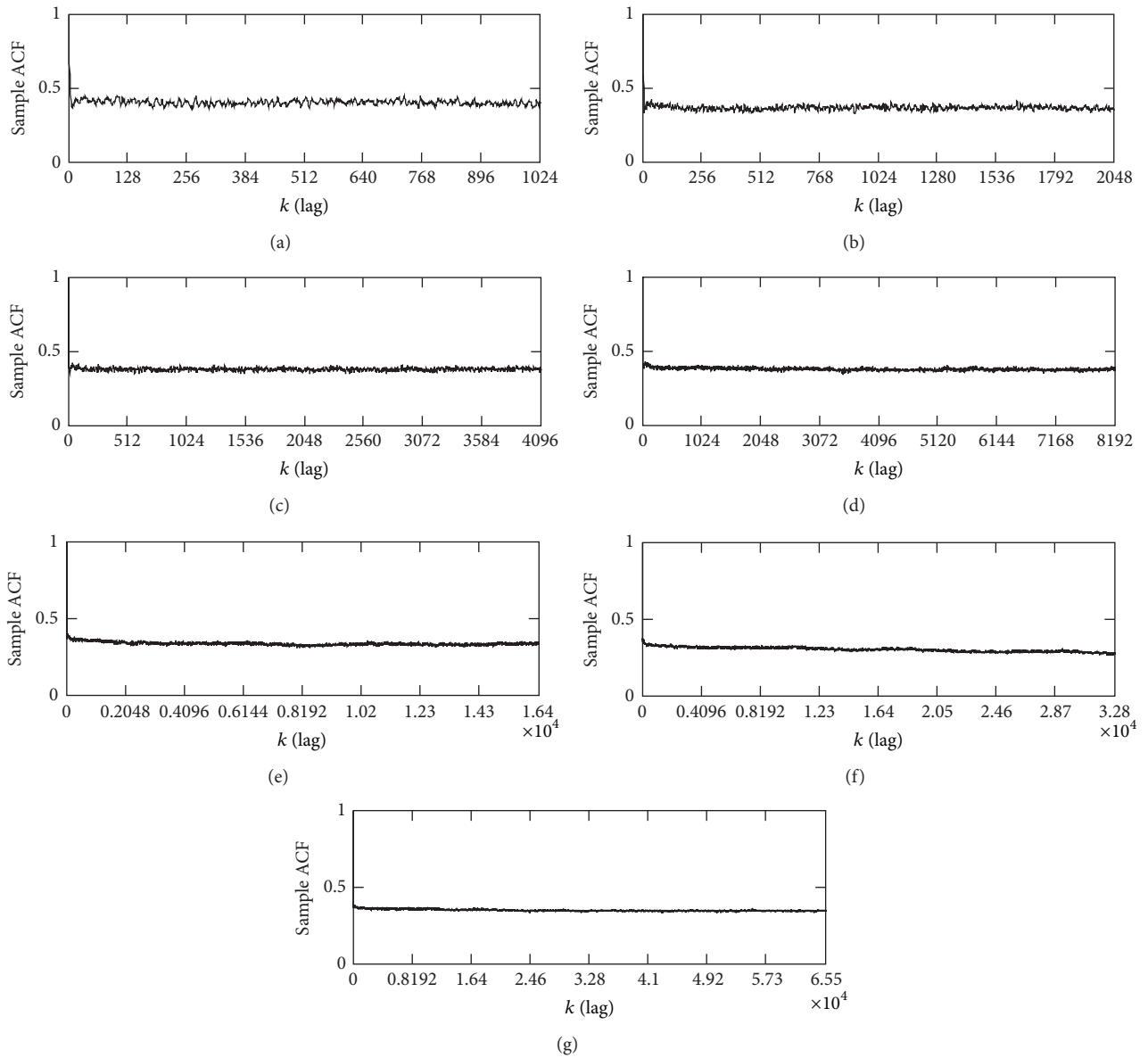


FIGURE 2: Sample ACFs of BC-pOct89 with the different sample sizes. (a) Sample ACF of BC-pOct89 with the sample size  $I = 2048$ . (b) Sample ACF of BC-pOct89 with  $I = 4096$ . (c) Sample ACF of BC-pOct89 with  $I = 8192$ . (d) Sample ACF of BC-pOct89 with  $I = 16384$ . (e) Sample ACF of BC-pOct89 with  $I = 32768$ . (f) Sample ACF of BC-pOct89 with  $I = 65536$ . (g) Sample ACF of BC-pOct89 with  $I = 131072$ .



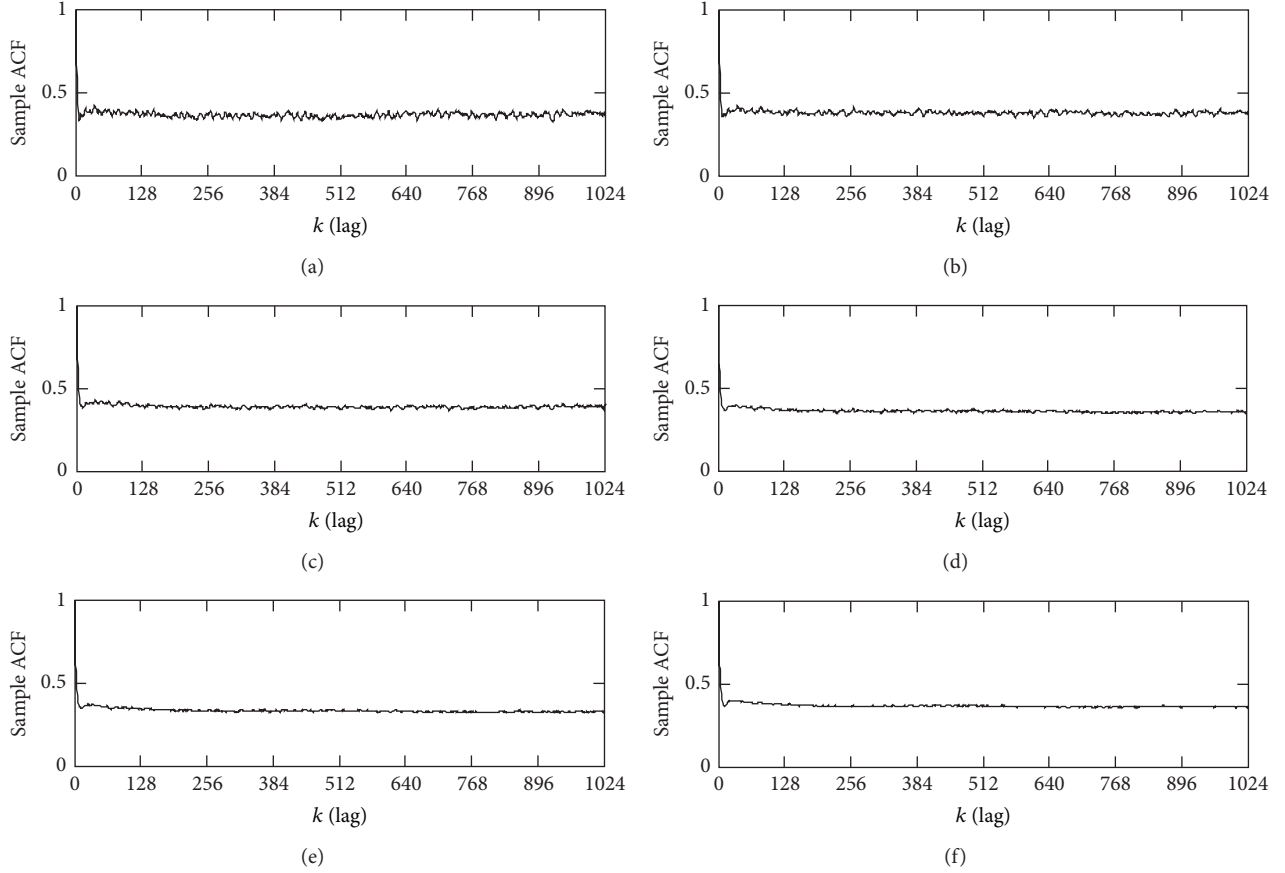


FIGURE 3: First 1024 points of sample ACFs of BC-pOct89 with the different sample sizes. (a) First 1024 points of sample ACF of BC-pOct89 with the sample size  $I = 4096$ . (b) First 1024 points of sample ACF of BC-pOct89 with  $I = 8192$ . (c) First 1024 points of sample ACF of BC-pOct89 with  $I = 16384$ . (d) First 1024 points of sample ACF of BC-pOct89 with  $I = 32768$ . (e) First 1024 sample ACF of BC-pOct89 with  $I = 65536$ . (f). First 1024 sample ACF of BC-pOct89 with  $I = 131027$ .

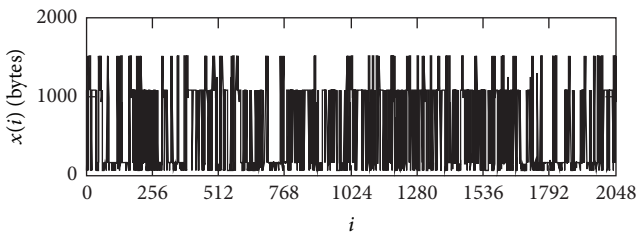


FIGURE 4: First 2048 points of packet-size series of traffic trace DEC-PKT-1 on a packet-by-packet basis.

Though we utilized traffic data in this research, the methodology described in this research might be possible for investigating the convergence of sample ACFs of other data series, for example, those in [36–43]. Finally, we note that this research does not imply something that might deviate from the point of view in traffic modeling using Levy stable structure, such as stable Levy motion [44], Levy flights [45],  $\alpha$ -stable models [8] or the standard Cauchy distribution [10, 11], when those correspond to random functions with infinite variance such that they

may yield divergent sample ACF. Rather, we suppose that it seems still faraway to thoroughly understand the statistics of traffic, without contradictions, with its commonly used models that may not be enough as Mandelbrot stated for modeling fractal random functions in general [46], but things may need developing; see, for example, Cohen and Lindner [47], Denby et al. [48], and Lazarou et al. [49].

## 5. Conclusions

We have exhibited that the sample ACFs of real-traffic data are convergent. Consequently, the sample ACFs of traffic exist. We have shown that the sample ACFs of traffic become smoother when the sample size increases.

## Appendix

### One More Case Study

The purpose of this appendix is to provide one more case study to demonstrate the convergence of the sample ACF of traffic using the real-traffic trace DEC-PKT-1.

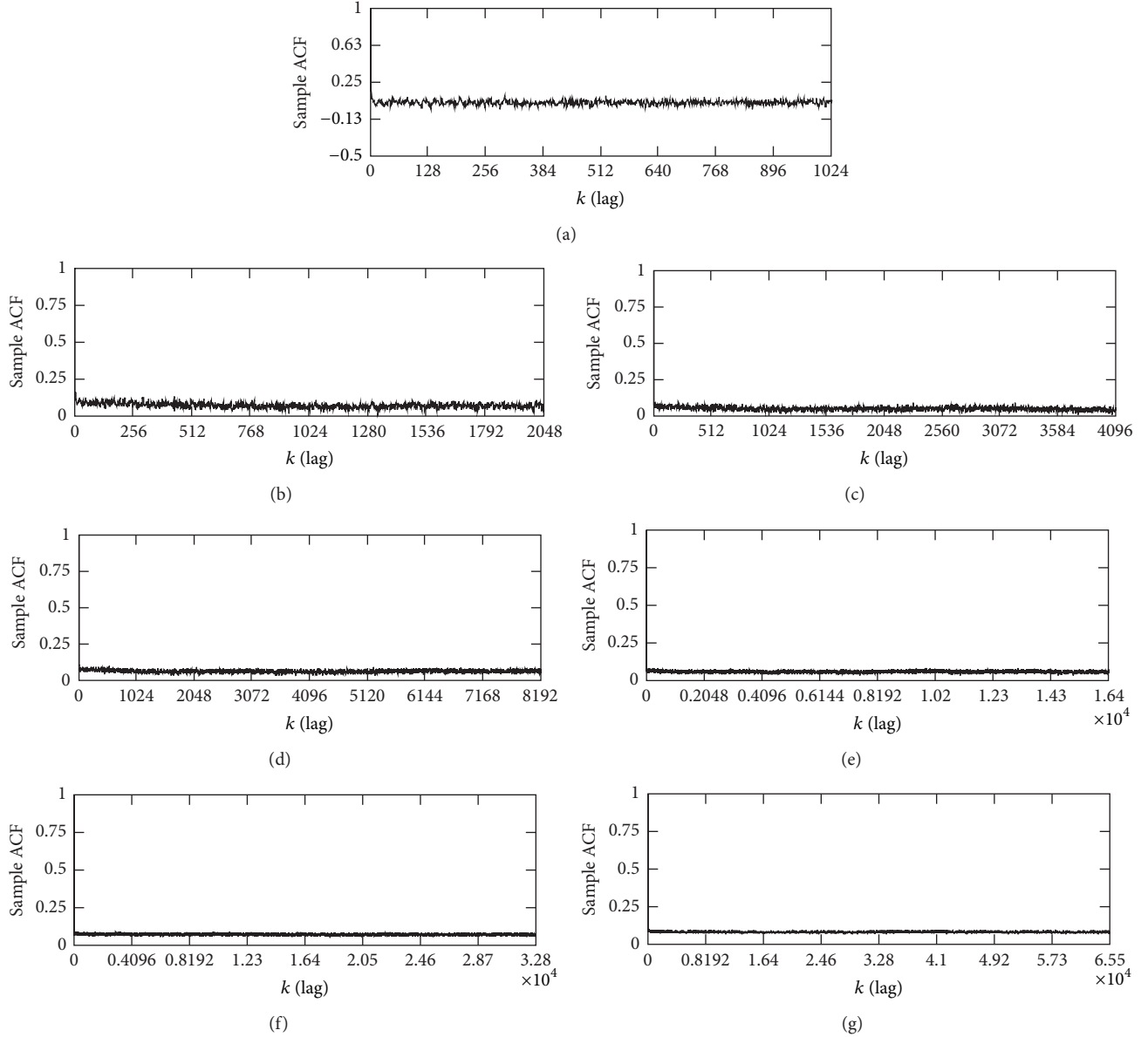


FIGURE 5: Plots of sample ACFs of DEC-PKT-1 with the different sample sizes. (a) Sample ACF of DEC-PKT-1 with the sample size  $I = 2048$ . (b) Sample ACF of DEC-PKT-1 with  $I = 4096$ . (c) Sample ACF of DEC-PKT-1 with  $I = 8192$ . (d) Sample ACF of DEC-PKT-1 with  $I = 16384$ . (e) Sample ACF of DEC-PKT-1 with  $I = 32768$ . (f) Sample ACF of DEC-PKT-1 with  $I = 65536$ . (g) Sample ACF of DEC-PKT-1 with  $I = 131072$ .

The first 2048 data points of DEC-PKT-1 are plotted in Figure 4. Figure 5 shows its plots of sample ACFs with different sample sizes from  $I = 2^{11} = 2048$  to  $I = 2^{17} = 131072$ .

Figure 5 implies that the sample ACF of DEC-PKT-1 with different sample sizes is a deterministic function. Besides, the fluctuation of its sample ACF decreases as the sample size increases. We refine the observation that the fluctuation of its sample ACF decreases as the sample size increases in Figure 6 by indicating the first 1024 points of each sample ACF, making

the result that the sample ACF of DEC-PKT-1 is convergent clearer.

## Acknowledgments

This work was supported in part by the 973 plan under the project Grant no. 2011CB302800, by the National Natural Science Foundation of China under the project Grant nos. 61272402, 61070214 and 60873264. The authors very much thank Will Leland (wel@bellcore.com), Dan Wilson

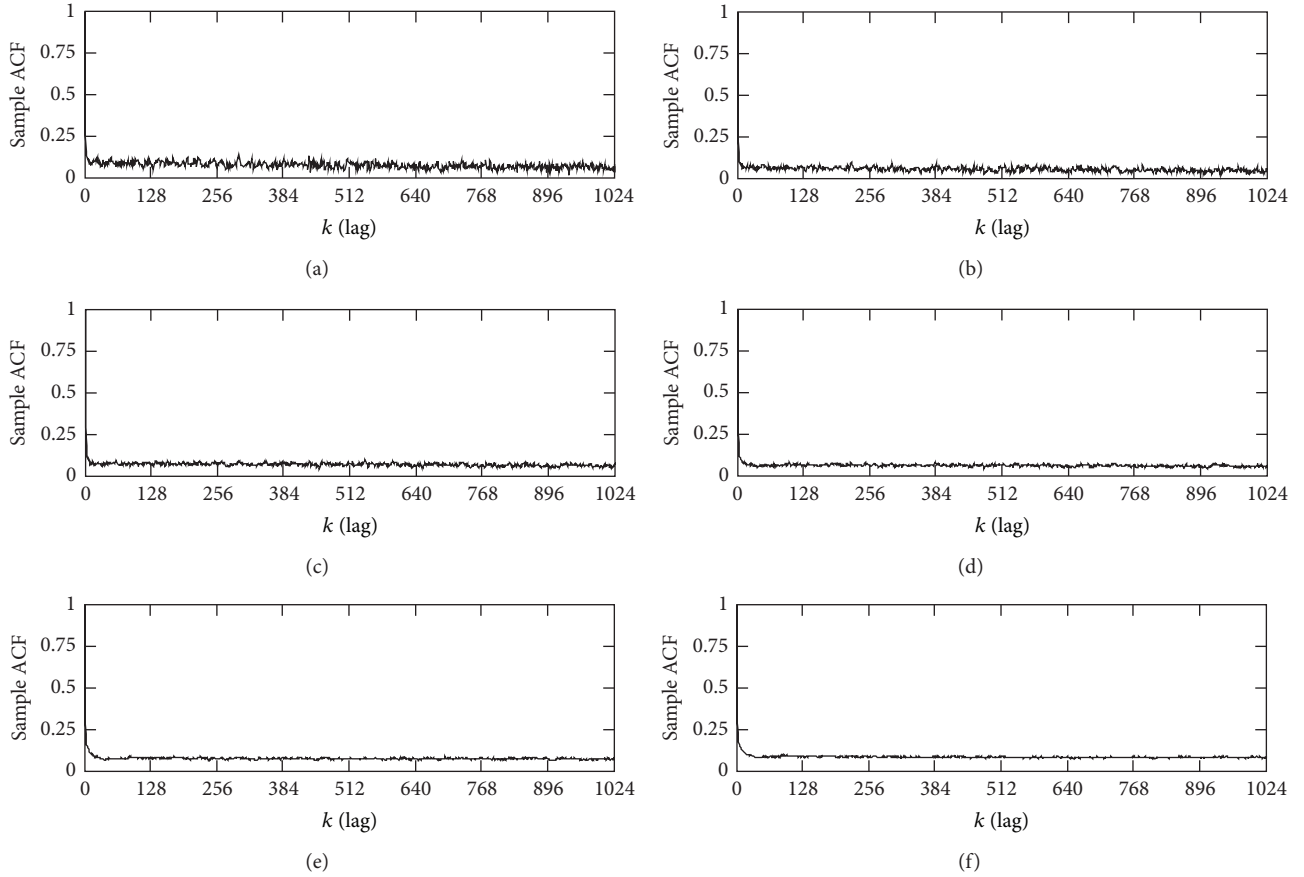


FIGURE 6: First 1024 points of sample ACFs of DEC-PKT-1 with the different sample sizes. (a) First 1024 points of sample ACF of DEC-PKT-1 with the sample size  $I = 4096$ . (b) First 1024 points of sample ACF of DEC-PKT-1 with  $I = 8192$ . (c) Sample ACF of DEC-PKT-1 with  $I = 16384$ . (d) First 1024 points of sample ACF of DEC-PKT-1 with  $I = 32768$ . (e) First 1024 sample ACF of DEC-PKT-1 with  $I = 65536$ . (f) First 1024 sample ACF of DEC-PKT-1 with  $I = 131027$ .

(dvw@bellcore.com), and Jeff Mogul (mogul@pa.dec.com), who provided them with their data in this research.

## References

- [1] A. M. Yaglom, *Correlation Theory of Stationary and Related Random Functions. Vol. I*, Springer, New York, NY, USA, 1987.
- [2] B. W. Lindgren and G. W. McElrath, *Introduction to Probability and Statistics*, The Macmillan Company, New York, NY, USA, 1959.
- [3] A. Papoulis, *Probability, Random Variables, and Stochastic Processes*, McGraw-Hill, New York, NY, USA, 3rd edition, 2002.
- [4] W. A. Fuller, *Introduction to Statistical Time Series*, John Wiley & Sons, New York, NY, USA, 2nd edition, 1996.
- [5] J. S. Bendat and A. G. Piersol, *Random Data: Analysis and Measurement Procedure*, John Wiley & Sons, New York, NY, USA, 3rd edition, 2000.
- [6] J. Beran, *Statistics for Long-Memory Processes*, Chapman & Hall, New York, NY, USA, 1994.
- [7] S. Resnick, G. Samorodnitsky, and F. Xue, "How misleading can sample ACFs of stable MAs be? (Very!)," *The Annals of Applied Probability*, vol. 9, no. 3, pp. 797–817, 1999.
- [8] A. Karasaridis and D. Hatzinakos, "Network heavy traffic modeling using  $\alpha$ -stable self-similar processes," *IEEE Transactions on Communications*, vol. 49, no. 7, pp. 1203–1214, 2001.
- [9] Ph. Barbe and W. P. McCormick, "Heavy-traffic approximations for fractionally integrated random walks in the domain of attraction of a non-Gaussian stable distribution," *Stochastic Processes and their Applications*, vol. 122, no. 4, pp. 1276–1303, 2012.
- [10] A. J. Field, U. Harder, and P. G. Harrison, "Measurement and modelling of self-similar traffic in computer networks," *IEE Proceedings-Communications*, vol. 151, no. 4, pp. 355–363, 2004.
- [11] T. Field, U. Harder, and P. Harrison, "Network traffic behaviour in switched Ethernet systems," *Performance Evaluation*, vol. 58, no. 2-3, pp. 243–260, 2004.
- [12] Y. Afek, A. Bremler-Barr, and Y. Koral, "Space efficient deep packet inspection of compressed web traffic," *Computer Communications*, vol. 35, no. 7, pp. 810–819, 2012.
- [13] V. N. G. J. Soares, F. Farahmand, and J. J. P. C. Rodrigues, "Traffic differentiation support in vehicular delay-tolerant networks," *Telecommunication Systems*, vol. 48, no. 1-2, pp. 151–162, 2011.
- [14] A. H. Taherinia and M. Jamzad, "A two-step watermarking attack using long-range correlation image restoration," *Security and Communication Networks*, vol. 5, no. 6, pp. 625–635, 2012.

- [15] Y. Cai, P. P. C. Lee, W. Gong, and D. Towsley, "Analysis of traffic correlation attacks on router queues," *Computer Networks*, vol. 55, no. 3, pp. 734–747, 2011.
- [16] Y. Zhu, X. Fu, B. Graham, R. Bettati, and W. Zhao, "Correlation-based traffic analysis attacks on anonymity networks," *IEEE Transactions on Parallel and Distributed Systems*, vol. 21, no. 7, pp. 954–967, 2010.
- [17] S. Lee, B. Chung, H. Kim, Y. Lee, C. Park, and H. Yoon, "Real-time analysis of intrusion detection alerts via correlation," *Computers and Security*, vol. 25, no. 3, pp. 169–183, 2006.
- [18] J. Zhou, M. Heckman, B. Reynolds, A. Carlson, and M. Bishop, "Modeling network intrusion detection alerts for correlation," *ACM Transactions on Information and System Security*, vol. 10, no. 1, article 4, 2007.
- [19] G. Min and M. Ould-Khaoua, "Prediction of communication delay in torus networks under multiple time-scale correlated traffic," *Performance Evaluation*, vol. 60, no. 1–4, pp. 255–273, 2005.
- [20] B. Balcioglu, D. L. Jagerman, and T. Altıok, "Merging and splitting autocorrelated arrival processes and impact on queueing performance," *Performance Evaluation*, vol. 65, no. 9, pp. 653–669, 2008.
- [21] L. B. Lim, L. Guan, A. Grigg, I. W. Phillips, X. G. Wang, and I. U. Awan, "Controlling mean queuing delay under multi-class bursty and correlated traffic," *Journal of Computer and System Sciences*, vol. 77, no. 5, pp. 898–916, 2011.
- [22] M. Ashour and T. Le-Ngoc, "Priority queuing of long-range dependent traffic," *Computer Communications*, vol. 31, no. 17, pp. 3954–3963, 2008.
- [23] <http://ita.ee.lbl.gov/html/contrib/BC.html>.
- [24] <http://ita.ee.lbl.gov/html/contrib/DEC-PKT.html>.
- [25] W. E. Leland, M. S. Taqqu, W. Willinger, and D. V. Wilson, "On the self-similar nature of Ethernet traffic (extended version)," *IEEE/ACM Transactions on Networking*, vol. 2, no. 1, pp. 1–15, 1994.
- [26] H. J. Fowler and W. E. Leland, "Local area network traffic characteristics, with implications for broadband network congestion management," *IEEE Journal on Selected Areas in Communications*, vol. 9, no. 7, pp. 1139–1149, 1991.
- [27] V. Paxson and S. Floyd, "Wide area traffic: The failure of Poisson modeling," *IEEE/ACM Transactions on Networking*, vol. 3, no. 3, pp. 226–244, 1995.
- [28] J. Cao, W. S. Cleveland, and D. X. Sun, "Bandwidth estimation for best-effort internet traffic," *Statistical Science*, vol. 19, no. 3, pp. 518–543, 2004.
- [29] S. Resnick, "On the foundations of multivariate heavy-tail analysis," *Journal of Applied Probability*, vol. 41, pp. 191–212, 2004.
- [30] B. D'Auria and S. I. Resnick, "The influence of dependence on data network models," *Advances in Applied Probability*, vol. 40, no. 1, pp. 60–94, 2008.
- [31] A. Feldmann, A. C. Gilbert, W. Willinger, and T. G. Kurtz, "The changing nature of network traffic: scaling phenomena," *ACM SIGCOMM Computer Communication Review*, vol. 28, no. 2, pp. 5–29, 1998.
- [32] M. Li, W. Zhao, W. Jia, D. Long, and C.-H. Chi, "Modeling autocorrelation functions of self-similar teletraffic in communication networks based on optimal approximation in Hilbert space," *Applied Mathematical Modelling*, vol. 27, no. 3, pp. 155–168, 2003.
- [33] M. Li, "Modeling autocorrelation functions of long-range dependent teletraffic series based on optimal approximation in Hilbert space-A further study," *Applied Mathematical Modelling*, vol. 31, no. 3, pp. 625–631, 2007.
- [34] M. Li and S. C. Lim, "Modeling network traffic using generalized Cauchy process," *Physica A*, vol. 387, no. 11, pp. 2584–2594, 2008.
- [35] P. Borgnat, G. Dewaele, K. Fukuda, P. Abry, and K. Cho, "Seven years and one day: sketching the evolution of internet traffic," in *Proceedings of the 28th IEEE Conference on Computer Communications (INFOCOM '09)*, pp. 711–719, Rio de Janeiro, Brazil, April 2009.
- [36] C. Cattani, E. Laserra, I. Bochicchio, and K. K. Nandi, "Correct light deflection in Weyl conformal gravity," *Physical Review D*, vol. 87, no. 4, Article ID 47503, 4 pages, 2013.
- [37] C. Cattani, "Fractional calculus and Shannon wavelet," *Mathematical Problems in Engineering*, vol. 2012, Article ID 502812, 26 pages, 2012.
- [38] C. Cattani, G. Pierro, and G. Altieri, "Entropy and multifractality for the myeloma multiple TET 2 gene," *Mathematical Problems in Engineering*, vol. 2012, Article ID 193761, 14 pages, 2012.
- [39] C. Toma, "Advanced signal processing and command synthesis for memory-limited complex systems," *Mathematical Problems in Engineering*, vol. 2012, Article ID 927821, 13 pages, 2012.
- [40] E. G. Bakhoum and M. H. M. Cheng, "Miniature carbon monoxide detector based on nanotechnology," *IEEE Transactions on Instrumentation and Measurement*, vol. 62, no. 1, pp. 240–245, 2013.
- [41] E. G. Bakhoum, "High-sensitivity miniature smoke detector," *IEEE Sensors Journal*, vol. 12, no. 10, pp. 3031–3035, 2012.
- [42] E. G. Bakhoum and C. Toma, "Modeling transitions in complex systems by multiplicative effect of temporal patterns extracted from signal flows," *Mathematical Problems in Engineering*, vol. 2012, Article ID 409856, 11 pages, 2012.
- [43] E. G. Bakhoum and C. Toma, "Specific mathematical aspects of dynamics generated by coherence functions," *Mathematical Problems in Engineering*, vol. 2011, Article ID 436198, 10 pages, 2011.
- [44] T. Mikosch, S. Resnick, H. Rootzén, and A. Stegeman, "Is network traffic approximated by stable Lévy motion or fractional Brownian motion?" *The Annals of Applied Probability*, vol. 12, no. 1, pp. 23–68, 2002.
- [45] G. Terdik and T. Gyires, "Lévy flights and fractal modeling of internet traffic," *IEEE/ACM Transactions on Networking*, vol. 17, no. 1, pp. 120–129, 2009.
- [46] B. B. Mandelbrot, *Multifractals and 1/f Noise*, Springer, New York, NY, USA, 1999.
- [47] S. Cohen and A. Lindner, "A central limit theorem for the sample autocorrelations of a Lévy driven continuous time moving average process," *Journal of Statistical Planning and Inference*, vol. 143, no. 8, pp. 1295–1306, 2013.
- [48] L. Denby, J. M. Landwehr, C. L. Mallows et al., "Statistical aspects of the analysis of data networks," *Technometrics*, vol. 49, no. 3, pp. 318–334, 2007.
- [49] G. Y. Lazarou, J. Baca, V. S. Frost, and J. B. Evans, "Describing network traffic using the index of variability," *IEEE/ACM Transactions on Networking*, vol. 17, no. 5, pp. 1672–1683, 2009.

## Research Article

# Adaptive Synchronization of Complex Dynamical Multilinks Networks with Similar Nodes

Weiping Wang,<sup>1</sup> Lixiang Li,<sup>2</sup> Haipeng Peng,<sup>2</sup> Jialiang Yuan,<sup>2</sup>  
Jinghua Xiao,<sup>1</sup> and Yixian Yang<sup>2,3</sup>

<sup>1</sup> School of Science, Beijing University of Posts and Telecommunications, Beijing 100876, China

<sup>2</sup> Information Security Center, Beijing University of Posts and Telecommunications, Beijing 100876, China

<sup>3</sup> National Engineering Laboratory for Disaster Backup and Recovery, Beijing University of Posts and Telecommunications, Beijing 100876, China

Correspondence should be addressed to Lixiang Li; [li.lixiang2006@163.com](mailto:li.lixiang2006@163.com)

Received 2 May 2013; Accepted 21 May 2013

Academic Editor: Ming Li

Copyright © 2013 Weiping Wang et al. This is an open access article distributed under the Creative Commons Attribution License, which permits unrestricted use, distribution, and reproduction in any medium, provided the original work is properly cited.

This paper studies the synchronization of complex dynamical networks with multilinks and similar nodes. The dynamics of all the nodes in the networks are impossible to be completely identical due to the differences of parameters or the existence of perturbations. Networks with similar nodes are universal in the real world. In order to depict the similarity of the similar nodes, we give the definition of the minimal similarity of the nodes in the network for the first time. We find the threshold of the minimal similarity of the nodes in the network. If the minimal similarity of the nodes is bigger than the threshold, then the similar nodes can achieve synchronization without controllers. Otherwise, adaptive synchronization method is adopted to synchronize similar nodes in the network. Some new synchronization criteria are proposed based on the Lyapunov stability theory. Finally, numerical simulations are given to illustrate the feasibility and the effectiveness of the proposed theoretical results.

## 1. Introduction

Complex dynamical networks have attracted increasing attention in recent years, since they have been widely exploited to model many complex systems in the science, engineering, and society [1, 2]. Synchronization of complex network has been found to be a universal phenomenon in nature and it has important potential applications to real-world dynamical systems. As an important and interesting collective behavior, synchronization of complex network has been studied extensively [3–8], such as complete synchronization, projective synchronization [9], impulsive synchronization [10, 11], exponential synchronization [12], adaptive synchronization [13–15], and pinning synchronization [16–21].

Most previous research assumes that the dynamics of all nodes are identical. Consequently, the synchronization problem is significantly simplified. However, the assumption

that the nodes are completely identical is not realistic in many real-world networks [22], such as in the neural networks, where the internal neurons in the nervous system are impossible to be completely identical due to the differences of the parameters. And the authors of [23, 24] studied synchronization of complex dynamical networks with nonidentical nodes. While, in normal circumstances, the neurons are not completely identical or completely nonidentical. They are similar to each other and they will achieve synchronization to transmit information which shows that the neural system has certain robustness. At this time, we want to know the answers of the following questions, which have a practical meaning for us to analyze and control many realistic networks with similar nodes. How to depict the similarity of the similar nodes? What is the condition that the similar nodes have to satisfy in the network in order to achieve synchronization without controllers? If there is a mutation or a pathological change, then some neurons may have many different characteristics,



and they can not synchronize with other neurons. When the similarity of the similar nodes is broken, how to synchronize the nodes in the network?

Furthermore, enormous works have been done on the synchronization in complex networks with single-link, and a lot of meaningful conclusions have been obtained. The authors of [19] propose that single-link network is a special case of multilinks network. Therefore, research on multilinks networks are more representative. Multilinks means that there is more than one link between two nodes and each of them has its own property. For instance, there are relationship networks, transportation networks, World Wide Web, and so forth. The transportation network as an example of a network with multilinks, which is made up by combining the corresponding airline network, railway network, and highway network. We can split the multilinks networks into many subnetworks based on the property of the connections. For a transportation network, the transmission speed is different among airline network, railway network, and highway network. In our previous work [19], time-delay was introduced to split complex dynamical networks into subnetworks, upon which a model of complex networks with multilinks has been constructed. However, the important issue of synchronization for complex dynamical networks with similar nodes and multilinks has so far received little attention. The study of the synchronization problem with similar nodes in the complex multilinks network becomes an interesting and challenging topic.

In this paper, we give a model of complex multilinks networks with similar nodes. A definition of similar nodes is given and the minimal similarity of similar nodes in the network is analyzed for the first time. We find a threshold of the minimal similarity of similar nodes. If the minimal similarity of similar nodes is bigger than the threshold in the network, then the similar nodes can achieve synchronization. Otherwise, we should add some controllers to the nodes in order to get synchronization. Then some new adaptive synchronization criteria are proposed. Finally, numerical simulations of dynamical networks with similar nodes are presented to demonstrate the feasibility and the effectiveness of the results.

## 2. Model and Preliminaries

The model of complex multilinks network consisting of  $N$  similar nodes with  $m$  kinds of properties can be described by

$$\begin{aligned} \dot{x}_i(t) = & A_i x_i(t) + f(x_i(t)) + c \sum_{j=1}^N b_{(0)ij} \Gamma_0 x_j(t) \\ & + c \sum_{l=1}^{m-1} \sum_{j=1}^N b_{(l)ij} \Gamma_l x_j(t - \tau_l), \quad i = 1, 2, \dots, N, \end{aligned} \quad (1)$$

where  $x_i(t) = (x_{i1}(t), x_{i2}(t), \dots, x_{iN}(t))^T$  is the state vector of node  $i$ ,  $A_i$  is a matrix,  $f(x_i(t))$  is a smooth nonlinear vector function,  $c > 0$  is the coupling strength,  $\Gamma_0$  and  $\Gamma_l$  are the inner-coupling matrices,  $B_l = (b_{(l)ij})_{N \times N}$ ,  $0 \leq l \leq m-1$  represents the topological structure of the  $l$ th subnetwork,

and  $\tau_l$  is the time-delay of the  $l$ th subnetwork compared with the basic network ( $\tau_0 = 0$ ). We define  $b_{(l)ij} = b_{(l)ji} = 1$  if there is a connection between node  $i$  and node  $j$  ( $j \neq i$ ) in the  $l$ th subnetwork, otherwise  $b_{(l)ij} = b_{(l)ji} = 0$ . And we define  $b_{(l)ii} = -\sum_{j=1, j \neq i}^N b_{(l)ij}$ .

Network (1) is in a state of asymptotical synchronization, if

$$x_1(t) = x_2(t) = \dots = x_N(t) \longrightarrow s(t) \quad (2)$$

as  $t \rightarrow \infty$  ( $1 \leq i \leq N$ ), where  $s(t) \in \mathbb{R}^n$  is a synchronous solution of the node system  $\dot{x}_i(t) = A_i x_i(t) + f(x_i(t))$ . We define the error vectors as

$$e_i(t) = x_i(t) - s_i(t). \quad (3)$$

Hereafter, the definitions of similar nodes and the minimal similarity of the similar nodes are given, and a useful assumption and two lemmas are introduced.

**Definition 1.** If  $A_i$  and  $A_j$  are matrices with the similar element values, then the node  $i$  and  $j$  are similar nodes. In the network (1), we define  $A$  as the matrix of basic node and  $A_i$  ( $1 \leq i \leq N-1$ ) as matrices of other nodes. Because  $A$  and  $A_i$  are matrices with similar element values, we define  $\delta_i = 1 - (\|A - A_i\|_F / \|A\|_F)$ ,  $\nu = \min(\delta_i)$ , ( $1 \leq i \leq N-1$ ), and  $\nu$  ( $0 < \nu < 1$ ) represents the minimal similarity of the nodes in the network. The norm of matrix  $A$  is  $\|A\|_F = (\sum_{i,j=1}^N a_{ij}^2)^{1/2}$ , and  $a_{ij}$  ( $1 \leq i, j \leq N$ ) are elements of matrix  $A$ .

**Remark 2.** From Definition 1, we know  $\nu$  is an important parameter. When  $\nu$  approaches to 1, the nodes in the network are similar. If  $\nu$  satisfies a certain condition, then the similar nodes of the network can achieve synchronization without controllers. On the contrary, when  $\nu$  is far away from 1, the nodes in the network become not similar, so the nodes cannot achieve synchronization without controllers. That is to say, there exists a threshold, if  $\nu$  is bigger than the threshold; then the similar nodes in the network can get synchronization without controllers. And the threshold is what we tried to find in the following.

**Assumption 3.** The smooth nonlinear function  $f(\cdot)$  satisfies the following Lipschitz condition:

$$\|f(x_i(t)) - f(s(t))\| \leq L \|x_i(t) - s(t)\|, \quad (4)$$

where  $L$  is a positive constant.

**Lemma 4.** For any two vectors  $x$  and  $y$ , and a matrix  $Q > 0$  with compatible dimensions, one has

$$2x^T y \leq x^T Q x + y^T Q^{-1} y. \quad (5)$$

**Lemma 5.** If  $A \in \mathbb{C}^{N \times N}$ , the eigenvalues of  $A$  are  $\lambda_i$  ( $i = 1, 2, \dots, N$ ), then  $\max(\lambda_i) \leq \|A\|$ , where  $\|A\|$  is an arbitrary matrix norm.

## 3. Synchronization Analysis

In this section, suppose there is not a control scheme to synchronize a delayed complex multilinks network with

similar nodes. According to system (1), the error dynamical system can be derived as

$$\begin{aligned} \dot{e}_i(t) = & A_i e_i(t) + f(x_i(t)) - f(s(t)) + c \sum_{j=1}^N b_{(0)ij} \Gamma_0 e_j(t) \\ & + c \sum_{l=1}^{m-1} \sum_{j=1}^N b_{(l)ij} \Gamma_l e_j(t - \tau_l), \end{aligned} \quad (6)$$

where  $A_i = A + \Delta A_i$ ,  $A_i$  is the matrix of node  $i$ , and  $A$  is the matrix of basic node. Because  $A$  and  $A_i$  are matrices with similar element values,  $\Delta A_i = A_i - A$ . It is easy to see that the synchronization of the complex network (1) is achieved if the zero solution of the error system (6) is globally asymptotically stable, which is ensured by the following theorem. And we find that the minimal similarity of the similar nodes satisfies an inequality for synchronization.

**Theorem 6.** Consider network (1), if the minimal similarity of the nodes  $\nu$  is bigger than the threshold, where the threshold of  $\nu$  is

$$\begin{aligned} & \left( \lambda_{\max}(A) + L + c \lambda_{\max}(P_0) + \frac{c}{2} \sum_{l=1}^{m-1} \lambda_{\max}(P_l P_l^T) \right. \\ & \left. + \frac{c}{2} (m-1) + \|A\|_F \right) (\|A\|_F)^{-1}, \end{aligned} \quad (7)$$

and it also satisfies the following inequality:

$$\begin{aligned} & \frac{\lambda_{\max}(A) + L + c \lambda_{\max}(P_0) + (c/2) \sum_{l=1}^{m-1} \lambda_{\max}(P_l P_l^T)}{\|A\|_F} \\ & + \frac{(c/2) (m-1) + \|A\|_F}{\|A\|_F} < \nu < 1, \end{aligned} \quad (8)$$

then the system (1) is synchronized without controllers.

*Proof.* Construct the following Lyapunov function:

$$V(t) = \frac{1}{2} \sum_{i=1}^N e_i(t)^T e_i(t) + \frac{c}{2} \sum_{l=1}^{m-1} \int_{t-\tau_l}^t \sum_{i=1}^N e_i(\theta)^T e_i(\theta) d\theta. \quad (9)$$

We get

$$\begin{aligned} \dot{V}(t) = & \sum_{i=1}^N e_i(t)^T \dot{e}_i(t) \\ & + \frac{c}{2} \sum_{l=1}^{m-1} \sum_{i=1}^N [e_i(t)^T e_i(t) - e_i(t - \tau_l)^T e_i(t - \tau_l)] \\ = & \sum_{i=1}^N e_i(t)^T A e_i(t) + \sum_{i=1}^N e_i(t)^T \Delta A_i e_i(t) \\ & + \sum_{i=1}^N e_i(t) [f(x_i(t)) - f(s(t))] \end{aligned}$$

$$\begin{aligned} & + \sum_{i=1}^N c e_i(t)^T \sum_{j=1}^N b_{(0)ij} \Gamma_0 e_j(t) \\ & + \sum_{i=1}^N c e_i(t)^T \sum_{l=1}^{m-1} \sum_{j=1}^N b_{(l)ij} \Gamma_l e_j(t - \tau_l) \\ & + \frac{c}{2} \sum_{i=1}^N \sum_{l=1}^{m-1} e_i(t)^T e_i(t) \\ & - \frac{c}{2} \sum_{i=1}^N \sum_{l=1}^{m-1} e_i(t - \tau_l)^T e_i(t - \tau_l). \end{aligned} \quad (10)$$

Let  $e(t) = (e_1(t), e_2(t), \dots, e_N(t))$ , then we get

$$\begin{aligned} \dot{V}(t) \leq & [e(t)^T A e(t) + e(t)^T \Delta A e(t) + L e(t)^T e(t)] \\ & + c e(t)^T (B_0 \otimes \Gamma_0) e(t) \\ & + c e(t)^T (B_1 \otimes \Gamma_1) e(t - \tau_1) \\ & + c e(t)^T (B_2 \otimes \Gamma_2) e(t - \tau_2) \\ & + \dots + c e(t)^T (B_{m-1} \otimes \Gamma_{m-1}) e(t - \tau_{m-1}) \\ & + \frac{c}{2} (m-1) e(t)^T e(t) \\ & - \frac{c}{2} e(t - \tau_1)^T e(t - \tau_1) - \frac{c}{2} e(t - \tau_2)^T e(t - \tau_2) \\ & - \dots - \frac{c}{2} e(t - \tau_{m-1})^T e(t - \tau_{m-1}). \end{aligned} \quad (11)$$

Let

$$\begin{aligned} P_0 &= B_0 \otimes \Gamma_0, \\ P_1 &= B_1 \otimes \Gamma_1, \\ P_2 &= B_2 \otimes \Gamma_2, \\ &\vdots \\ P_{m-1} &= B_{m-1} \otimes \Gamma_{m-1}, \end{aligned} \quad (12)$$

where  $\otimes$  represents the Kronecker product. Then by Lemma 4, we have

$$\begin{aligned} \dot{V}(t) \leq & \lambda_{\max}(A) e(t)^T e(t) + \lambda_{\max}(\Delta A_i) e(t)^T e(t) \\ & + L e(t)^T e(t) + c \lambda_{\max}(P_0) e(t)^T e(t) \\ & + \frac{c}{2} \lambda_{\max}(P_1 P_1^T) e(t)^T e(t) \\ & + \frac{c}{2} \lambda_{\max}(P_2 P_2^T) e(t)^T e(t) \\ & + \dots + \frac{c}{2} \lambda_{\max}(P_{m-1} P_{m-1}^T) e(t)^T e(t) \end{aligned}$$

$$\begin{aligned}
& + \frac{c}{2} (m-1) e(t)^T e(t) \\
& \leq \left[ \lambda_{\max}(A) + \|\Delta A_i\|_F + L + c\lambda_{\max}(P_0) \right. \\
& \quad \left. + \frac{c}{2} \sum_{l=1}^{m-1} \lambda_{\max}(P_l P_l^T) + \frac{c}{2} (m-1) \right] e(t)^T e(t) \\
& \leq \left[ \lambda_{\max}(A) + (1-\nu) \|A\|_F + L + c\lambda_{\max}(P_0) \right. \\
& \quad \left. + \frac{c}{2} \sum_{l=1}^{m-1} \lambda_{\max}(P_l P_l^T) + \frac{c}{2} (m-1) \right] e(t)^T e(t).
\end{aligned} \tag{13}$$

Therefore, if we have

$$\begin{aligned}
& \lambda_{\max}(A) + (1-\nu) \|A\|_F + L + c\lambda_{\max}(P_0) \\
& + \frac{c}{2} \sum_{l=1}^{m-1} \lambda_{\max}(P_l P_l^T) + \frac{c}{2} (m-1) < 0,
\end{aligned} \tag{14}$$

then  $\dot{V}(t) \leq 0$ . So we get the synchronization criterion as follows:

$$\begin{aligned}
& \frac{\lambda_{\max}(A) + L + c\lambda_{\max}(P_0) + (c/2) \sum_{l=1}^{l=m-1} \lambda_{\max}(P_l P_l^T)}{\|A\|_F} \\
& + \frac{(c/2)(m-1) + \|A\|_F}{\|A\|_F} < \nu < 1.
\end{aligned} \tag{15}$$

If  $\nu$  satisfies (15), the nodes are synchronized. Thus we complete the proof.  $\square$

*Remark 7.* The matrix of basic node can be chosen at random from  $A_i$  ( $1 \leq i \leq N$ ). No matter which one we choose, Theorem 6 also holds.

Furthermore, noise plays an important role in the process of synchronization. Here we consider the influence of the noise. If there is an additive noise in the system (1) in the form of

$$\begin{aligned}
\dot{x}_i(t) &= A_i x_i(t) + f(x_i(t)) + c \sum_{j=1}^N b_{(0)ij} \Gamma_0 x_j(t) \\
& + c \sum_{l=1}^{m-1} \sum_{j=1}^N b_{(l)ij} \Gamma_l x_j(t - \tau_l) + \eta_i(t), \\
& i = 1, 2, \dots, N,
\end{aligned} \tag{16}$$

where  $\eta_i(t) \in \mathbb{R}^n$  is the zero mean bounded noise. Using system (16), we can easily get the following error system:

$$\begin{aligned}
\dot{e}_i(t) &= (A + \Delta A_i) e_i(t) + f(x_i(t)) - f(s(t)) \\
& + c \sum_{j=1}^N b_{(0)ij} \Gamma_0 e_j(t) \\
& + c \sum_{l=1}^{m-1} \sum_{j=1}^N b_{(l)ij} \Gamma_l e_j(t - \tau_l) + \eta_i(t),
\end{aligned} \tag{17}$$

then we get

$$\begin{aligned}
E(\dot{e}_i(t)) &= (A + \Delta A_i) E[e_i(t)] + E[f(x_i(t)) - f(s(t))] \\
& + c \sum_{j=1}^N b_{(0)ij} \Gamma_0 E[e_j(t)] \\
& + c \sum_{l=1}^{m-1} \sum_{j=1}^N b_{(l)ij} \Gamma_l E[e_j(t - \tau_l)] + E[\eta_i(t)].
\end{aligned} \tag{18}$$

Finally, we get the theorem as follows.

**Theorem 8.** When there is a noise or perturbation, considering the network (16), if the following condition holds

$$\begin{aligned}
& \frac{\lambda_{\max}(A) + L + c\lambda_{\max}(P_0) + (c/2) \sum_{l=1}^{l=m-1} \lambda_{\max}(P_l P_l^T)}{\|A\|_F} \\
& + \frac{(c/2)(m-1) + \|A\|_F}{\|A\|_F} < \nu < 1,
\end{aligned} \tag{19}$$

then  $E[e_i(t)]$  approaches to zero.

The proof process of Theorem 8 is similar to the proof process of Theorem 6, so here it is omitted.

#### 4. Adaptive Synchronization

In this section, a control scheme is developed to synchronize a delayed complex multilinks network with similar nodes, which do not satisfy the synchronization criterion (15). And the following adaptive controllers are used:

$$u_i = -d_i e_i(t), \quad 1 \leq i \leq N. \tag{20}$$

And the updating laws are

$$\dot{d}_i = k_i e_i(t)^T e_i(t), \quad 1 \leq i \leq N, \tag{21}$$

where  $k_i$  ( $1 \leq i \leq N$ ) are positive constants. The adaptive controllers (20) are widely used in solving many synchronous problems.

Then the controlled network can be characterized as

$$\begin{aligned}\dot{x}_i(t) &= A_i x_i(t) + f(x_i(t)) + c \sum_{j=1}^N b_{(0)ij} \Gamma_0 x_j(t) \\ &+ c \sum_{l=1}^{m-1} \sum_{j=1}^N b_{(l)ij} \Gamma_l x_j(t - \tau_l) + u_i, \\ i &= 1, 2, \dots, N.\end{aligned}\quad (22)$$

According to system (22), the following error dynamical system can be derived:

$$\begin{aligned}\dot{e}_i(t) &= (A + \Delta A_i) e_i(t) + f(x_i(t)) - f(s(t)) \\ &+ c \sum_{j=1}^N b_{(0)ij} \Gamma_0 e_j(t) \\ &+ c \sum_{l=1}^{m-1} \sum_{j=1}^N b_{(l)ij} \Gamma_l e_j(t - \tau_l) - d_i e_i(t).\end{aligned}\quad (23)$$

It is clear to see that the synchronization of the controlled complex network (22) is achieved if the zero solution of the error system (23) is globally asymptotically stable, which is ensured by the following theorem.

**Theorem 9.** Consider the network (22) under the actions of the controllers (20) and the updating laws (21). If the following condition holds:

$$\begin{aligned}\lambda_{\max}(A) + (1 - \gamma) \|A\|_F + L + c \lambda_{\max}(P_0) \\ + \frac{c}{2} \sum_{l=1}^{m-1} \lambda_{\max}(P_l P_l^T) + \frac{c}{2} (m-1) < d^*,\end{aligned}\quad (24)$$

where  $d^*$  is a sufficiently large positive constant to be determined, then the system (1) is synchronized.

*Proof.* Construct the following Lyapunov function:

$$\begin{aligned}V(t) &= \frac{1}{2} \sum_{i=1}^N e_i(t)^T e_i(t) \\ &+ \frac{c}{2} \sum_{l=1}^{m-1} \int_{t-\tau_l}^t \sum_{i=1}^N e_i(\theta)^T e_i(\theta) d\theta \\ &+ \frac{1}{2} \sum_{i=1}^N \frac{(d_i - d^*)^2}{k_i}.\end{aligned}\quad (25)$$

Clearly,  $V(t)$  is positive. Then the derivative of  $V(t)$  is obtained as

$$\begin{aligned}\dot{V}(t) &= \sum_{i=1}^N e_i(t)^T \dot{e}_i(t) \\ &+ \frac{c}{2} \sum_{l=1}^{m-1} \sum_{i=1}^N [e_i(t)^T e_i(t) \\ &\quad - e_i(t - \tau_l)^T e_i(t - \tau_l)] \\ &+ \sum_{i=1}^N [d_i e_i(t)^T e_i(t) - d^* e_i(t)^T e_i(t)] \\ &= \sum_{i=1}^N \left\{ e_i(t)^T A e_i(t) + e_i(t)^T \Delta A_i e_i(t) + e_i(t) \right. \\ &\quad \times [f(x_i(t)) - f(s(t))] \\ &\quad + c e_i(t)^T \sum_{j=1}^N b_{(0)ij} \Gamma_0 e_j(t) \\ &\quad + c e_i(t)^T \sum_{l=1}^{m-1} \sum_{j=1}^N b_{(l)ij} \Gamma_l e_j(t - \tau_l) \\ &\quad - d_i e_i(t)^T e_i(t) + \frac{c}{2} \sum_{l=1}^{m-1} e_i(t)^T e_i(t) \\ &\quad - \frac{c}{2} \sum_{l=1}^{m-1} e_i(t - \tau_l)^T e_i(t - \tau_l) \\ &\quad \left. + d_i e_i(t)^T e_i(t) - d^* e_i(t)^T e_i(t) \right\}.\end{aligned}\quad (26)$$

Let  $e(t) = (e_1(t), e_2(t), \dots, e_N(t))$ , then we get

$$\begin{aligned}\dot{V}(t) &\leq [e(t)^T A e(t) + e(t)^T \Delta A_i e(t) + L e(t)^T e(t)] \\ &+ c e(t)^T (B_0 \otimes \Gamma_0) e(t) \\ &+ c e(t)^T (B_1 \otimes \Gamma_1) e(t - \tau_1) + c e(t)^T \\ &\times (B_2 \otimes \Gamma_2) e(t - \tau_2) \\ &+ \dots + c e(t)^T (B_{m-1} \otimes \Gamma_{m-1}) e(t - \tau_{m-1}) \\ &+ \frac{c}{2} (m-1) e(t)^T e(t) - \frac{c}{2} e(t - \tau_1)^T e(t - \tau_1) \\ &- \frac{c}{2} e(t - \tau_2)^T e(t - \tau_2) \\ &- \dots - \frac{c}{2} e(t - \tau_{m-1})^T e(t - \tau_{m-1}) - d^* e(t)^T e(t).\end{aligned}\quad (27)$$

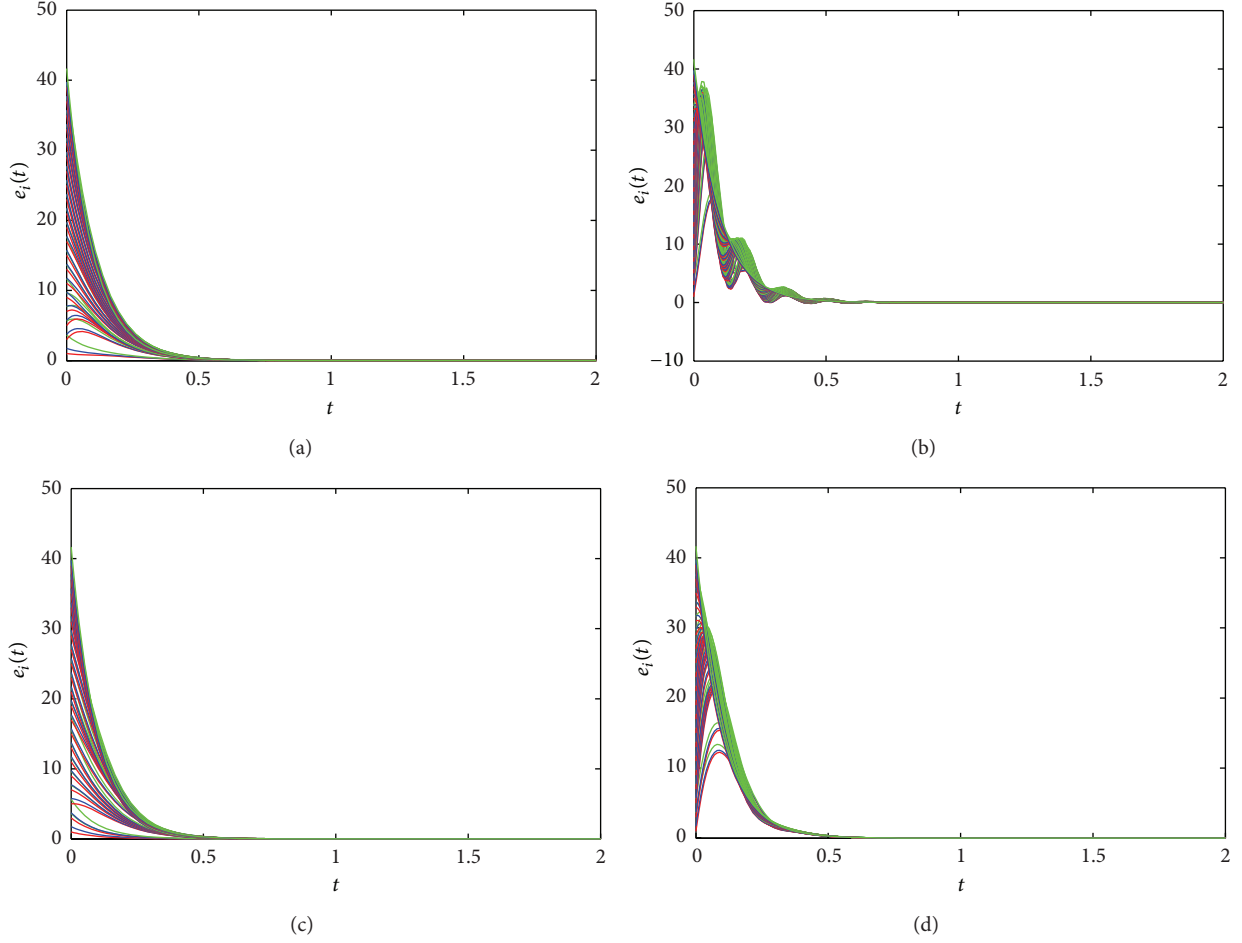


FIGURE 1: Separate synchronous variables  $e_{i1}$ ,  $e_{i2}$ ,  $e_{i3}$  ( $1 \leq i \leq 30$ ) of different network models where  $e_{i1}$  are shown by the red line,  $e_{i2}$  are shown by the blue line, and  $e_{i3}$  are shown by the green line.  $c = 2$ ;  $\tau = 0.01$ . (a)  $B_0$  and  $B_1$  are small-world network models, and the rewiring probability among nodes is 0.3 and 0.6. (b)  $B_0$  and  $B_1$  are scale-free network models, and their minimum degrees are 2 and 3. (c)  $B_0$  and  $B_1$  are random network models, and their connection probability among nodes is 0.1 and 0.3. (d)  $B_0$  is a small-world network model, and the rewiring probability among nodes is 0.3.  $B_1$  is a scale-free network model, and the minimum degree is 2. Those similar nodes can achieve synchronization without controllers (color online).

Let

$$\begin{aligned}
 P_0 &= B_0 \otimes \Gamma_0, \\
 P_1 &= B_1 \otimes \Gamma_1, \\
 P_2 &= B_1 \otimes \Gamma_2, \\
 &\vdots \\
 P_{m-1} &= B_{m-1} \otimes \Gamma_{m-1},
 \end{aligned} \tag{28}$$

where  $\otimes$  represents the Kronecker product. Then by Lemma 4, we have

$$\begin{aligned}
 \dot{V}(t) &\leq \lambda_{\max}(A) e(t)^T e(t) \\
 &\quad + \lambda_{\max}(\Delta A_i) e(t)^T e(t) + L e(t)^T e(t) \\
 &\quad + c \lambda_{\max}(P_0) e(t)^T e(t) \\
 &\quad + \frac{c}{2} \lambda_{\max}(P_1 P_1^T) e(t)^T e(t) \\
 &\quad + \cdots + \frac{c}{2} \lambda_{\max}(P_{m-1} P_{m-1}^T) e(t)^T e(t)
 \end{aligned}$$

$$\begin{aligned}
 &+ \frac{c}{2} (m-1) e(t)^T e(t) - d^* e(t)^T e(t) \\
 &\leq \left[ \lambda_{\max}(A) + \|\Delta A_i\|_F + L \right. \\
 &\quad \left. + c \lambda_{\max}(P_0) + \frac{c}{2} \sum_{l=1}^{m-1} \lambda_{\max}(P_l P_l^T) \right. \\
 &\quad \left. + \frac{c}{2} (m-1) - d^* \right] e(t)^T e(t) \\
 &\leq \left[ \lambda_{\max}(A) + (1-\gamma) \|A\|_F + L \right. \\
 &\quad \left. + c \lambda_{\max}(P_0) + \frac{c}{2} \sum_{l=1}^{m-1} \lambda_{\max}(P_l P_l^T) \right. \\
 &\quad \left. + \frac{c}{2} (m-1) - d^* \right] e(t)^T e(t).
 \end{aligned}$$

(29)



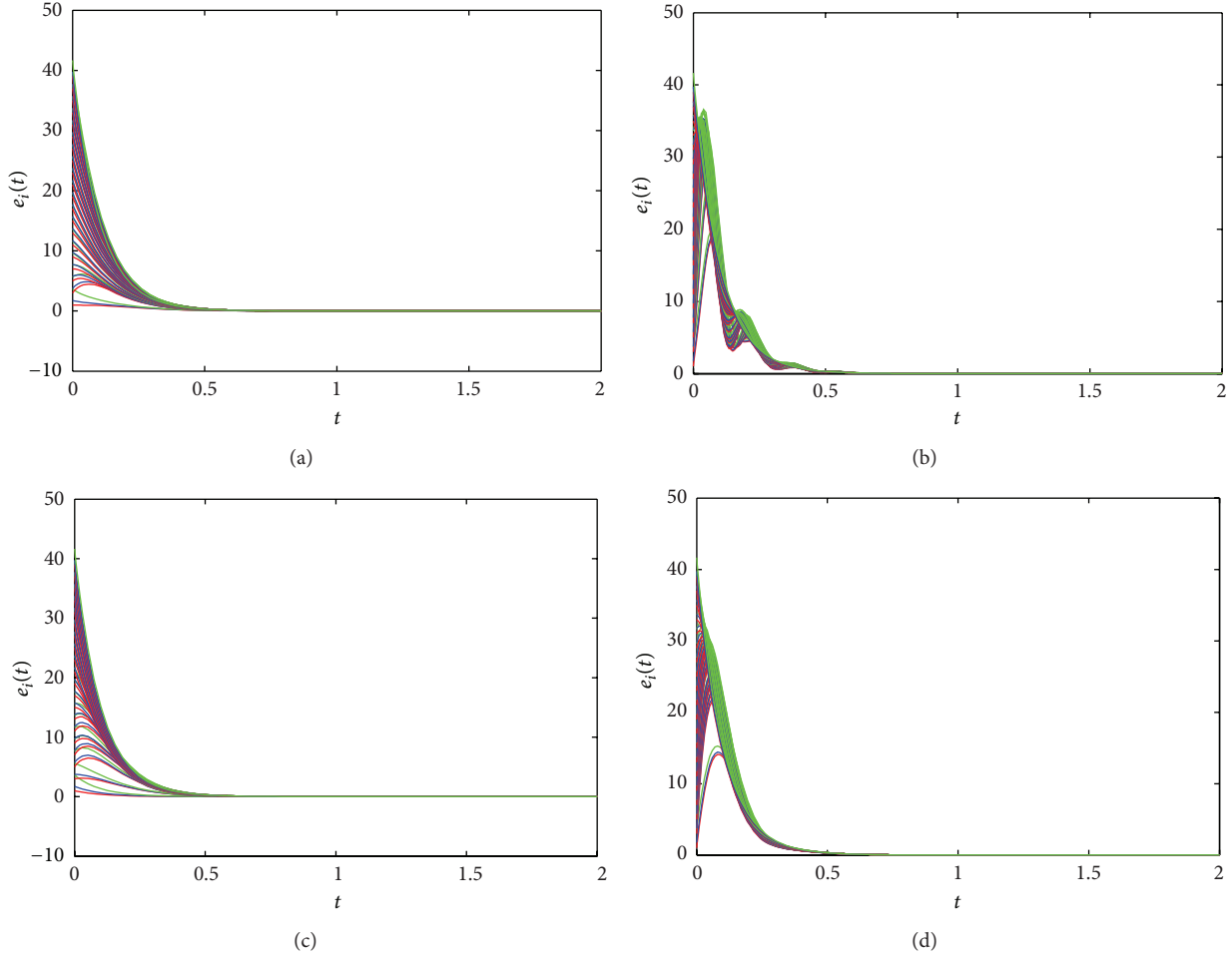


FIGURE 2: The similar nodes can achieve synchronization without controllers when the Brownian motion satisfies  $E\omega(t) = 0$ ,  $D\omega(t) = 1$ . And separate synchronous variables  $e_{i1}$ ,  $e_{i2}$ ,  $e_{i3}$  ( $1 \leq i \leq 30$ ) of different network models where  $e_{i1}$  are shown by the red line,  $e_{i2}$  are shown by the blue line, and  $e_{i3}$  are shown by the green line.  $c = 2$ ;  $\tau = 0.01$ . The network models of (a)–(d) are the same with Figures 1(a)–1(d) (color online).

Therefore, if we have

$$\lambda_{\max}(A) + (1 - \nu) \|A\|_F + L + c\lambda_{\max}(P_0) + \frac{c}{2} \sum_{l=1}^{m-1} \lambda_{\max}(P_l P_l^T) + \frac{c}{2} (m-1) < d^*, \quad (30)$$

then  $\dot{V}(t) \leq 0$ . Here we complete the proof.  $\square$

**Remark 10.** If there is not a nonlinear function in system (1), then the network (1) is transferred into

$$\begin{aligned} \dot{x}_i(t) &= A_i x_i(t) + c \sum_{j=1}^N b_{(0)ij} \Gamma_0 x_j(t) \\ &\quad + c \sum_{l=1}^{m-1} \sum_{j=1}^N b_{(l)ij} \Gamma_l x_j(t - \tau_l), \end{aligned} \quad (31)$$

$$i = 1, 2, \dots, N.$$

Likewise, we can design the controllers as in (20) and (21). If the following condition holds:

$$\lambda_{\max}(A) + (1 - \nu) \|A\|_F + c\lambda_{\max}(P_0) + \frac{c}{2} \sum_{l=1}^{m-1} \lambda_{\max}(P_l P_l^T) + \frac{c}{2} (m-1) < d^*, \quad (32)$$

then the system (31) is synchronized, where  $d^*$  is a sufficiently large positive constant to be determined.

**Remark 11.** The single-link network is a special case of multilinks networks [19]. When there is not a delay, the network (1) is transferred into the following single-link network:

$$\begin{aligned} \dot{x}_i(t) &= A_i x_i(t) + f(x_i(t)) \\ &\quad + c \sum_{j=1}^N b_{(0)ij} \Gamma_0 x_j(t), \quad i = 1, 2, \dots, N, \end{aligned} \quad (33)$$

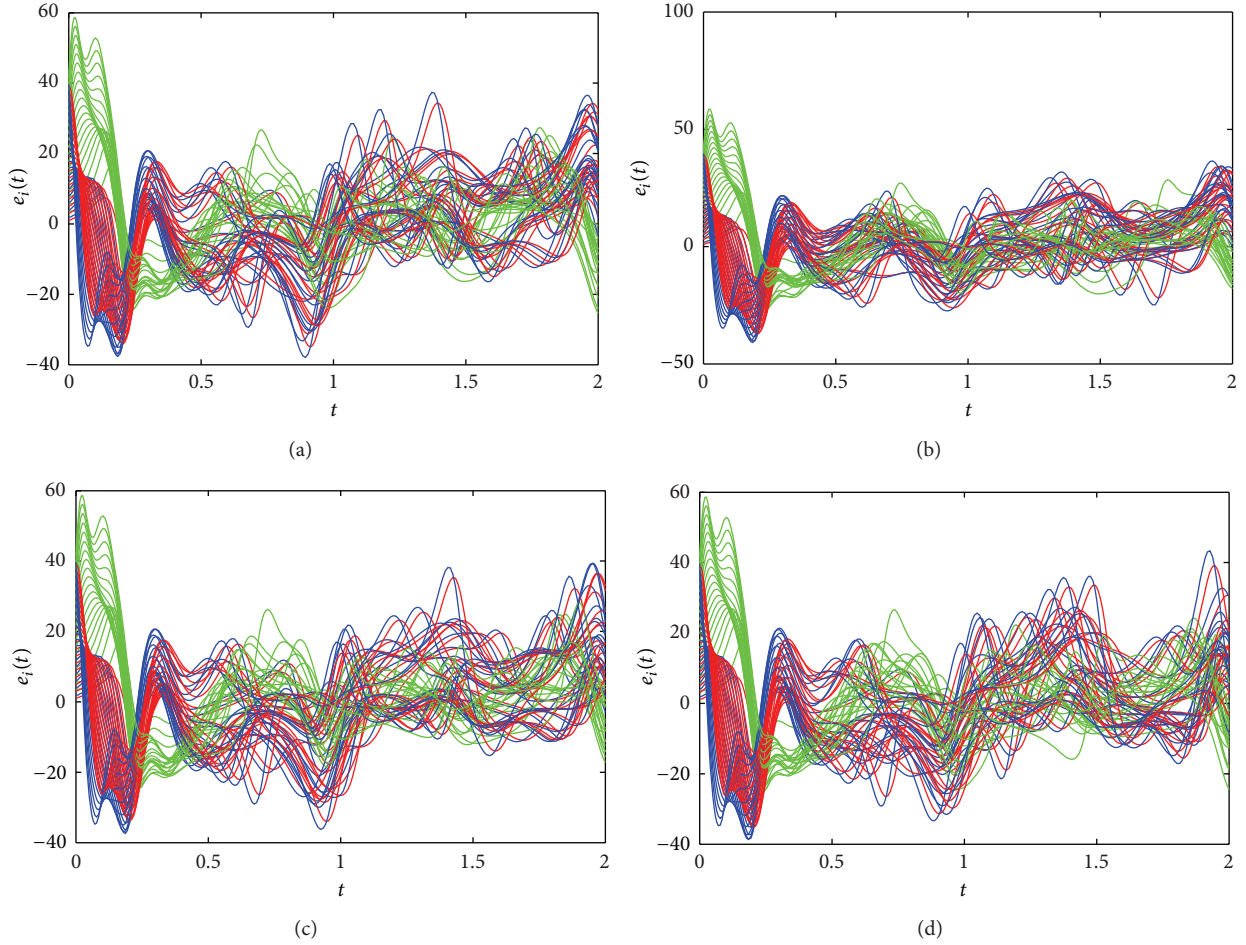


FIGURE 3: Separate synchronous variables  $e_{i1}, e_{i2}, e_{i3}$  ( $1 \leq i \leq 30$ ) of different network models where  $e_{i1}$  are shown by the red line,  $e_{i2}$  are shown by the blue line, and  $e_{i3}$  are shown by the green line.  $c = 2$ ;  $\tau = 0.01$ . The dynamics of nodes satisfy the Lü system. The nodes of the network cannot achieve synchronization without controllers. The network models of (a)–(d) are the same with Figures 1(a)–1(d) (color online).

and the controllers are designed as in (20)–(21). If the following condition holds:

$$\lambda_{\max}(A) + (1 - \nu) \|A\|_F + L + c \lambda_{\max}(P_0) < d^*, \quad (34)$$

then the system (33) is synchronized, where  $d^*$  is a sufficiently large positive constant to be determined.

## 5. Numerical Simulation

In this section, we use some examples to explain the influence of the proposed criteria, and we consider a network consisting of 30 similar nodes. The multilinks network with 2 properties can be described as follows:

$$\begin{aligned} \dot{x}_i(t) = & A_i x_i(t) + f(x_i(t)) + c \sum_{j=1}^{30} b_{(0)ij} \Gamma_0 x_j(t) \\ & + c \sum_{j=1}^{30} b_{(1)ij} \Gamma_1 x_j(t - \tau), \end{aligned} \quad (35)$$

where  $1 \leq i \leq 30$ ,  $B_0 = (b_{(0)ij})_{30 \times 30}$ , and  $B_1 = (b_{(1)ij})_{30 \times 30}$  are symmetrically diffusive coupling matrixes with  $b_{(0)ij}$ ,

$b_{(1)ij} = 0$  or  $1$ .  $\Gamma_0 = \Gamma_1 = \text{diag}(1, 1, 1)$ ,  $c = 2$ ,  $\tau = 0.01$ ,  $f(x_i(t)) = (0.6 \sin(x_{i1}), 0.6 \sin(x_{i2}), 0.6 \sin(x_{i3}))^T$ . According to Assumption 3, we can know that  $L = 0.6$ :

$$A_i = \begin{pmatrix} -10 + 0.1 * \text{rand} & 0.1 * \text{rand} & 0.1 * \text{rand} \\ 0.1 * \text{rand} & -10 + 0.1 * \text{rand} & 0.1 * \text{rand} \\ 0.1 * \text{rand} & 0.1 * \text{rand} & -10 + 0.1 * \text{rand} \end{pmatrix}, \quad (36)$$

where the function of rand can produce a random number between 0 and 1. According to the definition of similar nodes, we know  $A_i$ ,  $1 \leq i \leq 30$  are matrices of the similar nodes. And

$$A = \begin{pmatrix} -10 & 0 & 0 \\ 0 & -10 & 0 \\ 0 & 0 & -10 \end{pmatrix} \quad (37)$$

is the matrix of the basic node. So

$$\Delta A_i = \begin{pmatrix} 0.1 * \text{rand} & 0.1 * \text{rand} & 0.1 * \text{rand} \\ 0.1 * \text{rand} & 0.1 * \text{rand} & 0.1 * \text{rand} \\ 0.1 * \text{rand} & 0.1 * \text{rand} & 0.1 * \text{rand} \end{pmatrix}. \quad (38)$$

According to the precise calculation,  $\lambda_{\max}(A) = -10$ ,  $\lambda_{\max}(P_0) = 0$ ,  $\lambda_{\max}(P_1^T P_1) = 18.5139$ . Based on

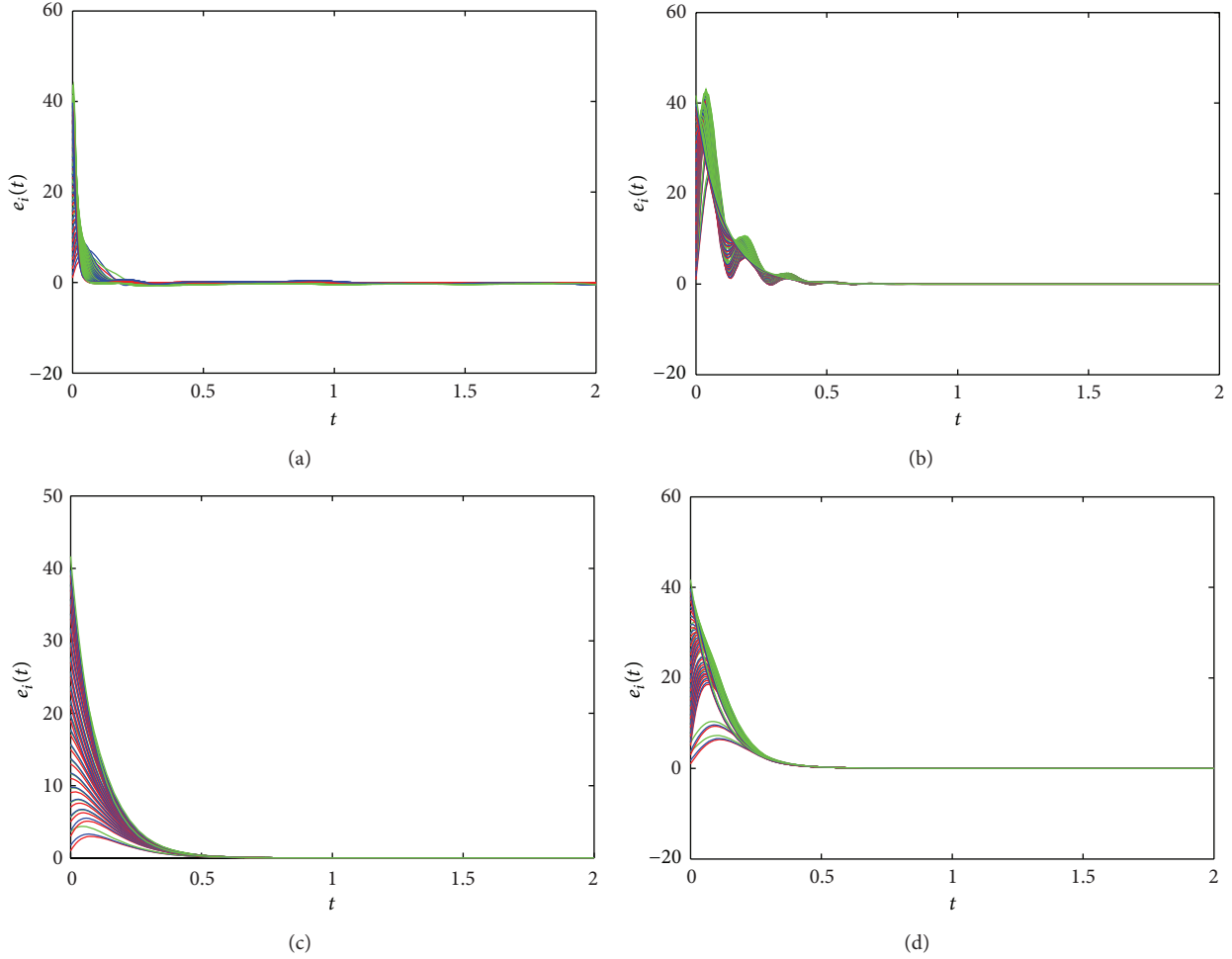


FIGURE 4: Separate synchronous variables  $e_{i1}$ ,  $e_{i2}$ ,  $e_{i3}$  ( $1 \leq i \leq 30$ ) of different network models where  $e_{i1}$  are shown by the red line,  $e_{i2}$  are shown by the blue line, and  $e_{i3}$  are shown by the green line.  $c = 2$ ;  $\tau = 0.01$ . The dynamics of nodes satisfy the Lü system. The nodes are controlled by the adaptive controllers (20) and (21). The network models of (a)–(d) are the same with Figures 1(a)–1(d) (color online).

the stability analysis, we get  $(\lambda_{\max}(A) + L + c\lambda_{\max}(P_0) + (c/2)\sum_{l=1}^{l=m-1}\lambda_{\max}(P_l P_l^T) + (c/2)(m-1) + \|A\|_F)(\|A\|_F)^{-1} = (-100 + 0.6 + 18.5139 + 1 + \sqrt{300000})/\sqrt{300000} = 0.5388$ . According to (38), because  $0 < \text{rand} < 1$ , the biggest changes are

$$\Delta A_i = \begin{pmatrix} 0.1 & 0.1 & 0.1 \\ 0.1 & 0.1 & 0.1 \\ 0.1 & 0.1 & 0.1 \end{pmatrix}. \quad (39)$$

Then we compute the  $\nu = 0.9983$ ,  $0.5388 < \nu < 1$ , so the similar nodes can achieve synchronization which satisfies Theorem 6. From Figures 1(a)–1(d), we know that the similar nodes in the network achieved synchronization under different network models.

Furthermore, in order to verify Theorem 9, we choose the model (16) as the second example, where the Brownian motion satisfies  $E\omega(t) = 0$ ,  $D\omega(t) = 1$ , and the parameters are the same with the first example. Figures 2(a)–2(d) plot the synchronous errors converge to 0 in finite time under

different network models with noise, which reflects that similar nodes have a certain robustness. In our future work, we will consider the model (35) with Gaussian noise [25] or  $1/f$  noise [26], and the stochastic bounded model like [27] in the complex network with similar nodes will be studied.

Next, another example as the third one describes the controlled network using Lü systems and considers the network consisting of 30 nodes. The node dynamical system is  $\dot{x}_i = (-36x_{i1} + 36x_{i2}; 20x_{i2} - x_{i1}x_{i3}; -3x_{i3} + x_{i1}x_{i2})$ , for  $i = 1, 2, \dots, 30$ . And  $\Delta A_i$  are the same with the first example. Since Lü attractor is bounded, we suppose that all nodes are running in the given bounded region. There exists the constants  $M_1 = 25$ ,  $M_2 = 30$ ,  $M_3 = 45$  satisfying  $\|x_{ij}\|_2, \|s_j\|_2 \leq M_j$  for  $1 \leq i \leq 30$  and  $1 \leq j \leq 3$  [28]. Thus we have

$$\|f(x_i) - f(s)\| \leq \sqrt{2M_1^2 + M_2^2 + M_3^2} \|e_i\|_2 \approx 64.6142 \|e_i\|_2, \quad (40)$$

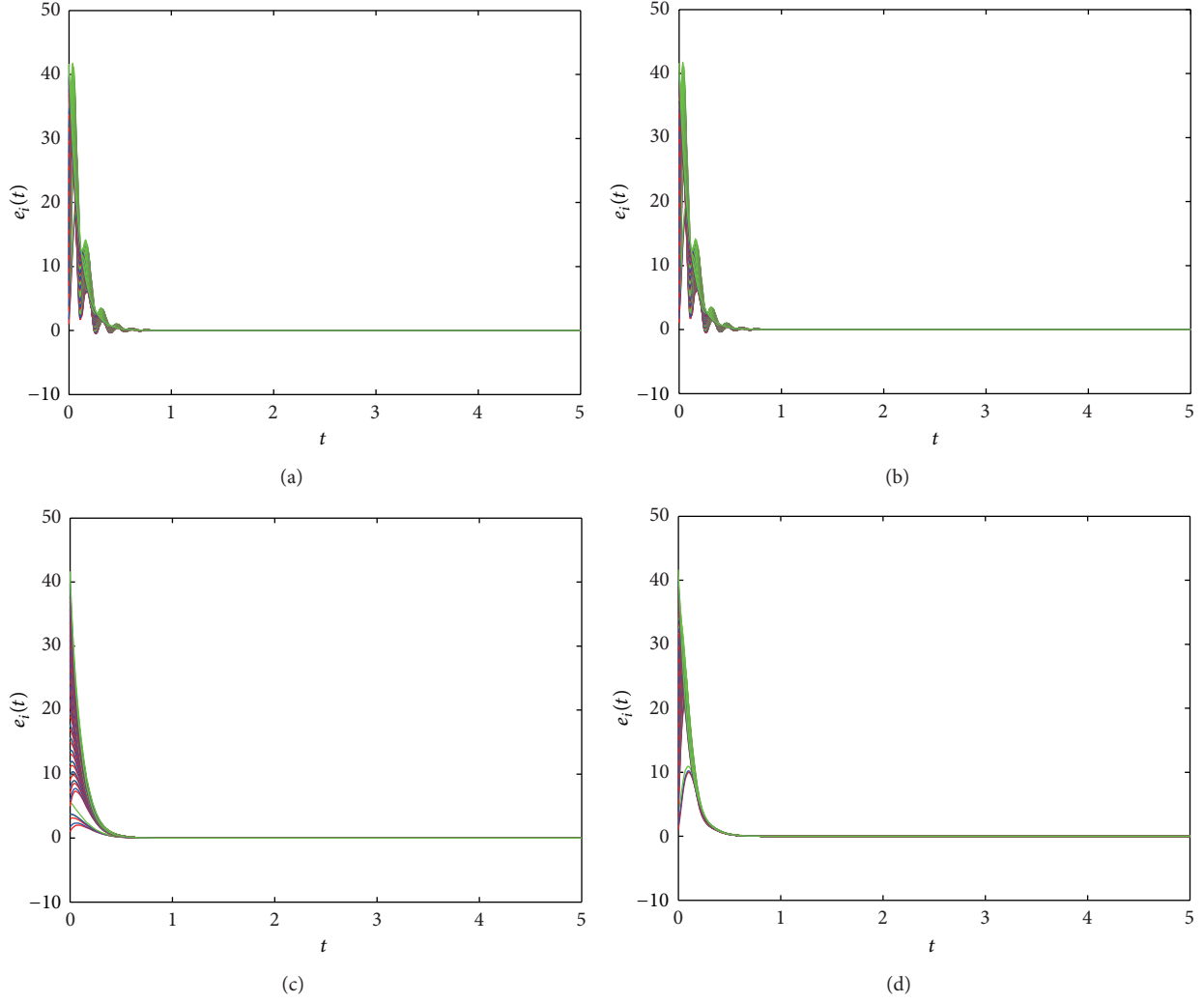


FIGURE 5: Separate synchronous variables  $e_{i1}, e_{i2}, e_{i3}$  ( $1 \leq i \leq 30$ ) of different network models where  $c = 2$ ,  $\tau = 0.01$ , and  $\tau_1 = 0.01$ . (a)  $B_0, B_1$ , and  $B_2$  are small-world network models, the rewiring probability among nodes is 0.3, 0.6, and 0.7. (b)  $B_0, B_1$ , and  $B_2$  are scale-free network models, and their minimum degrees are 1, 2, and 3. (c)  $B_0, B_1$ , and  $B_2$  are random network models, and their connection probability among nodes is 0.1, 0.3, and 0.5. (d)  $B_0$  is a small-world network model, and the rewiring probability among nodes is 0.3.  $B_1$  is a scale-free network model, and the minimum degree is 2.  $B_2$  is a random network model, and the connection probability among nodes is 0.1. The dynamics of nodes satisfy the Lü system. The multilinks network can achieve synchronization under the adaptive controllers (color online).

then we can know that  $L = 64.6142$ . And other parameters are the same with the first example. We have  $\lambda_{\max}(A) = 20$ , and

$$\begin{aligned}
 & \left( \lambda_{\max}(A) + L + c\lambda_{\max}(P_0) \right. \\
 & \quad \left. + \frac{c}{2} \sum_{l=1}^{l=m-1} \lambda_{\max}(P_l P_l^T) \frac{c}{2} (m-1) + \|A\|_F \right) (\|A\|_F)^{-1} \\
 & = \frac{20 + 64.6142 + 18.5139 + 1 + \sqrt{3001}}{\sqrt{3001}} = 2.9008.
 \end{aligned} \tag{41}$$

It does not satisfy Theorem 6. So the nodes cannot achieve synchronization without controllers. Simulation results are given in Figures 3(a)–3(d) which show the evolution process

of 30 state variables in three dimensions. And it verified that the similar nodes cannot achieve synchronization without controllers.

According to the adaptive synchronization criteria, we add the adaptive controllers (20) and (21) to these similar nodes of the network.  $k_1 = k_2 = k_3 = 1$ . The curves of error vectors  $e_{i1}, e_{i2}, e_{i3}$  ( $i = 1, 2, 3$ ) are shown in Figures 4(a)–4(d).

To be more persuadable, with the same calculation method, Figures 5(a)–5(d) plot the synchronous errors of networks with links owning 3 properties. Figures 5(a)–5(d) have different network models, and  $\tau_1 = 0.01$ . This demonstrates that our theorem is not only applicable to multilinks network owning two links properties but also to real networks with multiple links. From Figures 1(a)–1(d) to Figures 5(a)–5(d), we attain that our theorems are feasible in different network models under different conditions. This

result is more helpful to real networks not just to model networks. From the above simulation results, we can see that these similar nodes can achieve synchronization under the impacts of the adaptive controllers. In the future, we will consider the possible application of this paper to packet delay issue in computer communications.

## 6. Conclusion

In this paper, we present the definition of similar nodes and analyze their minimal similarity in the network for the first time. We find the threshold of the minimal similarity of the similar nodes if it is bigger than the threshold, then the similar nodes can achieve synchronization without controllers. Otherwise, we have to add some controllers in order to get synchronization. So some new adaptive synchronization criteria are proposed to realize the synchronization of multilinks networks with similar nodes. Finally, numerical simulations are provided to show the effectiveness and the correctness of the proposed criteria. The model and the principles designed in this paper are very useful to analyze and control the dynamical multilinks networks with similar nodes, such as heart cells networks and neural networks.

## Acknowledgments

This paper is supported by the Foundation for the Author of National Excellent Doctoral Dissertation of PR China (Grant no. 200951), the National Natural Science Foundation of China (Grant nos. 61100204, 61070209, and 61121061), and the Asia Foresight Program under NSFC Grant (Grant no. 61161140320).

## References

- [1] S. H. Strogatz, "Exploring complex networks," *Nature*, vol. 410, no. 6825, pp. 268–276, 2001.
- [2] A.-L. Barabási and R. Albert, "Emergence of scaling in random networks," *Science*, vol. 286, no. 5439, pp. 509–512, 1999.
- [3] M. Chen, "Some simple synchronization criteria for complex dynamical networks," *IEEE Transactions on Circuits and Systems II*, vol. 53, no. 11, pp. 1185–1189, 2006.
- [4] J. Lü and G. Chen, "A time-varying complex dynamical network model and its controlled synchronization criteria," *IEEE Transactions on Automatic Control*, vol. 50, no. 6, pp. 841–846, 2005.
- [5] J. Cao, P. Li, and W. Wang, "Global synchronization in arrays of delayed neural networks with constant and delayed coupling," *Physics Letters A*, vol. 353, no. 4, pp. 318–325, 2006.
- [6] J. Zhou, L. Xiang, and Z. Liu, "Global synchronization in general complex delayed dynamical networks and its applications," *Physica A*, vol. 385, no. 2, pp. 729–742, 2007.
- [7] Y. Xu, W. Zhou, J. Fang, and H. Lu, "Structure identification and adaptive synchronization of uncertain general complex dynamical networks," *Physics Letters A*, vol. 374, no. 2, pp. 272–278, 2009.
- [8] H. Peng, N. Wei, L. Li, W. Xie, and Y. Yang, "Models and synchronization of time-delayed complex dynamical networks with multi-links based on adaptive control," *Physics Letters A*, vol. 374, no. 23, pp. 2335–2339, 2010.
- [9] H. Du, P. Shi, and N. Lü, "Function projective synchronization in complex dynamical networks with time delay via hybrid feedback control," *Nonlinear Analysis: Real World Applications*, vol. 14, no. 2, pp. 1182–1190, 2013.
- [10] J. Lu, D. W. C. Ho, and J. Cao, "A unified synchronization criterion for impulsive dynamical networks," *Automatica*, vol. 46, no. 7, pp. 1215–1221, 2010.
- [11] Z.-H. Guan, Z.-W. Liu, G. Feng, and Y.-W. Wang, "Synchronization of complex dynamical networks with time-varying delays via impulsive distributed control," *IEEE Transactions on Circuits and Systems I*, vol. 57, no. 8, pp. 2182–2195, 2010.
- [12] J. Lu, D. W. C. Ho, J. Cao, and J. Kurths, "Exponential synchronization of linearly coupled neural networks with impulsive disturbances," *IEEE Transactions on Neural Networks*, vol. 22, no. 2, pp. 329–335, 2011.
- [13] Y. Xu, W. Zhou, J. Fang, and W. Sun, "Adaptive lag synchronization and parameters adaptive lag identification of chaotic systems," *Physics Letters A*, vol. 374, no. 34, pp. 3441–3446, 2010.
- [14] Y. Xu, W. Zhou, J. Fang, and W. Sun, "Adaptive synchronization of the complex dynamical network with non-derivative and derivative coupling," *Physics Letters A*, vol. 374, no. 15–16, pp. 1673–1677, 2010.
- [15] A. Das and F. L. Lewis, "Distributed adaptive control for synchronization of unknown nonlinear networked systems," *Automatica*, vol. 46, no. 12, pp. 2014–2021, 2010.
- [16] X. F. Wang and G. Chen, "Pinning control of scale-free dynamical networks," *Physica A*, vol. 310, no. 3–4, pp. 521–531, 2002.
- [17] X. Li, X. Wang, and G. Chen, "Pinning a complex dynamical network to its equilibrium," *IEEE Transactions on Circuits and Systems I*, vol. 51, no. 10, pp. 2074–2087, 2004.
- [18] F. Sorrentino, M. Bernardo, F. Garofalo, and G. Chen, "Controllability of complex networks via pinning," *Physical Review E*, vol. 75, no. 4, Article ID 046103, 6 pages, 2007.
- [19] Q. Hu, H. Peng, Y. Wang, Z. Hu, and Y. Yang, "Pinning adaptive synchronization of complex dynamical network with multilinks," *Nonlinear Dynamics*, vol. 69, no. 4, pp. 1813–1824, 2012.
- [20] J. Zhou, J.-A. Lu, and J. Lü, "Pinning adaptive synchronization of a general complex dynamical network," *Automatica*, vol. 44, no. 4, pp. 996–1003, 2008.
- [21] W. Yu, G. Chen, and J. Lü, "On pinning synchronization of complex dynamical networks," *Automatica*, vol. 45, no. 2, pp. 429–435, 2009.
- [22] Y. Wang, Y. Fan, Q. Wang, and Y. Zhang, "Stabilization and synchronization of complex dynamical networks with different dynamics of nodes via decentralized controllers," *IEEE Transactions on Circuits and Systems I*, vol. 59, no. 8, pp. 1786–1795, 2012.
- [23] Q. Song, J. Cao, and F. Liu, "Synchronization of complex dynamical networks with nonidentical nodes," *Physics Letters A*, vol. 374, no. 4, pp. 544–551, 2010.
- [24] S. Cai, Q. He, J. Hao, and Z. Liu, "Exponential synchronization of complex networks with nonidentical time-delayed dynamical nodes," *Physics Letters A*, vol. 374, no. 25, pp. 2539–2550, 2010.
- [25] M. Li and W. Zhao, "Quantitatively investigating locally weak stationarity of modified multifractional Gaussian noise," *Physica A*, vol. 391, no. 24, pp. 6268–6278, 2012.
- [26] M. Li and W. Zhao, "On  $1/f$  noise," *Mathematical Problems in Engineering*, vol. 2012, Article ID 673648, 23 pages, 2012.
- [27] M. Li and W. Zhao, "Representation of a stochastic traffic bound," *IEEE Transactions on Parallel and Distributed Systems*, vol. 21, no. 9, pp. 1368–1372, 2010.



- [28] D. Li, J.-A. Lu, X. Wu, and G. Chen, "Estimating the ultimate bound and positively invariant set for the Lorenz system and a unified chaotic system," *Journal of Mathematical Analysis and Applications*, vol. 323, no. 2, pp. 844–853, 2006.

## Research Article

# On the Long-Range Dependence of Fractional Brownian Motion

**Ming Li**

*School of Information Science & Technology, East China Normal University, No. 500 Dong-Chuan Road, Shanghai 200241, China*

Correspondence should be addressed to Ming Li; [ming\\_lihk@yahoo.com](mailto:ming_lihk@yahoo.com)

Received 5 May 2013; Accepted 15 May 2013

Academic Editor: Massimo Scalia

Copyright © 2013 Ming Li. This is an open access article distributed under the Creative Commons Attribution License, which permits unrestricted use, distribution, and reproduction in any medium, provided the original work is properly cited.

This paper clarifies that the fractional Brownian motion,  $B_H(t)$ , is of long-range dependence (LRD) for the Hurst parameter  $0 < H < 1$  except  $H = 1/2$ . In addition, we note that the fractional Brownian motion is positively correlated for  $0 < H < 1$  except  $H = 1/2$ . Moreover, we present a theorem to state that the differential or integral of a random function,  $X(t)$ , may substantially change the statistical dependence of  $X(t)$ . One example is that the differential of  $B_H(t)$ , in the domain of generalized functions, changes the LRD of  $B_H(t)$  to be of short-range dependence (SRD) when  $0 < H < 0.5$ .

## 1. Introduction

Fractional Brownian motion (fBm) is widely used [1–10]. Its theory and applications attract the interests of researchers in various fields, ranging from telecommunications to biomedical engineering; see, for example, [11–44], simply citing a few.

There is a set of statistical properties of fBm, such as nonstationarity and being nondifferentiable in the domain of ordinary functions [45]. Two properties, namely, nonstationarity and nondifferentiable property, are the basic properties of standard Brownian motion (Bm) [46–52], which is well known in the fields of time series as well as stochastic processes [53, 54]. As the substantial generalization of Bm, fBm has a property that Bm lacks, that is, its statistical dependence [1–4, 45]. The measure of the statistical dependence of fBm is characterized by the Hurst parameter  $H \in (0, 1)$ .

Note that the fBm for the Hurst parameter  $H \in (0, 1)$  and  $H \neq 1/2$  is of LRD [11, 12, 45, 55, 56]. In addition, fBm is positively correlated for  $H \in (0, 1)$  but  $H \neq 1/2$  [57]. However, the LRD property of fBm may be sometimes conservatively expressed. For example, the LRD property of fBm was restricted by  $H \in (0.5, 1)$  as can be seen from [58, page 2341] and [59, page 708]. For this reason, it may be meaningful to clarify, which this paper aims at.

The remaining paper is organized as follows. In Section 2, we describe that the range of  $H$  for fBm to be of LRD is  $H \in (0, 1)$  and  $H \neq 1/2$ . Discussions are in Section 3, which is followed by conclusions.

## 2. FBm Is LRD for $0 < H < 1$ except $H = 0.5$

In what follows, a random function in general is denoted by  $X(t)$  for  $t \in (0, \infty)$ . We denote  $B_H(t)$  for  $t \in (0, \infty)$  as fBm with  $H \in (0, 1)$ .

Without generality losing, we assume that  $X(t)$  is a random function with mean zero. The autocorrelation function (ACF) of  $X(t)$  is, for  $t, s \in (0, \infty)$ , denoted by

$$C_{XX}(t, s) = E[X(t)X(s)]. \quad (1)$$

By LRD [1, 2], we mean that

$$\int_0^\infty C_{XX}(t, s) dt = \infty. \quad (2)$$

If

$$\int_0^\infty C_{XX}(t, s) dt < \infty, \quad (3)$$

$X(t)$  is of short-range dependence (SRD).

Denote by  $S_{XX}(\omega, t)$  the power spectrum density function (PSD) of  $X(t)$ . Denote by  $F$  the operator of the Fourier transform. Then [60–64],

$$S_{XX}(\omega, t) = F[C_{XX}(t, s)]. \quad (4)$$

The LRD condition described in the frequency domain is expressed by

$$\lim_{\omega \rightarrow 0} S_{XX}(\omega, s) = \infty. \quad (5)$$

The above expression implies the property of  $1/f$  noise regarding random functions with LRD [1–4, 65–70]. On the other hand,  $X(t)$  is of SRD if

$$\lim_{\omega \rightarrow 0} S_{XX}(\omega, s) < \infty. \quad (6)$$

Let  $W^{-\nu}$  be the Weyl integral of order  $\nu > 0$ . Then, for random function  $X(t)$ ; see, for example, [71–75], one has

$$W^{-\nu} X(t) = \frac{1}{\Gamma(\nu)} \int_t^\infty (u-t)^{\nu-1} X(u) du. \quad (7)$$

Thus, the fBm of the Weyl type is in the form:

$$\begin{aligned} B_H(t) - B_H(0) &= \frac{1}{\Gamma(H + 1/2)} \\ &\times \left\{ \int_{-\infty}^0 [(t-u)^{H-0.5} - (-u)^{H-0.5}] dB(u) \right. \\ &\quad \left. + \int_0^t (t-u)^{H-0.5} dB(u) \right\}. \end{aligned} \quad (8)$$

Following [76], the PSD of the fBm of the Weyl type is expressed by

$$S_{B_H B_H}(\omega, t) = \frac{1}{|\omega|^{2H+1}} (1 - 2^{1-2H} \cos 2\omega t). \quad (9)$$

Therefore, we have the following theorem.

**Theorem 1.** *fBm is of LRD for  $H \in (0, 1)$  except  $H = 1/2$ .*

*Proof.* Because  $\lim_{\omega \rightarrow 0} S_{B_H B_H}(\omega, t) = \infty$  for all  $t > 0$  and for  $H \in (0, 1)$  except  $H = 1/2$ , the theorem holds.  $\square$

As a matter of fact, fBm reduces to the standard Bm if  $H = 1/2$ . The PSD of BM, see [11], is given by

$$S_{B_{1/2} B_{1/2}}(t, \omega) = \frac{1}{\omega^2} (1 - \cos 2\omega t). \quad (10)$$

Thus,

$$\lim_{\omega \rightarrow 0} S_{B_{1/2} B_{1/2}}(t, \omega) = 2t^2 \neq \infty. \quad (11)$$

From the theorem, we have the following corollary.

**Corollary 2.** *fBm is not SRD for  $H \in (0, 1)$ .*

In passing, we mention that the ACF of  $B_H(t)$  of the Weyl type is in the form:

$$\begin{aligned} C_{B_H B_H}(t, s) &= \frac{V_H}{(H + 1/2) \Gamma(H + 1/2)} \\ &\times [ |t|^{2H} + |s|^{2H} - |t-s|^{2H} ], \end{aligned} \quad (12)$$

where  $V_H$  is the strength of  $B_H(t)$ . It is given by

$$V_H = \text{Var}[B_H(1)] = \Gamma(1 - 2H) \frac{\cos \pi H}{\pi H}. \quad (13)$$

Following [57, page 4], we have the following remark.

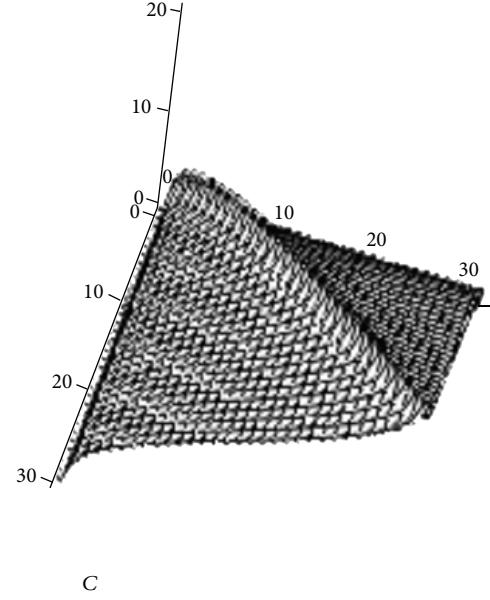


FIGURE 1: ACF of fBm for  $t, s = 0, 1, \dots, 30$  and  $H = 0.2$ .

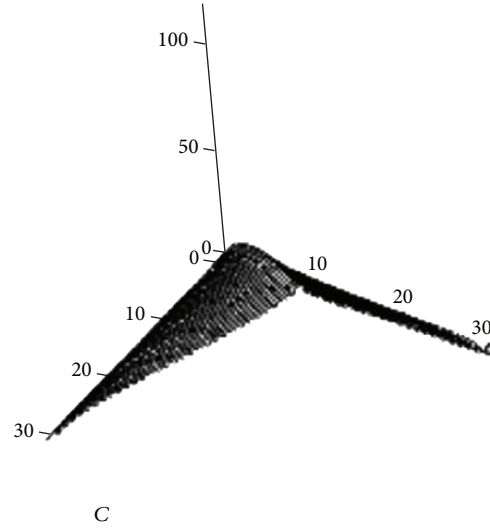


FIGURE 2: ACF of fBm for  $t, s = 0, 1, \dots, 30$  and  $H = 0.4$ .

**Remark 3.** The ACF of fBm is positively correlated for  $H \in (0, 1)$  except  $H = 1/2$ . That is,  $C_{B_H B_H}(t, s) \geq 0$  for  $t, s \in (0, \infty)$ . Figures 1 and 2 indicate the plots of  $C_{B_H B_H}(t, s)$  for  $t, s = 0, 1, \dots, 30$  with  $H = 0.2$  and  $0.4$ , respectively.

### 3. Discussions

Let  $G_H(t)$  be the fractional Gaussian noise (fGn). Then, in the domain of generalized functions over the Schwartz space of test functions [45], we write

$$G_H(t) = \frac{dB_H(t)}{dt}. \quad (14)$$

Denote by  $C_{G_H G_H}(\tau, s)$  the ACF of  $G_H(t)$ . Then, for  $\varepsilon > 0$  [19, 45], one has

$$C_{G_H G_H}(\tau; \varepsilon) = \frac{V_H \varepsilon^{2H-2}}{2} \times \left[ \left( \left| \frac{\tau}{\varepsilon} \right| + 1 \right)^{2H} + \left| \frac{\tau}{\varepsilon} - 1 \right|^{2H} - 2 \left| \frac{\tau}{\varepsilon} \right|^{2H} \right]. \quad (15)$$

From the contents in Section 2, we have the following theorem.

**Theorem 4.** *Let  $X(t)$  be a random function. Then, the statistical dependence of  $dX(t)/dt$  may substantially differ from that of  $X(t)$ , where the differential is in the domain of generalized functions.*

*Proof.* To prove the theorem, we only need an example to show it. Let  $X(t) = B_H(t)$ . Then,  $dX(t)/dt = G_H(t)$ . It is well known that fGn is LRD when  $H \in (0.5, 1)$  as  $C_{G_H G_H}$  is nonintegrable if  $H \in (0.5, 1)$ . On the other hand, for  $H \in (0, 0.5)$ , the integral of  $C_{G_H G_H}$  is zero. Hence, fGn is SRD when  $H \in (0, 0.5)$ . In passing, we note that  $C_{G_H G_H}(\tau; \varepsilon)$  changes its sign and becomes negative for some  $\tau$  proportional to  $\varepsilon$  in this parameter domain [45, page 434]. Since  $B_H(t)$  is LRD for  $H \in (0, 1)$  except  $H = 1/2$ , the statistical dependence of  $G_H(t)$  substantially differs from that of  $B_H(t)$ . This completes the proof.  $\square$

From Theorem 4, we immediately obtain the corollary below.

**Corollary 5.** *Let  $X(t)$  be a random function. Then, the statistical dependence of  $D^{-1}X(t)$  may substantially differ from that of  $X(t)$ , where  $D^{-1}$  is the integral operator of order one.*

*Proof.* Let  $X(t) = G_H(t)$ . Then,  $D^{-1}X(t) = B_H(t)$ . Since  $B_H(t)$  is LRD for  $H \in (0, 0.5)$  while  $G_H(t)$  is SRD when  $H \in (0, 0.5)$ , one sees that the statistical dependence of  $D^{-1}X(t)$  substantially differs from that of  $X(t)$ . Thus, Corollary 5 results.  $\square$

## 4. Conclusions

We have clarified that fBm is LRD and positively correlated for  $H \in (0, 1)$  except  $H = 1/2$ . In addition, we have proved that the differential or integral of a random function may considerably change its statistical dependence.

## Acknowledgments

This work was supported in part by the 973 plan under the project Grant no. 2011CB302800 and by the National Natural Science Foundation of China under the project Grants nos. 61272402, 61070214, and 60873264.

## References

- [1] B. B. Mandelbrot, *Gaussian Self-Affinity and Fractals*, Springer, New York, NY, USA, 2001.
- [2] J. Beran, *Statistics for Long-Memory Processes*, Chapman and Hall, New York, NY, USA, 1994.
- [3] J. Levy-Vehel, E. Lutton, and C. Tricot, Eds., *Fractals in Engineering*, Springer, 1997.
- [4] P. Doukhan, G. Oppenheim, and M. S. Taqqu, Eds., *Theory and Applications of Long-Range Dependence*, Birkhäuser, Boston, Mass, USA, 2002.
- [5] J. B. Bassingthwaite, L. S. Liebovitch, and B. J. West, *Fractal Physiology*, Oxford University Press, 1994.
- [6] J.-P. Bouchaud and A. Georges, "Anomalous diffusion in disordered media: statistical mechanisms, models and physical applications," *Physics Reports*, vol. 195, no. 4-5, pp. 127–293, 1990.
- [7] W. Willinger and V. Paxson, "Where mathematics meets the internet," *Notices of the American Mathematical Society*, vol. 45, no. 8, pp. 961–970, 1998.
- [8] V. Paxson and S. Floyd, "Wide area traffic: the failure of Poisson modeling," *IEEE/ACM Transactions on Networking*, vol. 3, no. 3, pp. 226–244, 1995.
- [9] S. C. Lim and L. P. Teo, "Modeling single-file diffusion with step fractional Brownian motion and a generalized fractional Langevin equation," *Journal of Statistical Mechanics*, vol. 2009, no. 8, Article ID P08015, 24 pages, 2009.
- [10] S. Kim, S. Y. Nam, and D. K. Sung, "Effective bandwidth for a single server queueing system with fractional Brownian input," *Performance Evaluation*, vol. 61, no. 2-3, pp. 203–223, 2005.
- [11] V. M. Sithi and S. C. Lim, "On the spectra of Riemann-Liouville fractional Brownian motion," *Journal of Physics*, vol. 28, no. 11, pp. 2995–3003, 1995.
- [12] S. V. Muniandy and S. C. Lim, "Modeling of locally self-similar processes using multifractional Brownian motion of Riemann-Liouville type," *Physical Review E*, vol. 63, no. 4, part 2, Article ID 461047, 2001.
- [13] D. Feyel and A. de La Pradelle, "On fractional Brownian processes," *Potential Analysis*, vol. 10, no. 3, pp. 273–288, 1999.
- [14] R. F. Peltier and J. Levy-Vehel, "Multifractional Brownian motion: definition and preliminaries results," INRIA TR 2645, 1995.
- [15] T. G. Sinai, "Distribution of the maximum of a fractional Brownian motion," *Russian Mathematical Surveys*, vol. 52, no. 2, pp. 119–138, 1997.
- [16] S. C. Lim and S. V. Muniandy, "On some possible generalizations of fractional Brownian motion," *Physics Letters A*, vol. 266, no. 2-3, pp. 140–145, 2000.
- [17] M. D. Ortigueira and A. G. Batista, "On the relation between the fractional Brownian motion and the fractional derivatives," *Physics Letters A*, vol. 372, no. 7, pp. 958–968, 2008.
- [18] S. C. Lim and L. P. Teo, "Weyl and Riemann-Liouville multifractional Ornstein-Uhlenbeck processes," *Journal of Physics A*, vol. 40, no. 23, pp. 6035–6060, 2007.
- [19] M. Li and S. C. Lim, "A rigorous derivation of power spectrum of fractional Gaussian noise," *Fluctuation and Noise Letters*, vol. 6, no. 4, pp. C33–C36, 2006.
- [20] M. Li and W. Zhao, "On bandlimitedness and lag-limitedness of fractional Gaussian noise," *Physica A*, vol. 392, no. 9, pp. 1955–1961, 2013.
- [21] M. Li and W. Zhao, "Quantitatively investigating locally weak stationarity of modified multifractional Gaussian noise," *Physica A*, vol. 391, no. 24, pp. 6268–6278, 2012.

- [22] V. Paxson, "Fast approximate synthesis of fractional gaussian noise for generating self-similar network traffic," *ACM SIGCOMM Computer Communication Review*, vol. 27, no. 5, pp. 5–18, 1997.
- [23] C. Cattani, M. Scalia, E. Laserra, I. Bochicchio, and K. K. Nandi, "Correct light deflection in Weyl conformal gravity," *Physical Review D*, vol. 87, no. 4, Article ID 47503, 4 pages, 2013.
- [24] C. Cattani, "Harmonic wavelet approximation of random, fractal and high frequency signals," *Telecommunication Systems*, vol. 43, no. 3–4, pp. 207–217, 2010.
- [25] C. Cattani, G. Pierro, and G. Altieri, "Entropy and multifractality for the myeloma multiple TET 2 gene," *Mathematical Problems in Engineering*, vol. 2012, Article ID 193761, 14 pages, 2012.
- [26] C. Cattani, "Fractals and hidden symmetries in DNA," *Mathematical Problems in Engineering*, vol. 2010, Article ID 507056, 31 pages, 2010.
- [27] S. Hu, Z. Liao, and W. Chen, "Sinogram restoration for low-dosed X-ray computed tomography using fractional-order Perona-Malik diffusion," *Mathematical Problems in Engineering*, vol. 2012, Article ID 391050, 13 pages, 2012.
- [28] Z. W. Liao, S. X. Hu, D. Sun, and W. F. Chen, "Enclosed Laplacian operator of nonlinear anisotropic diffusion to preserve singularities and delete isolated points in image smoothing," *Mathematical Problems in Engineering*, vol. 2011, Article ID 749456, 15 pages, 2011.
- [29] J. W. Yang, Y. J. Chen, and M. Scalia, "Construction of affine invariant functions in spatial domain," *Mathematical Problems in Engineering*, vol. 2012, Article ID 690262, 11 pages, 2012.
- [30] H. E. Stanley, S. V. Buldyrev, A. L. Goldberger, S. Havlin, C.-K. Peng, and M. Simons, "Long-range power-law correlations in condensed matter physics and biophysics," *Physica A*, vol. 200, no. 1–4, pp. 4–24, 1993.
- [31] B. Podobnik, P. C. Ivanov, K. Biljakovic, D. Horvatic, H. E. Stanley, and I. Grosse, "Fractionally integrated process with power-law correlations in variables and magnitudes," *Physical Review E*, vol. 72, no. 2, Article ID 026121, 7 pages, 2005.
- [32] A. Carbone, G. Castelli, and H. E. Stanley, "Time-dependent Hurst exponent in financial time series," *Physica A*, vol. 344, no. 1–2, pp. 267–271, 2004.
- [33] Z. Chen, P. C. Ivanov, K. Hu, and H. E. Stanley, "Effect of nonstationarities on detrended fluctuation analysis," *Physical Review E*, vol. 65, no. 4, Article ID 041107, 15 pages, 2002.
- [34] C. Toma, "Advanced signal processing and command synthesis for memory-limited complex systems," *Mathematical Problems in Engineering*, vol. 2012, Article ID 927821, 13 pages, 2012.
- [35] E. G. Bakhoum and C. Toma, "Specific mathematical aspects of dynamics generated by coherence functions," *Mathematical Problems in Engineering*, vol. 2011, Article ID 436198, 10 pages, 2011.
- [36] E. G. Bakhoum and C. Toma, "Mathematical transform of traveling-wave equations and phase aspects of quantum interaction," *Mathematical Problems in Engineering*, Article ID 695208, 15 pages, 2010.
- [37] G. Korvin, *Fractal Models in the Earth Science*, Elsevier, 1992.
- [38] E. E. Peters, *Fractal Market Analysis—Applying Chaos Theory to Investment and Economics*, John Wiley & Sons, 1994.
- [39] S.-C. Liu and S. Chang, "Dimension estimation of discrete-time fractional Brownian motion with applications to image texture classification," *IEEE Transactions on Image Processing*, vol. 6, no. 8, pp. 1176–1184, 1997.
- [40] S. Chang, S.-T. Mao, S.-J. Hu, W.-C. Lin, and C.-L. Cheng, "Studies of detrusor-sphincter synergy and dyssynergia during micturition in rats via fractional brownian motion," *IEEE Transactions on Biomedical Engineering*, vol. 47, no. 8, pp. 1066–1073, 2000.
- [41] C. Fortin, R. Kumaresan, W. Ohley, and S. Hofer, "Fractal dimension in the analysis of medical images," *IEEE Engineering in Medicine and Biology Magazine*, vol. 11, no. 2, pp. 65–71, 1992.
- [42] A. Eke, E. P. Herman, J. B. Bassingthwaite et al., "Physiological time series: distinguishing fractal analysis noises from motions," *European Journal of Physiology*, vol. 439, no. 4, pp. 403–415, 2000.
- [43] G. M. Raymond, D. B. Percival, and J. B. Bassingthwaite, "The spectra and periodograms of anti-correlated discrete fractional Gaussian noise," *Physica A*, vol. 322, pp. 169–179, 2003.
- [44] H. E. Schepers, J. H. G. M. van Beek, and J. B. Bassingthwaite, "Four methods to estimate the fractal dimension from self-affine signals," *IEEE Engineering in Medicine and Biology Magazine*, vol. 11, no. 2, pp. 57–64, 1992.
- [45] B. B. Mandelbrot and J. W. Van Ness, "Fractional Brownian motions, fractional noises and applications," *SIAM Review*, vol. 10, pp. 422–437, 1968.
- [46] G. E. Uhlenbeck and L. S. Ornstein, "On the theory of the Brownian motion," *Physical Review*, vol. 36, no. 5, pp. 823–841, 1930.
- [47] T. Hida, *Brownian Motion*, Springer, 1980.
- [48] J. Dunkel and P. Hänggi, "Relativistic Brownian motion," *Physics Reports*, vol. 471, no. 1, pp. 1–73, 2009.
- [49] M. Peligrad and S. Utev, "Another approach to Brownian motion," *Stochastic Processes and their Applications*, vol. 116, no. 2, pp. 279–292, 2006.
- [50] E. Frey and K. Kroy, "Brownian motion: a paradigm of soft matter and biological physics," *Annalen der Physik*, vol. 14, no. 1–3, pp. 20–50, 2005.
- [51] P. Hänggi, F. Marchesoni, and F. Nori, "Brownian motors," *Annalen der Physik*, vol. 14, no. 1–3, pp. 51–70, 2005.
- [52] F. Cecconi, M. Cencini, M. Falcioni, and A. Vulpiani, "Brownian motion and diffusion: from stochastic processes to chaos and beyond," *Chaos*, vol. 15, no. 2, Article ID 026102, p. 9, 2005.
- [53] A. Papoulis, *Probability, Random Variables and Stochastic Processes*, McGraw-Hill Book, 2nd edition, 1984.
- [54] W. A. Fuller, *Introduction to Statistical Time Series*, John Wiley & Sons, New York, NY, USA, 2nd edition, 1996.
- [55] S. C. Lim and S. V. Muniandy, "Generalized Ornstein-Uhlenbeck processes and associated self-similar processes," *Journal of Physics A*, vol. 36, no. 14, pp. 3961–3982, 2003.
- [56] H. Qian, "Fractional brownian motion and fractional gaussian noise," *Lecture Notes in Physics*, vol. 621, pp. 22–33, 2003.
- [57] F. Aurzada and C. Baumgarten, "Persistence of fractional Brownian motion with moving boundaries and applications," *Journal of Physics A*, vol. 46, no. 12, Article ID 125007, 2013.
- [58] V. Maroulas and J. Xiong, "Large deviations for optimal filtering with fractional Brownian motion," *Stochastic Processes and their Applications*, vol. 123, no. 6, pp. 2340–2352, 2013.
- [59] R. Scheffer and R. Maciel Filho, "The fractional Brownian motion as a model for an industrial airlift reactor," *Chemical Engineering Science*, vol. 56, no. 2, pp. 707–711, 2001.
- [60] M. Sun, C. C. Li, L. N. Sekhar, and R. J. Scabassi, "Wigner spectral analyzer for nonstationary signals," *IEEE Transactions on Instrumentation and Measurement*, vol. 38, no. 5, pp. 961–966, 1989.



- [61] M. B. Priestley, "Evolutionary spectra and non-stationary processes," *Journal of the Royal Statistical Society B*, vol. 27, pp. 204–237, 1965.
- [62] J. S. Bendat and A. G. Piersol, *Random Data: Analysis and Measurement Procedure*, John Wiley & Sons, 3rd edition, 2010.
- [63] J. Xiao and P. Flandrin, "Multitaper time-frequency reassignment for nonstationary spectrum estimation and chirp enhancement," *IEEE Transactions on Signal Processing*, vol. 55, no. 6, pp. 2851–2860, 2007.
- [64] P. Borgnat, P. Flandrin, P. Honeine, C. Richard, and J. Xiao, "Testing stationarity with surrogates: a time-frequency approach," *IEEE Transactions on Signal Processing*, vol. 58, no. 7, pp. 3459–3470, 2010.
- [65] M. Li and W. Zhao, "On  $1/f$  noise," *Mathematical Problems in Engineering*, vol. 2012, Article ID 673648, 22 pages, 2012.
- [66] K. Fraedrich, U. Luksch, and R. Blender, " $1/f$  model for long-time memory of the ocean surface temperature," *Physical Review E*, vol. 70, no. 3, Article ID 037301, pp. 1–4, 2004.
- [67] W. T. Li and D. Holste, "Universal  $1/f$  noise, crossovers of scaling exponents, and chromosome-specific patterns of guanine-cytosine content in DNA sequences of the human genome," *Physical Review E*, vol. 71, no. 4, Article ID 041910, 9 pages, 2005.
- [68] F. N. Hooge, " $1/f$  noise," *Physica B*, vol. 83, no. 1, pp. 14–23, 1976.
- [69] M. S. Keshner, " $1/f$  noise," *Proceedings of the IEEE*, vol. 70, no. 3, pp. 212–218, 1982.
- [70] G. Aquino, M. Bologna, P. Grigolini, and B. J. West, "Beyond the death of linear response:  $1/f$  optimal information transport," *Physical Review Letters*, vol. 105, no. 6, Article ID 069901, 1 page, 2010.
- [71] J. Klafter, S. C. Lim, and R. Metzler, *Fractional Dynamics: Recent Advances*, World Scientific, 2012.
- [72] A. A. Kilbas, H. M. Srivastava, and J. J. Trujillo, *Theory and Applications of Fractional Differential Equations*, Elsevier Science, Amsterdam, The Netherlands, 2006.
- [73] S. Samko, A. A. Kilbas, and D. I. Marichev, *Integrals and Derivatives of the Fractional Order and Some of Their Applications*, Gordon and Breach, Amsterdam, The Netherlands, 1993.
- [74] G. M. Zaslavsky, *Hamiltonian Chaos and Fractional Dynamics*, Oxford University Press, Oxford, UK, 2008.
- [75] R. C. Blei, *Analysis in Integer and Fractional Dimensions*, University Press, Cambridge, UK, 2003.
- [76] P. Flandrin, "On the spectrum of fractional Brownian motions," *IEEE Transactions on Information Theory*, vol. 35, no. 1, pp. 197–199, 1989.